New physics, Dark matter and cosmology in the light of Large Hadron Collider

Ahmad Tarhini

$N°$d'ordre: 108-2013 Année 2013

THÈSE DE DOCTORAT DE L'UNIVERSITÉ DE LYON

délivrée par L'UNIVERSITÉ CLAUDE BERNARD LYON 1

ÉCOLE DOCTORALE DE PHYSIQUE ET D'ASTROPHYSIQUE DE LYON

DIPLÔME DE DOCTORAT

(arrêté du 7 août 2006)

Spécialité

Physique théorique / Physique des particules

Présentée par

M. Ahmad TARHINI

Nouvelle physique, Matière noire et cosmologie à l'aurore du Large Hadron Collider

Soutenue publiquement le 05 Juillet 2013 devant la commission d'examen formée de:

M.	D.	Tsimpis	*Président du jury*	-	IPN Lyon
M.	U.	Ellwanger	*Rapporteur*	-	LPT Orsay
M.	G.	Moreau	*Rapporteur*	-	LPT Orsay
Mme	F.	Mahmoudi	*Examinatrice*	-	LPC Clermont & CERN
M.	G.	Moultaka	*Examinateur*	-	L2C Montpellier
M.	A. S.	Cornell	*Examinateur*	-	NITheP Johannesburg
M.	A.	Deandrea	*Directeur de thèse*	-	IPN Lyon
M.	A.	Arbey	*Co-directeur de thèse*	-	IPN Lyon & CERN

Order $N°$: 108-2013 Year 2013

PHD THESIS of the UNIVERSITY of LYON

Delivered by the UNIVERSITY CLAUDE BERNARD LYON 1

Subject:

Theoretical Physics / Particles Physics

submitted by

Mr. Ahmad TARHINI

for the degree of

DOCTOR OF PHILOSOPHY

New physics, Dark matter and cosmology in the light of Large Hadron Collider

---

defended July 5th, 2013 in front of the following Examining Committee:

Mr.	D.	Tsimpis	*President*	-	IPN Lyon
M.	U.	Ellwanger	*Reviewer*	-	LPT Orsay
M.	G.	Moreau	*Reviewer*	-	LPT Orsay
Mrs.	F.	Mahmoudi	*Examiner*	-	LPC Clermont & CERN
Mr.	G.	Moultaka	*Examiner*	-	L2C Montpellier
Mr.	A. S.	Cornell	*Examiner*	-	NITheP Johannesburg South Africa
Mr.	A.	Deandrea	*Supervisor*	-	IPN Lyon
Mr.	A.	Arbey	*Co-supervisor*	-	IPN Lyon & CERN

Abstract

In the first part of this thesis, we review the Universal Extra-Dimensional Model compactified on a S^1/Z_2 orbifold, and the renormalisation group evolution of quark and lepton masses, mixing angles and phases both in the UED extension of the Standard Model and of the Minimal Supersymmetric Standard Model (the five-dimensional MSSM). We consider two typical scenarios: all matter fields propagating in the bulk, and matter fields constrained on the brane. The two possibilities give rise to quite different behaviours. For the quark sector we study the Yukawa couplings and various flavor observables and for the neutrino sector, we study the evolution of neutrino masses, mixing angles and phases. The analysis is performed in the two cases for different values of $\tan\beta$ and different radii of compactification. The resulting renormalisation group evolution equations in these scenarios are compared with the existing results in the literature, together with their implications.

In the second part, we present a simulation study about anomaly mediated supersymmetry breaking and its extensions. Anomaly mediation is a popular and well motivated supersymmetry breaking scenario. Different possible detailed realisations of this set-up are studied and actively searched for at colliders. Apart from limits coming from flavour, low energy physics and direct collider searches, these models are usually constrained by the requirement of reproducing the observations on dark matter density in the universe. We reanalyse these bounds and in particular we focus on the dark matter bounds both considering the standard cosmological model and alternative cosmological scenarios. We briefly discuss the implications for phenomenology and in particular at the Large Hadron Collider. After that we update our analysis by using new limits from observables and adding recent Higgs boson measurements for the mass and signal strengths in different decay channels.

Keywords:

Beyond the Standard Model, Extra Dimensional Model, Renormalization Group Equations, Supersymmetry, CKM Matrix, PMNS Matrix, Neutrinos, Dark Matter, Cosmology, Large Hadron Collider, Higgs Boson.

Résumé

Dans la première partie de cette thèse, je présenterai le 5D MSSM qui est un modèle supersymétrique avec une dimension supplémentaire. (Five Dimensional Minimal Supersymmetric Standard Model). Après compactification sur l'orbifold $S1/Z2$, le calcul des équations du groupe de renormalisation (RGE) à une boucle montre un changement dans l'évolution des paramètres phénoménologiques. Dès que l'énergie $E = 1/R$ est atteinte, les états de Kaluza-Klein interviennent et donnent des contributions importantes. Plusieurs possibilités pour les champs de matière sont discutés : ils peuvent se propager dans le "bulk" ou ils sont localisés sur la "brane".

Je présenterai d'une part l'évolution des équations de Yukawa dans le secteur des quarks ainsi que les paramètres de la matrice CKM, d'autre part, les effets de ce modèle sur le secteur des neutrinos notamment les masses, les angles de mélange, les phases de Majorana et de Dirac.

Dans la deuxième partie, je parlerai du modèle AMSB et ses extensions (MM-AMSB et HC-AMSB). Ces modèles sont des scénarios de brisure assez bien motivés en supersymétrie. En calculant des observables issues de la physique des particules puis en imposant des contraintes de cosmologie standard et alternative sur ces scénarios, j'ai déterminé les régions qui respectent les contraintes de la matière noire et les limites de la physique des saveurs.

Je reprendrai ensuite l'analyse de ces modèles en utilisant de nouvelles limites pour les observables. La nouvelle analyse est faite en ajoutant les mesures récentes sur la masse du Higgs et les rapports de branchement pour plusieurs canaux de désintégrations.

Mots-clés :

Au delà du Modèle Standard, Dimensions supplémentaires, Equations du Groupe de Renormalisation, Supersymétrie, Matrice CKM, Matrice PMNS, Neutrinos, Matière noire, Cosmologie, Large Hadron Collider, Boson de Higgs.

Remerciements

En premier lieu, je tiens à remercier mon directeur de thèse, Aldo Deandrea, avec qui j'ai partagé plus de 3 années de recherches pendant lesquelles j'ai énormement appris. J'ai apprécié son soutien, son optimisme et nos discussions de physique.

Je remercie ensuite les membres de mon jury de thèse: Prof. Dimitrios Tsimpis, Prof. Ulrich Ellwanger, Prof. Grégory Moreau, Prof. Nazila Mahmoudi, Prof. Alan S. Cornell, Prof. Gilbert Moultaka.

Mes remerciements vont aussi à mon codirecteur Alexandre Arbey et mes collaborateurs avec qui j'ai beaucoup travaillé, beaucoup discuté et de ce fait beaucoup appris.

Je voudrais aussi remercier tous les membres de l'Institut de Physique Nucléaire de Lyon (IPNL) pour leur accueil notamment le groupe de physique théorique, ainsi que le directeur Guy Chanfray et l'ex directeur Benard Ille.

Un grand merci à l' école doctorale ED 52 PHAST ainsi que son directeur Prof. Christophe Dujardin et Sylvie Flores.

Je voudrais aussi remercier très chaleureusement tous mes amis du laboratoire, mes amis libanais et syriens en France, et tous mes amis dans mon village.

Enfin, mes remerciements les plus chaleureux vont à mes parents, mes frères, toute ma grande famille, mon oncle Younes, à ma fiancée Dalal. À ces derniers, je dédie cette thèse.

Contents

Introduction

The Standard Model (SM) of elementary particle physics is one of the cornerstones of all science and one of the great triumphs of the 20th century. It has been carefully experimentally verified in many ways, especially during the past decades and it provides a correct description of virtually all known microphysical nongravitational phenomena. However, there are a number of theoretical and phenomenological issues that the SM fails to address adequately: the gauge hierarchy problem, description of gravity, triggering electroweak symmetry breaking, gauge coupling unification, explanation of family structure and fermion (neutrino) masses, cosmological challenges including the issue of dark matter...

The masses of the quarks and charged leptons are determined in the Standard Model (SM) via Yukawa couplings to the Higgs boson. The origin of their structure (masses and mixing angles) has no explanation within the SM and presents as one of the major challenges for physics beyond the SM. Among these models those with extra spatial dimensions offer many possibilities for model building and TeV-scale physics scenarios which can now be explored or constrained at the Large Hadron Collider (LHC). Extra-dimensional models give, for example, a way to generate electroweak symmetry breaking or supersymmetry breaking through the choice of appropriate boundary conditions. In addition, for the case of flat extra-dimensions, the presence of towers of excited Kaluza-Klein (KK) states induces a power-law enhancement of the gauge couplings, leading to possible low-scale unification. This effect can be applied to other couplings, such as Yukawa couplings, giving an original way to generate mass hierarchies.

SUSY is a lovely theoretical construct, which is included in the most general set of symmetries of local relativistic field theories, has the virtue of solving the gauge hierarchy problem and it has captured the imagination of many theoretical physicists. It allows for a new synthesis of particle interactions, and offers a new direction for the incorporation of gravity into particle physics. The supersymmetric extension of the Standard Model also ameliorates the situation of phenomenological problems in the physics of elementary particles, if superpartners exist at the TeV scale. These new states may well be discovered in experiments at high energy colliders. Since SUSY relates the scalar and fermionic sectors, the chiral symmetries which protect the masses of the fermions, also protect the masses of the scalars from quadratic divergences, leading to an elegant solution of the hierarchy problem. We saw that apart from this, SUSY leads to unification of gauge couplings, provides cold dark matter candidate and provides a framework to discuss gravity.

The study of the renormalisation group equations (RGEs) provides a way by which partial explorations of the physics implications at a high energy scale is possible, as the theories at asymptotic energies may reveal new symmetries or other interesting properties which may lead

to deeper insights into the physical content.

The RGEs help us to study the asymptotic properties of the Lagrangian parameters like the Yukawa coupling constants and mixing angles, and explore the possibility of a model in which the CKM matrix might have a simple, special form at asymptotic energies. We will also treat the neutrino masses and several parameters of the PMNS matrix. However, our results will be limited by the fact that extra-dimensional theories are only effective ones, limited by a cut-off in their physical description of fundamental phenomena. Therefore the following study can only be used as an indication of the behaviour of couplings and mixing parameters at an intermediate scale between the electroweak scale (at which these parameters are measured) and the higher scale at which the effective theory ceases to be valid. However, in the range of the LHC energies (of the order of a few TeV), and beyond, one can indeed test if the departure from the usual behaviour of the coupling evolution can be seen in precision flavour measurements.

String theory is a realistic attempt to provide a unified quantum picture of all known interactions in physics. Consistent string theories indicate the existence of supersymmetry and compactified extra dimensions in their low energy phenomenology. Though a rigorous connection between string theory and low energy phenomenological models with extra dimensions has not yet been possible, it provides enough motivation to study higher dimensional supersymmetric theories. From a purely phenomenological point of view, such higher dimensional supersymmetric theories have various virtues to their credit, including the explanation of the fermion mass hierarchy from a different angle, providing a cosmologically viable dark matter candidate, possible interpretation of the Higgs as a composite leading to a successful electroweak symmetry breaking without the necessity of a fundamental Yukawa interaction, and lowering the unification scale down to a few TeV. Supersymmetrization provides a natural mechanism to stabilize the Higgs mass in extra dimensional scenarios. We note that all supersymmetric models in four dimensions necessarily introduce the paradigm of further new physics that controls SUSY breaking in this class of models. Embedding supersymmetric models in extra dimension provides various avenues to realize soft breaking of supersymmetry.

In order to present the results, I divided this thesis in three parts:

– Part 1 is an introduction to the main concepts necessary to understand the Standard Model of particle physics, supersymmetry, cosmology and dark matter.
– Part 2 consists of two chapters in which I describe my work about phenomenology in the 5D MSSM and the comparison between different observables in our model and others UED models. I present in chapter 2 a theoretical description of the model, describe in a compact form the RGE of various parameters as well as results related to quarks sector and CKM matrix. I will discuss a five dimensional $\mathcal{N} = 1$ supersymmetric model compactified on the S^1/Z_2 orbifold as a simple testing ground for the effects of the extra-dimension on the quark Yukawa couplings and the CKM matrix observables.
  In chapter 3 I present the results related to neutrino sector and PMNS matrix.

Part 2 is based on the following papers:

1. A. Cornell, A. Deandrea, L. Liu, A. Tarhini. Scaling of the CKM Matrix in the 5D MSSM [arXiv:1110.1942],
   Published in Phys. Rev. D85 (2012) 056001.
2. A. Cornell, A. Deandrea, L. Liu, A. Tarhini. The evolution of neutrino masses and mixings in the 5D MSSM [arXiv:1206.5988],
   Published in Eur.Phys.J.Plus 128 (2013) 6.
3. A. Cornell, A. Deandrea, L. Liu, A. Tarhini. Renormalisation running of masses and mixings in UED models [arXiv:1209.6239],
   Published in Mod. Phys. Lett. A 28, 1330007 (2013).

– Part 3 also consists of two chapters. I study the scan of parameter space in various anomaly mediation SUSY breaking scenarios and how it is constrained by the flavour physics, Higgs physics and the dark matter limits using the SuperIso Relic program. In chapter 4 I present a detailed study with many observables from B-physics and I see how the alternative cosmology can lead to new favoured regions in the parameter space. In chapter 5 I will use updated results and more constrained limits on flavour observables. I study also the effects of Higgs mass and branching ratios to these models.

Part 3 is based on the following papers:

1. A. Arbey, A. Deandrea, A. Tarhini. Anomaly mediated SUSY breaking scenarios in the light of cosmology and in the dark (matter) [arXiv:1103.3244],
   Published in JHEP 1105:078,2011.
2. A. Arbey, A. Deandrea, F. Mahmoudi, A. Tarhini. Anomaly mediated supersymmetric models and Higgs data from the LHC [arXiv:1304.0381],
   Published in Phys. Rev. D 87 (115020) 2013.

Part 2 and part 3 are independent. Finally some appendices will help the reader to find details about concepts and equations in the different chapters.

Chapter 1

General context and overview

1.1 The Standard Model of particle physics

1.1.1 Description and particle content

Our current understanding of High Energy Physics can be summarized in the theory known as the Standard Model (SM) [1]. It is a renormalizable quantum field theory describing the elementary particles of matter and their fundamental interactions. The SM describes collectively the electromagnetic, weak and strong interactions between the fundamental constituents of matter, quarks and leptons. In mathematical terms, the SM is a non-Abelian gauge theory based on the symmetry group $G_{SM} = SU(3)_C \times SU(2)_L \times U(1)_Y$. As a gauge theory, the Standard Model is based on the fundamental concept of gauge symmetries. Unlike global symmetries, gauge symmetries are not new symmetries of nature, in the sense that they do not imply the existence of new conserved charges. However, their existence is of a much deeper significance, since they determine in a unique way how the the fields (particles) interact.

The development of the SM proved to be difficult, due to the fact that gauge symmetries can be broken, i.e. they may not be manifest in physical observables. Symmetry breaking in the form of phase transitions was well known in classical physics and had been formalized by Landau [2, 3]. Considering for instance a ferromagnet, we know that, above the Curie temperature, the net magnetization is zero, the spins are randomly oriented and the system displays a symmetry under SO(3) transformations (3-dimensional rotations). Below the Curie temperature, the system obtains a net magnetization with the spins pointing along a certain direction and the symmetry being reduced ("broken") from SO(3) to SO(2) (rotations about the external field direction). In this less symmetric phase, one needs additional degrees of freedom in order to describe the system. These have been dubbed *order parameters*.

In an analogous way, Higgs, Brout, Englert, Guralnik, Hagen and Kibble proposed a way to apply these principles in systems of quantum fields [4–8]. Glashow, Weinberg and Salam then applied the idea of symmetry breaking to the description of the electromagnetic and weak interactions as a unified gauge field theory.
In the electroweak theory [9–11], one starts from a symmetric phase which is invariant under the transformations of the gauge group $SU(2) \times U(1)_Y$, where $Y = Q - \frac{I_3}{2}$ is the hypercharge, Q

is the charge and I_3 the projection of the isospin along the z axis. Along with the electroweak gauge bosons, the electroweak theory predicts the existence of a scalar field (called the *Higgs field*), which plays the role of the order parameter of the theory. Below a certain energy scale, the Higgs field acquires a non-zero vacuum expectation value and the $SU(2) \times U(1)_Y$ symmetry is broken down to $U(1)_Q$, which is the gauge symmetry of electromagnetism. In the process, the weak bosons acquire masses and appear thus to be non-invariant under the gauge transformations [1]. The electroweak theory has been consolidated by the discovery of the neutral current interactions and the W and Z bosons by the Gargamelle and UA1 experiments at CERN. This paved the way towards the construction of the Standard Model, which started with the works of Glashow, Weinberg and Salam [9–11].

The development of Quantum Chromodynamics (QCD) as the gauge theory of strong interactions began with the introduction of the quark model for the classification of hadron resonances [12,13]. The colour charge was introduced as a new degree of freedom in an attempt to solve the Δ^{++} puzzle, i.e. to allow for the existence of resonances with antisymmetric wavefunctions comprised of three quarks with identical flavour and spin [14]. The measurement of the cross-section ratio $\sigma(e^+e^- \to hadrons)/\sigma(e^+e^- \to \mu^+\mu^-)$ at SLAC [15] provided evidence for the existence of three colours and the discovery of 3-jet events in e^+e^- collisions by the TASSO experiment at DESY [16] established the existence of gluons thus proving that the strong interactions could be described as a gauge theory with a SU(3) symmetry group.

The SM accommodates twelve fundamental fermions of spin 1/2 that are divided into two categories: leptons which do not interact with strong interactions and quarks which interact with strong interactions and come in three colours; and three generations. To each of these particles one associates an antiparticle by charge conjugation. The fundamental fermions are described by different representations of the SM gauge group G_{SM}. Right-handed quarks and right-handed leptons are $SU(2)$ singlets and the right-handed neutrinos are G_{SM} singlets. Fermion interactions are mediated by the gauge bosons that transform under the adjoint representation of G_{SM}. The standard model also predicts the existence of a Higgs boson, which is a spin 0 particle. Its recent discovery in 2012opens the way to the detailed study of its properties. In the table 1.1, we give the SM field content and their charges under the three different gauge groups and their electric charges.

1.1.2 Standard Model Lagrangian

The Standard Model Lagrangian can be split into four parts [17]: the gauge sector $\mathcal{L}_G$, the fermion sector $\mathcal{L}_F$, the Higgs sector $\mathcal{L}_H$ and the Yukawa sector $\mathcal{L}_y$.

$$\mathcal{L}_{SM} = \mathcal{L}_G + \mathcal{L}_F + \mathcal{L}_H + \mathcal{L}_y \tag{1.1}$$

1. In the electroweak sector (weakly coupled sector), the associated gauge fields are respectively $W^{1,2,3}$ and B. The gauge symmetry breaking introduces masses for three new mass-eigenstates: $W^{\pm}$ and Z. One eigenstate will remain massless, the photon γ.

Field	Notation	$SU(3)_C$	$SU(2)_W$	$U(1)_Y$	$U(1)_{EM}$
Quarks (s=1/2)	$Q_L = \begin{pmatrix} u_L \\ d_L \end{pmatrix}, \begin{pmatrix} c_L \\ s_L \end{pmatrix}, \begin{pmatrix} t_L \\ b_L \end{pmatrix}$	3	2	1/6	$\begin{pmatrix} 2/3 \\ -1/3 \end{pmatrix}$
	$u_R,\ c_R,\ t_R$	3	1	2/3	2/3
	$d_R,\ s_R,\ b_R$	3	1	$-1/3$	$-1/3$
Leptons (s=1/2)	$L_L = \begin{pmatrix} \nu_e \\ e_L \end{pmatrix}, \begin{pmatrix} \nu_\mu \\ \mu_L \end{pmatrix}, \begin{pmatrix} \nu_\tau \\ \tau_L \end{pmatrix}$	1	2	$-1/2$	$\begin{pmatrix} 0 \\ -1 \end{pmatrix}$
	$e_R,\ \mu_R,\ \tau_R$	1	1	1	-1
Gauge (s=1)	g	8	1	0	0
	$W^3,\ W\pm$	1	3	0	$0,\ \pm 1$
	B	1	1	0	0
Higgs (s=0)	$\Phi = \begin{pmatrix} \phi^+ \\ \phi_0 = \frac{1}{\sqrt{2}}(v + h + i\varphi_0) \end{pmatrix}$	1	2	1/2	$\begin{pmatrix} 1 \\ 0 \end{pmatrix}$

Table 1.1: The SM fields with their representations under $SU(3)_C$ and $SU(2)_W$ and their charges under $U(1)_Y$ and $U(1)_{EM}$. Q is the electric charge and s is the spin of the field.

Gauge sector

The first term is the kinetic term of the gauge fields:

$$\mathcal{L}_G = -\frac{1}{4g_1^2} B^{\mu\nu} B_{\mu\nu} - \frac{1}{4g_w^2} \sum_{a=1}^{3} W^{a,\mu\nu} W_{a,\mu\nu} - \frac{1}{4g_s^2} \sum_{A=1}^{8} G^{A,\mu\nu} G_{A,\mu\nu} \tag{1.2}$$

where $B^{\mu\nu}$, $W^{a,\mu\nu}$ and $G^{A,\mu\nu}$ are the field strength of the associated gauge fields given by:

$$\begin{aligned} B^{\mu\nu} &= \partial^\mu B^\nu - \partial^\nu B^\mu \\ W^{a,\mu\nu} &= \partial^\mu W^{a,\nu} - \partial^\nu W^{a,\mu} + g_w\ \epsilon^{abc}\ W^{b,\mu} W^{c,\nu} \\ G^{A,\mu\nu} &= \partial^\mu G^{A,\nu} - \partial^\nu G^{A,\mu} + g_s\ f^{ABC}\ G^{B,\mu} G^{C,\nu} \end{aligned} \tag{1.3}$$

g_s, g_w and g_1 are the coupling constants associated to $SU(3)_C$, $SU(2)_W$ and $U(1)_Y$. ϵ^{abc} and f^{ABC} are the structure constants of $SU(2)$ and $SU(3)$. They are defined by the commutation

relation between the generators t^a for $SU(2)$ or T^A for $SU(3)$ [2], where $a = 1..3$ and $A = 1..8$.

$$[t^a, t^b] = i\epsilon^{abc}t^c \text{ and } \quad [T^A, T^B] = if^{ABC}T^C \tag{1.4}$$

Fermion sector

The gauge interaction of fermions can be derived from the covariant derivative, once the various charges of the fields are known. The peculiarity of the SM is that the left-handed part of a fermion has a different coupling compared to the right-handed one. For instance, only left-handed fields couple to W bosons.

$$\mathcal{L}_F = i\bar{Q}^i_L \not{D} Q^i_L + i\bar{u}^i_R \not{D} u^i_R + i\bar{d}^i_R \not{D} d^i_R + i\bar{e}^i_R \not{D} e^i_R + i\bar{L}^i_L \not{D} L^i_L \tag{1.5}$$

The index $i = 1..3$ is a flavour index which takes into account the three families of quarks and leptons, $\not{D} = \gamma_\mu D^\mu$ where γ_μ are the Dirac's matrices. The colour indices have been removed for more readability and the covariant derivative is given by:

$$D^\mu = \partial^\mu - ig_s\theta_S G^{\mu,A}T^A - ig_w\theta_W W^{\mu,a}t^a - ig_1 Y B^\mu \tag{1.6}$$

$\theta_S = 0$ for singlets and 1 for triplets of $SU(3)_C$, $\theta_W = 0$ for singlets and 1 for doublets of $SU(2)_W$ and Y is the charge under $U(1)_Y$.

Higgs sector

This part of the Lagrangian will generate the spontaneous breaking of gauge symmetry. The gauge Lagrangian Eq.(1.2) contains massless gauge bosons because a mass term such as $\frac{1}{2}m^2 B_\mu B^\mu$ is forbidden by the gauge symmetry, which also forbids fermion mass terms $m\bar{f}f = m(\bar{f}_R f_L + \bar{f}_L f_R)$ in the fermion Lagrangian Eq.(1.5) because the left-chiral and right-chiral components of the fields transform differently under the gauge symmetry. To generate masses of the gauge bosons (other than the photon) and the chiral fermions in a gauge invariant way, we introduce a new complex scalar field Φ whose Lagrangian will respect all the symmetry of the SM but whose vacuum expectation value will not, and the gauge symmetries are respected everywhere in the theory but are broken by the vacuum state.

$$\Phi = \begin{pmatrix} \phi^+ \\ \phi^0 \end{pmatrix} \rightarrow \langle\Phi\rangle = \frac{1}{\sqrt{2}}\begin{pmatrix} 0 \\ v \end{pmatrix} \tag{1.7}$$

The Lagrangian of the Higgs field is given by:

$$\mathcal{L}_H = (D^\mu\Phi)^\dagger(D_\mu\Phi) - \mu^2\Phi^\dagger\Phi + \lambda(\Phi^\dagger\Phi)^2 \tag{1.8}$$

2. $t^a = \sigma^a/2$ with $a = 1..3$ for the fundamental representation of $SU(2)$. Here σ^a are the Pauli matrices.

where $D^\mu = \partial^\mu - ig_w W^{\mu,a} t^a - ig_1 Y_h B^\mu$. This expression of the potential is the easiest renormalizable possibility. For $\mu^2 < 0$ and $\lambda > 0$ we can show that it will generate the vacuum expectation value (vev) for the Higgs field $v = \sqrt{-\frac{\mu^2}{\lambda}}$. We notice that the charged component of Φ does not take a (vev) in order to conserve the invariance under $U(1)_{EM}$.

Then we can do an expansion of the Higgs field around the minimum v in function of real fields $\theta_{1,2,3}$ and H:

$$\Phi = \begin{pmatrix} \theta_1 + i\theta_2 \\ \frac{1}{\sqrt{2}}(v+H) - i\theta_3 \end{pmatrix} = e^{i\theta_a t^a} \begin{pmatrix} 0 \\ \frac{1}{\sqrt{2}}(v+H) \end{pmatrix} \tag{1.9}$$

Here, one can use the $SU(2)_L$ gauge invariance of Φ and we can eliminate the degrees of freedom $\theta_{1,2,3}$ which become non-physical:

$$\Phi(x) \to e^{-i\theta_a(x)t^a}\Phi(x) = \frac{1}{\sqrt{2}} \begin{pmatrix} 0 \\ (v+H) \end{pmatrix} \tag{1.10}$$

By expanding the kinetic term of the Lagrangian, we will generate mass terms for the gauge bosons:

$$\begin{aligned} (D^\mu\Phi)^\dagger(D_\mu\Phi) &= \left| \left(\partial^\mu - ig_w W^{\mu,a} t^a - \frac{i}{2} g_1 B^\mu \right) \Phi \right|^2 \\ &= \frac{1}{2}(\partial_\mu H)^2 + \frac{1}{8} {g_w}^2 (v+H)^2 \left| {W_\mu}^1 + i {W_\mu}^2 \right|^2 + \frac{1}{8}(v+H)^2 \left| g_w {W_\mu}^3 - g_1 B_\mu \right|^2 . \end{aligned} \tag{1.11}$$

If we define the physical gauge fields ${W_\mu}^\pm$, Z_μ and A_μ

$${W_\mu}^\pm = \frac{1}{2}({W_\mu}^1 \mp i {W_\mu}^2), \; Z_\mu = \frac{g_w {W_\mu}^3 - g_1 B_\mu}{\sqrt{g_w^2 + g_1^2}}, \; A_\mu = \frac{g_w {W_\mu}^3 + g_1 B_\mu}{\sqrt{g_w^2 + g_1^2}} \tag{1.12}$$

the equation Eq.(1.11) can be rewritten as:

$$(D^\mu\Phi)^\dagger(D_\mu\Phi) = \frac{1}{2}(\partial_\mu H)^2 + {M_W}^2 {W_\mu}^+ W^{-\mu} + \frac{1}{2}{M_Z}^2 Z_\mu Z^\mu + \frac{1}{2}{M_A}^2 A_\mu A^\mu. \tag{1.13}$$

The diagonalization of the mass matrix of the gauge fields gives the eigenstates Z^μ and A^μ of the theory:

$$\begin{pmatrix} Z_\mu \\ A_\mu \end{pmatrix} = \begin{pmatrix} \cos\theta_W & -\sin\theta_W \\ \sin\theta_W & \cos\theta_W \end{pmatrix} \begin{pmatrix} W_\mu^3 \\ B_\mu \end{pmatrix} \tag{1.14}$$

where θ_W is the Weinberg angle given by:

$$\cos\theta_W = \frac{g_w}{\sqrt{g_w^2 + g_1^2}} \quad \text{and} \quad \sin\theta_W = \frac{g_1}{\sqrt{g_w^2 + g_1^2}}\,. \tag{1.15}$$

The masses of vector bosons are therefore given by

$$M_W = \frac{v g_w}{2}, \quad M_Z = \frac{v}{2}\sqrt{g_w^2 + g_1^2}, \quad M_A = 0. \tag{1.16}$$

The photon A is always massless because it is protected by the $U(1)_{EM}$ symmetry which is not broken. We have four initial degrees of freedom of Φ, three of them are being absorbed by $W^\pm$ and Z, and the last one will correspond to the new scalar particle: the Higgs boson.

Yukawa sector

From symmetry considerations we are free to add gauge-invariant interactions between the scalar fields and the fermions[3]. These are called the Yukawa terms in the Lagrangian and they are responsible of generating fermion masses and the mixing between different families.

$$\mathcal{L}_Y = -\sum_{i=1}^{3} Y^u_{ij} Q^\dagger_{Li} (i\sigma_2 H^*) u_{Rj} - \sum_{i=1}^{3} Y^d_{ij} Q^\dagger_{Li} H d_{Rj} - \sum_{i=1}^{3} Y^e_{ij} L^\dagger_{Li} H e_{Rj} + h.c. \tag{1.17}$$

where Y^u, Y^d and Y^l are the 3×3 complex Yukawa matrices. Once the Higgs field gets a vev v, we will have fermion masses:

$$(m_u)_{ij} \sim (Y^u)_{ij} v, \quad (m_d)_{ij} \sim (Y^d)_{ij} v, \quad (m_l)_{ij} \sim (Y^l)_{ij} v. \tag{1.18}$$

These mass matrices are in the flavour basis, and not in the mass basis. To diagonalize them and define the real mass eigenstates, we introduce unitary matrices which affect, in the quark sector, the interactions containing both quark types with $W^\pm$. This lead to a non diagonal term in the Lagrangian which ensures couplings between different quark generations through the CKM matrix (see more details in section 2.6). It should be noted that due to the absence of their right chiral components, the neutrinos remain massless in the SM; this consideration has changed after the observation of neutrinos oscillation and this is a way how to go beyond the SM.

1.1.3 Electroweak precision tests of the Standard Model

The Standard Model is a consistent, renormalizable quantum field theory that accounts for a wide variety of experimental data over an energy range up to about 100 GeV. Initially, the SM was tested at the tree level, but the remarkable agreement between SM predictions and

3. We use the Higgs doublet in order to write down a mass term which connects right-handed and left-handed components which are respectively singlets and doublets of $SU(2)_W$.

the precision measurements at the CERN LEP collider and TEVATRON have confirmed the SM to at least a part per mille and have established that radiative corrections as given by the SM are essential for agreement with these data. The SM also qualitatively explains why baryon and lepton numbers appear to be approximately conserved: with its particle content, it is impossible to write renormalizable interactions that do not conserve baryon and lepton numbers, so that these interactions (if they exist) must be suppressed by (powers of) some new physics scale [18].

There are 19 parameters within the SM [4]: 9 for the masses of charged fermions, 2 for the Higgs boson (Higgs vev v and quartic coupling λ), 3 gauge couplings constants (related to α_s,α_{ew} and $sin\ \theta_W$), 4 parameters from the CKM matrix and the QCD θ parameter. We use three input parameters to compare theoretical predictions of SM and the experimental data: the Z-mass determined by LEP1, $M_Z = 91.1876\pm\ 0.0021$ GeV, the fine structure constant $\alpha = 1/137.035999084(51)$, extracted from measurement of the anomalous magnetic moment of the electron, and the Fermi constant extracted from the muon lifetime, $G_F = 1.166364(5) \times 10^{-5}\ GeV^{-2}$.

From these inputs we can predict the other observables of the SM, which can be observed in colliders, by including quantum correction effects. The main progress in the domain was made in LEP e^+e^- collider in 1990, and it has already permitted us to give bounds on the top and Higgs masses. The observation of the top quark was confirmed in 1995 by the TEVATRON (a $p\bar{p}$ collider) [19, 20]. Recently the new results from ATLAS and CMS indicate the presence of a Higgs like boson with a mass about 126 GeV (see fig. 1.1), this discovery opens up an era of precision studies of its production and decay properties.

The Z pole observables experiments [23] included the variables, M_Z, Γ_Z, σ, branching ratios into e^+e^-, $\mu^+\mu^-$, $\tau^+\tau^-$, $q\bar{q}$, $c\bar{c}$, $b\bar{b}$. From these data we can obtain constraint on the number of families of neutrino $N_\nu = 2.984 \pm 0.009$ which give the first experimental indication of the three generation flavour structure of the SM. These experiments also measured a number of asymmetries, including forward-backward (FB), polarization and mixed FB polarization which can determine θ_W. Some of the results in fig. 1.2 show how the precision of these measurements allows deviations which are often under the percent level. There is a hint of tension between the lepton and quark asymmetries which appears in $A_{fb}^{0,b}$. This may suggest new physics affecting the third family. For more details about experimental status of the SM and discussion of different observables, the reader can refer to [20].

Constraints on new physics

The radiative corrections to the gauge boson self-energies dominate the radiative effects on electroweak observables because all fermions couple to $SU(2)_L$ gauge fields. The ρ_0 parameter describes new sources of electroweak symmetry breaking [20] and can test some new physics models

$$\rho_0 = \frac{m_W^2}{m_Z^2 cos^2\theta_W \rho_{SM}} \tag{1.19}$$

4. There are also 9 additional parameters from neutrino sector: 3 masses, 3 mixing angles and 3 phases.

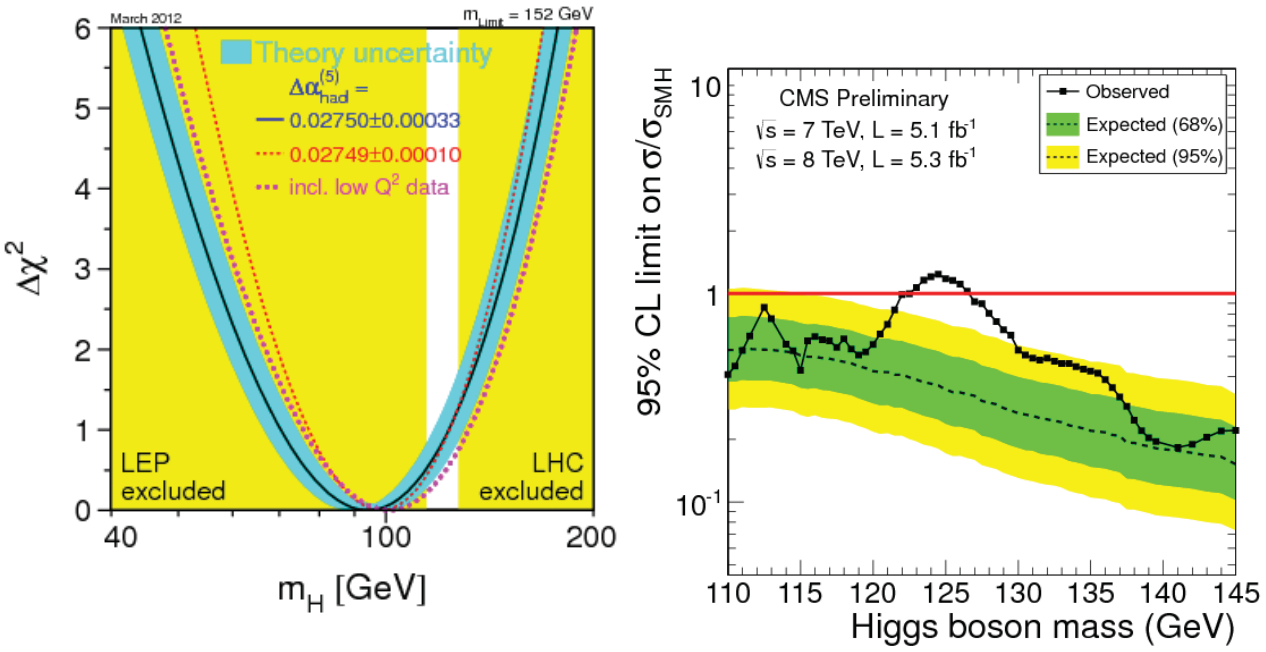

Figure 1.1: **Left panel :** The $\Delta\chi^2$ of the Standard Model fit of the electroweak precision observables as a function of the Higgs mass. The minimum of this curve, at 94 GeV, is the mass of the Higgs bosons which is preferred by EWPT with an experimental uncertainty of +29 and -24 GeV (at 68% confidence level). Extracted from Ref. [21].
Right panel : The 95% CL upper limits on the cross section ratio σ/σ_{SM} for the SM Higgs boson hypothesis as function of m_h. The observed values are shown by the solid line. The dashed line indicates the expected median of results for the background only hypothesis, while the green and yellow bands indicate the ranges that are expected to contain 68% and 95% of all observed excursions from the median, respectively. Extracted from Ref. [22].

where $\rho_{SM} = m_W^2/(m_Z^2 cos^2\theta_W)$ is the default parameter assuming the validity of the SM. Another set of parameters, S, T and U can be used to constrain many new physics models beyond SM; they give constraints about heavy physics which affect the gauge self-energies and it can be applied to precision observables [5]. We denote the contributions of new physics to the

5. The STU-parametrization [24]: T measures the difference between the new physics contributions of neutral and charged current processes at low energies and S (U) describe new physics contributions to neutral (charged) current processes at different energy scales.

Quantity	Value	Standard Model	Pull	Dev.
M_Z [GeV]	91.1876 ± 0.0021	91.1874 ± 0.0021	0.1	0.0
Γ_Z [GeV]	2.4952 ± 0.0023	2.4961 ± 0.0010	−0.4	−0.2
Γ(had) [GeV]	1.7444 ± 0.0020	1.7426 ± 0.0010	—	—
Γ(inv) [MeV]	499.0 ± 1.5	501.69 ± 0.06	—	—
$\Gamma(\ell^+\ell^-)$ [MeV]	83.984 ± 0.086	84.005 ± 0.015	—	—
$\sigma_{\rm had}$[nb]	41.541 ± 0.037	41.477 ± 0.009	1.7	1.7
R_e	20.804 ± 0.050	20.744 ± 0.011	1.2	1.3
R_μ	20.785 ± 0.033	20.744 ± 0.011	1.2	1.3
R_τ	20.764 ± 0.045	20.789 ± 0.011	−0.6	−0.5
R_b	0.21629 ± 0.00066	0.21576 ± 0.00004	0.8	0.8
R_c	0.1721 ± 0.0030	0.17227 ± 0.00004	−0.1	−0.1
$A_{FB}^{(0,e)}$	0.0145 ± 0.0025	0.01633 ± 0.00021	−0.7	−0.7
$A_{FB}^{(0,\mu)}$	0.0169 ± 0.0013		0.4	0.6
$A_{FB}^{(0,\tau)}$	0.0188 ± 0.0017		1.5	1.6
$A_{FB}^{(0,b)}$	0.0992 ± 0.0016	0.1034 ± 0.0007	−2.6	−2.3
$A_{FB}^{(0,c)}$	0.0707 ± 0.0035	0.0739 ± 0.0005	−0.9	−0.8
$A_{FB}^{(0,s)}$	0.0976 ± 0.0114	0.1035 ± 0.0007	−0.5	−0.5
$\bar{s}_\ell^2(A_{FB}^{(0,q)})$	0.2324 ± 0.0012	0.23146 ± 0.00012	0.8	0.7
	0.23200 ± 0.00076		0.7	0.6
	0.2287 ± 0.0032		−0.9	−0.9
m_t [GeV]	173.4 ± 1.0	173.5 ± 1.0	−0.1	−0.3
M_W [GeV]	80.420 ± 0.031	80.381 ± 0.014	1.2	1.6
	80.376 ± 0.033		−0.2	0.2

Figure 1.2: This table is extracted from PDG review [20] on electroweak precision test. The *Pull* column give the deviation considering the Higgs mass as a free parameter and the *Dev* column is given for $m_h = 124.5$GeV. Γ's represent the partial and total width of the Z and $R_x = \Gamma_{had}/\Gamma_x$, A_{FB} the forward-backward asymmetry in the distribution of $f\bar{f}$ production which originates from interferences between the vector and the axial-vector couplings.

various self-energies by Π_{ij}^{new}, we have [20]:

$$\begin{aligned}
\hat{\alpha}(M_Z)T &= \frac{\Pi_{WW}^{new}(0)}{M_W^2} - \frac{\Pi_{ZZ}^{new}(0)}{M_Z^2}, \\
\frac{\hat{\alpha}(M_Z)}{4\hat{s}_Z^2\hat{c}_Z^2}S &= \frac{\Pi_{ZZ}^{new}(M_Z^2) - \Pi_{ZZ}^{new}(0)}{M_Z^2} - \frac{\hat{c}_Z^2 - \hat{s}_Z^2}{\hat{c}_Z\hat{s}_Z}\frac{\Pi_{Z\gamma}^{new}(M_Z^2)}{M_Z^2} - \frac{\Pi_{\gamma\gamma}^{new}(M_Z^2)}{M_Z^2}, \\
\frac{\hat{\alpha}(M_Z)}{4\hat{s}_Z^2}(S+U) &= \frac{\Pi_{WW}^{new}(M_W^2) - \Pi_{WW}^{new}(0)}{M_W^2} - \frac{\hat{c}_Z}{\hat{s}_Z}\frac{\Pi_{Z\gamma}^{new}(M_Z^2)}{M_Z^2} - \frac{\Pi_{\gamma\gamma}^{new}(M_Z^2)}{M_Z^2}\,,
\end{aligned} \tag{1.20}$$

where $\hat{s}_Z^2 = \sin^2\hat{\theta}_W(M_Z)$, $\hat{c}_Z^2 = \cos^2\hat{\theta}_W(M_Z)$ and $\hat{\alpha}(M_Z)^{-1} = 127.944 \pm 0.014$. Setting STU

equal to zero in the SM case and assuming that 115.5 GeV $< m_h <$ 127 GeV, present limits on these parameters are given by [20]:

$$\begin{array}{ll} S = 0.00^{+0.11}_{-0.10} & sin^2\theta_W = 0.23125 \pm 0.00016 \\ T = 0.00^{+0.11}_{-0.12} & \alpha_s(m_Z) = 0.1197 \pm 0.0018 \\ U = 0.08 \pm 0.11 & m_t = 173.4 \pm 1.0\ GeV \end{array} \tag{1.21}$$

These variables depend on m_h and give constraints on some exotic extensions of the SM by calculating the masses and couplings of extra-particles. For example, a heavy degenerate family of fermions [6] is excluded by the current electroweak precision test because the S parameter present a deviation of 5.7 σ.

1.1.4 Problems with the Standard Model

The SM is not a complete model. Some of the experimental arguments in support of this are:

- The SuperKamiokande collaboration in 1998 and other new experiments on the neutrino sector gives the solar and atmospheric neutrino data and presents definitive evidence for neutrino oscillations. This strongly implies masses for neutrinos.
- The presence of Dark Matter (discussed in section 1.3) in the Universe which suggests (a) new stable particle(s), not predicted by the SM. This is due to the Zwicky's observations in 1933 and the study of fluctuations in the spectrum of Cosmic Microwave Background.
- Observations of type Ia supernovae and CMB radiation suggest that the bulk of the energy of the Universe resides in a novel form called *dark energy* which constitutes 74 % of the energy density. This could be the cosmological constant introduced by Einstein.

There is more in nature than the SM. Some theoretical questions and considerations going in this way are:

- **Quantum Gravity :** At the quantum level, the SM describes three of the four fundamental interactions. However, gravity is only treated classically and quantum discussion of gravity should be an effective field theory valid at scales smaller than M_{Pl}.
- **Gauge group :** The SM does not explain the choice of $G_{SM} = SU(3)_C \times SU(2)_L \times U(1)_Y$. Why are there three families and four interactions? Why 3+1 space time dimensions?
- **Strong CP problem :** In the QCD sector, there is a coupling allowed by SM symmetries which takes the form of $\theta\epsilon^{\mu\nu\rho\sigma}G^A_{\mu\nu}G^A_{\rho\sigma}$, where θ is an arbitrary dimensionless parameter. This term breaks the CP symmetry (charge conjugation followed by parity). The experimental bound on the neutron electric dipole moment implies $\theta < 10^{-11}$ but we cannot simply set θ to zero because of the CP violation in the electroweak sector. The main problem refers to the fact that θ is *unnaturally* small and if a parameter is naturally small, then one can set it to zero with a symmetry protecting its value (for example the Peccei-Quinn symmetry) but this is not the case here.

6. This is not the case of the heavy non-chiral fermions (known as vector-like particles) which do not contribute to STU parameters (or to ρ_0).

– **Confinement :** Why is it only possible for quarks to exist confined in hadrons such as protons and neutrons? The value of the strong coupling increases with decreasing energy so the strong interactions are asymptotically free, and at low energies, they are so strong that they do not allow quarks to separate.
– **Hierarchy problem :** There exists a large mass hierarchy in the matter sector of the SM: the electron mass is about 0.511 MeV and the top mass is around 173 GeV. Another issue is why there are totally different energy scales: $M_{ew} \sim 10^2$ GeV and $M_{Pl} \sim 10^{19}$ GeV. This we will refer to as a *naturalness* problem, then a *fine tuning* should be performed at each order in perturbation theory to avoid M_{ew} to take the value of the cutoff scale (which can be $\sim M_{Pl}$).
– **Fine-Tuning :** The chiral symmetry protects fermion masses from large radiative corrections. However, as seen in fig. 1.3, the Higgs boson mass receives radiative corrections from its self-couplings, gauge boson loops and fermion loops. These corrections are quadratically divergent and very sensitive to the UV physics, they are given by:

$$\delta m_h^2 \sim \frac{1}{32\pi^2}((\frac{1}{4}(3g_w^2 + g_1^2) + 6\lambda - 6y_t^2)\Lambda^2 + \mathcal{O}(\log\Lambda)) \tag{1.22}$$

The physical mass is obtained by adding the bare mass and the one-loop correction $m_h^2(phys) \sim m_h^2(bare) + \frac{c}{16\pi^2}\Lambda^2$, where we have dropped the $(\ln\Lambda)$ terms and the c coefficient depends on the various coupling constants of the SM. If we take $\Lambda = M_{GUT} \sim 10^{16}$ GeV, then the Lagrangian mass parameter m_h^2 will have to be fine tuned to 1 part in 10^{26} to cancel this quadratic effect and provide a physical Higgs mass around 100 GeV. This makes the SM less natural and this is know as *naturalness* or *fine-tuning* problem.

Beyond the Standard Model

For the above reasons, SM cannot represent a fundamental theory of the Universe but it can be an effective field theory at low energies. We need to find an extension that could solve some or all problems of the SM in order to generalize it. The above arguments all point to *new physics* but they do not indicate decisively the scale for this new physics except the last

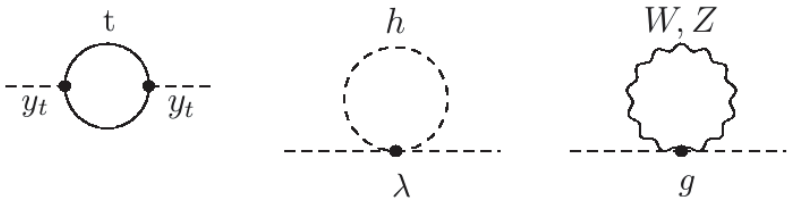

Figure 1.3: Radiative corrections to Higgs mass in SM from top, Higgs self-interaction and W, Z.

argument because we have an idea about the Higgs mass, so we can choose the value of Λ in Eq.(1.22) to be around TeV. In this case one can avoid *fine-tuning* problem.

One of the important ideas to go beyond SM is to try to generalize symmetries of SM [25]:

- **Internal symmetry :** Consider for example *Grand Unified Theories* (GUT) in which the SM symmetries are themselves the result of the breaking of a larger symmetry (containing as an example new gauge groups SU(5), SO(10), ...). This extension is elegant because it unifies in one single symmetry the three gauge interactions of the SM and it decreases the number of parameters. However, it does not solve the open problems of the SM and with our present precision understanding, the running of the three gauge couplings does not unify at a single point at higher energies.
- **Space-time symmetry I :** *Extra Dimensions* models (for example: Large Extra Dimension (ADD), Warped Extra Dimension (RS), UED) that try to bridge the gap between the two scales of the SM. They have a more general coordinate transformations and this idea is similar to extra dimensions in *Kaluza Klein* theory. Our 4 dimensional Universe is restricted on a *brane* or a surface inside a larger dimensional one. These models can solve many problems of the SM such as the hierarchy problem.
- **Space-time symmetry II :** *Supersymmetry* is a symmetry under the exchange of bosons and fermions, it solves the most important problem of the SM, the naturalness issue of the hierarchy problem due to cancellations between contributions of fermions and bosons to the Higgs mass. SUSY also solves the unification of the gauge couplings and provides the best candidate for cold dark matter.

There is also *models with no fundamental scalars* in which there is a possibility to describe the elementary Higgs fields in terms of some dynamical symmetry breaking mechanism based on new strong dynamics such as *technicolour*, *composite Higgs model*.

1.2 Supersymmetry

Supersymmetry (SUSY) is a proposed invariance under generalized space-time transformations linking fermions and bosons. One can say that it is one of the most beautiful ideas in Physics. SUSY enables a fermion to transform into a boson and vice versa. It admits supermultiplets with fermionic and bosonic members. The couplings of those members get related and their masses are split by SUSY breaking effects. For more details or further explanation of any part of this section, the reader can refer to [18, 26–30].

1.2.1 Motivations for SUSY

The motivations for *supersymmetry* are numerous and in the following we list some of them:

- **Solving the hierarchy problem :** Due to the symmetry between bosons and fermions in SUSY, we have cancellation of quadratic divergences for scalar masses and we avoid the *fine-tuning* problem. As an example, let us consider just the top correction to Higgs in equation (1.23):

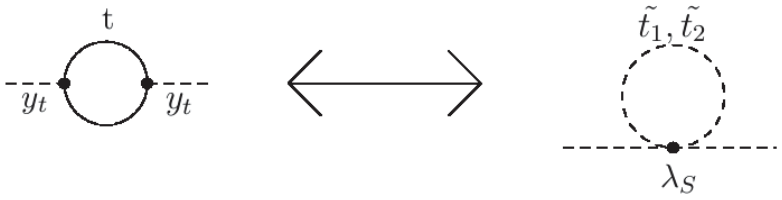

Figure 1.4: Radiative corrections to Higgs mass in SM from the top quark and new cancelling contribution from the two top partners: $\tilde{t_1}, \tilde{t_2}$.

$$\Delta m_h^2 \sim -\frac{y_t^2}{16\pi^2}(2\Lambda^2 + 6m_t^2 \log\left(\frac{\Lambda}{m_t}\right) + ...) \tag{1.23}$$

Here Λ is the cut-off scale of SM which is expected to be around M_{Pl}. Therefore, if we add two new scalars to the SM, with the same quantum number as the top quark, one superpartner for each top's chirality as it is shown in the fig. 1.4, and we denote λ_S their couplings with the Higgs and m_S, their masses, then they will give corrections to the Higgs mass:

$$\Delta m_h^2 \sim 2 \times \left(\frac{\lambda_S}{16\pi^2}(\Lambda^2 + 2m_{\tilde{t}}^2 \log\left(\frac{\Lambda}{m_{\tilde{t}}}\right) + ...)\right) \tag{1.24}$$

If $\lambda_S = y_t^2$, there is a compensation between the two loops and the divergence is now logarithmic.

- **Unification of the gauge coupling :** The values of running gauge couplings do not unify if we evolve these to high energies using the renormalisation group equations of the SM. However, if we use supersymmetric evolution equations, they unify at the scale $M_{GUT} \sim 2 \times 10^{16}$ GeV as we can see in fig. 1.5.
- **Cold dark matter candidate :** SUSY with conserved R-parity can provide a dark matter candidate [26]. The lightest supersymmetric particle (LSP) cannot decay due to the R-parity that forbids vertices with odd number of supersymmetric particles. Then the LSP is stable and could thereby become a viable candidate for the observed cold Dark Matter in the Universe.
- **Connection to Gravity :** if we consider the local SUSY transformations rather than global ones, we will have a spin 2 massless gauge field, the *graviton* [18], which mediates gravitational interactions together with its superpartner is the *gravitino* (in the same way as the local gauge invariance requires to introduce gauge bosons). The local supersymmetry dictates the dynamics of supergravity which includes Einstein general relativity [7].

7. Taking the parameters to be local or space-time dependent in Eq.(1.33), one gets a local translations that result in a theory of (super) gravity.

1.2.2 Algebra

Supersymmetry (SUSY) is based on a new symmetry between fermionic and bosonic degrees of freedom. From a technical point of view, this can be formulated in the following way: the new generators of this transformation will extend the Poincaré algebra into a superalgebra. This is allowed by Coleman-Mandula theorem only by adding also anticommuting generators. In the minimal extension, we add to the translation generator P^μ and Lorentz transformation generator $M^{\mu\nu}$, one new fermionic generator $Q = \left(Q_\alpha, \bar{Q}^{\dot{\alpha}}\right)^T$ which transforms like a spin-1/2 [26]. These operators change the spin of the state

$$Q_\alpha|fermion>=|boson> \qquad \bar{Q}_{\dot{\alpha}}|boson>=|fermion> \tag{1.25}$$

The new coordinates are Grassmann variables transforming as two-compnent Weyl spinors

$$\{\theta_\alpha, \theta_\beta\} = 0 \qquad \{\bar{\theta}_{\dot{\alpha}}, \bar{\theta}_{\dot{\beta}}\} = 0 \tag{1.26}$$

where the $\alpha, \beta, \dot{\alpha}, \dot{\beta}$ indices take the values 1 or 2.

The new superalgebra becomes

$$\begin{aligned}
[P_\mu, P_\nu] = 0,\ [M_{\mu\nu}, P_\rho] &= i(g_{\mu\rho}P_\nu - g_{\nu\rho}P_\mu), \\
[M_{\mu\nu}, M_{\rho\sigma}] &= i(M_{\mu\sigma}g_{\nu\rho} + M_{\nu\sigma}g_{\mu\rho} - M_{\mu\rho}g_{\nu\sigma} - M_{\nu\sigma}g_{\mu\rho}) \\
[M_{\mu\nu}, Q_\alpha] = (\sigma_{\mu\nu})^\beta_\alpha Q_\beta,\ \text{and} \quad [P_\mu, Q_\alpha] &= 0 \\
\{Q_\alpha, Q_\beta\} = 0,\ \text{and} \quad \{Q_\alpha, \bar{Q}_{\dot{\beta}}\} &= 2\sigma^\mu_{\alpha\dot{\beta}} P_\mu
\end{aligned} \tag{1.27}$$

where $g_{\mu\nu}$ is Minkowski's metric, $\sigma_\mu = (1, \sigma_i)$ are Pauli's matrices, $\sigma_{\mu\nu} = \frac{1}{4}[\sigma_\mu, \sigma_\nu]$ and

$$P_\mu = i\partial_\mu, \quad iQ_\alpha = \frac{\partial}{\partial\theta^\alpha} - i\sigma^\mu_{\alpha\dot{\alpha}}\bar{\theta}^{\dot{\alpha}}\partial_\mu, \quad i\bar{Q}_{\dot{\alpha}} = -\frac{\partial}{\partial\bar{\theta}^{\dot{\alpha}}} + i\theta^\alpha\sigma^\mu_{\alpha\dot{\alpha}}\partial_\mu\ . \tag{1.28}$$

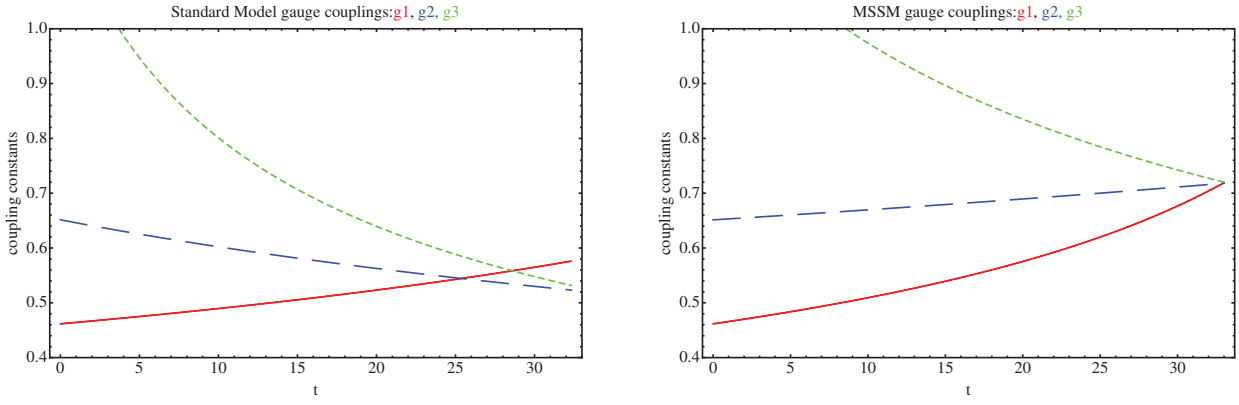

Figure 1.5: Gauge couplings g_1 (red), g_2 (blue), g_3 (green) in the SM (left panel), and in the MSSM (right panel) as a function of a scale parameter $t = ln(\frac{\mu}{M_Z})$.

We define the covariant fermionic derivatives

$$D_\alpha = \frac{\partial}{\partial\theta^\alpha} + i\sigma^\mu_{\alpha\dot\alpha}\bar\theta^{\dot\alpha}\partial_\mu \qquad \bar D_{\dot\alpha} = -\frac{\partial}{\partial\bar\theta^{\dot\alpha}} - i\theta^\alpha\sigma^\mu_{\alpha\dot\alpha}\partial_\mu \ . \tag{1.29}$$

The derivatives D_α and $\bar D_{\dot\alpha}$ anticommute with the generators of SUSY and they obey algebra :

$$\{D_\alpha, \bar D_{\dot\alpha}\} = 2i\sigma^\mu_{\alpha\dot\alpha}\partial_\mu \qquad \{D_\alpha, D_\beta\} = \{\bar D_{\dot\alpha}, \bar D_{\dot\beta}\} = 0. \tag{1.30}$$

1.2.3 Superspace and Superfields

The superfield formalism is quite useful in SUSY [26, 28–30]. These superfields describe the quantum fields, their superpartners and the auxiliary fields in the same object which are reducible representations of SUSY algebra [8]. The calculation using superfields is easier than the calculation with each component of superfields (the fermionic fields, scalars, vector bosons, ...) because one supergraph contains many graphs of standard fields. Superspace corresponds to our standard space-time with the addition of two spinorial anticommuting coordinates , θ_α and $\bar\theta^{\dot\alpha}$. The superfields live in superspace in which the integration over the variables θ and $\bar\theta$ is defined as [9]

$$\int d^2\theta = 0, \quad \int d^2\bar\theta = 0, \quad \int d^2\theta\ \theta^2 = 1, \quad \int d^2\bar\theta\ \bar\theta^2 = 1. \tag{1.31}$$

The elements of integration are

$$\begin{aligned} d^2\theta &= -\frac{1}{4}d\theta^\alpha d\theta^\beta\epsilon_{\alpha\beta}, \qquad d^4\theta = d^2\theta d^2\bar\theta, \\ d^2\bar\theta &= -\frac{1}{4}d\bar\theta_{\dot\alpha}d\bar\theta_{\dot\beta}\epsilon^{\dot\alpha\dot\beta}, \qquad d^8z = d^4x d^4\theta. \end{aligned} \tag{1.32}$$

In the superspace, the functions $\delta(\theta) = \theta^2$ and $\delta(\bar\theta) = \bar\theta^2$ act as Dirac delta distributions.

The supertranslation in superspace of the coordinates x^μ, θ and $\bar\theta$ are

$$\begin{aligned} x_\mu &\to x_\mu + a_\mu + i\theta\sigma_\mu\bar\xi - i\xi\sigma_\mu\bar\theta, \\ \theta &\to \theta + \xi, \\ \bar\theta &\to \bar\theta + \bar\xi, \end{aligned} \tag{1.33}$$

where ξ and $\bar\xi$ play a role of Grassmannian transformation parameters.

8. Irreducible representations of the SUSY algebra are obtained by imposing constraints which are covariant under the supersymmetry algebra

9. Integration and derivation are identical for the anticommuting Grassmann variables.

A superfield is a function of x^μ, θ, $\bar{\theta}$ and its expansion is finite because the anticommuting propriety of the coordinates θ and $\bar{\theta}$

$$\begin{aligned} F(x^\mu,\theta,\bar{\theta}) = f(x) + \theta\chi(x) + \bar{\theta}\bar{\chi}(x) + \theta^2 m(x) + \bar{\theta}^2 n(x) + \theta\sigma^\mu\bar{\theta}v_\mu(x), \\ + \theta^2\bar{\theta}\bar{\lambda}(x) + \theta\bar{\theta}^2\lambda(x) + \theta^2\bar{\theta}^2 d(x) \ . \end{aligned} \tag{1.34}$$

This superfield contains 16 bosonic and 16 fermionic degrees of freedom. The action of the SUSY algebra on the superfields

$$F(x^\mu,\theta,\bar{\theta}) \to e^{i(-a^\mu P_\mu + \xi Q + \bar{\xi}\bar{Q})} F(x^\mu,\theta,\bar{\theta}) \ . \tag{1.35}$$

Chiral superfield

A chiral superfield (left) $\Phi(x,\theta,\bar{\theta})$ satisfies the condition

$$\bar{D}_{\dot{\alpha}}\Phi(x,\theta,\bar{\theta}) = 0 \ , \tag{1.36}$$

When we develop the chiral superfield, the usual fields arise as the coefficients in an expansion of $F(x^\mu,\theta,\bar{\theta})$ in powers of θ and $\bar{\theta}$

$$\begin{aligned} \Phi(x,\theta,\bar{\theta}) = \phi(x) + i\theta\sigma^\mu\bar{\theta}\partial_\mu\phi(x) + \frac{1}{4}\theta^2\bar{\theta}^2\partial^2\phi(x), \\ + \sqrt{2}\theta\psi(x) - \frac{i}{\sqrt{2}}\theta^2\partial_\mu\psi(x)\sigma^\mu\bar{\theta} \ , \\ + \theta^2 F(x) \ , \end{aligned} \tag{1.37}$$

where ϕ is a complex scalar field, ψ is a left-handed Weyl spinor field and F is an auxiliary complex scalar field.

One can also construct an antichiral (right) superfield $\Phi^\dagger(x,\theta,\bar{\theta})$ that has the component field expansion

$$\begin{aligned} \Phi^\dagger(x,\theta,\bar{\theta}) = \phi^\dagger(x) - i\theta\sigma^\mu\bar{\theta}\partial_\mu\phi^\dagger(x) + \frac{1}{4}\theta^2\bar{\theta}^2\partial^2\phi^\dagger(x), \\ + \sqrt{2}\bar{\theta}\bar{\psi}(x) + \frac{i}{\sqrt{2}}\bar{\theta}^2\theta\sigma^\mu\partial_\mu\bar{\psi}(x) \ , \\ + \bar{\theta}^2 F^\dagger(x) \ , \end{aligned} \tag{1.38}$$

which obeys the condition

$$D_\alpha\Phi^\dagger(x,\theta,\bar{\theta}) = 0 \ , \tag{1.39}$$

The SUSY transformation of a chiral superfield in Eq.(1.35) induces transformations of its components. Under an infinitesimal SUSY transformation the left-handed superfield change as follows

$$\Phi \to \Phi + \delta\Phi \ ,$$
$$\delta\Phi = i(\xi Q + \bar{\xi}\bar{Q})\Phi = \delta\phi(x) + \sqrt{2}\theta\delta\psi(x) + \theta^2\delta F(x) + ... \tag{1.40}$$

If we use the explicit expressions in Eq.(1.28), we find

$$\delta\phi = \sqrt{2}\xi\psi \ ,$$
$$\delta\psi = i\sqrt{2}\sigma^\mu\bar{\xi}\partial_\mu\phi + \sqrt{2}\xi F \ ,$$
$$\delta F = i\sqrt{2}\partial_\mu\psi\sigma^\mu\bar{\xi} \ . \tag{1.41}$$

As expected the change in the bosonic (fermionic) component of the superfield is proportional to the fermionic (bosonic) fields. It is important to notice that the change in F component under a SUSY transformation is a total derivative. This can be used for the construction of SUSY Lagrangians as we will see in section 1.2.4. The product of chiral (antichiral) superfields is a chiral (antichiral) one, but this is not the case of a term such as $\bar{\Phi}\Phi$.

Vector Superfield

One can also define the vector superfield with the hermitian constraint

$$V = V^\dagger \ . \tag{1.42}$$

Its expansion in terms of the coordinates θ and $\bar{\theta}$ gives

$$\begin{aligned} V(x,\theta,\bar{\theta}) = {} & C(x) + i\theta\xi(x) - i\bar{\theta}\bar{\xi}(x) \\ & + \frac{i}{2}\theta^2[M(x) + iN(x)] - \frac{i}{2}\bar{\theta}^2[M(x) - iN(x)] - \theta\sigma^\mu\bar{\theta}v_\mu(x) \\ & + i\theta^2\bar{\theta}[\bar{\lambda}(x) + \frac{i}{2}\bar{\sigma}^\mu\partial_\mu\xi(x)] - i\bar{\theta}^2\theta[\lambda(x) + \frac{i}{2}\sigma^\mu\partial_\mu\bar{\xi}(x)] \\ & + \frac{1}{2}\theta^2\bar{\theta}^2[D(x) + \frac{1}{2}\partial^2 C(x)] \end{aligned} \tag{1.43}$$

where C, D, M, N are real scalar fields, ξ is a Weyl spinor and v_μ is a vector field (gauge boson).

The supersymmetric generalization of the abelian gauge transformation is given by

$$V \to V + i(\Phi - \Phi^\dagger) \ . \tag{1.44}$$

In the Wess-Zumino gauge, this transformation will be an ordinary gauge transformation for the vector field v_μ and the other fields C, M, N and χ are eliminated. Therefore

$$V_{WZ} = -\theta\sigma^\mu\bar{\theta}v_\mu(x) + i\theta^2\bar{\theta}\bar{\lambda}(x) - i\bar{\theta}^2\theta\lambda(x) + \frac{1}{2}\theta^2\bar{\theta}^2 D(x) \tag{1.45}$$

where v_μ should be associated with the gauge field (vector boson), λ is a Weyl fermion (the gaugino) and D is an auxiliary field. As for the chiral superfield, we can determine the transformation properties of the component fields of $V(x,\theta,\bar{\theta})$ under infinitesimal SUSY transformation

$$\begin{aligned}\delta\lambda_\alpha &= -iD\xi_\alpha - \frac{1}{2}(\sigma^\mu\bar{\sigma}^\nu)_\alpha^\beta\xi_\beta V_{\mu\nu}\ ,\\ \delta V^\mu &= i(\xi\sigma^\nu\bar{\lambda} - \lambda\sigma^\nu\bar{\xi}) - \partial^\mu(\xi\chi + \bar{\xi}\bar{\chi})\ ,\\ \delta D &= \partial_\mu(-\xi\sigma^\nu\bar{\lambda} + \lambda\sigma^\nu\bar{\xi})\ ,\end{aligned} \tag{1.46}$$

where $V_{\mu\nu} = \partial_\mu V_\nu - \partial_\nu V_\mu$. Note that the variation of the D field is a total derivative as in the case of F field. Since total divergences vanish when integrated over the space time, the F (D) component of chiral (vector) superfields can be used to construct SUSY Lagrangians.

For an arbitrary V, *not necessarily in the Wess-Zumino gauge*, one can construct left and right chiral spinorial field-strength superfields

$$W_\alpha = -\frac{1}{4}\bar{D}^2 D_\alpha V \qquad \bar{W}_{\dot{\alpha}} = -\frac{1}{4}D^2\bar{D}_{\dot{\alpha}}V \tag{1.47}$$

as superfield generalizations of the abelian field-strength tensor ($F_{\mu\nu}$ is in the θ component of W_α).

1.2.4 SUSY Lagrangians

The general form of a renormalizable action for a chiral field theory is

$$\begin{aligned}S &= \int d^8z\left(\bar{\Phi}_i\Phi_i + W(\Phi_i)\delta(\bar{\theta}) + W^\dagger(\Phi_i)\delta(\theta)\right)\\ &= \int d^8z\ \bar{\Phi}_i\Phi_i + \left(a_i\Phi_i + \frac{1}{2}m_{ij}\Phi_i\Phi_j + \frac{1}{3!}\lambda_{ijk}\Phi_i\Phi_j\Phi_k\right)\delta(\bar{\theta}) + h.c.\end{aligned} \tag{1.48}$$

The first term correspond to the kinetic contribution of Φ. In the expansion of $\bar{\Phi}_i\Phi_i$, we have a term proportional to $\theta^2\bar{\theta}^2$ which is called the D term. The second part of the Lagrangian is the superpotential W which corresponds to the mass and Yukawa coupling terms. We have in the expansion components with θ^2 which is called the F term. We set $a_i = 0$ in the following since Φ_i will not be a gauge singlet.

The kinetic Lagrangian of a free vector superfield is

$$\mathcal{L}_{gauge} = \frac{1}{4}W^\alpha W_\alpha|_{\theta^2} + \frac{1}{4}\bar{W}_{\dot{\alpha}}\bar{W}^{\dot{\alpha}}|_{\bar{\theta}^2} \tag{1.49}$$

Abelian case of a supersymmetric gauge theory

The (anti) chiral superfields transform under the $U(1)$ gauge transformations as

$$\Phi_l \to e^{-iQ_l\Lambda}\Phi_l, \qquad \overline{\Phi}_l \to e^{iQ_l\overline{\Lambda}}\overline{\Phi}_l \tag{1.50}$$

where Λ is the scalar chiral superfield associated with the $U(1)$ gauge transformation and Q_l are charges of matter superfields Φ_l. In order to have an invariant kinetic part in Eq.(1.48), one should modify it

$$\mathcal{L}_{kinetic} = \overline{\Phi}_l e^{i2Q_l V}\Phi_l \tag{1.51}$$

Therefore, we have the most general renormalizable action in the abelian SUSY gauge

$$\begin{aligned} S &= \int d^8z[\overline{\Phi}_l e^{i2Q_l V}\Phi_l + \frac{1}{4}W^\alpha W_\alpha \delta(\bar{\theta}) + \frac{1}{4}\overline{W}_{\dot{\alpha}}\overline{W}^{\dot{\alpha}}\delta(\theta) \\ &+ (\frac{1}{2}m_{ij}\Phi_i\Phi_j + \frac{1}{3!}\lambda_{ijk}\Phi_i\Phi_j\Phi_k)\delta(\bar{\theta}) + h.c.] \end{aligned} \tag{1.52}$$

Non-Abelian case of a supersymmetric gauge theory

In the non-abelian case, the Lie algebra of the gauge group generators is

$$[T^a, T^b] = if^{abc}T^c \tag{1.53}$$

where f^{abc} is the structure constants and the generators T^a are normalized as

$$Tr(T^aT^b) = k\delta^{ab}, k > 0 \tag{1.54}$$

The chiral superfields transformations are generalized to

$$\Phi_i \to e^{-i\Lambda_{ij}}\Phi_j, \qquad \overline{\Phi}_i \to e^{i\overline{\Lambda}_{ij}}\overline{\Phi}_j \tag{1.55}$$

where $\Lambda_{ij} = T^a_{ij}\Lambda_a$.

In order to insure the gauge invariance of the chiral kinetic term, the vector superfield has to be transformed as

$$e^{2gV} \to e^{-i\bar{\Lambda}}e^{2gV}e^{i\Lambda} \tag{1.56}$$

where $V = T^aV^a$. And the field-strenght superfields are written as

$$W_\alpha = -\frac{1}{4}\overline{D}^2 e^{-2gV}D_\alpha e^{2gV} \tag{1.57}$$

$$\overline{W}_{\dot{\alpha}} = -\frac{1}{4}D^2 e^{-2gV}\overline{D}_{\dot{\alpha}} e^{2gV} \tag{1.58}$$

and should be transformed as

$$W_\alpha \to e^{-i\Lambda}W_\alpha e^{i\Lambda}, \qquad \overline{W}_{\dot{\alpha}} \to e^{i\bar{\Lambda}}\overline{W}_{\dot{\alpha}}e^{-i\bar{\Lambda}} \tag{1.59}$$

The most general renormalizable action is therefore

$$S_{SYM} = S_{gauge} + S_{mat} \tag{1.60}$$

where

$$S_{gauge} = \int d^8z \frac{Tr}{16kg^2}(W^\alpha W_\alpha \delta(\bar{\theta}) + \overline{W}_{\dot{\alpha}}\overline{W}^{\dot{\alpha}}\delta(\theta)) \tag{1.61}$$

and

$$S_{mat} = \int d^8z \left[\overline{\Phi}_l e^{i2Q_l V}\Phi_l + (\frac{1}{2}m_{ij}\Phi_i\Phi_j + \frac{1}{3!}\lambda_{ijk}\Phi_i\Phi_j\Phi_k)\delta(\bar{\theta})\right] \tag{1.62}$$

The quantification of this action introduce a gauge fixing term $\int d^8z\ \mathcal{L}_{GF}$ and a Faddeev-Popov ghost term $\int d^8z\ \mathcal{L}_{FP}$, which we do not detail here. We can find them and the Feynmann rules in [31].

1.2.5 Minimal Supersymmetric Standard Model (MSSM)

The MSSM is the minimal SUSY extension of the SM. It contains scalar degrees of freedom associated with the left-handed and right-handed SM fermions, i.e. the left-handed and right-handed *sfermions*. It must also includes the fermionic partners of the SM gauge bosons (*gauginos*) and Higgs boson (*Higgsinos*).

We use one Higgs doublet in the SM to generate masses for fermions through Yukawa interactions. The first term in Eq.(1.17) gives the mass for up-types quarks using the conjugate Higgs doublet. In SUSY, the Higgs-fermion Yukawa interactions originate from superpotential only which can not involve any conjugate superfield ($W(\Phi_i)$ is an analytic function of chiral superfields). Therefore we introduce a second Higgs doublet H_2 with the opposite hypercharge which gives masses to the up-type quarks [27]. It also ensures the cancellation of anomalies. The MSSM includes the following sets of chiral superfields presented in table 1.2.

Names		spin 0	spin 1/2	$SU(3)_C, SU(2)_L, U(1)_Y$
quarks, squarks (×3 families)	Q	$(\tilde{u}_L\ \tilde{d}_L)$	$(u_L\ d_L)$	$(3, 2, \frac{1}{6})$
	$\bar{u}$	$\tilde{u}^*_R$	$u^\dagger_R$	$(3, 1, -\frac{2}{3})$
	$\bar{d}$	$\tilde{d}^*_R$	$d^\dagger_R$	$(\bar{3}, 1, \frac{1}{3})$
leptons, sleptons (×3 families)	L	$(\tilde{\nu}\ \tilde{e}_L)$	$(\nu\ e_L)$	$(1, 2, -\frac{1}{2})$
	$\bar{e}$	$\tilde{e}^*_R$	$e^\dagger_R$	$(1, 1, 1)$
Higgs, higgsinos	H_u	$(H^+_u\ H^0_u)$	$(\tilde{H}^+_u \tilde{H}^0_u)$	$(1, 2, \frac{1}{2})$
	H_d	$(H^0_d\ H^-_d)$	$(\tilde{H}^0_d \tilde{H}^-_d)$	$(1, 2, -\frac{1}{2})$

Table 1.2: Chiral supermultiplets in the MSSM. The spin-0 fields are complex scalars, and the spin-1/2 fields are left-handed two-component Weyl fermions [26].

The Higgs scalar fields in the MSSM consist of two complex SU(2) doublet, or eight real scalar degrees of freedom. When the electroweak symmetry is broken, three of them will be the Nambu-Goldstone bosons G^0, $G^\pm$ and they represent the longitudinal modes for Z^0 and $W^\pm$. Five Higgs scalar eigenstates remain which consist of two CP-even neutral scalars h and H ($m_h < m_H$), one CP-odd neutral scalar A^0 and two charged Higgs $H^\pm$.

After electroweak symmetry breaking, the neutral Higgsinos ($\tilde{H}^0_u$ and $\tilde{H}^0_d$) and the neutral gauginos ($\tilde{B}$ and $\tilde{W}^0$) mix to form four neutral mass eigenstates called *Neutralinos* $\tilde{N}_i$ ($i = 1, 2, 3, 4$). The charged Higgsinos ($\tilde{H}^+_u$ and $\tilde{H}^-_d$) and Winos ($\tilde{W}^+$ and $\tilde{W}^-$) combine to form two charged mass eigenstates called *Charginos* $\tilde{C}^\pm_j$ ($j = 1, 2$).

The gauge bosons are put in vector superfields with their superpartners (the *gauginos*). the gauge supermultiplets are presented in table 1.3.

Names	spin 1/2	spin 1	$SU(3)_C, SU(2)_L, U(1)_Y$
gluino, gluon	$\tilde{g}$	g	$(8,1,0)$
winos, W bosons	$\tilde{W}^{\pm}\ \tilde{W}^0$	$W^{\pm}\ W^0$	$(1,3,0)$
bino, B boson	$\tilde{B}^0$	B^0	$(1,1,0)$

Table 1.3: Gauge supermultiplets in the MSSM [26].

After presenting the particles content of the MSSM, we need to include to the MSSM Lagrangian the *superpotential* which is the sum of the products of chiral superfields.

$$W_{MSSM} = y^U_{ij} Q_i u^c_j H_2 + y^D_{ij} Q_i d^c_j H_1 + y^L_{ij} L_i e^c_j H_1 + \mu H_1 H_2 \ , \tag{1.63}$$

where i and j are family indices. The Yukawa couplings are dimensionless 3×3 matrices that determine the masses of quarks and charged leptons as well as the phase of the CKM matrix. The $\mu H_1 H_2$ term is responsible of the masses of Higgsinos.

One can add the following term to the superpotential which violate either lepton and baryon number

$$W_{\not{B}\not{L}} = \lambda^1_{ijk} L_i L_j e_k + \lambda^2_{ijk} L_i Q_j d_k + \lambda^3_{ijk} u^c_i d^c_j d^c_k + \mu^1_i L_i H_2 \ , \tag{1.64}$$

This term lead to a rapid proton decay and it is absent in the SM. The most general renormalizable gauge invariant superpotential of the simplest SUSY extension is $W_{MSSM} + W_{\not{B}\not{L}}$.

The baryon and lepton number violating processes could be suppressed by postulating invariance under R-Parity transformations which forbids all terms in $W_{\not{B}\not{L}}$

$$R = (-1)^{3(B-L)+2S} \tag{1.65}$$

where S is the spin of the particle and $R = +1$ (-1) for all observed particles (superpartners). The existence of R-parity would have important phenomenological implications:

- The lightest superpartner (LSP) is stable and can play the role of non-baryonic dark matter. In most SUSY scenarios, the neutralino is the (LSP) which is a mixture of Higgsinos, Binos and Winos. It is a heavy weakly interacting particle which can provide the correct dark matter relic abundance if its mass is around EW scale.
- In colliders, superparticles are produced in pairs which then decay to (LSP) and give a signal of missing energy.

1.2.6 SUSY Breaking

SUSY predicts mass degenerate superpartners of the SM fields but they have not been observed in colliders. Therefore SUSY must be broken at some scale M_{SUSY} and all sparticles have to be heavy. Simultaneously, the correlation between different couplings does not change

in order to preserve the cancellation of quadratic divergences of scalar mass corrections. The terms that fulfill these conditions are called *soft* SUSY breaking terms.

SUSY can be broken spontaneously as any other gauge theory. We introduce a simple example in the following.

A field ϕ_i in a gauge theory transforms under finite and infinitesimal group elements as [25]

$$\phi_i \to (e^{i\alpha^a T^a})_i^j \phi_j \ , \qquad \delta\phi_i = i\alpha^a (T^a)_i^j \phi_j \ . \tag{1.66}$$

We know that a gauge symmetry is broken if the vacuum state $(\phi_{vac})_i$ transforms in a non-trivial way

$$(\alpha^a T^a)_i^j (\phi_{vac})_j \neq 0 \ . \tag{1.67}$$

In $U(1)$ symmetry, we have $\phi = \rho e^{i\theta}$, then infinitesimally

$$\delta\phi = i\alpha\phi \quad \Rightarrow \quad \delta\rho = 0, \quad \delta\theta = \alpha \tag{1.68}$$

where the last term corresponds to a *Goldstone Boson*.

Similary, SUSY is broken if the vacuum state $|vac\rangle$ satisfies $Q_\alpha|vac\rangle \neq 0$. From SUSY algebra in Eq.(1.27), one can show that

$$(\bar{\sigma}^0)^{\dot{\beta}\alpha}\{Q_\alpha, \bar{Q}_{\dot{\beta}}\} = \sum_{\alpha=1}^{2}(Q_\alpha Q_\alpha^\dagger + Q_\alpha^\dagger Q_\alpha) = 4P^0 = 4E \tag{1.69}$$

Since $\langle vac|Q_\alpha Q_\alpha^\dagger + Q_\alpha^\dagger Q_\alpha|vac\rangle > 0$, then in broken SUSY, the energy is strictly positive $E > 0$.

As an example, let us take the case of the F-term breaking: we should have at least one of the three transformations different from zero in Eq.(1.41) to break SUSY. To preserve Lorentz invariance, we need to have

$$\langle\psi\rangle = \langle\partial_\mu\phi\rangle = 0 \tag{1.70}$$

So our SUSY breaking condition simplifies to

$$\langle F\rangle \neq 0 \quad \Rightarrow \quad \delta\psi \neq 0 \tag{1.71}$$

In this case, we call ψ a *Goldstone fermion* or *Goldstino*[10]. Since the F-term in the scalar potential is $V_F = \sum_i F_i^\dagger F$, this will affect the shape of V.

However, This picture of spontaneous breaking of SUSY cannot be implemented in the MSSM because we will have problems with the F and D-terms when they develop a (vev) [32].

Soft SUSY breaking in the MSSM

We have two sectors in the SM: the observable sector (quarks) and the symmetry breaking mechanism (Higgs). These sectors are related through Yukawa couplings. In SUSY, we have an additional sector since it is broken in a hidden sector. The observable and SUSY breaking sectors are related via a *messenger sector* which involves three types of mediation [25].

10. It is not the supersymmetric partner of some Goldstone boson.

– **Gravity mediation**
In this scenario, the mediating field couples to the SM with gravitational strength and the coupling is suppressed by the inverse planck mass which is the natural scale of gravity. One can include a mass square to have a right dimension for mass splitting in the observable sector.

$$\delta m = \frac{M_{SUSY}^2}{M_{Pl}} \tag{1.72}$$

We want $\Delta m \sim 1$ TeV and we know that $M_{Pl} \sim 10^{18}$ GeV, so $M_{SUSY} \sim 10^{11}$ GeV. The gravitino gets a mass $m_{3/2}$ of the order of Δm (around TeV).

– **Gauge mediation**

$$G = G_{SM} \times G_{SUSY} = (SU(3) \times SU(2) \times U(1)) \times G_{SUSY}$$

Matter fields are charged under G which gives a M_{SUSY} of order of Δm in the TeV range. In that case, the gravitino $m_{3/2}$ is given by $\frac{M_{SUSY}^2}{M_{Pl}} \sim 10^{-3}$ eV.

– **Anomaly mediation**
Auxiliary field of supergravity get a vacuum expectation value and the conformal anomaly play an important role in this case. We will see this scenario with more details in section 4.1.

In all scenarios, the Lagrangian for the observable sector has contributions $\mathcal{L} = \mathcal{L}_{SUSY} + \mathcal{L}_{SUSY}$ where $\mathcal{L}_{SUSY}$ is the summation of Eq.(1.61) and Eq.(1.62) and

$$\mathcal{L}_{SUSY} = m_0^2 \phi^* \phi + (M_\lambda \lambda\lambda + c.c.) + (a\phi^3 + c.c.) \tag{1.73}$$

where the first, second and third term correspond respectively to the scalar masses, gaugino masses and the trilinear couplings. M_λ, m_0^2 and a are called *soft breaking terms*.

The soft SUSY breaking terms in the MSSM are

$$\begin{aligned} -\mathcal{L}_{soft}^{MSSM} &= \frac{1}{2}\left(M_3 \tilde{g}\tilde{g} + M_2 \tilde{W}\tilde{W} + M_1 \tilde{B}\tilde{B} + c.c.\right) \\ &+ \left(\tilde{\bar{u}} a_u \tilde{Q} H_u - \tilde{\bar{d}} a_d \tilde{Q} H_d - \tilde{\bar{e}} a_e \tilde{L} H_d + c.c.\right) \\ &+ \tilde{Q}^\dagger m_Q^2 \tilde{Q} + \tilde{L}^\dagger m_L^2 \tilde{L} + \tilde{\bar{u}} m_{\bar{u}}^2 \tilde{\bar{u}}^\dagger + \tilde{\bar{d}} m_{\bar{d}}^2 \tilde{\bar{d}}^\dagger + \tilde{\bar{e}} m_{\bar{e}}^2 \tilde{\bar{e}}^\dagger \\ &+ m_{H_u}^2 H_u^* H_u + m_{H_d}^2 H_d^* H_d + (b H_u H_d + c.c.) \end{aligned} \tag{1.74}$$

To avoid fine-tuning, the SUSY breaking mass parameters are expected to be in the TeV range. We note that most of the parameters of the MSSM (>100) come from this part of the Lagrangian.

1.3 Cosmology and Dark Matter

1.3.1 Standard Model of cosmology

How the universe behaves and has behaved is of course linked to what it is made of. Therefore, from the observation of the universe on its large scales, it is possible to find constraints on particle physics. This is one of the aims of cosmology, studying the largest scales we can observe.

In the same way that there is a Standard Model of Particle Physics, there is a Standard Model of Cosmology. Since Hubble's observation of a global isotropic expansion of our universe, and through the assumption that this isotropy is homogeneous, meaning that our viewpoint should not be peculiar in any way, the image we have of the universe has evolved into the one of a space expanding ever since a hot big-bang occured.

When using these constraints of homogeneity and isotropy, the most general metric that can be written is the Friedmann-Lemaître-Robertson-Walker metric [33]:

$$ds^2 = dt^2 - a(t)^2 \left[\frac{dr^2}{1 - kr^2} + r^2(d\theta^2 + \sin^2\theta d\phi^2) \right] \tag{1.75}$$

where t is time, r the co-moving distance, $a(t)$ the scale factor that we will study further in this section, and k the spatial curvature. The value of the curvature k depends on the geometry of the universe and can be taken as 1, 0 or -1 wihout loss of generality thanks to the rescaling factor a. If $k = 0$, the universe is flat and the co-moving coordinates are Euclidean. If $k = -1$, the geometry of the universe is hyperbolic and the universe is open and infinite. Finally, the case $k = 1$ corresponds to the geometry of a sphere, and the universe has a finite volume.

What interests us then is how the universe decribed this way behaves. In order to study this behaviour, we should first find the meaning of the scale factor $a(t)$. We can see from the metric that $a(t)$ is defined as the scale factor between the physical distance between two points in space dl and their co-moving coordinate difference dr, $dl = a(t)dr$. Therefore when considering the rate dv at which this physical distance evolves, we obtain $dv = H\ dl$, with:

$$H(t) = \frac{\dot{a}(t)}{a(t)} \tag{1.76}$$

and H is the Hubble constant. Hubble's discovery in 1929 that all galaxies are moving away from us at a speed proportional to their distance from us leads to believe that this movement due to the expansion of the universe with a homogeneous Hubble constant H rather than a movement in co-moving coordinates of the galaxies. It is therefore interesting to study the evolution of the Hubble constant and of the scale factor, which is determined by the Einstein equations:

$$R_{\mu\nu} - \frac{1}{2} g_{\mu\nu} R = 8\pi G T_{\mu\nu}$$

where $R_{\mu\nu}$ and R are the Ricci tensor and scalar.

The solution to these equations depends on the energy density in the universe, which can be divided in three parts: the non-relativistic matter ρ_M (baryons, Dark Matter, heavy leptons), relativistic matter ρ_{rad} (photons, light neutrinos with mass less than 10^{-4} eV) and Dark Energy ρ_Λ. If considered to be perfect gases, the various ρ obey the equation of state $p = w\ \rho$, with $w = 1/3$ for relativistic gases, $w = 0$ for non-relativistic matter, and $w = -1$ for Dark Energy. This leads to a solution of the Einstein equation of the form:

$$H^2 = \frac{8\pi G}{3}\rho_R + \frac{8\pi G}{3}\rho_M + \frac{8\pi G}{3}\rho_\Lambda - \frac{k}{a^2} \quad \text{with} \quad \rho \propto a^{-3(w+1)} \tag{1.77}$$

where G is Newton's gravitation constant. We can see that a critical density appears in this expression $\rho_c = \frac{3H^2}{8\pi G}$, defining the ratios $\Omega_i = \frac{\rho_i}{\rho_c}$. The solution for H then transforms for a flat universe into:

$$1 = \Omega_{tot} = \Omega_R + \Omega_M + \Omega_\Lambda \quad \text{with} \quad k = 0 \tag{1.78}$$

In the end, the set of five parameters Ω_M, Ω_{rad}, Ω_Λ, H_0, k is sufficient to describe the shape and evolution of the FLRW universe [33]. This is the reason why for the last 30 years one of the goals of observational cosmology has been to measure them more and more precisely.

1.3.2 A brief history of the universe

Another point of interest in the history of the universe is the first stages of its evolution, when its content changed radically to become the most part of what it is now. This is what a few scientists tried to think about for the few years after the discovery of the FLRW metric. The first model developed, called "Cold Big Bang" was proposed, with the assumption of an expansion due to the dominant presence of the pressureless matter that makes up galaxies. It was then abandonned in favor of the Hot Big Bang scenario, which turned out to be more consistent with nucleosynthesis studies. In the Hot Big Bang scenario, the early universe was dominated by radiation, modifying the way nucleosynthesis occured with respect to the cold one. Since then, many efforts have been put into the study of this scenario, as well in experimental observations as in theoretical predictions.

The very first moments of the universe are not yet fully understood and not well described, such as inflation. According to the most common theories, gravitation became classical when the temperature of the universe went under the so-called Planck scale, about $10^{-43}s$ giving $\rho \sim (M_{Pl} = 10^{18}GeV)^4$ after the time $t = 0$ such that $a(0) = 0$. Then follows a brief period of brutal expansion called inflation possibly linked to the breaking of the symmetry of a Grand Unified Theory around $t \sim 10^{-32}s$. After that, a step called reheating occured, when the scalar field responsible tfor inflation decayed into the various particles of the Standard Model. When temperature reached the whereabouts of the Higgs boson mass, $T \sim 100$ GeV, for $t \sim 10^{-6}s$, the electroweak symmetry was spontaneously broken, followed shortly at $t \sim 10^{-4}s$, $T \sim 100$ MeV by the QCD phase transition, producing hadrons form unconfined quarks and gluons [33].

The next step, lasting for the few first hundred seconds of the universe, was nucleosynthesis, where the hadrons formed previously combined into the light nuclei such as H, He and Li. The observation of the composition of today's Universe, compared to theoretical predictions from Big Bang Nucleosynthesis models, allows us to estimate the density of baryons in the universe: $\Omega_B h^2 = 0.021 \pm 0.005$, making up only for 4% of the universe energy density. In this part of History, the energy density was dominated by radiation, until around $t \sim 10^4 yr$, when matter became predominant, changing the rate of expansion. At that time, through electromagnetic interaction, the nuclei, electrons and photons were in thermal equilibrium. At $t \sim 10^5 yr$, the electrons and nuclei formed atoms in the step called recombination, forming neutral states and therefore decoupling from photons. From this time on, photons propagated almost freely until now, forming what we see as the Cosmic Microwave Background and from which we can therefore get direct information from that time. The final step of the formation of the universe was the gravitational evolution of small inhomogeneities, leading to the formation of stars and galaxies from dust clouds. This brief description can be shown in fig. 1.6.

The future of the Universe is now mainly determined by its curvature, and the energy density, the struggle between the momentum of expansion and the pull (or push) of gravity. The current rate of expansion is measured by the Hubble Constant, while the strength of gravity depends on the density and pressure of the matter in the universe.

If the density of the universe is less than the critical density, meaning negative curvature, then the universe will expand forever, like the green or blue curves in fig. 1.6. For such a universe, ever expanding, there might be a "Big Rip", where the Universe tears apart, or a "Big Freeze", because the expansion of the Universe causes its cooling. If the density of the universe is greater than the critical density (positive curvature), then expansion will stop at some point, and gravity will have the Universe collapse in the so called Big Crunch, like the orange curve on fig. 1.6.

Recent observations of distant supernova have suggested that the expansion of the universe is actually accelerating, like the graph's red curve, which implies the existence of a form of matter with a strong negative pressure, such as the cosmological constant, which would make the Universe expand forever if dominant.

1.3.3 Evidences of Dark Matter

One of the fundamental questions in particle physics and cosmology is the nature of *dark matter*. Currently, there are several evidence leading us to believe that a big part of the Universe is made of a material having a nature still unknown. For a review about this subject, the reader can refer for example to [35].

As shown in fig. 1.7, WMAP (Wilkinson Microwave Anisotropy Probe) data reveals that the content of our Universe include 4.6% atoms, the building blocks of stars and planets. Dark matter comprises 23% of the universe. This matter, different from atoms, does not emit or absorb light. It has only been detected indirectly by its gravity. 72% of the universe, is composed of "dark energy", that acts as a sort of an anti-gravity. This energy, distinct from dark matter, is responsible for the present-day acceleration of the universal expansion. WMAP data is accurate to two digits, so the total of these numbers is not 100%. This reflects the

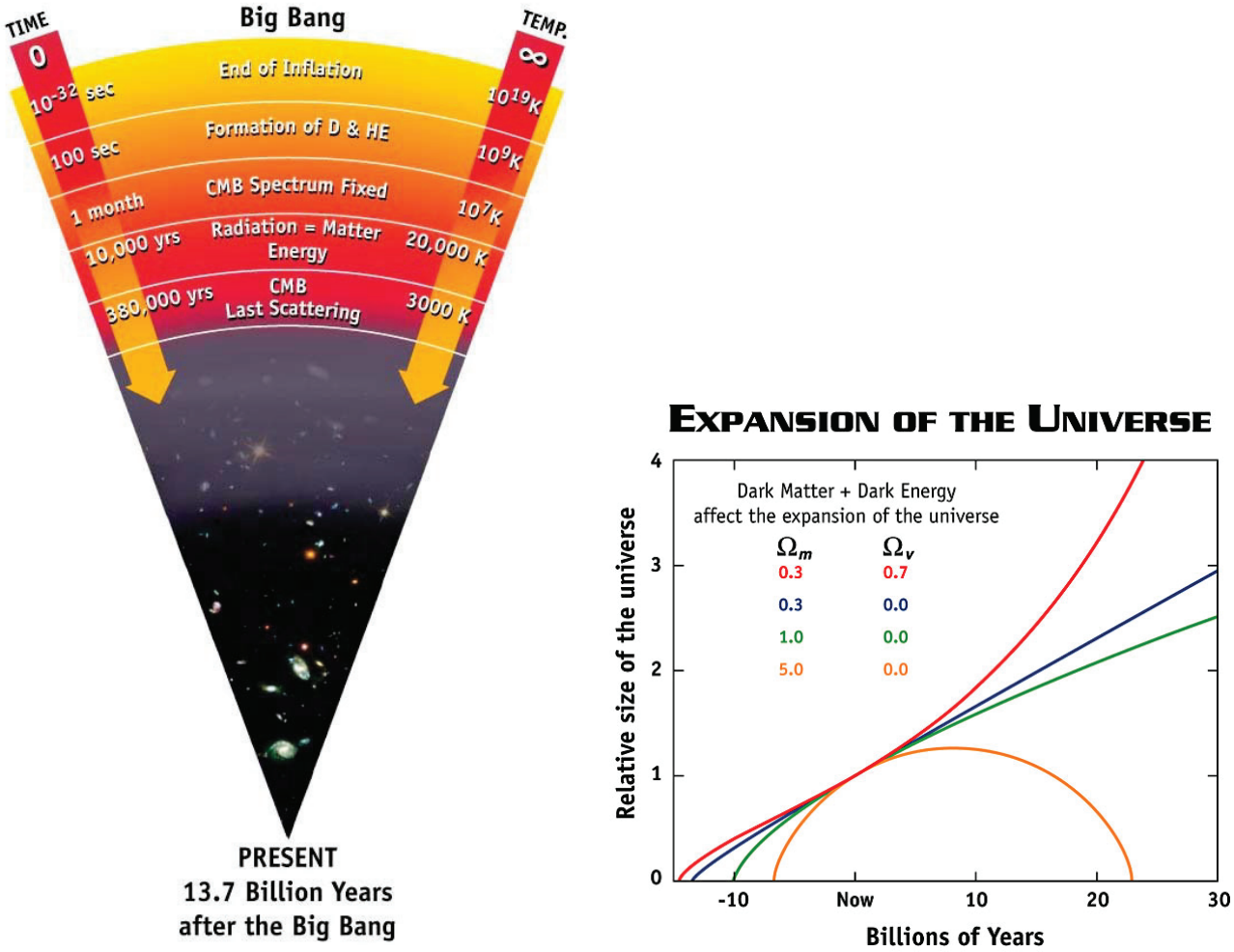

Figure 1.6: **Left Panel :** The past history of the Universe. **Right Panel :** Possible fates of the Universe. Those plots are extracted from WMAP collaboration website [34].

current limits of WMAP's ability to define Dark Matter and Dark Energy.

Some of the observations which suggest the presence of Dark Matter from astrophysical to cosmological scale are presented below:

Galaxy clusters and Gravitational lensing

The first evidence of the existence of dark matter comes from Zwicky in 1933 when he studied the speed distribution of galaxies in the Coma cluster. A cluster of galaxies is a combination of more than one hundred galaxies linked together by gravitational interactions. After estimating the gravitational mass of the cluster, he found that this mass is much greater than the total sum of the masses of the luminous objects in the cluster (visible matter). Therefore, to explain the existence of clusters, it was necessary to assume the presence of a gravitationally

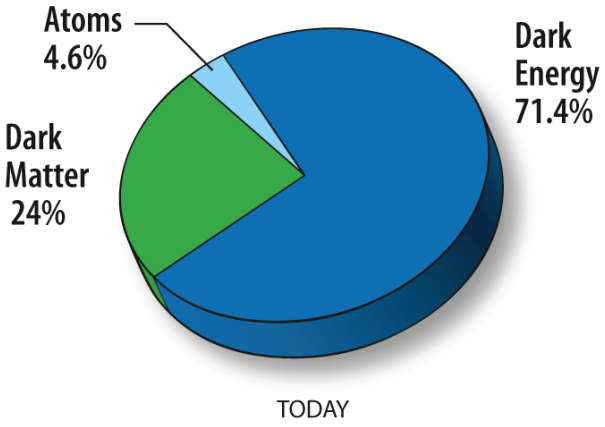

Figure 1.7: Content of the Universe. This plot is extracted from WMAP collaboration website [34].

interacting non-luminous matter.

From Einstein general relativity predictions, we know that the curvature of the space-time produced by the matter leads to a deviation in the path of light. This phenomena is called *Gravitational lensing*. The deviation angle depends from the mass of the object causing this deviation. We can estimate the mass of astrophysical objects (planets, galaxies, clusters, ...) and consider that some of these objects are very brilliant. By observing the deviation in the path of light, one can have an idea about the mass located beyond the cluster. These observations show also the existence of large amount of Dark Matter in the clusters [36].

Another hint of Dark Matter evidence at the galaxy scale is the observation of the *Bullet cluster* [37]. In fig. 1.8, we see the collision of two galaxy clusters: in red and yellow, the famous bullet shape represents the X-rays emissions coming from the heating of interacting baryonic matter. On the other hand, the green contours show the distribution of mass which is quite isotropic and seems not affected by the collisions. This observation is difficult to explain with modified gravity while it can be understood by the presence of a massive and weakly interacting kind of *invisible* matter.

Galaxy rotation curves

The direct evidence of the presence of dark matter at the galactic scale comes from the measurements of the galaxy rotation curves. These measurements have been done in 1970s and were originally performed by V.C. Rubin and other astronomers [38]. Consider a mass $M(R)$ inside a sphere of radius R with an equilibrium between kinetic and gravitational energies. From Newton's mechanics, the circular velocity v of an object on a stable orbital of radius R is given by

$$\frac{v^2}{R} = \frac{GM(R)}{R^2} \quad \Rightarrow \quad v = \sqrt{\frac{GM(R)}{R}} \tag{1.79}$$

where G is the gravitational constant and v the velocity of the stars. Beyond the visible part of the galaxy, $M(R)_{visible}$ is constant and we expect that v decreases as $1/\sqrt{R}$ when we go away from the galaxy centre for large distances. However, the measurements of the velocities of stars and gas clouds in function of their distance from the galactic centre show a flat behaviour at large distances (see fig. 1.8). The discrepancy between the expected "Keplerian" behaviour and the observations can be explained by the existence of a halo of non-visible matter which will play a gravitational role. It will have a mass $M(r) \propto r$ and density $\rho(r) \propto 1/r^2$ for large distances with

$$M(r) = 4\pi \int_0^r r^2 \rho(r) dr. \tag{1.80}$$

Note that there are other ways to explain the rotation curves of galaxies and clusters, the effect of gravitational lensing and CMB anisotropies, which does not require the introduction of dark matter. In these models, the gravity is modified at galactic scale. For example, the theory MOND (MOdified Newtonian Dynamics) [39] proposed that gravity does not follow the predictions of Newtonian dynamics for very small accelerations. In general, this theory can

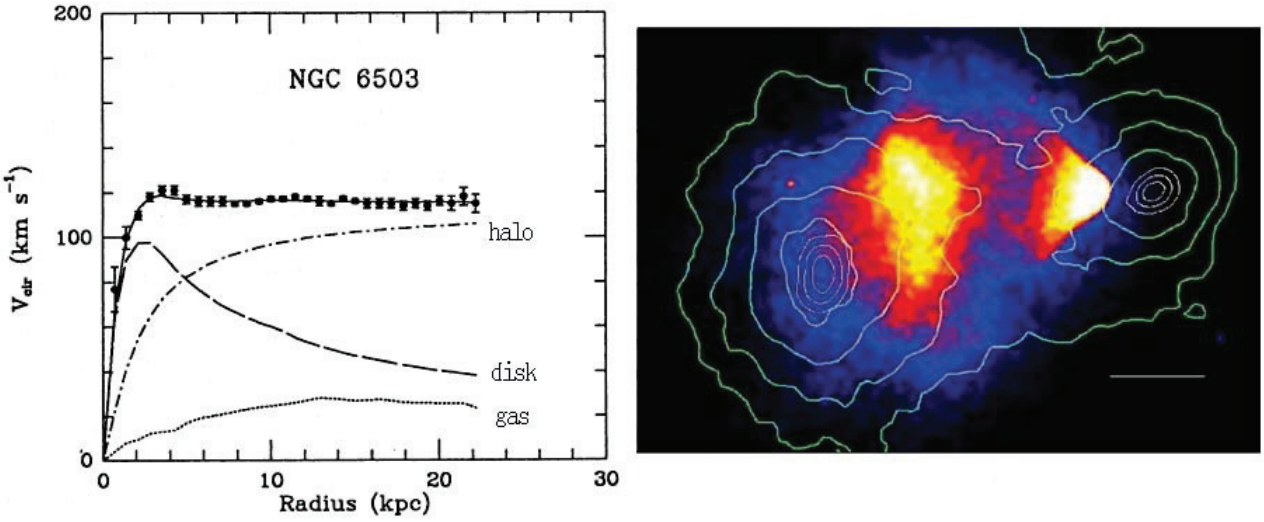

Figure 1.8: **Left Panel :** Rotation curve for the spiral galaxy NGC6530, extracted from [38]. **Right Panel :** Direct evidence for Dark Matter in the *bullet cluster* (1E0657-56). In this plot reproduced from [37]: the visible matter (red and yellow), observed in X-rays by the CHANDRA satellite, only contributes little to the total mass of the two colliding clusters (density contours in green). This total mass has been measured by gravitational lensing with VLT and Hubble satellite.

explain some astrophysical observations, but new data about some galaxy clusters disfavour such theories of gravity modification and they are not satisfactory to describe the current cosmological observations.

Cosmology

The observation of galaxy clusters and spiral galaxy rotation curves give a clear signature of the dark matter existence. However, they do not permit to determine the quantity of this matter in the Universe. This quantity could be extracted from the precision measurements of the Cosmic Microwave Background (CMB).

Firstly discovered by Penzias and Wilson [40], the temperature distribution of those photons has been extremely well measured at 2.725K by experiment of Cosmical Microwave Background (CMB) detection. As we will see, the CMB is a probe of the early universe structure and will contain information of the content of matter and radiation in the earlier universe (fig. 1.9). This radiation comes from the propagation of photons which are decoupled from the matter in the primordial Universe.

The first observations of the CMB started with COBE (Cosmic Background Explorer) in 1989 which is the predecessor to the WMAP Project [41, 42]. COBE was launched by NASA into an Earth Orbit in 1989 to make a full sky map of the Cosmic Microwave Background (CMB) radiation leftover from the Big Bang. After many decades of experimental effort, the CMB is known to be isotropic at the 10^{-5} level and to follow with extraordinary precision the spectrum of a black body corresponding to a temperature $T = 2.725K$. Today, the analysis of CMB anisotropies and fluctuations enables accurate testing of cosmological models and puts stringent constraints on cosmological parameters.

From the analysis of the WMAP data alone, the following values are found for the abundance of baryonic matter density Ω_b and the total one in the Universe Ω_M [43].

$$\Omega_b h^2 = 0.02260 \pm 0.00053 \ , \qquad \Omega_M h^2 = 0.13334^{+0.0056}_{-0.0055} \tag{1.81}$$

where $h = H_0/100$ km.s^{-1}.Mpc^{-1} $= 0.704$. This implies that the dark matter density $\Omega_{DM} h^2 = 0.1123 \pm 0.0035$ makes about 83% of the total mass density.

The CMB data show the small scale fluctuations (fig. 1.9) in the primordial plasma which allow us to infer the cosmological parameters.The angular spectrum of the CMB is fitted by the ΛCDM model assuming a gaussian, adiabatic and nearly scale invariant power spectrum of primordial fluctuations. The structure of this spectrum requires the introduction of a cold dark matter to our description of the Universe [44]. We can try to explain such effects with relic density of neutrinos which are also weakly interacting but WMAP estimates their relic abundance at $\Omega_\nu h^2 \leq 0.0145$ which is not sufficient (this value is measured by WMAP and the combined result is given in table 1.4).

Other studies on cosmological scale are the analyses of the large scale structure of the Universe which give evidence for dark matter. By calculating the distance to galaxies using their redshifts, cosmologists have been able to map out the approximate locations of more than 1.5 million galaxies. For instance, the Sloan Digital Sky Surveys (SDSS) has created a map of the sky with more than 900,000 galaxies, 120,000 quasars and 400,000 stars [45]. Using these

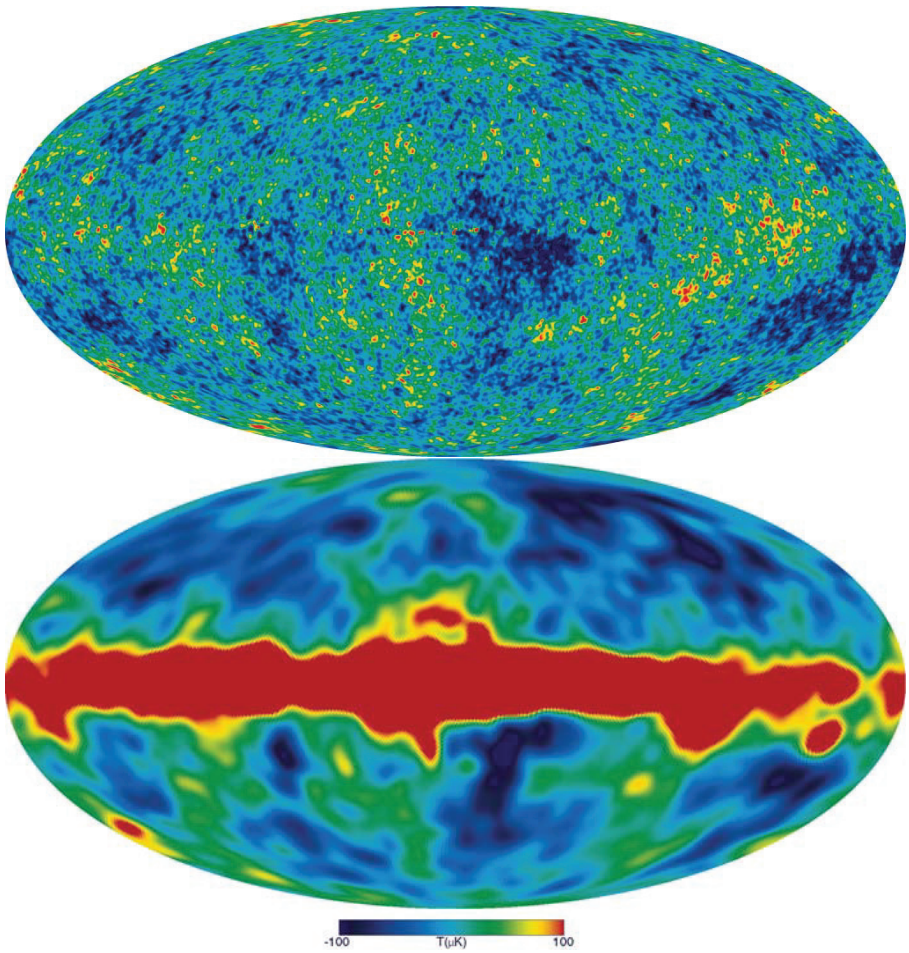

Figure 1.9: **Top :** The detailed, all-sky picture of the infant universe from three years of WMAP data. The image reveals 13.7 billion year old temperature fluctuations (shown as colour differences) that correspond to the seeds that grew to become the galaxies. This image shows a temperature range of ± 200 mK.
Bottom : The all-sky image produced by the COBE Satellite. It is a low resolution image of the sky (7 degree resolution), but obvious cold and hot regions are apparent in the image. The large red band is the microwave emissions from our own galaxy. This image shows a temperature range of ± 100 mK. It was processed through the same data pipe as the first year WMAP data. The largest version of the image has a scale added.
Extracted from the WMAP collaboration website [34].

maps, we can look at the signatures of density perturbations which were in the primordial plasma (Baryonic Acoustic Oscillation) [46]. Then we can generate the small fluctuations at early time from the large scale structures. Therefore, by measuring these structures, we can infer the power spectrum of those initial fluctuations. This leads to an estimate of matter abundance of $\Omega_M = 0.286 \pm 0.018$.

Another studies that can lead to an evidence of dark matter existence are the measurements of luminosity curves of Supernovae Ia as a function of their redshifts [43]. With these data, we can then estimate the deviations from Hubble law and constrain the Hubble parameter and $\Omega_M - \Omega_\Lambda$ as shown in fig. 1.10.

The set of parameters which define the ΛCDM model will be constrained by these experiments, as it is presented in table 1.4. In this table, the total density is $\Omega_{tot} = 1$ which means that we assume that the universe is flat ($k = 0$). Then we remark that the dark energy component is quite important and dominates the dynamics of our present universe. We do not know the physical origin of such term which could be related to gravity and early Universe dynamics. Finally we can stress that the amount of baryonic matter is very small compared to the total matter density.

Ω_γ	Ω_ν	Ω_b	Ω_{dm}	Ω_Λ	$H_0(\mathrm{km/s/Mpc})$
$4.6^{+0.5}_{-0.5} \times 10^{-5}$	< 0.0125	$0.0456^{+0.0016}_{-0.0016}$	$0.227^{+0.014}_{-0.014}$	$0.728^{+0.015}_{-0.016}$	$70.4^{+1.3}_{-1.4}$

Table 1.4: Constraints on ΛCDM model obtained combination of Cosmic Microwave Background, Baryonic Acoustic Oscillations and the SuperNovae Surveys assuming $\Omega_{tot} = 1$ [47] in the Supernova Cosmology Project Collaboration.

1.3.4 Dark matter candidates

As we have seen in the previous section, the evidence for non-baryonic dark matter is compelling at all observed astrophysical scales. It is therefore natural to ask what is the dark matter made of? In this section, we present some of the candidates discussed in the literature [35].

In general, if the dark matter particles have a low mass, we call them *warm* dark matter; and if they have masses about few GeV, they are called *cold* dark matter. Actually, the observations of galaxy and cluster dynamics prefer the cold dark matter. In the SM, the only stable and neutral particle which can be responsible for the relic abundance of dark matter is the *neutrino*. However, its very tiny mass and very high velocity lead to a big problem in the formation of structures. This is not the case if the dark matter is heavy since the ordinary matter will gather to form galaxies and clusters.

Supersymmetric candidates

As we mentioned, a solution to dark matter candidates can be brought by particle physics by considering a Weakly Interacting Massive Particle (WIMP), whose abundance remains unchanged after decoupling from the primordial plasma. Since the SM does not contain any heavy candidate that interacts weakly with the matter, we are required to study models of new physics. As we already seen in SUSY models with conserved R-parity, the LSP is stable and could be a good candidate for dark matter. In the MSSM, the possible candidates are the

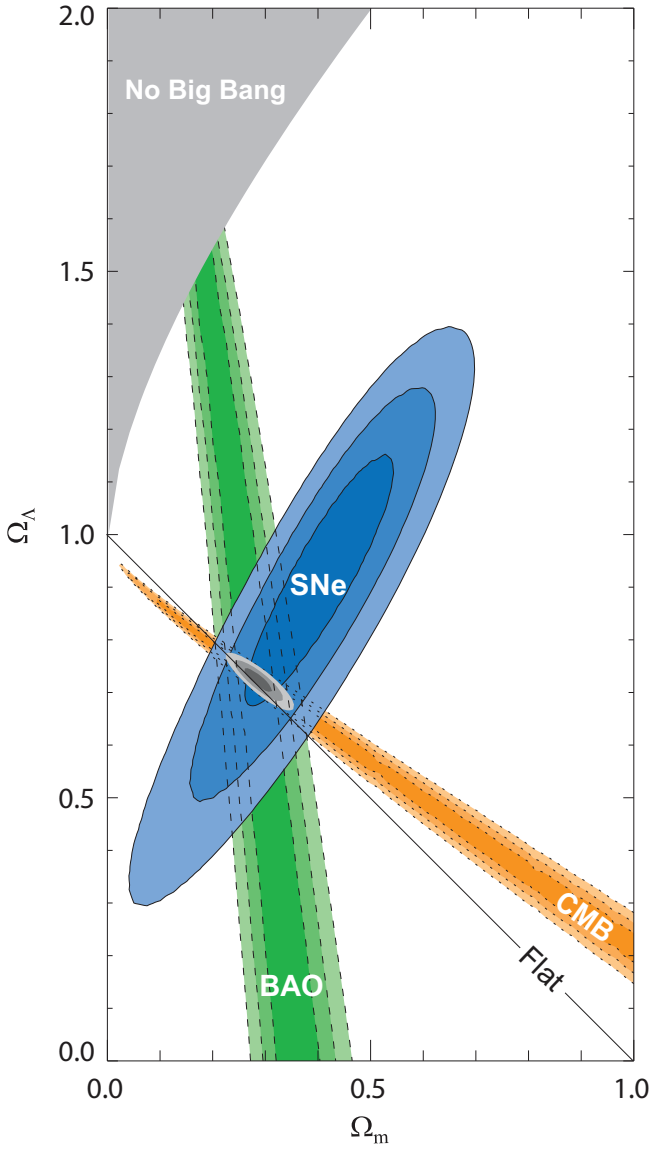

Figure 1.10: 68.3%, 95.4% and 99.7% confidence level contours on Ω_Λ and Ω_M obtained from the Supernova Cosmology Project Collaboration: Cosmic Microwave Background, Baryonic Acoustic Oscillations and the SuperNovae Surveys as well as their combinations (assuming $w = -1$ for the dark energy), extracted from [43].

sneutrino, the *neutralino* and in some cases the *gravitino*. The other supersymmetric particles are excluded because they are charged.

– **Neutralino**
In the MSSM, the lightest neutralino χ_1^0, described in section 1.2.5, is the candidate for the dark matter. The neutralino is formed from the mixing of gauginos and higgsinos; this mixing will determine the characteristics of neutralino and its coupling to others

particles. Its mass vary from a few GeV to a few hundred GeV depending on the model in which we work. We can learn about the properties of χ_1^0 by studying the annihilation of two neutralinos to quarks, leptons, vector bosons, Higgs bosons ...

– **Sneutrino**
A *sneutrino* is the superpartner of a SM neutrino in supersymmetric models. Its mass and couplings are typically at the electroweak scale and it is a good candidate for WIMPs. However, it has an important coupling to the Z boson and that leads to a quick annihilation which generates a very small relic density. It has been shown that sneutrinos will have a cosmologically interesting relic density if their mass is in the range of 550 to 2300 GeV. However, the scattering cross section of a sneutrino with nucleons is easily calculated and is much larger than the limits found by direct dark matter detection experiments [48].

– **Gravitino**
Supersymmetric theories which contain gravity predict the existence of spin 3/2 particle, the *gravitino*, which takes a mass after the spontaneous SUSY breaking. In the gauge mediated supersymmetry for example, gravitinos can be the lightest supersymmetric particle and be stable. Theoretically, they are strongly motivated but it is very difficult to observe and detect them in direct searches since they are only sensitive to gravitational interactions [49]. There is also a problem in theories with conserved R-parity: if the *gravitino* is the LSP, the Next-LSP particle should decay to the LSP and others SM particles via gravitational interaction. So the NLSP will have a very long life-time which lead to cosmological problems related to the abundances of light elements in the primordial nucleosynthesis. In this case, the *gravitino* mass has to be less than 1 GeV [50],which does not correspond to a good candidate for cold dark matter. However, this problem can be solved in some scenarios [51] with R-parity violation with $5 < m_{3/2} < 300$ GeV.

Others candidates

We present here some candidates for the dark matter.

– **Axions**
Axions could be also considered as a dark matter candidate. They are introduced in order to solve the problem of CP violation in particle physics. Laboratory searches, stellar cooling and the dynamics of supernova 1987A constrain axions to be very light ($\leq$ 0.01 eV). Furthermore, they are expected to be extremely weakly interacting with ordinary particles, which implies that they were not in thermal equilibrium in the early Universe. Its relic density calculation is uncertain but it is possible to find an acceptable range where axions satisfy constraints and represent a possible dark matter candidate [52].

– **Axinos**
The superpartners of the axion, were believed until recently to only be capable of acting as a warm, or hot, dark matter candidate [53]. It has been shown, however, that for quite low reheating temperatures, cold axino dark matter may be possible [54].

– **Lightest Kaluza-Klein particle**
Universal Extra Dimension (UED) models offer another candidate for cold dark matter. In these models as described in section 2.1, the SM fields can propagate in the spatial

extra dimensions compactified on a circle of radius R. For every SM particle ϕ^0 correspond a tower of Kaluza-Klein states ϕ^n with masses proportional to n/R. A remnant of momentum conservation along the fifth coordinate implies the KK number conservation at tree level and the KK parity conservation at loop level. This KK parity ensures the stability of the lightest KK particle in the same way that R-parity makes the LSP stable. The Lightest Kaluza-Klein Particle (LKP) provide a good candidate for the cold dark matter [55].

1.3.5 Cold WIMP relic density calculation

We have presented, in the previous section, the current model used to describe our universe and we have emphasized the fact that a Dark Matter component has to be added to our description. In the early Universe, very energetic and massive particles were created and existed in thermal equilibrium. As the Universe expanded and cooled, lighter particles do not have sufficient energy to produce heavier ones through interactions and the expansion dilutes the density of particles such that interactions did not occur as frequently.

The probability of interaction between individual particles depends on a cross-section σ and on their relative velocity v. In thermal equilibrium, the interaction between two species i and $j$is characterized by a thermally averaged cross-section $\langle\sigma v\rangle$. The interaction rate (or scattering rate) of i is given by $\Gamma_i = n_j\langle\sigma v\rangle$. The scattering is efficient enough for maintaining i in thermal equilibrium with j provided that the scattering rate Γ_i is larger than the inverse of the characteristic time set by the universe expansion $\Gamma_i > H$. When $\Gamma_i < H$, the cross-section is so low or the species j is so diluted that the chance for i to scatter over j within a time comparable to the age of the universe becomes negligible. When all possible scattering reactions which could maintain i in thermal equilibrium have $\Gamma_i < H$, the species i decouples from thermal equilibrium. In this case, assuming that the particles are stable and non-interacting, they can only free-stream with a frozen distribution.

The exact moment or temperature of freeze-out can be calculated by equating the reaction rate to the Hubble expansion rate. We present in the following how SM extensions can solve this problem and how Dark Matter can contribute to the total matter budget of the universe.

Solving the Boltzmann equation

We present here the standard calculation of the relic abundance of a particle species χ which can explain the observed matter density. We will explain how this massive stable particle went out of the thermal equilibrium and decoupled, because of the universe expansion. We suppose that the particle is stable or long-lived, so that in the Boltzmann equation only the annihilation term is relevant. The relic abundance of χ can be found by solving the Boltzmann equation [55–57]:

$$\frac{dn}{dt} = -3Hn - \langle\sigma v\rangle(n^2 - n_{eq}^2) \tag{1.82}$$

where n is the density of the relic particle and n_{eq} is the density at the thermal equilibrium. v is the relative velocity of the two χ and $\langle\sigma v\rangle = \langle\sigma(\chi\chi \to SM)v\rangle$ is the thermally averaged total annihilation cross-section. The first term corresponds to a dilution term of the relic χ, the second one is the annihilation term and the third one is the production term from SM particles in the thermal bath. As we are interested in cold Dark Matter, we have to look at two different regimes: at high temperature ($T \gg m$), χ is still relativistic and its equilibrium density is given by

$$n_{eq} \sim T^3 \tag{1.83}$$

At low temperature ($T \ll m$), n_{eq} is given by the non-relativistic limit:

$$n_{eq} = g\left(\frac{mT}{2\pi}\right)^{3/2} e^{-m/T} \tag{1.84}$$

Here m is the mass of the relic particle χ, T is the temperature and g is the number of internal degrees of freedom such as spin, colour, and so on. As it can be seen from the numerical solution in fig. 1.11, at early time, χ annihilated (was created) with its own anti-particle into (from) Standard Model states. Then, because of the expansion, the temperature will drop ($a(t) \sim 1/T$) and the annihilation rate $\Gamma = n\langle\sigma v\rangle$ will be smaller than the Hubble parameter. In this case, the particles cannot annihilate anymore due to lack of reagents and their density will remain fixed. This decoupling of the stable particles from the thermal bath of the primordial plasma is called *freeze-out* and will occur at temperature denoted T_F which corresponds roughly to the time where $\Gamma \sim H$.

$\langle\sigma v\rangle$ is often approximated by its non-relativistic expansion:

$$\langle\sigma v\rangle = a + b\langle v^2\rangle + O(\langle v^4\rangle) \approx a + \frac{6b}{x} + O(1/x^2) \quad \text{where} \quad x = \frac{m}{T} \tag{1.85}$$

Then by solving the Boltzmann equation analytically, we obtain the relic density Ω_χ:

$$\Omega_\chi h^2 \approx \frac{1.04 \times 10^9}{M_P} \frac{x_F}{\sqrt{g_*(x_F)}} \frac{1}{a + 3b/x_F} \tag{1.86}$$

where $M_P = 1.22 \times 10^{19}$ GeV is the Planck mass and g_* is the total number of effectively massless degrees of freedom and is given to a first approximation by:

$$g_*(x) = \sum_{i=bosons} g_i + \frac{7}{8} \sum_{j=fermions} g_i \tag{1.87}$$

In g_*, the coefficient 7/8 comes from the Fermi-Dirac statistics and the dependence on temperature is due to the fact that the thermal bath will quickly lose a lot of massive species as the temperature will drop below their masses. The freeze-out "temperature", x_F, is found from the equation:

$$x_F = \ln\left(c(c+2)\sqrt{\frac{45}{8}}\frac{g}{2\pi^3}\frac{mM_P(a+6b/x_F)}{\sqrt{g_*(x_F)x_F}}\right) \tag{1.88}$$

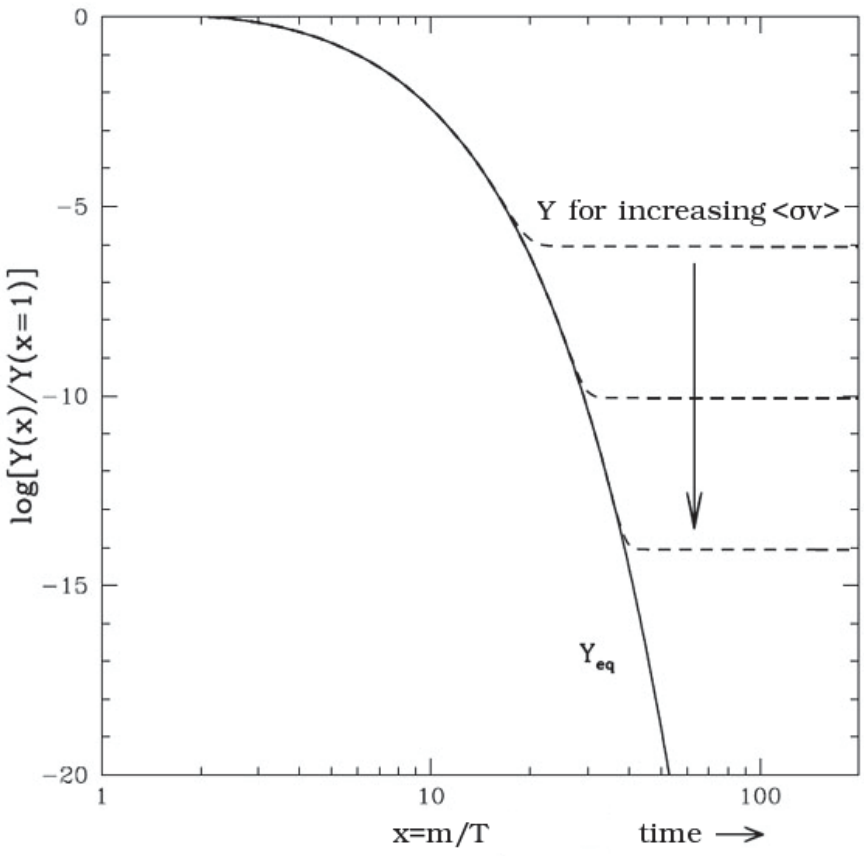

Figure 1.11: Numerical simulation for the evolution of the comoving relic density taken from Ref. [58]. This comoving density $Y \propto nT^{-3}$ includes the dilution effect coming from the expansion of the universe. The solid line represents the equilibrium density and the dashed one the current density .

where the value of the constant c can be found after numerical computation. Usually we use $c = 1/2$ because of the weak dependence of x_F on its value. Finally, sub-leading effects can be taken into account [56] like, for instance, relativistic corrections by the simple replacement $b \to b - \frac{1}{4}a$.

1.4 Alternative cosmological scenarios

In the following, we consider that dark matter is composed of exclusively one particle produced thermally.
The density number of supersymmetric particles is determined by the Boltzmann equation Eq.(1.82). The expansion rate H is determined by the Friedmann equation

$$H^2 = \frac{8\pi G}{3}\rho_{rad} \ , \tag{1.89}$$

and the entropy evolution reads

$$\frac{ds}{dt} = -3Hs \,, \tag{1.90}$$

where s is the total entropy density. Solving and evolving simultaneously Eqs.(1.82, 1.89) and Eq.(1.90) enable to compute the relic density in our present Universe. In the standard cosmology, the dominant component before Big-Bang Nucleosynthesis is considered to be radiation, which is constituted of all relativistic particles. This assumption is however relaxed in many cosmological scenarios. The last two equations can indeed be written more generally as [59]

$$H^2 = \frac{8\pi G}{3}(\rho_{rad} + \rho_D) \,, \tag{1.91}$$

$$\frac{ds}{dt} = -3Hs + \Sigma_D \,, \tag{1.92}$$

ρ_D parametrises a modified evolution of the total density of the Universe, beyond radiation density ρ_{rad}. Σ_D parametrises here effective entropy fluctuations due to unknown properties of the Early Universe. The radiation energy and entropy density evolutions are known and can be written as usual:

$$\rho_{rad} = g_{\rm eff}(T)\frac{\pi^2}{30}T^4 \,, \qquad s_{rad} = h_{\rm eff}(T)\frac{2\pi^2}{45}T^3 \,. \tag{1.93}$$

In the following, we consider two scenarios in which the energy density is modified, and two scenarios with a modified entropy content.

1.4.1 Quintessence

The quintessence model is one of the most well-known models for dark energy. It is based on a cosmological scalar field which has presently a negative constant pressure P and a positive constant energy density ρ such as $P \approx -\rho$ [60]. This behaviour is achieved when the kinetic term of the scalar field equilibrates the potential. However, in the early Universe, the scalar field has a dominating kinetic term, leading to a positive pressure such as $P \approx \rho$. During this period, the energy density was varying very quickly, such as $\rho \propto T^6$. We study here a quintessence scenario in which the quintessence field before Big-Bang Nucleosynthesis was dominating the expansion of the Universe. In this case [61]:

$$\rho_D(T) = \kappa_\rho \rho_{rad}(T_{BBN}) \left(\frac{T}{T_{BBN}}\right)^6 \,, \tag{1.94}$$

where κ_ρ is the proportion of quintessence to radiation at the BBN temperature ($\sim$1 MeV). We consider that κ_ρ is a free parameter, which can be constrained using the BBN abundance constraints. To compute the abundance of the elements produced during the primordial nucleosynthesis, we use the code AlterBBN [62] integrated into SuperIso Relic. Comparing the abundances to the observational constraints, we obtain limits on κ_ρ.

1.4.2 Late decaying inflaton

The second scenario we consider here is a late decay of an inflaton field. The inflaton field is a scalar field which is considered to be responsible for the rapid inflation of the early Universe. Generally, the inflaton is considered to decay into standard particles much before the relic decoupling from the primordial soup. However, several models evoke the possibility of a late decay of the inflaton, around the time of BBN. From [63,64], there exist cosmological models in which the late decay of a scalar field reheats the Universe to a low reheating temperature , which can be smaller than the freeze-out temperature, without spoiling primordial nucleosynthesis. The decay of this scalar field into radiation increases the entropy and modifies the expansion rate of the Universe. We consider here such a scenario in which we neglect the eventual entropy production, and we takes [61]

$$\rho_D(T) = \kappa_\rho \rho_{rad}(T_{BBN}) \left(\frac{T}{T_{BBN}}\right)^8 . \tag{1.95}$$

The exponent is here increased from 6 to 8 in comparison to the quintessence field, as mentioned also in [63, 64]. Such a modification of the expansion rate can be also achieved in a Universe with extra-dimensions modifying the Friedmann equations [65].

1.4.3 Primordial entropy production

In this third scenario, we assume that a primordial entropy production due to an unknown component occurs. In general, such an entropy production should be accompanied with energy production, but to better estimate the deviation of the relic density in such a cosmological scenario, we neglect here the energy production, and we consider that the Universe has, in addition to the standard radiation entropy density, a dark entropy density evolving like [59]

$$s_D(T) = \kappa_s s_{rad}(T_{BBN}) \left(\frac{T}{T_{BBN}}\right)^3 , \tag{1.96}$$

where κ_s is the ratio of effective dark entropy density over radiation entropy density at the time of BBN. The corresponding entropy production is related to s_D by the relation

$$\Sigma_D = \sqrt{\frac{4\pi^3 G}{5}} \sqrt{1+\tilde{\rho}_D} T^2 \left[\sqrt{g_{eff}} s_D - \frac{1}{3} \frac{h_{eff}}{g_*^{1/2}} T \frac{ds_D}{dT}\right] , \tag{1.97}$$

with

$$g_*^{1/2} = \frac{h_{eff}}{\sqrt{g_{eff}}} \left(1 + \frac{T}{3h_{eff}} \frac{dh_{eff}}{dT}\right) , \tag{1.98}$$

and

$$\tilde{\rho}_D = \frac{\rho_D}{\rho_{rad}} . \tag{1.99}$$

1.4.4 Late reheating

In this last scenario, the reheating temperature T_{RH} is smaller than the neutralino freeze out temperature ($T_{f.o.} \simeq m_\chi/20$ GeV) [64], T_{RH} should be considered as a cosmological parameter that can take any value around a few MeV and then the neutralinos decoupled from the plasma before the end of the reheating process so their relic density will differ from its standard value. We consider that the inflaton decays around the time of Big-Bang nucleosynthesis, generating entropy. From the standard late reheating scenarios, we assume that the entropy production evolves like [59]

$$\Sigma_D(T) = \kappa_\Sigma \Sigma_{rad}(T_{BBN}) \left(\frac{T_{BBN}}{T}\right) \tag{1.100}$$

for $T > 1$ MeV and that this entropy production stops at the time of BBN. We again neglect the energy production or non-thermal production of particles in order to better understand the effects of a reheating entropy production on the relic density. In term of entropy density, we have

$$s_D(T) = 3\sqrt{\frac{5}{4\pi^3 G}} h_{eff} T^3 \int_0^T dT' \frac{g_*^{1/2} \Sigma_D(T')}{\sqrt{1 + \frac{\rho_D}{\rho_{rad}}} h_{eff}^2 T'^6} \,. \tag{1.101}$$

Part I

Phenomenology in the 5D MSSM

Introduction

The Standard Model (SM), by meeting almost all confrontations with experiments, stands as a remarkably simple parameterisation of known physics. Yet it has many unsatisfactory aspects such as a large number of parameters, a triplication of chiral families, and three different gauge structures. Consequently, it is strongly believed among theorists that there must exist a simpler underlying structure of which the SM is the low energy piece. Many think that such a structure will make its appearance at much higher energies, somewhere in the unexplored region between a few TeV and the Planck scale. Experimentalists can only proceed one or two orders of magnitude at a time in their exploration of those scales. Theorists, on the other hand, have mainly a twofold approach in divining this structure. In the first, the quantum numbers of the SM are grouped into mathematically pleasing structures (constrained however by the predictions affecting the low energy part of the theory), resulting in an exercise in quantum pattern recognition. This has led to Grand Unified Theories (GUTs) [66]. The second approach is to use the renormalisation group to extrapolate the SM parameters to the unexplored scales [67]. The purpose is to find if those parameters satisfy interesting relations at higher energies. When used in conjunction with the former approach, this can give powerful hints of the physics expected at higher energies.

We shall also recall that in order to obtain finite results in quantum field theory, in a higher order than the tree level, one has to perform the renormalisation program. The independence of the renormalisation procedure from the renormalisation point leads to the dependence of the Lagrangian parameters on the point of renormalisation. This dependence is governed by the renormalisation Group Equations (RGEs) for the coupling constants and other parameters of the Lagrangian. As such, it all depends on having accurate data to input as initial conditions on the RGEs, as well as a strong theoretical basis for the evolution equations themselves. These theories, at asymptotic energies, may reveal some new symmetries or other interesting properties that give deeper insight into the physical content. Also, from the requirement of the stability of the theory one can, for example, give bounds on the physical parameters, like the Higgs mass in the SM or its extensions.

In the SM, the runnings of the gauge, Yukawa and quartic scalar couplings is logarithmic with the energy scale. Although the gauge couplings do not all meet at a point, they tend to unify near 10^{15}GeV. Extensions to the SM such as extra-dimensional scenarios accessible to SM fields have the virtue, thanks to the couplings now having a power law running, of bringing the unification scale down to an explorable range [68]. Note that many other extensions to the SM exist which alter the runnings in different ways, such as supersymmetry, where a range of new particles ensure the gauge couplings do meet at a point, but runnings remain logarithmic.

The story of extra-dimensional physics can be thought to begin in the 1920s with Kaluza (1919) and Klein (1926) [69] who had the idea to add a fifth dimension to unify the only two forces known at this time. Later in the 1970s and 1980s the birth of supergravity and superstring theories renewed the interest in extra-dimensional models. However these dimensions are

expected to be very small ($M_P \sim 10^{-35}m$) and will not be probed by experiments any time soon. However, beginning in the 1990s new extra-dimensional scenarios which could be larger than the Planck length appeared. Antoniadis [70] proposed TeV^{-1} scale extra-dimensions to explain the supersymmetry breaking, and in order to solve the hierarchy problem, the Large Extra Dimensions approach was introduced by Arkani-Hamed, Dimopoulos and Dvali (ADD) [71–74]. In these models, the metric is flat and the strength of the gravitational interaction is diluted, which leads to interesting consequences for low-energy phenomenology.

Another approach was introduced by Randall and Sundrum [75] with only one curved extra-dimension (warped extra-dimensions). The new dimension is compactified on a finite interval $0 \leq y \leq L$, with the endpoints of the interval being 3-branes. The metric of this space is not flat, where the gravity fields propagating in the fifth dimension suffer exponential suppression and live on a different brane to the SM particles.

Extra-dimensional models lead to many phenomenological implications which can be tested at colliders and also can be used as a tool to answer many issues in the SM, such as the hierarchy problem [71–75]; TeV scale extra-dimensional scenarios giving rise to new supersymmetry breaking mechanisms [70]; the generation of neutrino mass and new sources of CP violation [76]; the unification without supersymmetry (SUSY) with suppression of proton decay [77]; triggering electroweak symmetry breaking without a Higgs boson [78], providing cosmologically viable dark matter candidates [79] and many other applications related to black holes and gravity [80].

With the Large Hadron Collider (LHC) now up and running, exploration of the realm of new physics that may operate at the TeV scale has begun [81, 82]. Among these models those with extra spatial dimensions might be revealed in such higher energy collider experiments, where the UED model makes for an interesting TeV scale physics scenario [70, 83]; as it features a tower of Kaluza-Klein (KK) states for each of the SM fields, all of which have full access to the extended spacetime manifold [81, 84]. This particular scenario has recently been extensively studied in the literature, such as investigations of electroweak symmetry breaking, proton stability, gauge hierarchy and fermion mass hierarchy problems, B physics, dark matter etc. [85–91]. This model has been a fruitful playground for addressing a variety of puzzles in the SM.

We therefore collect in a comprehensive manner and in one place the necessary tools for making renormalisation group analyses of the SM and its UED extensions. We view this compendium as a template for general applications of the running of parameters from the m_Z scale to the Planck scale. The observable parameters of the SM are: 6 quark masses, 3 lepton masses, 4 parameters of the Cabibbo-Kobayashi-Maskawa (CKM) matrix [92] and 3 gauge couplings. The RGEs for the CKM matrix being obtained from the RGEs for the Yukawa couplings. This can also be extended to include neutrino masses and mixings possible in the leptonic sector.

In the following we first introduce the various models we shall consider (section 2.1 and section 2.2 for the supersymmetric extensions to this), next deriving the RGEs for the gauge

couplings constants (section 2.3) and Yukawa couplings for the SM and UED scenarios (section 2.4) and 5-dimensional Minimal Supersymmetric SMs (5D MSSM) (section 2.5). This shall be followed by a review of the CKM parameters evolution (sections 2.6 and 2.7). The summary of chapter 2 is in section 2.8.

In chapter 3, we start with a brief introduction in section 3.1. After that we present in section 3.2 extensions to massive neutrino scenarios and their mixing evolution. We summarize and give conclusions of our results in section 3.3.

Chapter 2

Quarks and CKM Matrix in UED models

2.1 The UED Standard Model

Space or Time extra dimensions ?

We should first precise the type of extra dimensions in our work. If we suppose that our theory is Lorentz invariant at D dimensions, the dispersion relation for a massless particle :

$$P^2 = 0 = g_{MN} P^M P^N \ , \tag{2.1}$$

If we choose a flat metric and one extra dimension $g_{MN} = (1, -1, -1, -1, \pm 1)$, then we have

$$P^2 = 0 = p_0^2 - \mathbf{p}^2 \pm p_5^2 \ , \tag{2.2}$$

so $p_\mu p^\mu = \mp p_5^2$. If the extra dimension is time-like, we have a massive particle $m^2 = -p_5^2$. The particle will be a *tachyon* and this leads to a serious problem of causality. In general, we only take spatial extra dimensions.

The UED model places particles of the SM in the bulk of one or more compactified extra dimensions [93]. In our case we have a single flat extra dimension of size R, compactified on an S_1/Z_2 orbifold. As such we will have an infinite tower of KK modes with the zero modes corresponding to the SM states. These KK modes are in the TeV scale and modify the running of the RGEs at relatively low energy scales [94]. The UED model, like any higher dimensional theory, is an effective field theory which is valid up to some scale Λ, at which a new physics theory emerges. Between the scale R^{-1} where the first KK states are excited and the cutoff scale Λ, there are finite quantum corrections to the Yukawa and gauge couplings from the ΛR number of KK states. Up to the scale R^{-1} the first step KK excitation occurs, the RG evolution is logarithmic, controlled by the SM beta functions. With the increasing of the energy, that is, when the KK threshold is crossed for each successive mode, new excitations come into play and govern new sets of beta functions. The values of physical parameters such as Yukawa couplings and gauge couplings do not run in the old SM fashion, instead they receive finite quantum

corrections whose magnitudes depend explicitly on the value of this cutoff parameter. As a result, once the KK states are excited, these couplings exhibit power law dependencies on Λ. This can be illustrated if $\Lambda R \gg 1$, to a very good accuracy, the generic SM beta function is shown to have the power law evolution behaviour [87]:

$$\beta^{4D} \to \beta^{4D} + (S(\mu) - 1)\,\tilde{\beta}\,, \tag{2.3}$$

where $\tilde{\beta}$ is a generic contribution from a single KK level, and where its coefficient is not a constant but instead $S(\mu) = \mu R$, with $\mu^{Max} = \Lambda$, reflecting the power law running behaviour. As a result of faster running, the gauge couplings tend to lower the unification scale down to a relatively low scale, which might be accessible to collider experiments, such as the LHC or the proposed International Linear Collider (ILC). Therefore, constraints from precision electroweak tests and current (or future) collider data would yield bounds on the compactification radius R. The RGE are an important tool for the search of the properties of the quark masses and the Cabibbo-Kobayashi-Maskawa (CKM) matrix at different energy scales. It is therefore of great interest to have an implementation of the UED model in studying these RGE.

The first version of this model we shall consider, the bulk UED model, sometimes known as the minimal UED model, has one extra dimension compactified on a circle of radius R with a Z_2 orbifolding which identifies the fifth coordinate $y \to -y$. The 5-dimensional KK expansions of the weak doublet and singlet as well as the Higgs and gauge fields are shown (the corresponding coupling constants among the KK modes are simply equal to the SM couplings up to normalisation factors, e.g. $Y_U = \dfrac{Y_U^5}{\sqrt{\pi R}}$) below:

$$\begin{aligned}
H(x,y) &= \frac{1}{\sqrt{\pi R}}\left\{H(x) + \sqrt{2}\sum_{n=1}^{\infty} H_n(x)\cos\left(\frac{ny}{R}\right)\right\}\,,\\
A_\mu(x,y) &= \frac{1}{\sqrt{\pi R}}\left\{A_\mu^0(x) + \sqrt{2}\sum_{n=1}^{\infty} A_\mu^n(x)\cos\left(\frac{ny}{R}\right)\right\}\,,\\
u(x,y) &= \frac{1}{\sqrt{\pi R}}\left\{u_R(x) + \sqrt{2}\sum_{n=1}^{\infty}\left[u_R^n(x)\cos\left(\frac{ny}{R}\right) + u_L^n(x)\sin\left(\frac{ny}{R}\right)\right]\right\}\,,\\
Q(x,y) &= \frac{1}{\sqrt{\pi R}}\left\{q_L(x) + \sqrt{2}\sum_{n=1}^{\infty}\left[Q_L^n(x)\cos\left(\frac{ny}{R}\right) + Q_R^n(x)\sin\left(\frac{ny}{R}\right)\right]\right\}\,,\\
d(x,y) &= \frac{1}{\sqrt{\pi R}}\left\{d_R(x) + \sqrt{2}\sum_{n=1}^{\infty}\left[d_R^n(x)\cos\left(\frac{ny}{R}\right) + d_L^n(x)\sin\left(\frac{ny}{R}\right)\right]\right\}\,,\\
L(x,y) &= \frac{1}{\sqrt{\pi R}}\left\{L_L(x) + \sqrt{2}\sum_{n=1}^{\infty}\left[L_L^n(x)\cos\left(\frac{ny}{R}\right) + L_R^n(x)\sin\left(\frac{ny}{R}\right)\right]\right\}\,,\\
e(x,y) &= \frac{1}{\sqrt{\pi R}}\left\{e_R(x) + \sqrt{2}\sum_{n=1}^{\infty}\left[e_R^n(x)\cos\left(\frac{ny}{R}\right) + e_L^n(x)\sin\left(\frac{ny}{R}\right)\right]\right\}\,.
\end{aligned} \tag{2.4}$$

The zero modes in the above equations are identified with the 4-dimensional SM fields, whilst the complex scalar field H and the gauge field A_μ are Z_2 even fields, and there is a left-handed

and a right-handed KK mode for each SM chiral fermion. Note that in models with UED momentum conservation in the extra dimensions, we are led to the conservation of KK number at each vertex in the interactions of the 4-dimensional effective theory (or strictly speaking, the KK parity $(-1)^n$ is what remains conserved, where n is the KK number). In the bulk we have the fermion and gauge field interactions as follows:

$$\begin{aligned}
\mathcal{L}_{Leptons} &= \int_0^{\pi R} dy\{i\bar{L}(x,y)\Gamma^M\mathcal{D}_M L(x,y) + i\bar{e}(x,y)\Gamma^M\mathcal{D}_M e(x,y)\} \,, \\
\mathcal{L}_{Quarks} &= \int_0^{\pi R} dy\{i\bar{Q}(x,y)\Gamma^M\mathcal{D}_M Q(x,y) + i\bar{u}(x,y)\Gamma^M\mathcal{D}_M u(x,y) + i\bar{d}(x,y)\Gamma^M\mathcal{D}_M d(x,y)\} \,,
\end{aligned} \tag{2.5}$$

where $\Gamma^M = (\gamma^\mu, i\gamma^5)$, and $M = 0, 1, 2, 3, 5$. Explicitly, the kinetic terms are given by:

$$\begin{aligned}
\mathcal{D}_M Q(x,y) &= \left(\partial_M + ig_3^5 G_M + ig_2^5 W_M + i\frac{1}{6}g_1^5 B_M\right) Q(x,y) \,, \\
\mathcal{D}_M u(x,y) &= \left(\partial_M + ig_3^5 G_M + i\frac{2}{3}g_1^5 B_M\right) u(x,y) \,, \\
\mathcal{D}_M d(x,y) &= \left(\partial_M + ig_3^5 G_M + i\frac{-1}{3}g_1^5 B_M\right) d(x,y) \,, \\
\mathcal{D}_M L(x,y) &= \left(\partial_M + ig_2^5 W_M + i\frac{-1}{2}g_1^5 B_M\right) L(x,y) \,, \\
\mathcal{D}_M e(x,y) &= \left(\partial_M - ig_1^5 B_M\right) e(x,y) \,.
\end{aligned} \tag{2.6}$$

The gauge couplings g_3^5, g_2^5 and g_1^5 refer to those of the $SU(3)$, $SU(2)$ and $U(1)$ gauge groups respectively, and are related to the 4-dimensional SM coupling constants by $g_i = \dfrac{g_i^5}{\sqrt{\pi R}}$, and the five dimensional gauge fields have the generic form $A_M = (A_\mu, A_5)$. After integrating out the compactified dimension, the 4-dimensional effective Lagrangian has interactions involving the zero mode and the KK modes. However, these KK modes cannot affect electroweak processes at tree level, and only contribute to higher order electroweak processes. For the one-loop diagrams of the Yukawa couplings we choose the Landau gauge in what follows, as many one-loop diagrams are finite in the Landau gauge and have no contribution to the renormalisation of the Yukawa couplings. We therefore consider the RGE for the quark- Higgs Yukawa couplings from which we obtain the evolution of the quark masses and the CKM matrix. The one-loop Feynman diagram contributions to the Yukawa couplings in the SM and UED model have been explicitly illustrated in [87, 95–97]. In the UED model, where for each energy level n_i, we effectively have a heavier duplicate copy of the entire SM particle content. That is, at each KK excited level, the KK tower corresponding to the fields in Eq.(2.4) exactly mirror the SM field

ground states. However, new contributions from the A_5,

$$A_5(x,y) = \sqrt{\frac{2}{\pi R}} \sum_{n=1}^{\infty} A_5^n(x) \sin\left(\frac{ny}{R}\right) \ , \tag{2.7}$$

interactions (that of the fifth component of the vector fields, i.e. $A_5 = \{G_5, W_5, B_5\}$) also contribute as illustrated in fig. 2.1. In contrast, the fifth component of the gauge bosons $A_5(x,y)$ is a real scalar and does not have any zero mode, transforming in the adjoint representation of the gauge group.

A simple alternative to this model is that of the brane localised UED model, where we have the same fields but where the fermion matter fields cannot propagate in the bulk and they are restricted to the brane. In the brane localised UED model, extra dimensional models make an interesting TeV scale physics scenario and as discussed earlier might be revealed in higher energy collider experiments, as they feature states that have full access to the extended spacetime manifold. For the case of brane localised matter fields, only the boson fields (the gauge fields and the scalar fields) can propagate in the bulk space. However, if the compactification radius R is sufficiently large, due to the power law running of the gauge couplings, it will enable us to bring the unification scale down to an exportable range at the LHC scale.

The information of the physical observables at the scale M_Z can be extrapolated to a higher energy scale by means of the RGE. It is well known from Eq.(1.17) that the evolution of the generic Yukawa coupling which describes the fermion-boson interactions, is given by the beta function. Although the bare constants are independent of the renormalisation scale, the renormalized coupling constants will depend on the choice of the scale parameter μ. As a result, the Yukawa coupling renormalisation depends on the corresponding beta functions, including contributions from the anomalous dimensions of the field operators. That is, its evolution is given by:

$$\mu\frac{\partial}{\partial\mu}\ln Y^R = \frac{1}{2}\mu\frac{\partial}{\partial\mu}\ln Z_{\psi_L} + \frac{1}{2}\mu\frac{\partial}{\partial\mu}\ln Z_{\psi_R} + \frac{1}{2}\mu\frac{\partial}{\partial\mu}\ln Z_{\phi} - \mu\frac{\partial}{\partial\mu}\ln Z_{couping} \ , \tag{2.8}$$

where Y^R is the renormalized Yukawa coupling constant, and Z_{ψ_L}, Z_{ψ_R} and Z_ϕ are the wave function renormalisation constants related to left-handed, right-handed fermions and Higgs

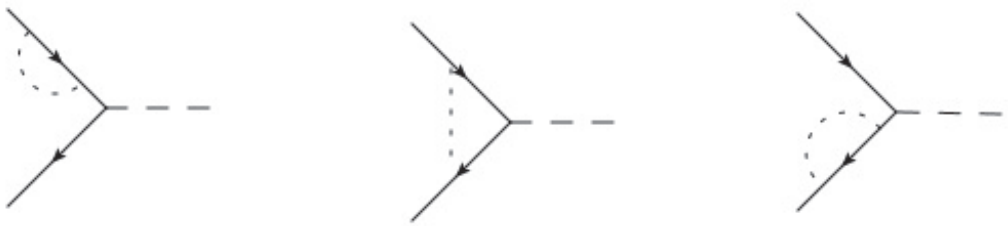

Figure 2.1: The one-loop corrections of the additional diagrams (to the SM type diagrams) from the fifth component of the vector fields to the Yukawa couplings, introduced at each KK excited level. The dashed line is for the Higgs field, the dotted line is for the A_5 scalar.

boson respectively, and $Z_{coupling}$ is the vertex renormalisation constant; or in terms of the anomalous dimensions, $\gamma_{wave} = \frac{1}{2}\mu\frac{\partial}{\partial\mu}\ln Z_{wave}, \gamma_{coupling} = \mu\frac{\partial}{\partial\mu}\ln Z_{coupling}$. After the calculation of these functions, one can obtain the coefficients of gauge couplings in section 2.4.2.

2.2 The 5D MSSM

Another useful model we shall consider is the 5D MSSM defined in [31,68,98–106]. The 5D MSSM is a five dimensional $\mathcal{N} = 1$ supersymmetric model compactified on the S_1/Z_2 orbifold which breaks the 5D Lorentz invariance to the usual 4D one. This breaking gives a momentum conservation along the fifth dimension which conserves the KK number at tree level and KK parity at loop level. One of the main implications of KK-parity invariance is that the lightest KK mode is stable and can be a cold dark matter candidate. In this compactification we can recover the MSSM at zero mode since we obtain chiral fermions. Note though, that since we are working with a supersymmetric model, the beta function can be derived in the superfield formalism, where we shall discuss $\mathcal{N} = 1$ supersymmetry in a five-dimensional Minkowski space and its description in terms of 4D superfields. The space-time coordinates being labeled by (x^μ, y).

The gauge sector is then described by a 5D $\mathcal{N} = 1$ vector supermultiplet which consists (on-shell) of a 5D vector field A^M, a real scalar S and two gauginos, λ and λ'. The action for which can be given by:

$$\begin{aligned} S_g &= \int \mathrm{d}^5x \frac{1}{2kg^2}\mathrm{Tr}\Big[-\frac{1}{2}F^{MN}F_{MN} - D^M S D_M S - i\overline{\lambda}\Gamma^M D_M\lambda \\ &\quad - i\overline{\lambda}'\Gamma^M D_M\lambda' + (\overline{\lambda}+\overline{\lambda}')[S,\lambda+\lambda']\Big] \ , \end{aligned} \tag{2.9}$$

with $D_M = \partial_M + iA_M$ and $\Gamma^M = (\gamma^\mu, i\gamma^5)$. $F^{MN} = -\frac{i}{g}[D^M, D^N]$ and k normalises the trace over the generators of the gauge groups.

From the decomposition of the 5D supercharge (which is a Dirac spinor) into two Majorana-type supercharges, which constitute a $\mathcal{N} = 2$ superalgebra in 4D, one can rearrange these fields in terms of a $\mathcal{N} = 2$, 4D vector supermultiplet, $\Omega = (V, \chi)$:

– V : $\mathcal{N} = 1$ vector supermultiplet containing A^μ and λ,

– χ : $\mathcal{N} = 1$ chiral supermultiplet containing λ' and $S' = S + iA^5$.

Both V and χ (and their component fields) are in the adjoint representation of the gauge group $\mathcal{G}$. Using the supermultiplets one can write the original 5D $\mathcal{N} = 1$ supersymmetric action Eq.(2.9) in terms of $\mathcal{N} = 1$ 4D superfields and the covariant derivative in the y direction [100]:

$$S_g = \int \mathrm{d}^5x\mathrm{d}^2\theta\mathrm{d}^2\overline{\theta}\frac{1}{4kg^2}\mathrm{Tr}\left[\frac{1}{4}(W^\alpha W_\alpha\delta(\overline{\theta}^2) + h.c) + (e^{-2gV}\nabla_y e^{2gV})^2\right] \ , \tag{2.10}$$

with $W^\alpha = -\frac{1}{4}\overline{D}^2 e^{-2gV}D_\alpha e^{2gV}$. D_α is the covariant derivative in the 4D $\mathcal{N} = 1$ superspace and $\nabla_y = \partial_y + \chi$. To find the Feynman rules to a given order in the gauge coupling g, one can expand and quantise the action [98]. The beta functions for the couplings of the

operators in the superpotential are governed by the wave function renormalisation constants $Z_{ij} = 1 + \delta Z_{ij}$ due to the non-renormalisation theorem [107] (there is no contribution from masses and gauge coupling constants renormalisation). The Feynman diagrams related to the wave-function renormalisation are given in fig. 2.2. For more details about superspace perturbation theory, supergraphs technics, Feynman rules, propagators in superfield theory, loop calculation methods, beta functions and all that, the reader can refer to [28, 29] as well as chapter 6 in Ref. [30].

Besides the renormalizable operators, there can be higher dimensional and non-renormalizable operators in an effective theory. But this is simplified in our case since we have a supersymmetric theory: due to the non-renormalisation theorem [30], only wave function renormalisation has to be considered for operators of the superpotential and no vertex corrections contribute. The supergraphs technique allows to use this theorem since SUSY is kept manifest and it has the advantage that the number of independent diagrams is reduced compared to the component field calculations. We avoid the quadratic divergences to the Higgs mass to all order in perturbation theory as a consequence of the non-renormalisation theorem and we do not have the *fine tuning* problem. This is the essence of *naturalness* due to SUSY.

The Higgs superfields and gauge superfields will always propagate into the fifth dimension. Different possibilities for the matter superfields will be discussed, where superfields containing SM fermions can propagate in the bulk or are restricted to the brane. For the case where all

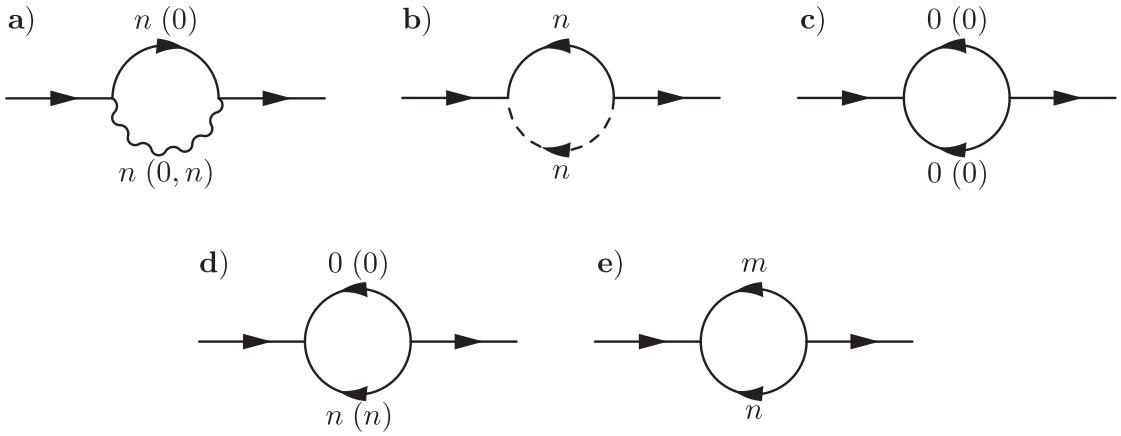

Figure 2.2: The one-loop diagrams related to the wave-function renormalisation of the matter superfields, in which diagrams a)-e) refer to the case where all the matter fields are in the bulk, and the excited KK states are labeled by the number without the bracket; whereas diagrams a), c) and d) are related to the brane localised matter fields case, in which the KK states are labeled by the number inside the bracket [98, 102].

fields can propagate in the bulk, the action for the matter fields would be [98]:

$$\begin{aligned} S_{matter} &= \int \mathrm{d}^8 z \mathrm{d}y \left\{ \bar{\Phi}_i \Phi_i + \Phi_i^c \bar{\Phi}_i^c + \Phi_i^c \partial_5 \Phi_i \delta(\bar{\theta}) - \bar{\Phi}_i \partial_5 \overline{\Phi}_i^c \delta(\theta) \right. \\ &\left. + \tilde{g}(2\bar{\Phi}_i V \Phi_i - 2\Phi_i^c V \bar{\Phi}_i^c + \Phi_i^c \chi \Phi_i \delta(\bar{\theta}) + \bar{\Phi}_i \bar{\chi} \bar{\Phi}_i^c \delta(\theta)) \right\} . \end{aligned} \tag{2.11}$$

Again, this action can be expanded and quantised. The χ-field should be odd under Z_2 symmetry because it appears together with a derivative ∂_y, whereas V is even. For the two matter superfields, we choose Φ to be even and the conjugate Φ^c to be odd such that Φ^c vanishes on the brane. Only the even fields have zero modes. The Fourier decomposition of the fields being:

$$\begin{aligned} V(x,y) &= \frac{1}{\sqrt{\pi R}} \left[V^{(0)}(x) + \sqrt{2} \sum_{n \geq 1} V^{(n)}(x) cos\left(\frac{ny}{R}\right) \right] , \\ \chi(x,y) &= \sqrt{\frac{2}{\pi R}} \sum_{n \geq 1} \chi^{(n)}(x) sin\left(\frac{ny}{R}\right) , \\ \Phi(x,y) &= \frac{1}{\sqrt{\pi R}} \left[\Phi^{(0)}(x) + \sqrt{2} \sum_{n \geq 1} \Phi^{(n)}(x) cos\left(\frac{ny}{R}\right) \right] , \\ \Phi^c(x,y) &= \sqrt{\frac{2}{\pi R}} \sum_{n \geq 1} \Phi^{c(n)}(x) sin\left(\frac{ny}{R}\right) . \end{aligned} \tag{2.12}$$

We can write the action for the second case where all superfields containing SM fermions are restricted to the brane. In which case the part of the action involving only gauge and Higgs fields is not modified, whereas the action for the superfields containing the SM fermions becomes:

$$S_{matter} = \int \mathrm{d}^8 z \mathrm{d}y \delta(y) \left\{ \bar{\Phi}_i \Phi_i + 2\tilde{g} \bar{\Phi}_i V \Phi_i \right\} . \tag{2.13}$$

Due to the 5D $\mathcal{N} = 1$ supersymmetry, Yukawa couplings are forbidden in the bulk. However, they can be introduced on the branes, which are 4D subspaces with reduced supersymmetry. One can also add the effective neutrino mass operator (also called lepton number violating Weinberg operator), with dimensionfull coupling $\tilde{k}_{ij}$ in which we are interested to show its evolution and therefore the Majorana mass term for neutrinos. We will write the following interaction terms, called brane interactions, containing Yukawa-type couplings:

$$S_{brane} = \int \mathrm{d}^8 z \mathrm{d}y \delta(y) \left\{ \left(\frac{1}{6} \tilde{\lambda}_{ijk} \Phi_i \Phi_j \Phi_k - \frac{\tilde{k}_{ij}}{4M} L_i H_u L_j H_u \right) \delta(\bar{\theta}) + \mathrm{h.c.} \right\} , \tag{2.14}$$

where L and H^u are the lepton and up-type Higgs doublet chiral superfields respectively. This operator is used to study neutrino masses and mixings, where RGEs for this effective operator have been derived in the context of the four-dimensional SM [108] and MSSM [109] and shall be discussed further in section 3.2. An extension to compactified extra-dimensions was considered in Ref [98], and we shall use a similar formalism in the next section.

From fig. 2.2 we obtain the wave function renormalisation of the matter superfields and then we calculate the beta function described in section 2.2.1. If we exclude the effects of extra

dimensions, one can obtain the beta function of the usual MSSM. The figs. 2.2 a)-e) refer to the case where matter superfields are able to propagate in the bulk (excited KK states are labeled by the number without brackets) and diagrams in figs. 2.2 a), c), d) represent the case of brane localised matter superfields (excited KK states are labeled by the number inside brackets).

Comments about cut-off regularization [18]

We could ask how interactions modify the photon mass: If one introduces a cut-off to regularize the integrals for vacuum polarization, it is well know that the corrections to the squared mass of the photon are quadratically divergent. This would imply that electromagnetic gauge invariance is broken! The cut-off is not a gauge invariant regulator: Under gauge transformations, $A_\mu(x) \to A_\mu(x) - \partial_\mu(x)$, or in k-space, $A_\mu(k) \to A_\mu(k) - ik_\mu\alpha(k)$ for all values of k. Even if we cut off the modes with $k > \Lambda$ in one gauge, these do not vanish in different gauge, so a cut-off of the momentum integrals is a gauge-dependent notion. If instead we use a gauge invariant regulator such as dimensional regularization, the radiative correction to the photon mass vanishes. We say that gauge invariance protects the photon from acquiring a mass. The leading divergence is logarithmic in any quantity in quantum electrodynamics of fermions. There are no quadratic or linear divergence.
However, this is not the case for scalars in field theories and especially in our model in which we should use the regularization by cut-off since we have linear and quadratic divergence which appear in supergraph calculations. If we use dimensional regularization, only logarithmic divergences appear.

2.2.1 β-functions in 5D MSSM

Usual result for 4D MSSM

We recall that, for a general gauge supersymmetric theory, the superpotential is given by the second term in Eq.(1.62). The beta functions for the couplings of the operators in the superpotential are governed by the wave function renormalisation constants $Z_{ij} = 1 + \delta Z_{ij}$. For the chiral superfields, they receive two types of corrections : one from loop with chiral superfields and the other from loop with chiral and vector superfields. Z_{ij} relate the bare to the renormalized superfileds

$$\Phi^i_B = \sum_{j=1}^{N_\Phi} Z^{1/2}_{ij} \Phi^j_R \,. \tag{2.15}$$

The sum runs over all N_Φ chiral superfileds of the model. The result for the wave function renormalisation constant at one loop for a chiral superfield reads [28]

$$-(16\pi^2)\delta Z_{ij} = \left(-4 \sum_{n=1}^{N_g} g_n^2 C_2(R^i_n)\delta_{ij} + \sum_{k,l=1}^{N_\Phi} \lambda^*_{ikl}\lambda_{jkl} \right) \frac{1}{\epsilon} \tag{2.16}$$

The sum over n runs over all gauge groups of the theory. The group-theoretical constants $C_2(R)$ are defined as

$$C_2(R)\delta_{ab} = \sum_A (T^A T^A)_{ab} \ , \tag{2.17}$$

where T^A are matrix representations of the generators of the gauge group corresponding to the irreducible representation R under which the fields Φ_i transform.

β-functions

In the paper [109], they develop a method to obtain the beta-function of the couplings for an arbitrary operator using the renormalisation constants for the wave functions (in a supersymmetric theory). The result for the Weinberg operator and its coupling k coupling is [110]

$$\begin{aligned} \beta_k^{5D} &= \frac{dk(\Lambda)}{d\,\log(\Lambda R)} \\ &= -\delta Z_{H_u}.k - \frac{1}{2}\delta Z_L^T.k - \frac{1}{2}k.\delta Z_L \end{aligned} \tag{2.18}$$

and for the Yukawa couplings

$$\begin{aligned} \beta_{Y_d} &= -\frac{1}{2}\Lambda\frac{\partial}{\partial\Lambda}(\delta Z_{D^c}^T Y_d + Y_d\delta Z_Q + Y_d\delta Z_{H_d}) \\ \beta_{Y_u} &= -\frac{1}{2}\Lambda\frac{\partial}{\partial\Lambda}(\delta Z_{U^c}^T Y_u + Y_u\delta Z_Q + Y_u\delta Z_{H_u}) \\ \beta_{Y_e} &= -\frac{1}{2}\Lambda\frac{\partial}{\partial\Lambda}(\delta Z_{E^c}^T Y_e + Y_e\delta Z_L + Y_e\delta Z_{H_d}) \end{aligned} \tag{2.19}$$

Firstly, we calculate the equivalent of the result in Eq.(2.16) in a 5D supersymmetric theory with a brane interaction between chiral superfields as described in Eq.(2.14). Due to the non-renormalisation theorem, we calculate only the renormalisation constants for the wave functions. The external superfileds do not have Kaluza-Klein excitations, and we will have different types of contributions (see fig. 2.2) :

- The bulk term contributions (modes $n > 0$) which consist in a loop of V and Φ, χ and Φ, or Φ and Φ.
- In the brane case, only the Higgs and gauge superfields can propagate in the fifth dimension. The term contributions consist in a loop of $V^{(n)}$ and Φ^0, or $\Phi^{(n)}$ and Φ^0.
- For the two above contributions, we add those of zero modes in the loop.

Bulk equations

In total, we obtain for the self-energy for chiral superfield

$$-(16\pi^2)\delta Z_\Phi^{5D} = \left(-8\sum_{n=1}^{N_g} g_n^2 C_2(R_n^i)\delta_{ij}\right)\Lambda R + \left(2\pi\sum_{k,l=1}^{N_\Phi}\lambda_{ikl}^*\lambda_{jkl}\right)\Lambda^2 R^2 \tag{2.20}$$

Some steps of the calculation of Eq.(2.20) is detailed in appendix A. This result can be applied to matter superfields as well as Higgs superfields (since both superfields are able to propagate in the bulk). Then, we have

$$\begin{aligned}
-(16\pi^2)\delta Z_{H_u} &= 12\pi Tr(Y_u^\dagger Y_u)\Lambda^2 R^2 - (\frac{6}{5}g_1^2 + 6g_2^2)\Lambda R \\
-(16\pi^2)\delta Z_{H_d} &= 4\pi[3Tr(Y_d^\dagger Y_d) + Tr(Y_e^\dagger Y_e)]\Lambda^2 R^2 - (\frac{6}{5}g_1^2 + 6g_2^2)\Lambda R \\
-(16\pi^2)\delta Z_L &= 4\pi(Y_e^\dagger Y_e)\Lambda^2 R^2 - (\frac{6}{5}g_1^2 + 6g_2^2)\Lambda R \\
-(16\pi^2)\delta Z_{E^c} &= 8\pi(Y_e^* Y_e^T)\Lambda^2 R^2 - (\frac{24}{5}g_1^2)\Lambda R \\
-(16\pi^2)\delta Z_{D^c} &= 8\pi(Y_d^* Y_d^T)\Lambda^2 R^2 - (\frac{8}{15}g_1^2 + \frac{32}{3}g_3^2)\Lambda R \\
-(16\pi^2)\delta Z_Q &= 4\pi(Y_u^\dagger Y_u + Y_d^\dagger Y_d)\Lambda^2 R^2 - (\frac{2}{15}g_1^2 + 6g_2^2 + \frac{32}{3}g_3^2)\Lambda R \\
-(16\pi^2)\delta Z_{U^c} &= 8\pi(Y_u^* Y_u^T)\Lambda^2 R^2 - (\frac{32}{15}g_1^2 + \frac{32}{3}g_3^2)\Lambda R
\end{aligned} \tag{2.21}$$

From Eqs.(2.18, 2.19, 2.21), we obtain Eqs.(2.38, 2.41).

Brane equations

To avoid the quadratic divergences when we localize the Yukawa interactions and the neutrino mass effective operator, we forbid fermions to propagate in the fifth dimension. Then the KK excitations for these fields are absent, we do not have a double sum of KK in the loop and no quadratic divergences. We will have in this case logarithmic or linear divergences. The Higgs can always propagate in the fifth dimension, so the renormalisation constants will be different between matter superfields and Higgs superfields. Then, we have

$$\begin{aligned}
-(16\pi^2)\delta Z_\Phi^f &= \left(-16\sum_{n=1}^{N_g} g_n^2 C_2(R_n^i)\delta_{ij} + 4\sum_{k,l=1}^{N_\Phi}\lambda_{ikl}^*\lambda_{jkl}\right)\Lambda R \\
-(16\pi^2)\delta Z_H &= \left(-8\sum_{n=1}^{N_g} g_n^2 C_2(R_n^i)\delta_{ij}\right)\Lambda R + \left(\sum_{k,l=1}^{N_\Phi}\lambda_{ikl}^*\lambda_{jkl}\right)\log(\Lambda R)
\end{aligned} \tag{2.22}$$

It is straightforward to deduce the following renormalisation constants for the matter and Higgs superfields

$$
\begin{aligned}
-(16\pi^2)\delta Z_{H_u} &= 6Tr(Y_u^\dagger Y_u)\log(\Lambda R) - (\frac{6}{5}g_1^2 + 6g_2^2)\Lambda R \\
-(16\pi^2)\delta Z_{H_d} &= 2[3Tr(Y_d^\dagger Y_d) + Tr(Y_e^\dagger Y_e)]\log(\Lambda R) - (\frac{6}{5}g_1^2 + 6g_2^2)\Lambda R \\
-(16\pi^2)\delta Z_L &= [8(Y_e^\dagger Y_e) - \frac{12}{5}g_1^2 - 12g_2^2]\Lambda R \\
-(16\pi^2)\delta Z_{E^c} &= [16(Y_e^* Y_e^T) - \frac{48}{5}g_1^2]\Lambda R \\
-(16\pi^2)\delta Z_{D^c} &= [16(Y_d^* Y_d^T) - \frac{16}{15}g_1^2\frac{64}{3}g_3^2]\Lambda R \\
-(16\pi^2)\delta Z_Q &= [8(Y_u^\dagger Y_u + Y_d^\dagger Y_d) - \frac{4}{15}g_1^2 - 12g_2^2 - \frac{64}{3}g_3^2)]\Lambda R \\
-(16\pi^2)\delta Z_{U^c} &= [16(Y_u^* Y_u^T) - \frac{64}{15}g_1^2 - \frac{64}{3}g_3^2]\Lambda R
\end{aligned}
\tag{2.23}
$$

From Eqs.(2.18, 2.19, 2.23), we obtain Eqs.(2.38, 2.42).

2.3 Gauge couplings

The evolution of the gauge couplings in four dimension at one loop are given by:

$$
16\pi^2 \frac{dg_i}{dt} = b_i {g_i}^3 , \tag{2.24}
$$

where $b_i^{SM} = (\frac{41}{10}, -\frac{19}{6}, -7)$ and $b_i^{MSSM} = (\frac{33}{5}, 1, -3)$ [18, 111], using a $SU(5)$ normalisation. If we consider our 5D theory as effective up to a scale Λ, we have contributions from the KK modes which give a power law evolution to the gauge couplings since extra-dimensions cause their running to vary much more rapidly. Eq.(2.3)can be written in terms of the scale parameter t:

$$
16\pi^2 \frac{dg_i}{dt} = [b_i + (S(t) - 1)\tilde{b}_i]{g_i}^3 , \tag{2.25}
$$

where $\tilde{b}_i$ take the following form in the case of the model UED SM [95, 112]:

$$
(\tilde{b}_1, \tilde{b}_2, \tilde{b}_3) = \left(\frac{1}{10}, -\frac{41}{6}, -\frac{21}{2}\right) + \frac{8}{3}\eta , \tag{2.26}
$$

with η being the number of generations of matter fields in the bulk. Therefore, for all our matter fields propagating in the bulk (that is, $\eta = 3$), we have for the UED SM bulk case:

$$
\tilde{b}_i = \left(\frac{81}{10}, \frac{7}{6}, -\frac{5}{2}\right) . \tag{2.27}
$$

Similarly, for all our matter fields localised to the 3-brane (that is, $\eta = 0$), we have for the UED SM brane case:

$$\tilde{b}_i = \left(\frac{1}{10}, -\frac{41}{6}, -\frac{21}{2}\right) . \tag{2.28}$$

Next we consider the beta functions of the gauge couplings in the 5D MSSM. In fact, after compactification of the 5D MSSM, we have two 4D $\mathcal{N} = 1$ chiral supermultiplets, Φ and Φ^c, where the zero modes of Φ give us the normal matter fields and Higgs fields as well as their super partners, while Φ^c is a new supermultiplet. In the component field formalism, at each KK level, aside from the quantum corrections that mirror those of the 4D MSSM, the only new one-loop contributions to the A_μ Feynman diagrams are from the wave function renormalisation of A_μ (which contribute via the coupling of A_μ to the complex scalar field and its super-partner in the superfield χ, and the coupling of A_μ with the new fermion field and its super-partner in the superfield Φ^c associated with the two doublets of the Higgs fields and the matter fields respectively in the bulk). This then gives rise to the master beta functions of the gauge couplings in the 5D MSSM as follows [102]:

$$(\tilde{b}_1, \tilde{b}_2, \tilde{b}_3) = \left(\frac{6}{5}, -2, -6\right) + 4\eta , \tag{2.29}$$

where η represents the number of generations of fermions which propagate in the bulk. This calculation is detailed in appendix B. So in the two cases we shall consider, that of all fields propagating in the bulk ($\eta = 3$) we have [113]:

$$\tilde{b}_i = \left(\frac{66}{5}, 10, 6\right) . \tag{2.30}$$

Similarly, for all our matter fields localised to the 3-brane (that is, $\eta = 0$), we have:

$$\tilde{b}_i = \left(\frac{6}{5}, -2, -6\right) . \tag{2.31}$$

In figs. 2.3 and 2.4 we have plotted the running of the gauge couplings for the UED SM case and the 5D MSSM respectively for the brane localised and bulk field cases, and for several choices of compactification scales for the extra-dimension (R). From these plots, and the discussion given in ref. [113], we find that for the three gauge coupling constants to approach a small region at some value of t requires an extremely large value of $1/R$, which is of no phenomenological interest at present. For the case of our fields being brane localised in the UED model, we see a similar behaviour: the extra-dimensions naturally lead to gauge coupling unification at an intermediate mass scale for the compactification radii considered here. Furthermore, as illustrated in fig. 2.3, the extra spacetime dimensions naturally lead to the appearance of GUTs at scales substantially below the usual GUT scale.

We assume the fundamental scale is not far from the range of LHC scale, and set the compactification radii to be $R^{-1} = 2$ TeV, 8 TeV, and 15 TeV respectively. In the limit when the energy scale is much smaller than R^{-1}, since the energy of the system is less than the excitations of the first KK modes, the theory reduces to the usual 4-dimensional SM, and the

existence of the KK excitations are ignored. When $\mu > R^{-1}$, excitations of many KK modes become possible, and the contributions of these KK states must be included in all physical calculations. This is characterized by the second term in Eq.(2.3) in the general beta function. Once the energy passes R^{-1} the excited KK modes tend to increase rapidly the running of the gauge couplings, and ultimately change the scale dependence of the gauge couplings from logarithmic to those of a power law as a function of μ. Quantitatively, due to the fast running of the gauge couplings, we find they nearly meet at around $t = 6.4$, 7.8, 8.4 for radii $R^{-1} = 2$, 8, 15 TeV respectively. The extra dimensions naturally lead to gauge coupling unification at an intermediate mass scale.

Similarly, in fig. 2.4 we have plotted the evolutions of the brane localised and bulk field cases for several choices of compactification scales for the 5D MSSM. From these plots, and as noted above, we find that for the three gauge coupling constants to approach a small region at some value t requires an extremely large value of $1/R$, whereas, for the case of our fields being brane localised, the extra dimensions naturally lead to gauge coupling unification at a similarly valued intermediate mass scale for the compactification radii considered here.

2.4 Yukawa evolutions in the SM and UED SM

In the quark sector of the SM, we have ten experimentally measurable parameters, i.e. six quark masses, three mixing angles, and one phase (these angles and phase being encoded in the CKM matrix which we shall discuss in section 2.6). A completely satisfactory theory of fermion masses and the related problem of mixing angles is certainly lacking at present, however, there has been considerable effort to understand the hierarchies of these mixing angles and fermion masses in terms of the RGEs [97, 111, 114–118]. First though we must recall that in order to

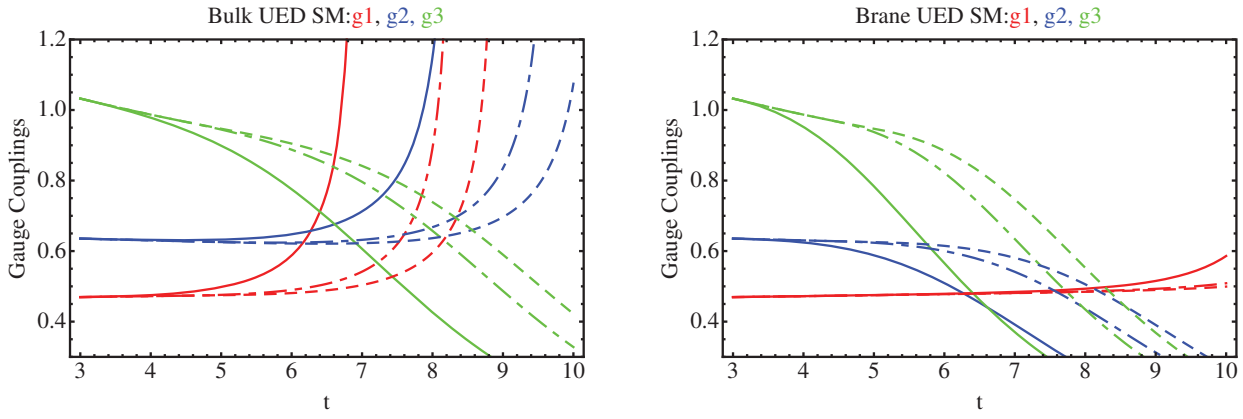

Figure 2.3: Gauge couplings g_1 (red), g_2 (blue), g_3 (green) with: in the left panel, all matter fields in the bulk (UED bulk); and the right panel for all matter fields on the brane (UED brane); for three different values of the compactification scales: 2 TeV (solid line), 8 TeV (dot-dashed line), 15 TeV (dashed line) as a function of the scale parameter t in the UED SM.

explore the physics at a high energy scale we use RGEs as a probe to study the momentum dependence of the Yukawa couplings, the gauge couplings, and from these the CKM matrix elements themselves. As such we can consider one of the primary goals of the LHC as being to uncover any new dynamics within the TeV range, where instead of assuming the RGE goes from the M_Z scale up to the GUT scale (10^{15} GeV) by using the $SU_C(3) \times SU_L(2) \times U_Y(1)$ symmetry, we know that models with extra dimensions may bring down the unification to a much lower energy scale. However, when using the RGEs as a probe, the initial values we shall adopt are very important, where we shall scale for the gauge couplings and the fermion masses at the M_Z scale are shown in Table 2.1.

Parameter	Value	Parameter	Value
α_1	0.01696	m_e	0.48657 MeV
α_2	0.03377	m_μ	102.718 MeV
α_3	0.1184	m_τ	1746.24 MeV
m_u	1.27 MeV	$\lvert V_{ub}\rvert$	0.00347
m_c	0.619 GeV	$\lvert V_{cb}\rvert$	0.0410
m_t	171.7 GeV	$\lvert V_{us}\rvert$	0.2253
m_d	2.90 MeV	J	2.91×10^{-5}
m_s	55 MeV		
m_b	2.89 GeV		

Table 2.1: Initial values for the gauge couplings, fermion masses and CKM parameters at M_Z scale. Data is taken from Ref [102, 119, 120].

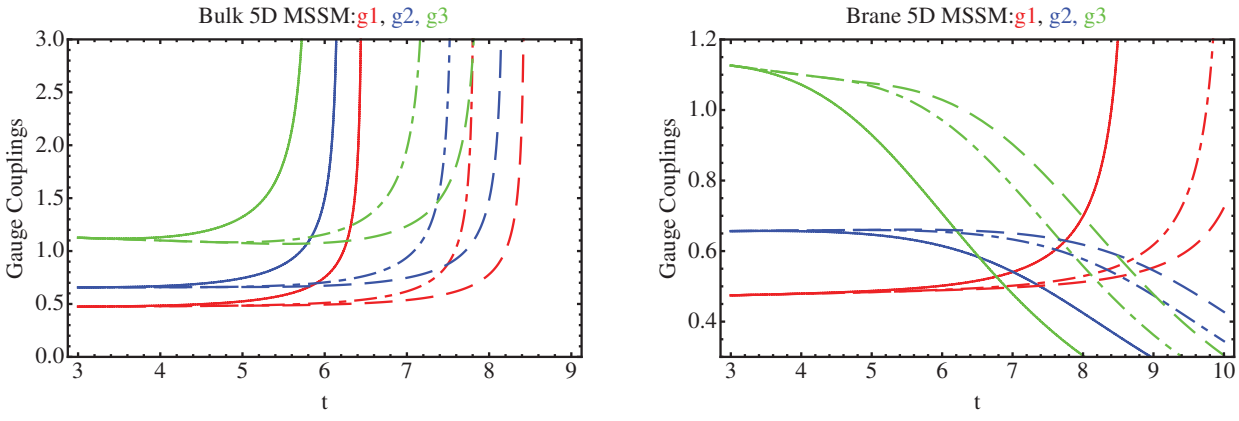

Figure 2.4: Gauge couplings g_1 (red), g_2 (blue), g_3 (green) with: in the left panel, all matter fields in the bulk; and the right panel for all matter fields on the brane; for three different values of the compactification scales: 2 TeV (solid line), 8 TeV (dot-dashed line), 15 TeV (dashed line) as a function of the scale parameter t in the 5D MSSM.

Furthermore, we shall also attempt, in section 3.2, to develop the RGEs of the lepton sector (including possible mixing angles and phases), which will require knowledge of the evolution of a parameter k, where the lowest order operator which generates Majorana neutrino masses after electroweak symmetry breaking (EWSB), is the lepton-number violating Weinberg operator [121]. This lowest order operator (appearing with dimension $d = 5$ in four space-time dimensions) can be written as:

$$-\frac{\tilde{k}_{ij}}{4M}(\bar{L}^{ci}_{\alpha}\epsilon^{\alpha\beta}\phi_{\beta})(L^{j}_{\delta}\epsilon^{\delta\gamma}\phi_{\gamma}) + h.c.\ , \tag{2.32}$$

where L and ϕ are the lepton and the Higgs doublet fields. M is the typical heavy energy scale for the range of validity of the low-energy effective theory. An operator of this type can be generated, for instance, by the usual see-saw mechanism. In which case the heavy scale M can be identified with the mass of the heavy right-handed neutrino. After EWSB the Higgs acquires a vacuum expectation value (vev) and the operator in Eq.(2.32) gives a Majorana mass term for the neutrinos. In the context of the MSSM it can be written in the form:

$$-\frac{\tilde{k}_{ij}}{4M}(L^{i}_{\alpha}\epsilon^{\alpha\beta}H^{u}_{\beta})(L^{j}_{\delta}\epsilon^{\delta\gamma}H^{u}_{\gamma})\ , \tag{2.33}$$

where L and H^u are the lepton and up-type Higgs doublet chiral superfields respectively. This operator is crucial for the study of neutrino masses and mixings, where renormalisation group equations for this effective operator have been derived in the context of the four-dimensional SM and MSSM [108, 109].

In the present case we consider the effective neutrino mass operator with dimensional coupling $\tilde{k}_{ij}$; after spontaneous symmetry breaking, the Majorana neutrino masses can be written as $m_\nu \equiv kv^2 sin^2\beta$ (v being the vev of the Higgs field and $\tan\beta$, the ratio of the vevs of our two Higgs doublets) and $k = \tilde{k}_{ij}/(2M\pi R)$ for bulk propagating, and $k = \tilde{k}/(2M)$ for brane localised matter superfield scenarios respectively.

As such, we have set M_Z as the renormalisation point, and use $t = \ln(\frac{\mu}{M_Z})$ and $S(t) = e^t M_Z R$. The general form of evolution equations for Yukawa couplings and neutrino k coupling at the one loop can be written in the following form Refs [122–124]:

$$\begin{aligned}
16\pi^2\frac{dY_d}{dt} &= Y_d\left\{T_t C_1 - G_d + \frac{3}{2}(Y_d^\dagger Y_d - Y_u^\dagger Y_u)C_2\right\}\ ,\\
16\pi^2\frac{dY_u}{dt} &= Y_u\left\{T_t C_1 - G_u + \frac{3}{2}(Y_u^\dagger Y_u - Y_d^\dagger Y_d)C_2\right\}\ ,\\
16\pi^2\frac{dY_e}{dt} &= Y_e\left\{T_t C_1 - G_e + \frac{3}{2}(Y_e^\dagger Y_e)C_2\right\}\ ,\\
16\pi^2\frac{dk}{dt} &= \alpha k + \left([{Y_e}^T Y_e^*]k + k[Y_e^\dagger Y_e]\right)C_3\ .
\end{aligned} \tag{2.34}$$

where $T_t = Tr\Big[3Y_d^\dagger Y_d + 3Y_u^\dagger Y_u + Y_e^\dagger Y_e\Big]$.

2.4.1 Standard Model

The SM is a limiting case for the UED, where the KK states decouple. The coefficients in the evolution equation are defined by:

$$\begin{aligned} G_{dSM} &= \left(\frac{1}{4}g_1^2 + \frac{9}{4}g_2^2 + 8g_3^2\right) , \\ G_{uSM} &= \left(\frac{17}{20}g_1^2 + \frac{9}{4}g_2^2 + 8g_3^2\right) , \\ G_{eSM} &= \left(\frac{9}{4}g_1^2 + \frac{9}{4}g_2^2\right) , \\ \alpha_{SM} &= 2\,T_t - 3g_2^2 + \lambda\,, \\ C_{1SM} &= 1\,, \\ C_{2SM} &= 1\,, \\ C_{3SM} &= -\frac{3}{2}\,. \end{aligned} \tag{2.35}$$

Note that there is a difference in the coefficients of the gauge coupling g_1 between Ref [122]. and Ref [123]. due to the $SU(5)$ normalisation factor 3/5.

2.4.2 UED SM Bulk

The UED contribution is obtained when KK states enter, where due to the orbifolding the zero mode for fermions are chiral, which are replaced by Dirac fermions at each KK level. This lead to the factor 2 appearing in C_1 and C_2 since the KK left and right-handed chiral states contribute to the closed fermion one loop diagrams. That is,

$$\begin{aligned} G_{dUEDBulk} &= \left(\frac{17}{120}g_1^2 + \frac{15}{8}g_2^2 + \frac{28}{3}g_3^2\right)(S(t)-1)\,, \\ G_{uUEDBulk} &= \left(\frac{101}{120}g_1^2 + \frac{15}{8}g_2^2 + \frac{28}{3}g_3^2\right)(S(t)-1)\,, \\ G_{eUEDBulk} &= \left(\frac{99}{40}g_1^2 + \frac{15}{8}g_2^2\right)(S(t)-1)\,, \\ \alpha_{UEDBulk} &= (S(t)-1)\left(4T_t - \frac{3}{20}g_1^2 - \frac{11}{4}g_2^2 + \lambda\right)\,, \\ C_{1UEDBulk} &= 2(S(t)-1)\,, \\ C_{2UEDBulk} &= (S(t)-1)\,, \\ C_{3UEDBulk} &= (S(t)-1)\,. \end{aligned} \tag{2.36}$$

Following the convention of Ref [95]. we use the coefficient $(S(t)-1) = (\mu R - 1)$, which depends on the energy scale and also lead to a reproduction of the SM before crossing the threshold of

the first KK state at $\mu = 1/R$. This coefficient corresponds to $s = \frac{\mu}{\mu_0}$ for the UED case only in Ref [122].

2.4.3 UED SM Brane

For the case where the fermions are restricted to the brane, we obtain the coefficients from Ref [112]. and Ref [122]. with a difference related to the $SU(5)$ normalisation factor:

$$\begin{aligned}
G_{dUEDBrane} &= \left(\frac{1}{4}g_1^2 + \frac{9}{4}g_2^2 + 8g_3^2\right) 2(S(t)-1)\,, \\
G_{uUEDBrane} &= \left(\frac{17}{20}g_1^2 + \frac{9}{4}g_2^2 + 8g_3^2\right) 2(S(t)-1)\,, \\
G_{eUEDBrane} &= \left(\frac{9}{4}g_1^2 + \frac{9}{4}g_2^2\right) 2(S(t)-1)\,, \\
\alpha_{UEDBrane} &= 2(S(t)-1)\Big(-3g_2^2 + \lambda\Big)\,, \\
C_{1UEDBrane} &= 0\,, \\
C_{2UEDBrane} &= 2(S(t)-1)\,, \\
C_{3UEDBrane} &= 2(S(t)-1)\,.
\end{aligned} \tag{2.37}$$

Note that the coefficient $C_1 = 0$ since we do not have a trace of fermionic loops as the fermions are restricted to the brane.

2.5 Yukawa evolutions in the MSSM and 5D MSSM

In the following we write the general form of the evolution equations for the various MSSMs we shall consider here, where we shall use a notation similar to the ones of Refs. [98, 124]. Note that the beta functions contain terms quadratic in the cut-off, where this part dominates the evolution of the Yukawa couplings and of k. The top Yukawa coupling becomes non-perturbative before the gauge couplings thus limiting the range of validity of the effective theory.

$$\begin{aligned}
16\pi^2\frac{dY_d}{dt} &= Y_d\left\{T_d\tilde{C} - G_d + (3Y_d^\dagger Y_d + Y_u^\dagger Y_u)C\right\}\,, \\
16\pi^2\frac{dY_u}{dt} &= Y_u\left\{T_u\tilde{C} - G_u + (3Y_u^\dagger Y_u + Y_d^\dagger Y_d)C\right\}\,, \\
16\pi^2\frac{dY_e}{dt} &= Y_e\left\{T_e\tilde{C} - G_e + (3Y_e^\dagger Y_e)C\right\}\,, \\
16\pi^2\frac{dk}{dt} &= \alpha k + \Big([{Y_e}^T Y_e^*]k + k[Y_e^\dagger Y_e]\Big)\,C\,.
\end{aligned} \tag{2.38}$$

where

$$\begin{aligned} T_d &= 3\,Tr(Y_d^\dagger Y_d) + Tr(Y_e^\dagger Y_e)\,, \\ T_u &= 3\,Tr(Y_u^\dagger Y_u)\,, \\ T_e &= 3\,Tr(Y_d^\dagger Y_d) + Tr(Y_e^\dagger Y_e)\,. \end{aligned} \tag{2.39}$$

2.5.1 MSSM

The MSSM, as a limiting case of the 5D models we shall consider in the following, and also when $0 < t < \ln(\frac{1}{M_Z R})$ (that is the energy we consider for the evolution from M_Z to $1/R$) the coefficients in the evolution equations are:

$$\begin{aligned} G_{dMSSM} &= \left(\frac{7}{15}g_1^2 + 3g_2^2 + \frac{16}{3}g_3^2\right)\,, \\ G_{uMSSM} &= \left(\frac{13}{15}g_1^2 + 3g_2^2 + \frac{16}{3}g_3^2\right)\,, \\ G_{eMSSM} &= \left(\frac{9}{5}g_1^2 + 3g_2^2\right)\,, \\ \alpha_{MSSM} &= 2\,T_u - \frac{6}{5}g_1^2 - 6g_2^2\,, \\ C_{MSSM} &= 1\,, \\ \tilde{C}_{MSSM} &= 1\,. \end{aligned} \tag{2.40}$$

These coefficients are modified when we enter the energy regime where the effects of the extra dimensions set in. The modifications depend on which particles are decoupled and on the structure of the model. We shall consider two cases, one in which all particles can propagate in the extra dimensions (bulk case) and the other in which fermionic matter fields are constrained to the brane (brane case).

2.5.2 Bulk

When the energy scale $E > 1/R$ or when the energy scale parameter $t > \ln(\frac{1}{M_Z R})$, the coefficients in the 5D MSSM, for all three generations propagating in the bulk, can be expressed

as:

$$\begin{aligned}
G_{d5Dbulk} &= \left(\frac{7}{15}g_1^2 + 3g_2^2 + \frac{16}{3}g_3^2\right) S(t) \,, \\
G_{u5Dbulk} &= \left(\frac{13}{15}g_1^2 + 3g_2^2 + \frac{16}{3}g_3^2\right) S(t) \,, \\
G_{e5Dbulk} &= \left(\frac{9}{5}g_1^2 + 3g_2^2\right) S(t) \,, \\
\alpha_{5Dbulk} &= 2\tilde{C}_{5Dbulk}T_u - (\frac{6}{5}g_1^2 + 6g_2^2)S(t) \,, \\
C_{5Dbulk} &= \pi S(t)^2 \,, \\
\tilde{C}_{5Dbulk} &= \pi S(t)^2 \,.
\end{aligned} \tag{2.41}$$

2.5.3 Brane

However, when all matter superfields are constrained to live on the 4D brane, the quadratic evolution due to the sum over the two KK towers will be milder. We note also that the traces are the same in the MSSM because we do not have a fermionic loop in the extra-dimension in the brane case. The coefficients of the evolution equations are given by:

$$\begin{aligned}
G_{d5Dbrane} &= \left(\frac{19}{30}g_1^2 + \frac{9}{2}g_2^2 + \frac{32}{3}g_3^2\right) S(t) \,, \\
G_{u5Dbrane} &= \left(\frac{43}{30}g_1^2 + \frac{9}{2}g_2^2 + \frac{32}{3}g_3^2\right) S(t) \,, \\
G_{e5Dbrane} &= \left(\frac{33}{10}g_1^2 + \frac{9}{2}g_2^2\right) S(t) \,, \\
\alpha_{5Dbrane} &= 2\ T_u - (\frac{9}{5}g_1^2 + 9g_2^2)S(t) \,, \\
C_{5Dbrane} &= 2S(t) \,, \\
\tilde{C}_{5Dbrane} &= 1 \,.
\end{aligned} \tag{2.42}$$

2.6 Scaling of the Yukawa couplings and the CKM matrix

It is well known that in the SM, the quark sector's flavour mixing is parameterized by the CKM matrix:

$$V_{CKM} = \begin{pmatrix} V_{ud} & V_{us} & V_{ub} \\ V_{cd} & V_{cs} & V_{cb} \\ V_{td} & V_{ts} & V_{tb} \end{pmatrix} = \begin{pmatrix} V_{11} & V_{12} & V_{13} \\ V_{21} & V_{22} & V_{23} \\ V_{31} & V_{32} & V_{33} \end{pmatrix} \,, \tag{2.43}$$

which makes it possible to explain all flavour changing weak decay processes and CP-violating phenomena to date, where the 10 year run of Babar at SLAC [125] and the Belle detector at KEK [126] has greatly improved our knowledge of the CKM matrix elements. In particular, for the standard parameterization of the CKM matrix, which has the form:

$$V_{CKM} = \begin{pmatrix} c_{12}c_{13} & s_{12}c_{13} & s_{13}e^{-i\delta} \\ -s_{12}c_{23} - c_{12}s_{23}s_{13}e^{i\delta} & c_{12}c_{23} - s_{12}s_{23}s_{13}e^{i\delta} & s_{23}c_{13} \\ s_{12}s_{23} - c_{12}c_{23}s_{13}e^{i\delta} & -c_{12}s_{23} - s_{12}c_{23}s_{13}e^{i\delta} & c_{23}c_{13} \end{pmatrix} , \tag{2.44}$$

where $s_{12} = \sin\theta_{12}$, $c_{12} = \cos\theta_{12}$ etc. are the sines and cosines of the three mixing angles θ_{12}, θ_{23} and θ_{13}, and δ is the CP violating phase.

The CKM matrix arises from a consideration of the square of the quark Yukawa coupling matrices being diagonalized by using two unitary matrices U and V,

$$\begin{aligned} \text{diag}\left(f_u^2, f_c^2, f_t^2\right) &= U Y_u^\dagger Y_u U^\dagger , \\ \text{diag}\left(h_d^2, h_s^2, h_b^2\right) &= V Y_d^\dagger Y_d V^\dagger , \end{aligned} \tag{2.45}$$

in which f_u^2, f_c^2, f_t^2 and h_d^2, h_s^2, h_b^2 are the eigenvalues of $Y_u^\dagger Y_u$ and $Y_d^\dagger Y_d$ respectively. It follows that the CKM matrix appears as a result of the transition from the quark flavour eigenstates to the quark mass eigenstates upon this diagonalization of the quark mass matrices:

$$V_{CKM} = U V^\dagger . \tag{2.46}$$

From the full set of one-loop coupled RGE for the Yukawa couplings and the CKM matrix, together with those for the gauge coupling equations, one can obtain the renormalisation group flow of all observables related to up- and down-quark masses and the CKM matrix elements.

The RGEs are very important tools to show the properties of the quark masses and the CKM matrix at different energy scales. We write down the general form for the evolution of f_i^2, h_j^2 and the variation of each element of the CKM matrix V_{ik} [95, 102, 112] in the SM, the UED SM, the MSSM and the 5D MSSM.

2.6.1 SM, UED Bulk SM and UED Brane SM

$$\begin{aligned} 16\pi^2 \frac{df_i^2}{dt} &= f_i^2[2(T_u A - G_u) + 3Bf_i^2 - 2B\sum_j h_j^2 |V_{ij}|^2] , \\ 16\pi^2 \frac{dh_j^2}{dt} &= h_j^2[2(T_d A - G_d) + 3Bh_j^2 - 2B\sum_i f_i^2 |V_{ij}|^2] , \\ 16\pi^2 \frac{dy_e^2}{dt} &= y_e^2[2(T_e A - G_e) + 3By_e^2] , \\ 16\pi^2 \frac{dV_{ik}}{dt} &= -\frac{3}{2}B\left[\sum_{m,j\neq i} \frac{f_i^2 + f_j^2}{f_i^2 - f_j^2} h_m^2 V_{im} V_{jm}^* V_{jk} + \sum_{j,m\neq k} \frac{h_k^2 + h_m^2}{h_k^2 - h_m^2} f_j^2 V_{jm}^* V_{jk} V_{im}\right] , \end{aligned} \tag{2.47}$$

where $A = B = 1$ in the SM, $A = 2S(t) - 1$, $B = S(t)$ in the UED Bulk SM and $A = 0$, $B = 2S(t)$ in the UED Brane SM. The gauge couplings G for the SM, the UED Bulk SM and the UED Brane SM are written in Eq.(2.35), Eq.(2.36) and Eq.(2.37) respectively.

2.6.2 MSSM, 5D bulk and 5D brane

$$\begin{aligned}
16\pi^2\frac{df_i^2}{dt} &= f_i^2[2(T_u\tilde{C} - G_u) + 6Cf_i^2 + 2C\sum_j h_j^2|V_{ij}|^2] \\
16\pi^2\frac{dh_j^2}{dt} &= h_j^2[2(T_d\tilde{C} - G_d) + 6Ch_j^2 + 2C\sum_i f_i^2|V_{ij}|^2] \,, \\
16\pi^2\frac{dy_e^2}{dt} &= y_e^2[2(T_e\tilde{C} - G_e) + 6Cy_e^2] \,, \\
16\pi^2\frac{dV_{ik}}{dt} &= C\left[\sum_{m,j\neq i}\frac{f_i^2+f_j^2}{f_i^2-f_j^2}h_m^2V_{im}V_{jm}^*V_{jk} + \sum_{j,m\neq k}\frac{h_k^2+h_m^2}{h_k^2-h_m^2}f_j^2V_{jm}^*V_{jk}V_{im}\right] \,,
\end{aligned} \tag{2.48}$$

where we use the same forms as in Eqs.(2.40,2.41,2.42) to fix the coefficients C, $\tilde{C}$ and gauge couplings G to describe each model.

2.7 Comparison of the models and implications

In the following we compare the main results for the different models and their physical meaning both in term of experimental limits and of the theoretical implications. However, as pointed out in the appendix C, there is a subtlety involved the running of the physical parameters in the UED bulk model. Although we plot their running up to the gauge unification scale, in fact, as illustrated in fig. C.1, the introduction of new ultraviolet cutoff becomes imperative due to the scalar potential stability condition, and beyond this scale new physics should appear. For further discussion and quantitative analysis in the UED bulk model, refer to Ref [127] for details. In contrast, in the UED brane model, the physics parameters have a full running till the gauge unification scale, since the Higgs self coupling evolution has a finite value which thus excludes the vacuum stability concern and validates the theory up its full scale [112].

2.7.1 Top Yukawa coupling

UED SM: Bulk and Brane cases

In fig. 2.5 the initial Yukawa couplings are given by the ratios of the fermion masses to the Higgs vacuum expectation value. The Yukawa couplings evolve in the usual logarithmic fashion when the energy is below 2 TeV, 8 TeV, and 15 TeV for the three different cases. However, once

the first KK threshold is reached, the contributions from the KK states become more and more significant. The evolution of f_t (see Eq.(2.47)) depends explicitly on the cutoff Λ, which have finite one-loop corrections to the beta functions at each massive KK excitation level. Therefore, the running of the Yukawa couplings, or more precisely, the one-loop KK corrected effective four dimensional Yukawa couplings, begins to deviate from their normal orbits and start to evolve faster and faster. For the compactification radius $R^{-1} = 2$ TeV, the Yukawa couplings evolve faster than the other two, reaching its minimum value at the unification scale, after that point their evolution will "blow-up" due to the faster running of the gauge couplings and new physics would come into play. For the radius $R^{-1} = 8$ TeV, we find similar behaviour to the $R^{-1} = 2$ TeV case, where the blow-up scale is not very far from that of 2 TeV case. However, for the third choice of radius, since the compactification radius is now much higher than the other two, we need more energy to push it further toward its "blow-up" point, which is at a higher unification scale. We also observe that the Yukawa couplings are quickly evolving to zero, however, a satisfactory unification of these seems to still be lacking. In the UED scenario, the unification of the Yukawa couplings is very desirable due to the fast power law running. As such, we have so far observed the Yukawa couplings all decrease with increasing energy, which agrees with what is observed in the SM, however, the Yukawa couplings are driven dramatically towards extremely weak values at a much faster rate. This is an interesting feature that distinguishes the UED model from that of the SM.

5D MSSM Bulk

The 4D MSSM contains the particle spectrum of a two-Higgs doublet model extension of the SM and the corresponding supersymmetric partners. After the spontaneous breaking of the electroweak symmetry, five physical Higgs particles are left in the spectrum. The two

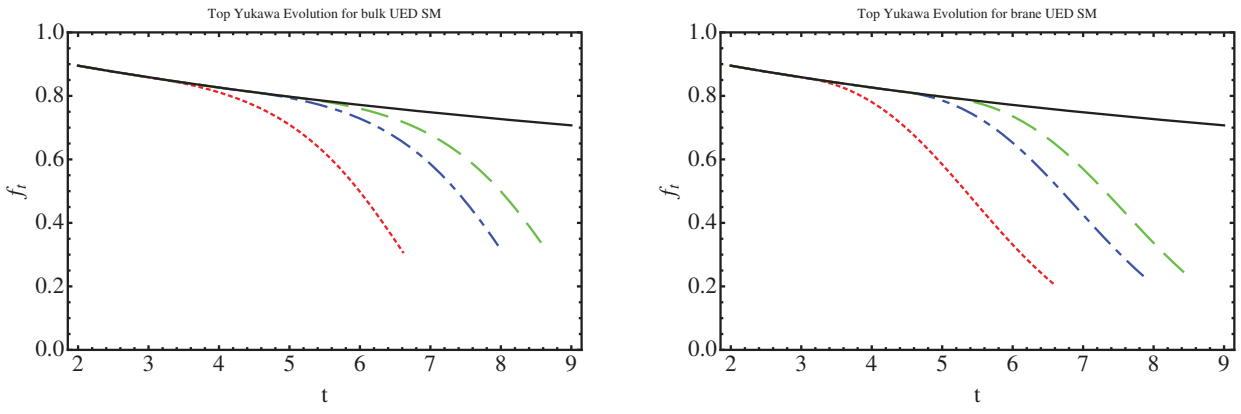

Figure 2.5: The Yukawa coupling f_t for the top quark in the UED SM as a function of the scale parameter t, for the bulk case (left panel) and the brane case (right panel) where the solid line is the SM evolution and for different compactification scales: $R^{-1} = 2$ TeV (red, dotted line), 8 TeV (blue,dot-dashed line), and 15 TeV (green,dashed line).

Higgs doublets H_u and H_d, with opposite hypercharges, are responsible for the generation of the up-type and down-type quarks respectively. The vacuum expectation values of the neutral components of the two Higgs fields satisfy the relation ${v_u}^2 + {v_d}^2 = \left(\frac{246}{\sqrt{2}}\right)^2 = (174GeV)^2$. The fermion mass matrices appear after the spontaneous symmetry breaking from the fermion-Higgs Yukawa couplings. As a result, the initial Yukawa couplings are given by the ratios of the fermion masses to the appropriate Higgs vacuum expectation values as follows:

$$f_{u,c,t} = \frac{m_{u,c,t}}{v_u} \quad , \quad h_{d,s,b} = \frac{m_{d,s,b}}{v_d} \quad , \quad y_{e,\mu,\tau} = \frac{m_{e,\mu,\tau}}{v_d} \ , \tag{2.49}$$

where we define $\tan\beta = v_u/v_d$, which is the ratio of vacuum expectation values of the two Higgs fields H_u and H_d.

From the complete sets of the RGEs we can run the renormalisation group flow of all observables related to up- and down-quark masses and the quark flavour mixings. For our numerical analysis we assume the fundamental scale is not far from the range of LHC scale, and set the compactification scale to be $R^{-1} = 2$ TeV, 8 TeV, and 15 TeV respectively.

Actually, below the supersymmetric breaking scale the Yukawa and gauge couplings run in the usual logarithmic fashion, giving a rather slow change for their values. Therefore, for supersymmetric breaking theories around TeV scales, for simplicity, we take the supersymmetric breaking scale $M_{SUSY} = M_Z$ in the present numerical study, and run the RGEs from M_Z up to the high energy scales for our three different compactification scales.

Additionally, as illustrated in fig. 2.6, for the case of universal 5D MSSM, once the first KK threshold is crossed at $\mu = R^{-1}$, the power law running of the various beta functions causes the Yukawa coupling to rapidly increase following the rapid increase in the gauge coupling constants in the left panel of fig. 2.4. From Eq.(2.48) and Eq.(2.41) we can find the quadratic term of $S(t)$ providing a positive contribution to the Yukawa beta functions, which is in contrast to beta functions of the gauge couplings (which include terms only linear in $S(t)$). Therefore, from Eq.(2.48), the positive contribution from $S(t)$ terms will dominate the negative contributions from the gauge couplings, and cause the Yukawa couplings to increase rapidly. This behaviour can be observed for both small and large $\tan\beta$ cases. However, as illustrated in the first graph of fig. 2.6, for small $\tan\beta$, the Yukawa coupling has a large initial value, therefore it blows up at a relatively low energy as compared with the case for large $\tan\beta$. As a result, as one evolves upward in the scale, the top Yukawa coupling is rising with a fast rate and is pushed up against the Landau pole where it becomes divergent and blows up. In the vicinity of this singular point the perturbative calculation becomes invalid, and the higher order corrections become significant. The Landau pole also indicates that there is an upper limit on the value of the gauge couplings where new physics must emerge before the Yukawa couplings diverge.

5D MSSM Brane

In the brane localised matter field scenario, the beta function has only linear terms in $S(t)$, which is comparable with the $S(t)$ term in the beta function for the gauge couplings. As depicted in fig. 2.7, for a small value of $\tan\beta$, we have a large initial value of f_t and the gauge coupling contribution to the Yukawa beta function is sub-dominant only. Therefore, as

discussed previously, the Yukawa coupling f_t increases rapidly as one crosses the KK threshold at $\mu = R^{-1}$, resulting in a rapid approach of the singularity before the unification scale is reached. However, for an intermediate value of $\tan\beta$, we have a relative smaller initial condition for the top Yukawa coupling and the Yukawa terms in the beta function become less important. The contributions from the gauge couplings may then become significant, which leads to a net negative contribution to the beta functions. Therefore, the curvature of the trajectory of the top Yukawa evolution might change direction, and the Yukawa evolution will decrease instead of increasing. This behaviour would become more obvious for a large value of $\tan\beta$. As observed in fig. 2.7, for $\tan\beta = 30$, we indeed observe the decreasing behaviour of the top Yukawa couplings. This behaviour provides a very clear phenomenological signature, especially for scenarios with a larger $\tan\beta$ and that are valid up to the unification scale where the gauge couplings converge.

2.7.2 CKM Matrix

Because of the arbitrariness in choice of phases of the quark fields, the phases of individual matrix elements of the V_{CKM} are not themselves directly observable. Among these we therefore use the absolute values of the matrix element $|V_{ij}|$ as the independent set of rephasing invariant variables. Of the nine elements of the CKM matrix, only four of them are independent, which is consistent with the four independent variables of the standard parametrisation of the CKM matrix. For definiteness we choose the $|V_{ub}|$, $|V_{cb}|$, $|V_{us}|$ and the Jarlskog rephasing invariant parameter $J = \mathrm{Im} V_{ud} V_{cs} V_{us}^* V_{cd}^*$ as the four independent parameters of V_{CKM}.

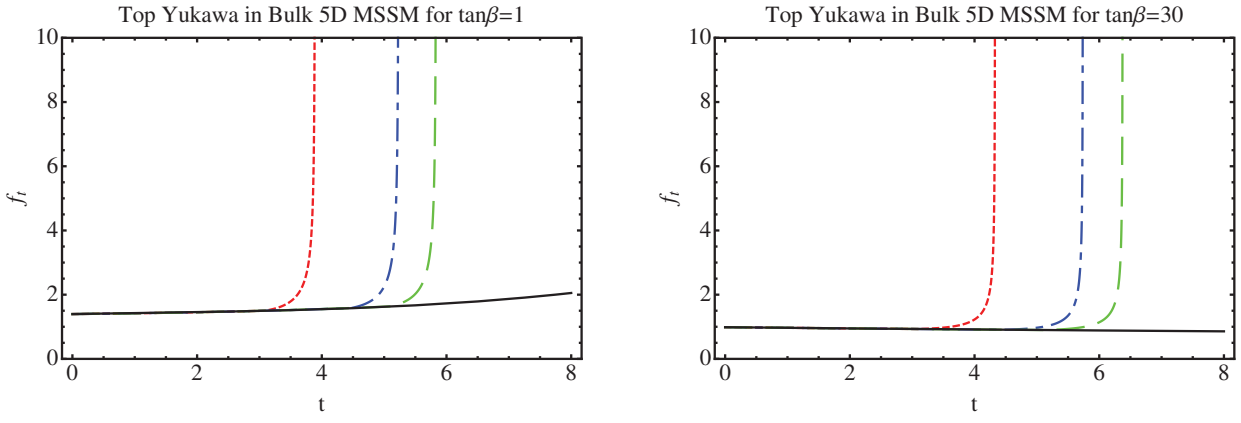

Figure 2.6: The Yukawa coupling f_t for the top quark in the bulk case of 5D MSSM as a function of the scale parameter t, for (left panel) $\tan\beta = 1$ and (right panel) $\tan\beta = 30$ where the solid line is the MSSM evolution and for different compactification scales: $R^{-1} = 2$ TeV (red, dotted line), 8 TeV (blue, dot-dashed line), and 15 TeV (green, dashed line).

UED SM

In fig. 2.8 we specially plot the evolution of $|V_{ub}|$ for the UED bulk and brane cases. For the evolution of $|V_{cb}|$ and $|V_{us}|$ we can observe similar behaviours, i.e., they all increase with the energy scale; the variation rate become faster once the KK threshold is passed. The absolute values of all the remaining magnitudes of the CKM matrix elements can be obtained from the unitarity equations, as depicted in fig. 2.8, with increasing energy the running of the CKM matrix shows a pronounced pattern at the point where the KK modes are excited, thus we could determine the renormalisation group evolutions of the full CKM matrix. As can be seen from Eq.(2.47), the evolution of the CKM matrix is governed by the Yukawa couplings and the factor $S(t)$. They evolve faster in the region where the power law scaling of the Yukawa couplings becomes substantial. Therefore, the renormalisation effect is explicit for mixings involving the third family, i.e., $|V_{ub}|$ and $|V_{cb}|$, due to the large value of their Yukawa couplings. Because of the smallness of the Yukawa coupling terms, the renormalisation group flow of the mixing between the first two families, i.e., the Cabibbo angle of $|V_{us}|$, turns out to be very small. Although the mixing angle increases all the time, it is rather inert, even in the UED model.

5D MSSM

In figs. 2.9 and 2.10 we plot the energy dependence of $|V_{ub}|$ from the weak scale all the way up to the high energy scales for different values of compactification radii R^{-1} for the bulk 5D MSSM case brane localised matter fields case respectively. In these sets of pictures we consider two indicative choices of $\tan\beta$, that of $\tan\beta = 1$ and $\tan\beta = 30$.

The running of the CKM matrix is governed by the terms related to the Yukawa couplings.

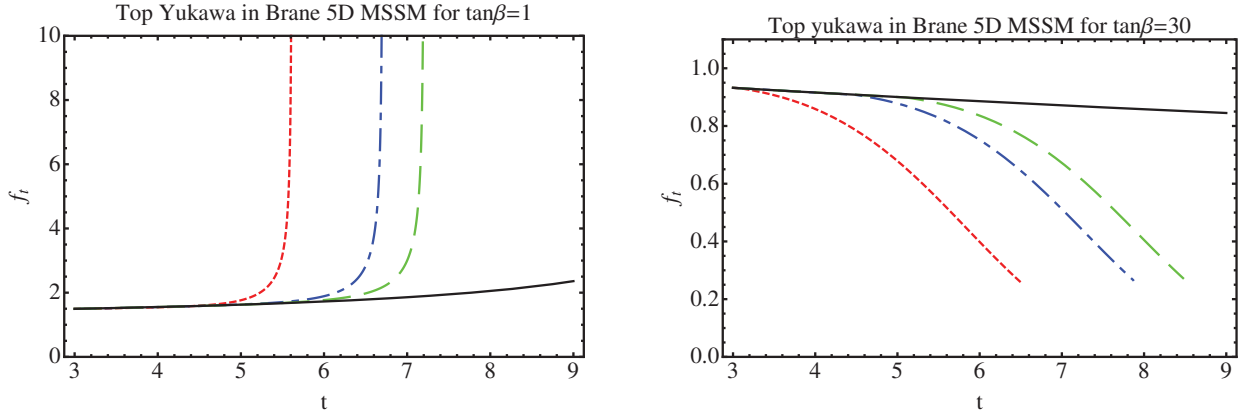

Figure 2.7: The Yukawa coupling f_t for the top quark in the brane case of 5D MSSM as a function of the scale parameter t, for (left panel) $\tan\beta = 1$ and (right panel) $\tan\beta = 30$ where the solid line is the MSSM evolution and for different compactification scales: $R^{-1} = 2$ TeV (red, dotted line), 8 TeV (blue, dot-dashed line), and 15 TeV (green, dashed line).

These Yukawa couplings are usually very small, except for the top Yukawa coupling (which could give a sizeable contribution). The CKM matrix element $V_{ub} \simeq \theta_{13} e^{-i\delta}$ can be used to observe the mixing angle, θ_{13}. It decreases with the energy scale in a similar manner regardless of whether $\tan\beta$ is small or large. However, for a large initial value of f_t (small $\tan\beta$), the mixing angles have a more rapid evolution and end in the regime where the top Yukawa diverges and develops a singularity. Quantitatively we observe from these plots that the value of $|V_{ub}|$ change by more than 50%.

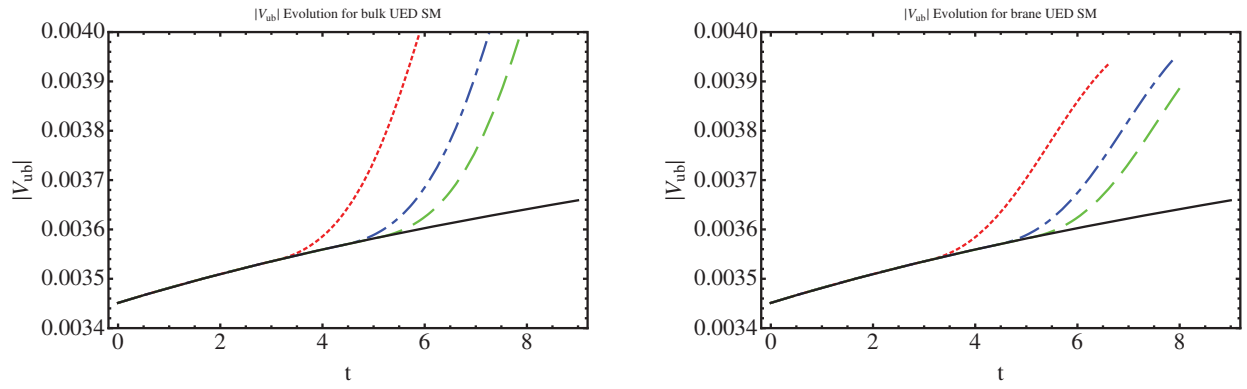

Figure 2.8: The CMK matrix elements $|V_{ub}|$ in the UED SM as a function of the scale parameter t, for the bulk case (left panel) and the brane case (right panel) where the solid line is the SM, for different compactification scales: $R^{-1} = 2$ TeV (red, dotted line), 8 TeV (blue,dot-dashed line), and 15 TeV (green, dashed line).

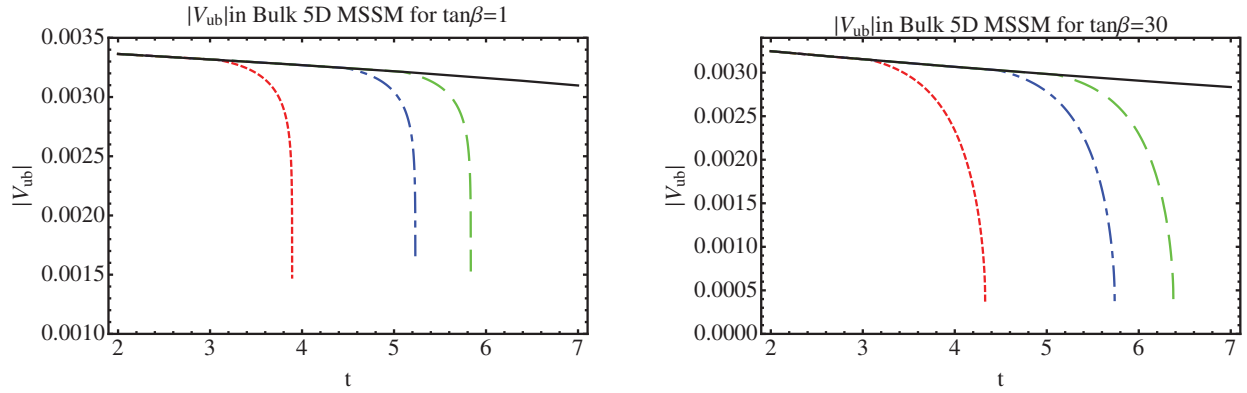

Figure 2.9: The CMK matrix elements $|V_{ub}|$ in the bulk case of 5D MSSM as a function of the scale parameter t, for (left panel) $\tan\beta = 1$ and (right panel) $\tan\beta = 30$ where the solid line is the MSSM evolution and for different compactification scales: $R^{-1} = 2$ TeV (red, dotted line), 8 TeV (blue, dot-dashed line), and 15 TeV (green, dashed line).

2.7.3 The Jarlskog parameter

UED SM

We next turn our attention to the quark flavour mixing matrix, especially the complex phase of the CKM matrix which characterizes CP-violating phenomena. This phenomena has been unambiguously verified in a number of $K - \bar{K}$ and $B - \bar{B}$ systems. For the parameter J (fig. 2.11), the characteristic parameter for the CP non-conservation effects, its variation becomes very significant. The larger the value of the compactification radius R, the faster J evolves to reach its maximum. We observe an approximate 30% increase for J at the unification scale compared with its initial value.

5D MSSM

From figs. 2.12, in contrast, the Jarlskog parameter decreases quite rapidly once the initial KK threshold is passed. However, when $\tan\beta$ is large, we have a relatively longer distance between the initial and terminating energy track, the evolution of J can be driven towards zero or even further. Besides, as can be seen explicitly in [111], the beta functions of the evolution equations of the CKM elements are up to the third order of the CKM elements, which are comparable smaller than that of Jarlskog parameter's quadratic dependence on the CKM elements. This fact then leads to the relatively large variation of J with the increase of energy. Furthermore, for $\tan\beta = 30$, the Jarlskog parameter drops almost to zero, which sets the effect of the SM CP violation to being very small. Note, however, that in a supersymmetric theory other sources of CP violation beyond the SM ones are typically present, therefore only a complete and detailed study of a specific model would allow us to establish the strength of the CP violating effects.

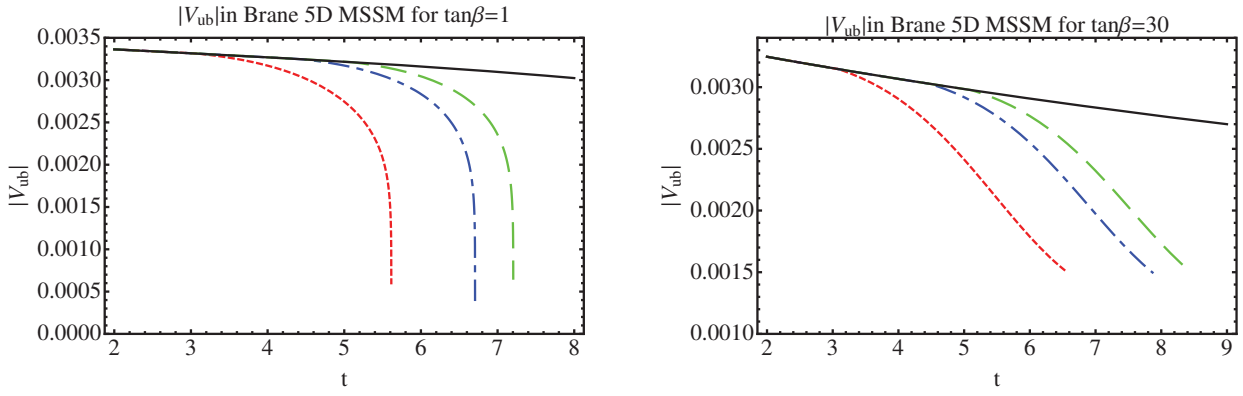

Figure 2.10: The CMK matrix elements $|V_{ub}|$ in the brane case of 5D MSSM as a function of the scale parameter t, for (left panel) $\tan\beta = 1$ and (right panel) $\tan\beta = 30$ where the solid line is the MSSM evolution and for different compactification scales: $R^{-1} = 2$ TeV (red, dotted line), 8 TeV (blue, dot-dashed line), and 15 TeV (green, dashed line).

For the matter fields constrained to the brane, in figs. 2.10 and 2.13 we observe that the evolutions of these mixing angles and CP violation parameter are decreasing irrespective of whether the top Yukawa coupling grows or not. For small $\tan\beta$ we see similar evolution behaviours for these parameters as in the bulk case. The decreases in the value of V_{ub} and J are much steeper, due to rapid growth of the top Yukawa coupling near the singular point. However, as $\tan\beta$ becomes larger, e.g. $\tan\beta = 30$, the top Yukawa coupling evolves downward instead of upward. The decreases in these CKM parameters then becomes much milder towards the unification scale; though the reduction to effectively zero in the Jarlskog parameter persists. As a result, for the brane localised matter field scenario, it is more desirable to have a large $\tan\beta$ for theories that are valid up to the gauge coupling unification scale.

2.8 Conclusion

In summary, for the two 5D MSSM scenarios with matter fields in the bulk or on the brane, we have performed the numerical analysis of the evolution of the various parameters of the CKM matrix, and both cases give us a scenario with small or no quark flavour mixings at high energies, especially for the mixings with the heavy generation. The evolution equations which relate various observables at different energies, and also allow the study of their asymptotic behaviours, are particularly important in view of testing the evolution of the Yukawa couplings. In the universal 5D MSSM model, the evolution of these CKM parameters have a rapid variation prior to reaching a cut-off scale where the top Yukawa coupling develops a singularity point and the model breaks down. For the brane localised matter fields model, we can only observe similar behaviours for small values of $\tan\beta$, while for large $\tan\beta$, the initial top Yukawa coupling becomes smaller, the gauge couplings then play a dominant role during the evolution of the Yukawa couplings, which cause the Yukawa couplings to decrease instead of increasing. As such

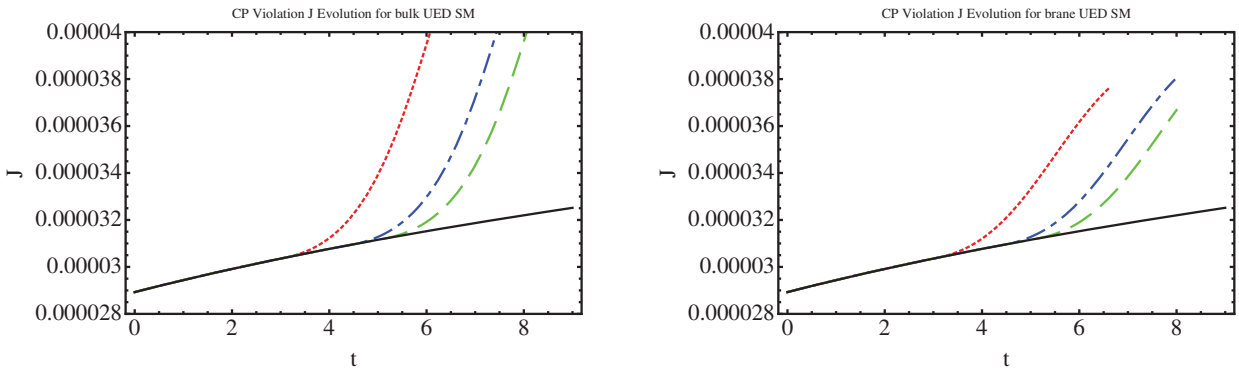

Figure 2.11: The Jarlskog parameter J in the UED SM as a function of the scale parameter t, for the bulk case (left panel) and the brane case (right panel) where the solid line is the SM, for different compactification scales: $R^{-1} = 2$ TeV (red, dotted line), 8 TeV (blue, dot-dashed line), and 15 TeV (green, dashed line).

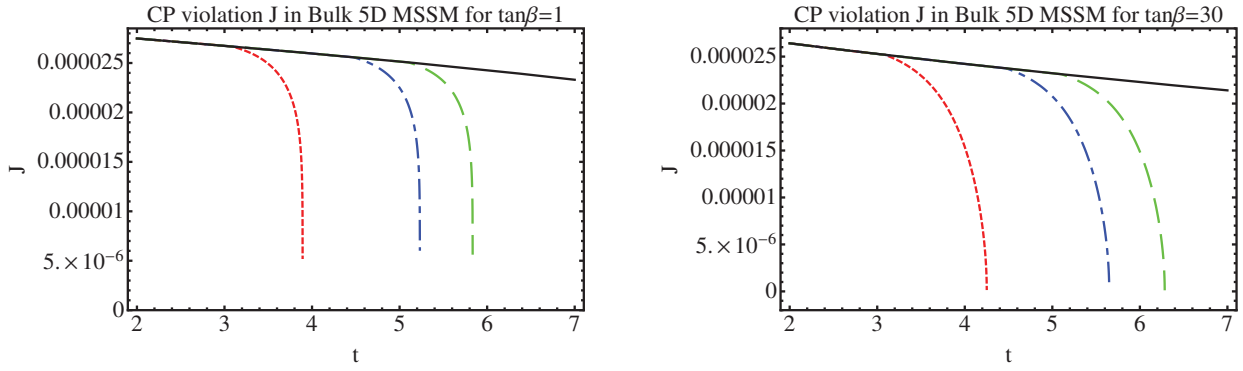

Figure 2.12: The Jarlskog parameter J in the bulk case of 5D MSSM as a function of the scale parameter t, for (left panel) $\tan\beta = 1$ and (right panel) $\tan\beta = 30$ where the solid line is the MSSM evolution and for different compactification scales: $R^{-1} = 2$ TeV (red, dotted line), 8 TeV (blue, dot-dashed line), and 15 TeV (green, dashed line).

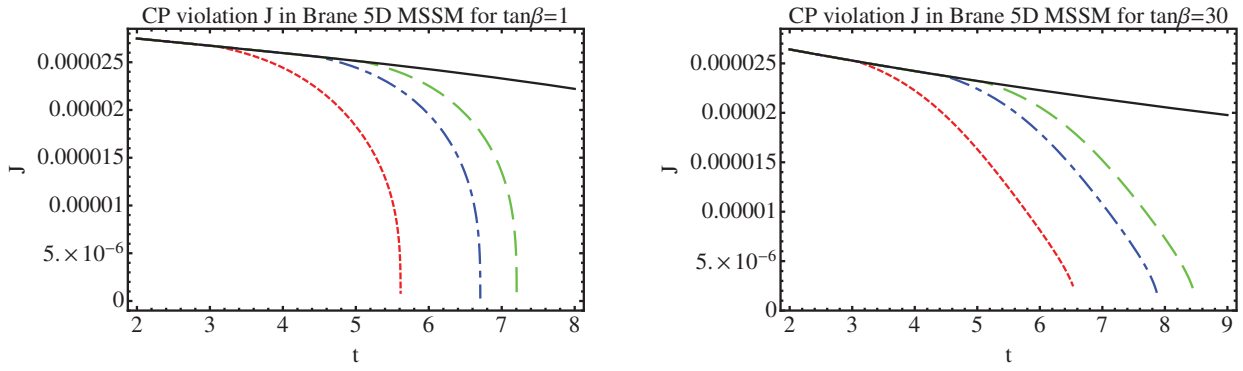

Figure 2.13: The Jarlskog parameter J in the brane case of 5D MSSM as a function of the scale parameter t, for (left panel) $\tan\beta = 1$ and (right panel) $\tan\beta = 30$ where the solid line is the MSSM evolution and for different compactification scales: $R^{-1} = 2$ TeV (red, dotted line), 8 TeV (blue, dot-dashed line), and 15 TeV (green, dashed line).

the variations of these CKM parameters have a relatively milder behaviour, and the theory is valid up the gauge coupling unification scale.

Chapter 3

Masses and Mixing angles evolution for neutrinos in UED models

3.1 Introduction

In the last decade, our perspectives in the search for physics Beyond the Standard Model (BSM) have seen the development of theories with extra (compact) dimensions. TeV-scale extra-dimensional models have allowed us to build effective models which can be tested at the present and next generation of colliders, where these wide varieties of extra-dimensional models have been proposed to solve, or at least understand from a geometrical perspective, different theoretical problems arising in the Standard Model (SM) and in its four-dimensional space-time extensions.

Another ingredient which can be introduced, supersymmetry, and in particular its minimal low energy construction, the MSSM, has long been held to play a central role in BSM physics; even if at present there is no evidence at colliders for the supersymmetric partners of the SM particles. From a theoretical point of view, supersymmetry plays a key role in resolving many problems in the SM and BSM physics; from gauge coupling unification, to the hierarchy problem, to the building of realistic grand unification models. The combination of supersymmetry and the physics of extra-dimensions has the added bonus of stabilising the extra-dimensional theory from quantum fluctuations, as well as the extra-dimensions potentially providing a mechanism for supersymmetry breaking. Indeed, four-dimensional supersymmetric models typically lack a simple mechanism for supersymmetry breaking, which the extra-dimensions may offer.

Neutrinos are generally taken to be massless in the SM, and the experimental evidence for nonzero neutrino masses implicit in the neutrino oscillations measurements, gives an important indication for physics BSM. In fact, neutrino masses are many orders of magnitude smaller than those of quarks and charged leptons. However, contrary to the small mixings in the quark sector, two of the lepton mixing angles are identified as being rather large, close to maximal. For an overview of the present knowledge of neutrino masses and mixings see Refs. [128,129] and references therein. The most recent experimental evidence of this fact is the measurement of the θ_{13} mixing parameter by the Daya Bay, Double Chooz and RENO experiments [130–132]. The implication of three sizable mixing angles are huge, and will surely boost the number

of investigations of the neutrino mixings and phases in the near future; in particular, this result suggests the possibility of measuring leptonic CP violation. The neutrino sector seems, therefore, to continue to play a special role in understanding BSM physics.

The generation of such masses and phases remains an open question. By including right-handed neutrinos into the Standard Model, it is possible to explain the neutrino masses with SM Higgs mechanism only. However the Yukawa couplings of neutrinos will be very small. In this context, theorists develop already some models, like the *see-saw* model [133], which address the smallness of the neutrino masses by giving large masses to right-handed neutrinos that will couple with left-handed neutrinos through Yukawa couplings. Moreover many properties of the PMNS matrix, like unitarity or majorana phases, need to be understood.

Recall also that quark and lepton masses and mixing angles are free parameters in minimal extensions to the SM. Also, as neutrino mixing angles show a pattern that is completely different from that of quark mixings, the relative wealth of the latest experimental data has motivated efforts on the theoretical side to understand the possible patterns of neutrino masses and mixings, and therefore to expose the underlying fundamental symmetries behind them. As such, understanding the evolution of these neutrino sector parameters will be critical as higher energy experiments probe this sector.

3.2 Neutrino parameter evolutions

In a similar way to what done for quark parameters, we can study the evolution of the masses, mixing and phases in the neutrino sector. In the following we first establish our conventions for these parameters and introduce the main present bounds and values from experiments. We than introduce the corresponding renormalisation evolution equations in the various models and discuss the numerical values obtained for the evolution of the parameters in different models, as previously done for the quark sector.

3.2.1 Conventions for masses and mixing parameters

The mixing matrix which relates gauge and mass eigenstates is defined to diagonalize the neutrino mass matrix in the basis where the charged lepton mass matrix is diagonal. It is usually parameterised as follows [134]:

$$U = \begin{pmatrix} c_{12}c_{13} & s_{12}c_{13} & s_{13}e^{-i\delta} \\ -s_{12}c_{23} - c_{12}s_{23}s_{13}e^{-i\delta} & c_{12}c_{23} - s_{12}s_{23}s_{13}e^{i\delta} & s_{23}c_{13} \\ s_{12}s_{23} - c_{12}c_{23}s_{13}e^{i\delta} & -c_{12}s_{23} - s_{12}c_{23}s_{13}e^{i\delta} & c_{23}c_{13} \end{pmatrix} \begin{pmatrix} e^{i\phi_1} & & \\ & e^{i\phi_2} & \\ & & 1 \end{pmatrix},$$

with $c_{ij} = \cos\theta_{ij}$ and $s_{ij} = \sin\theta_{ij}$ $(ij = 12, 13, 23)$. We follow the conventions of Ref. [124] to extract mixing parameters from the PMNS matrix.

Experimental information on neutrino mixing parameters and masses is obtained mainly from oscillation experiments. In general Δm^2_{atm} is assigned to a mass squared difference between ν_3 and ν_2, whereas Δm^2_{sol} to a mass squared difference between ν_2 and ν_1. The current observational values are summarized in Table 3.1. Data indicates that $\Delta m^2_{sol} \ll \Delta m^2_{atm}$, but

the masses themselves are not determined. In this work we have adopted the masses of the neutrinos at the M_Z scale as $m_1 = 0.1$ eV, $m_2 = 0.100379$ eV, and $m_3 = 0.11183$ eV, as the *normal* hierarchy (whilst any reference to an *inverted* hierarchy would refer to $m_3 = 0.1$ eV, with $m_3 < m_1 < m_2$ and satisfying the above bounds). For the purpose of illustration, we choose values for the angles and phases as the M_Z scale as: $\theta_{12} = 34^o$, $\theta_{13} = 8.83^o$, $\theta_{23} = 46^o$, $\delta = 30^0$, $\phi_1 = 80^o$ and $\phi_2 = 70^o$.

Parameter	Value (90% CL)
$\sin^2(2\theta_{12})$	$0.861(^{+0.026}_{-0.022})$
$\sin^2(2\theta_{23})$	> 0.92
$\sin^2(2\theta_{13})$	0.092 ± 0.017
Δm^2_{sol}	$(7.59 \pm 0.21) \times 10^{-5} eV^2$
Δm^2_{atm}	$(2.43 \pm 0.13) \times 10^{-3}\ eV^2$

Table 3.1: Present limits on neutrino masses and mixing parameters used in the text. Data is taken from Ref. [120] and from Ref. [130] for $\sin^2(2\theta_{13})$.

The evolution equation for the observables in our 5D MSSM are taken from [103]. As expected $\tan\beta$ plays an important role as all the mixing angles and phases depend on y_τ (see appendix D). However, the new degrees of freedom (the extra-dimensional fields giving rise to KK excitations of the zero modes) become important at energies corresponding to their masses. In the following we study the evolution of the relevant parameters, such as Δm^2_{sol}, Δm^2_{atm} and the angles and phases, as a function of the energy scale and of $\tan\beta$. Only some selected plots will be shown and we will comment on the other similar cases not explicitly shown.

3.2.2 Δm^2_{sol} and Δm^2_{atm}

For the UED SM, we see different behaviour for the brane case fig. 3.1 and bulk case fig. 3.2. Once the KK threshold is reached, both Δm^2_{sol} and Δm^2_{atm} decrease with increasing energy in the brane case, but they increase with the energy in the bulk case for the different radii of compactification. The evolution of masses depends on the evolution of y_τ and k coupling and the RG runnings in the UED SM bulk model are generally larger than those in UED SM brane model. This is due to the fact that the coefficient $C_1 = 0$ in the brane model (see Eq.(2.37)) and $2(S(t) - 1)$ in the bulk model (see Eq.(2.36)) and also there is difference in α in the two equations due to the trace of charged-fermion Yukawa couplings in bulk model whereas such a contribution does not exist in brane model due to the absence of fermion KK excitations (see the T term in Eq.(2.35)). This lead to the increasing of observables in the bulk case and the decreasing in the brane case.

For the 5D MSSM, in general, in the brane case, the evolution has the same form for the three masses m_1, m_2, m_3. This leads to a reduction of up to a factor of two for the masses at $t = 6$ (for a large radius, $R^{-1} = 1$ TeV) with respect to the MSSM values at low energies (smaller radii give a weaker effect as the KK excitations contribute to the evolution equations

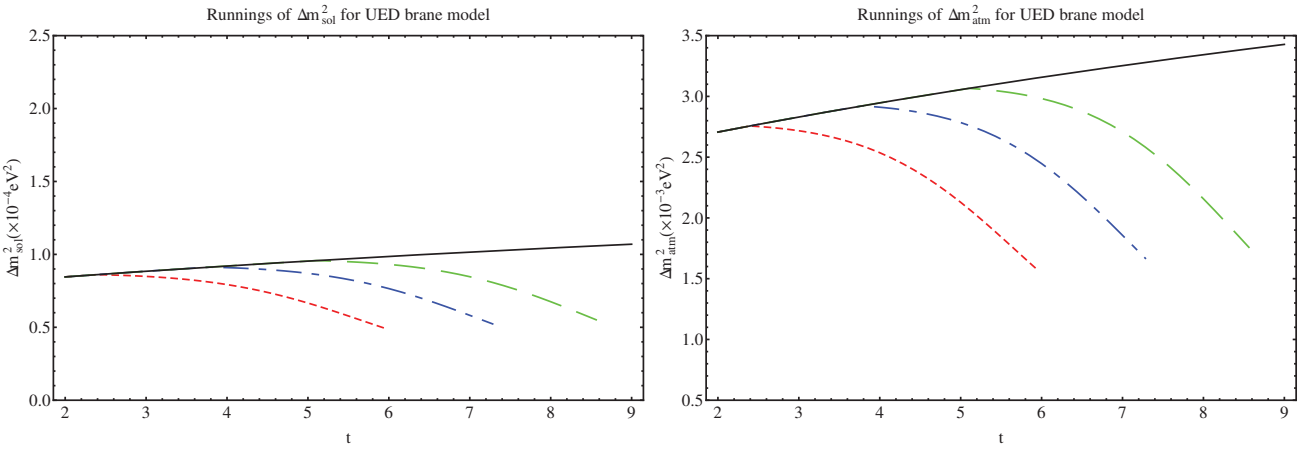

Figure 3.1: Evolution of Δm^2_{sol} (left panel) and Δm^2_{atm} (right panel) as a function of the scale $t = \ln(\mu/M_Z)$ with matter fields constrained to the brane in the UED SM. The black line is the SM evolution, the red (small dashes) is for $R^{-1} \sim 1$ TeV, the blue (dash-dotted) $R^{-1} \sim 4$ TeV, the green (large dashes) $R^{-1} \sim 15$ TeV.

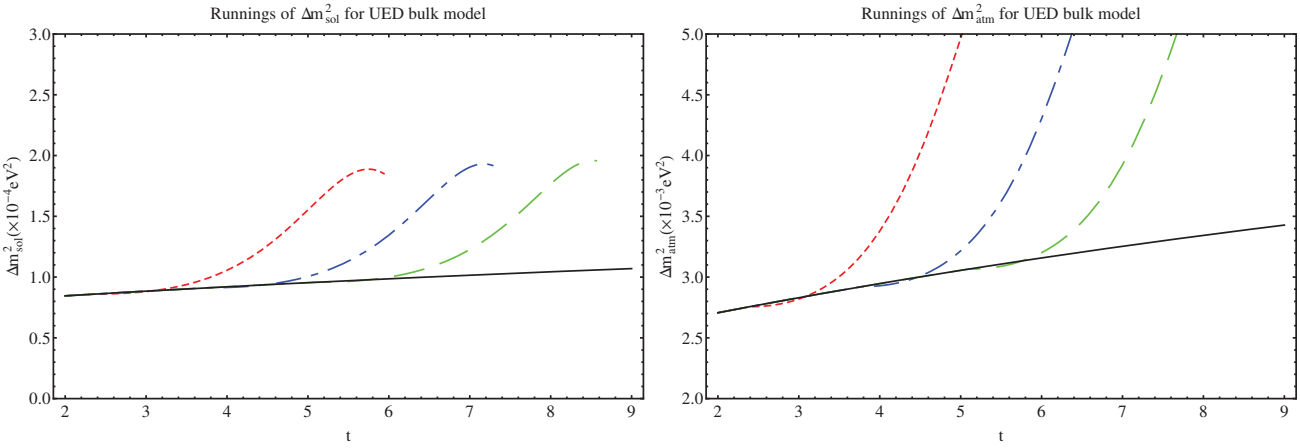

Figure 3.2: Evolution of Δm^2_{sol} (left panel) and Δm^2_{atm} (right panel) as a function of the scale $t = \ln(\mu/M_Z)$ with matter fields in the bulk in the UED SM. The black line is the SM evolution, the red (small dashes) is for $R^{-1} \sim 1$ TeV, the blue (dash-dotted) $R^{-1} \sim 4$ TeV, and the green (large dashes) $R^{-1} \sim 15$ TeV.

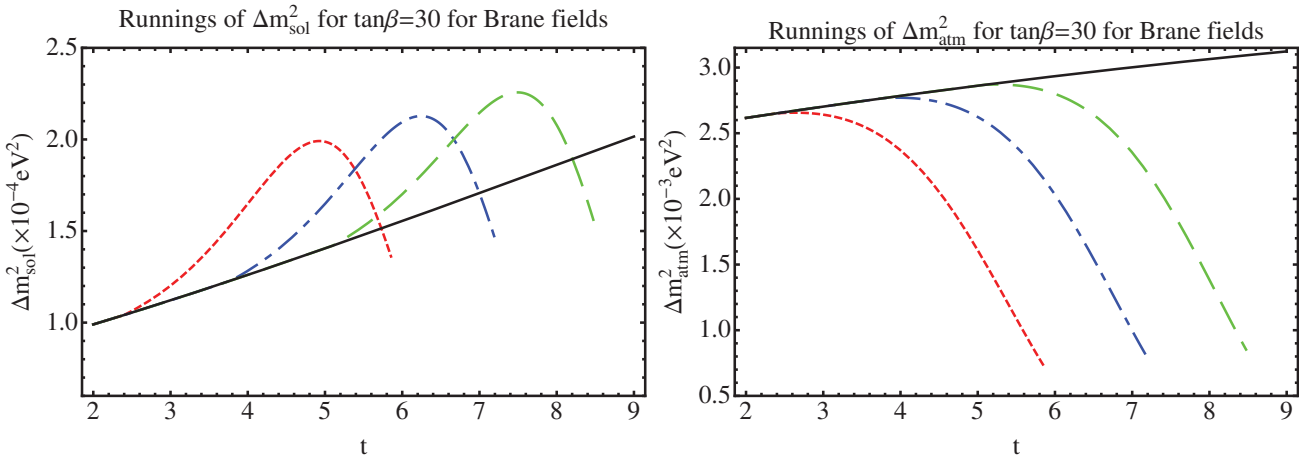

Figure 3.3: Evolution of Δm^2_{sol} (left panel) and Δm^2_{atm} (right panel) as a function of the scale $t = \ln(\mu/M_Z)$ with matter fields constrained to the brane for $\tan\beta = 30$ in the 5D MSSM. The black line is the MSSM evolution, the red (small dashes) is for $R^{-1} \sim 1$ TeV, the blue (dash-dotted) $R^{-1} \sim 4$ TeV, the green (large dashes) $R^{-1} \sim 15$ TeV.

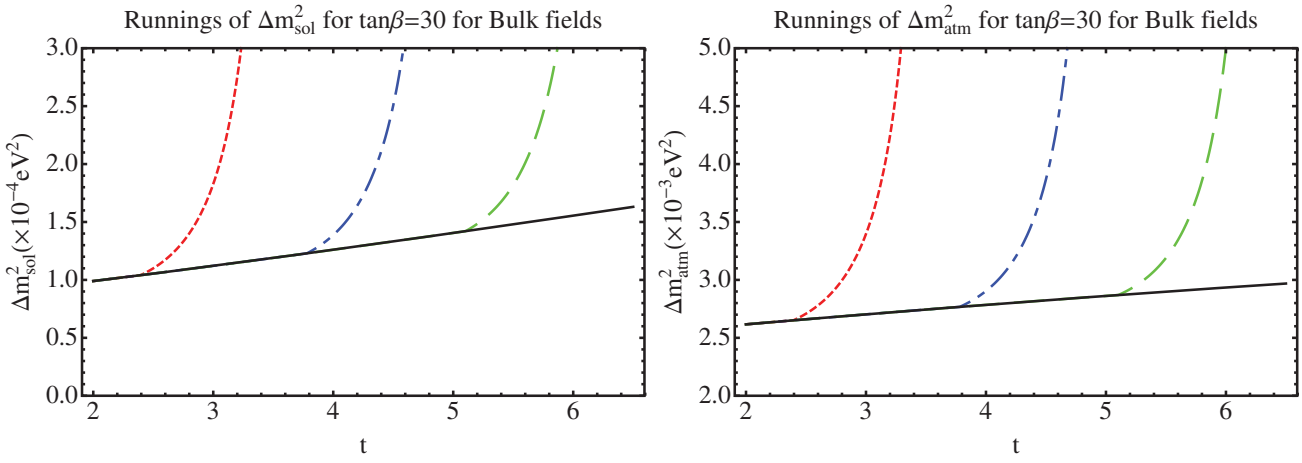

Figure 3.4: Evolution of Δm^2_{sol} (left panel) and Δm^2_{atm} (right panel) as a function of the scale $t = \ln(\mu/M_Z)$ with matter fields in the bulk for $\tan\beta = 30$ in the 5D MSSM. The black line is the MSSM evolution, the red (small dashes) is for $R^{-1} \sim 1$ TeV, the blue (dash-dotted) $R^{-1} \sim 4$ TeV, and the green (large dashes) $R^{-1} \sim 15$ TeV. The evolution is towards a non-perturbative regime, where the Yukawa coupling develops a Landau pole and the effective theory becomes invalid.

at higher energies). This prediction is extremely stable and can be explained as the evolution of the masses is governed by the equation

$$\dot{m}_i = \frac{1}{16\pi^2} m_i \left(\alpha + C_i y_\tau^2\right) \ , \tag{3.1}$$

where the coefficients C_i induce a non-universal behaviour and the parameter α contains the up Yukawa couplings and the gauge coupling terms (detailed in appendix D and Eq.(2.42). In contrast to the MSSM, the evolution in the brane case is completely dominated by the universal part. The essential point is that in the MSSM the positive contribution to α, approximately $6y_t^2$, is of the same order as the negative contribution from the gauge part. In our case the gauge part has a large pre-factor $S(t) = e^t M_Z R$ with respect to the MSSM which makes it completely dominant compared to any other contribution. As energy increases, we can write:

$$\dot{m}_i \sim \frac{1}{16\pi^2} m_i \left[6y_t^2 - \left(\frac{9}{5}g_1^2 + 9g_2^2\right) S(t)\right] < 0 \ . \tag{3.2}$$

From this approximation we immediately see that all masses decrease with increasing energy and eventually tend to zero if the evolution equations can be trusted up to a high energy.

In the 5D MSSM bulk case the evolution has again the same form for the three masses m_1, m_2, m_3, but the behaviour is the opposite as the masses increase at high energy because all matter fields propagate in the bulk and contribute to the evolution. In detail this can be seen by the fact that even if the gauge part gets a large pre-factor $S(t)$, the Yukawa part gets in this case a pre-factor $S(t)^2$, which changes the sign of the derivative with respect to the previous case:

$$\dot{m}_i \sim \frac{1}{16\pi^2} m_i \left[\pi S(t)^2 6y_t^2 - \left(\frac{6}{5}g_1^2 + 6g_2^2\right) S(t)\right] > 0 \ . \tag{3.3}$$

From this approximation we see that all masses increase with increasing energy scale.

The situation is more involved when analyzing the mass squared differences. We plot in figs. 3.3 and 3.4 the evolution of Δm^2_{sol} and Δm^2_{atm} both for the matter fields on the brane and for all fields in the bulk for tanβ=30 and different radii of compactification. In the brane case different behaviours as a function of the energy scale are possible as a relatively large interval in energy range is allowed for the effective theory. As explicitly illustrated in fig. 3.3, the relevant radiative corrections controlled by the gauge fields in Eq.(3.2) become dominant as energy goes up, which tends to reduce mass splitting, and an approximately degenerate neutrino masses spectrum at the high energy scale $m_1 \approx m_2 \approx m_3$ becomes favourable. This is in contrast with the MSSM, where the neutrino mass splitting becomes large at an ultraviolet cut-off. Therefore, it is very appealing that the neutrino mass splitting at low energy could be attributed to radiative corrections resulting from a degenerate pattern at a high energy scale. In fig. 3.4, the bulk case tends to a non-perturbative regime, where the unitarity bounds of the effective theory are reached much faster and only a much shorter running can be followed using the effective theory. As seen in Eq.(3.3), the quadratic terms related to $S(t)$ dominate during the fast evolution. As such, the neutrino mass splitting becomes even larger at a high energy scale.

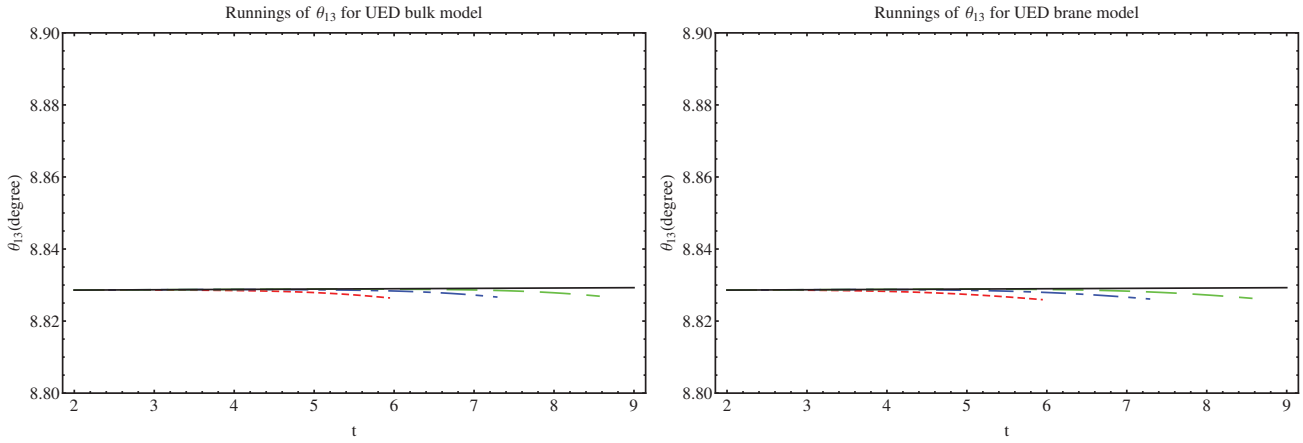

Figure 3.5: Evolution of θ_{13} as a function of the parameter $t = \ln(\mu/M_Z)$ with matter fields in the bulk (left panel) and on the brane (right panel) respectively in the UED SM. The black line is the SM evolution, the red (small dashes) is for $R^{-1} \sim 1$ TeV, the blue (dash-dotted) $R^{-1} \sim 4$ TeV, and the green (large dashes) $R^{-1} \sim 15$ TeV.

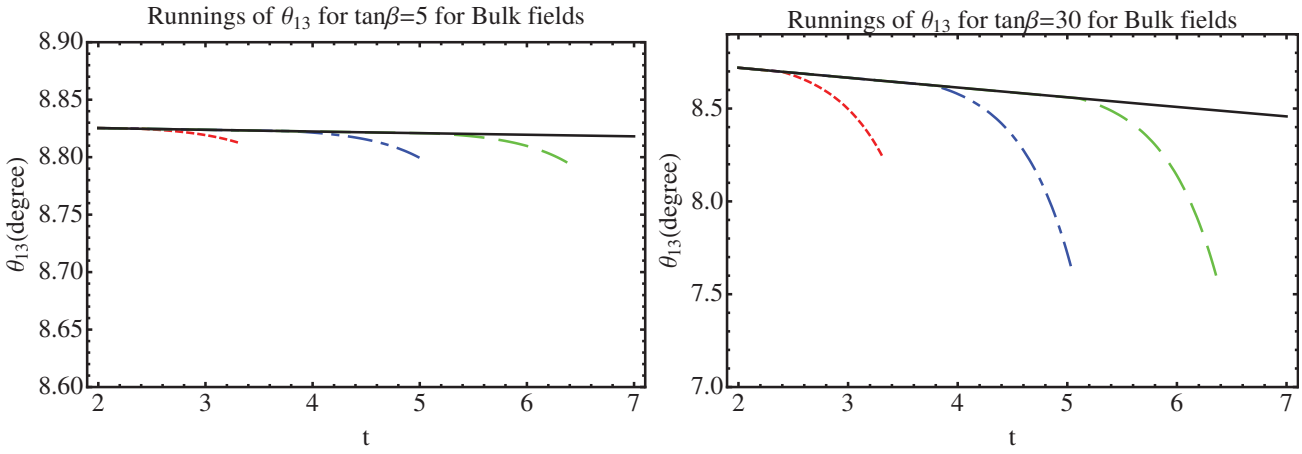

Figure 3.6: Evolution of θ_{13} as a function of the parameter $t = \ln(\mu/M_Z)$ with matter fields in the bulk for $\tan\beta = 5$ (left panel) and $\tan\beta = 30$ (right panel) in the 5D MSSM respectively. The black line is the MSSM evolution, the red (small dashes) is for $R^{-1} \sim 1$ TeV, the blue (dash-dotted) $R^{-1} \sim 4$ TeV, and the green (large dashes) $R^{-1} \sim 15$ TeV.

3.2.3 Mixing angles

Concerning the evolution of the mixing angles, as can be seen in figs. 3.5–3.10, in the UED bulk and brane cases, we have very small variation from the SM case because we do not have dependence on $\tan\beta$ and there is not a quadratic term of $S(t)$ in the RGEs so there is no strong enhancement in the running. However the mixing angles variation is more significant in the 5D MSSM in which the largest effect is for θ_{12}, with changes of more than 70% possible for the brane localised matter field scenario. As observed, due to the large quadratic term of $S(t)$ in the beta function, the θ_{12} has a rapid and steep variation in the bulk case. However, for the brane case, it has a relatively longer evolution track with the θ_{12} then being pulled further down until the termination point (where the effective theory becomes invalid). In contrast, the running of θ_{13} and θ_{23} is much milder. As demonstrated in figs. 3.6 and 3.7, changes in the values of θ_{13} vary only a couple of degrees. For a larger value of $\tan\beta$ we have a relatively large Yukawa coupling to τ, which leads to a large magnitude for its beta function, resulting in a relatively large variation during the evolution. However, a running to $\theta_{13} = 0$ cannot be observed in any situation. From the evolution behaviour of θ_{13}, one can see that the renormalisation group running effects or finite quantum corrections are almost impossible to generate $\theta_{13} = 0$ at a high energy scale, even though the power law enhanced evolution is considered during the running. Therefore, for the tri-bimaximal mixing pattern [135], in the current context with no other extreme conditions being taken into account, a slightly changed θ_{13} could not be accommodated during the whole range of the energy scale. Similar trajectories are also observed for θ_{23} (see fig. 3.10).

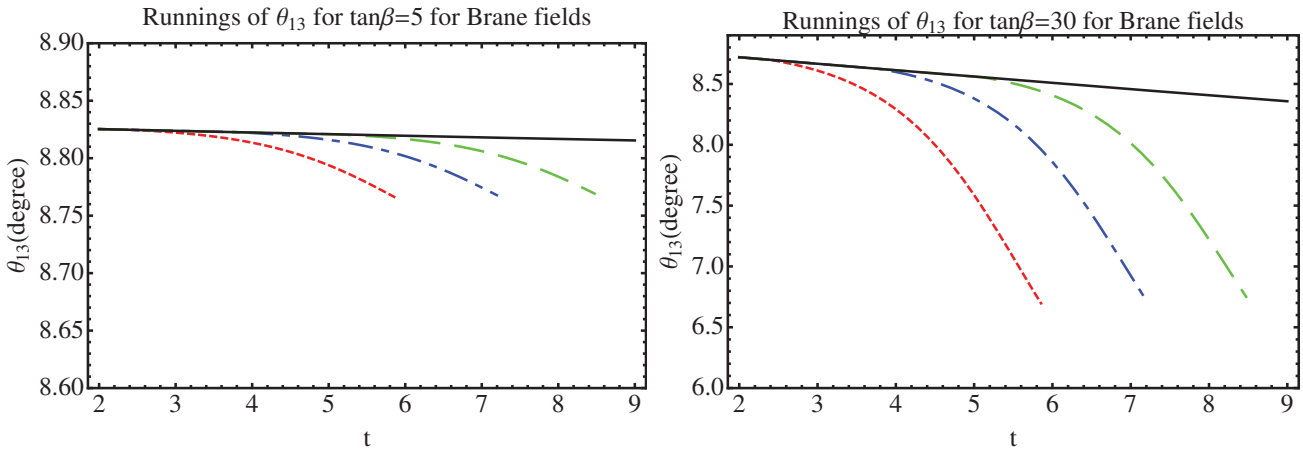

Figure 3.7: Evolution of θ_{13} as a function of the parameter $t = \ln(\mu/M_Z)$ with matter fields constrained to the brane for $\tan\beta = 5$ (left panel) and $\tan\beta = 30$ (right panel) in the 5D MSSM respectively. The black line is the MSSM evolution, the red one (small dashes) is for $R^{-1} \sim 1$ TeV, the blue (dash-dotted) $R^{-1} \sim 4$ TeV, and the green (large dashes) $R^{-1} \sim 15$ TeV.

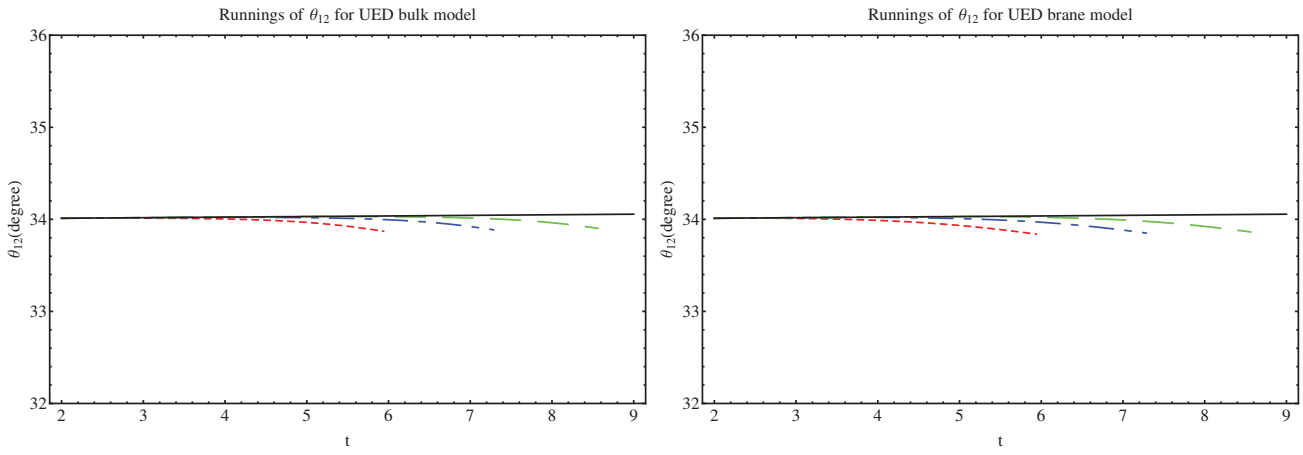

Figure 3.8: Evolution of θ_{12} as a function of the parameter $t = \ln(\mu/M_Z)$ with matter fields in the bulk (left panel) and on the brane (right panel) respectively in the UED SM. The black line is the SM evolution, the red (small dashes) is for $R^{-1} \sim 1$ TeV, the blue (dash-dotted) $R^{-1} \sim 4$ TeV, and the green (large dashes) $R^{-1} \sim 15$ TeV.

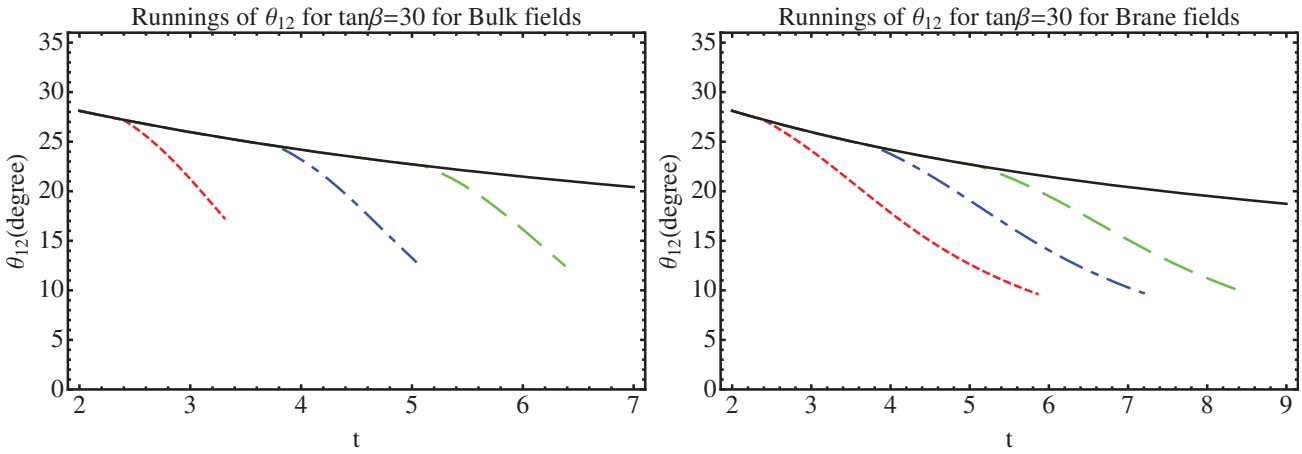

Figure 3.9: Evolution of θ_{12} in the bulk (left panel) and on the brane (right panel) as a function of the scale $t = \ln(\mu/M_Z)$ for $\tan\beta = 30$ in the 5D MSSM. The black line is the MSSM evolution, the red one (small dashes) is for $R^{-1} \sim 1$ TeV, the blue (dash-dotted) $R^{-1} \sim 4$ TeV, and the green (large dashes) $R^{-1} \sim 15$ TeV.

3.2.4 δ phase

The variation of the Dirac phase δ in the UED SM case is stable and similar for the bulk and brane cases, there is very small deviation from the SM because all other mixing angles vary only by small quantities and the coefficient C which appear in the variation of δ (see appendix E) are linear in $S(t)$ and there is no dependence on $\tan\beta$.

Noting that the Dirac phase δ determines the strength of CP violation in neutrino oscillations. In the 5D MSSM, the runnings we include follow the general features presented in figs. 3.11 and 3.12, with large increases possible once the first KK threshold is crossed. From these studies we have seen that the variation is bigger for high $\tan\beta$ with large changes appearing in the brane case when approaching the high energy scale. The recent results from the Daya bay and RENO reactor experiments have established a non zero values of θ_{13}. Therefore, the leptonic CP violation characterized by the Jarlskog invariant $J \sim \sin\theta_{12}\cos\theta_{12}\sin\theta_{23}\cos\theta_{23}\sin\theta_{13}\cos^2\theta_{13}\sin\delta$ becomes promising to be measured in the future long baseline neutrino oscillation experiments. As plotted, we can observe a relatively large evolution for the Dirac phase, even the maximum CP violation case $\delta = \frac{\pi}{2}$ could be achieved for relatively small input values. For leptogenesis related to the matter-antimatter asymmetry, we should note that the parameters entering the leptogenesis mechanism cannot be completely expressed in terms of low-energy neutrino mass parameters. Note that in some specific models the parameters of the PMNS matrix (which contains CP asymmetry effects) can be used [129, 136]. Here, the CP-violating effects induced by the renormalisation group corrections could lead to values of the CP asymmetries large enough for a successful leptogenesis, and the models predicting maximum leptonic CP violation, or where the CP-violating phase δ is not strongly suppressed, become especially appealing. Specific models with large extra dimensions in which leptogenesis is relevant at low scale can also

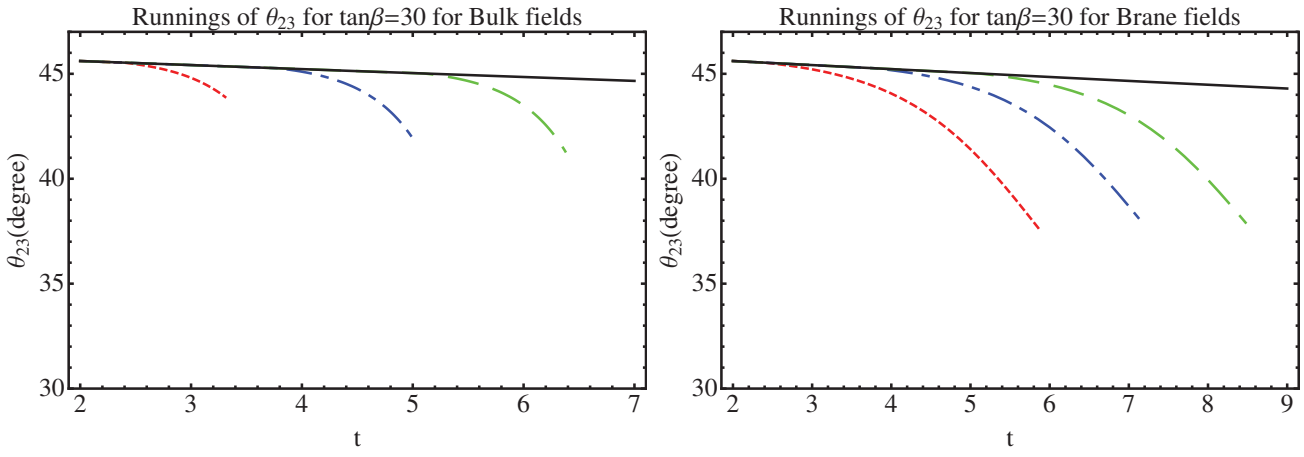

Figure 3.10: Evolution of θ_{23} in the bulk (left panel) and on the brane (right panel) as a function of the parameter $t = \ln(\mu/M_Z)$ for $\tan\beta = 30$ in the 5D MSSM. The black line is the MSSM evolution, the red one (small dashes) is for $R^{-1} \sim 1$ TeV, the blue (dash-dotted) $R^{-1} \sim 4$ TeV, and the green (large dashes) $R^{-1} \sim 15$ TeV.

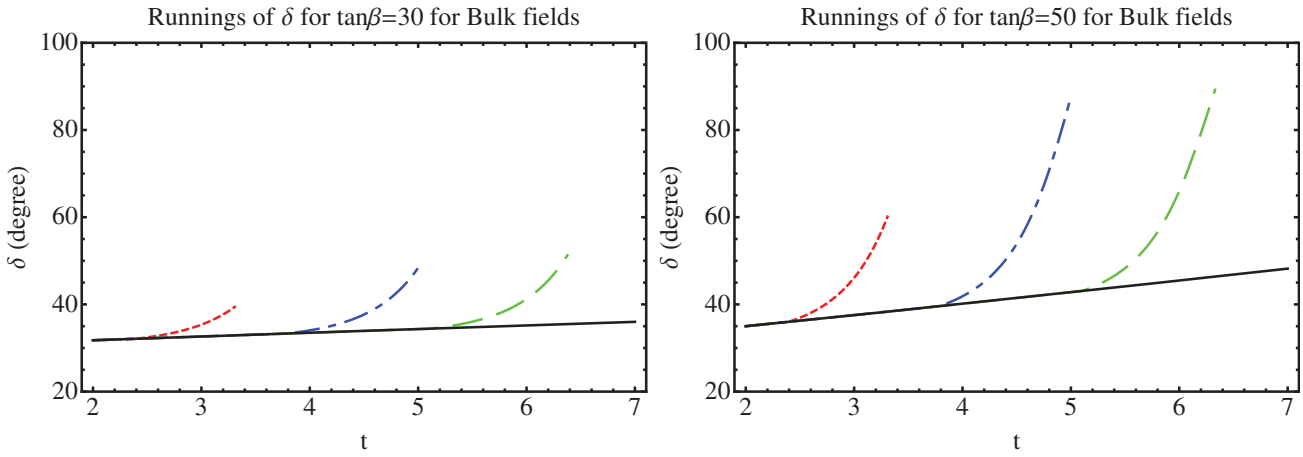

Figure 3.11: Evolution of the phase δ as a function of the parameter $t = \ln(\mu/M_Z)$ with matter fields in the bulk for $\tan\beta = 30$ (left panel) and $\tan\beta = 50$ (right panel) in the 5D MSSM respectively. The black line is the MSSM evolution, the red one (small dashes) is for $R^{-1} \sim 1$ TeV, the blue (dash-dotted) $R^{-1} \sim 4$ TeV, and the green (large dashes) $R^{-1} \sim 15$ TeV.

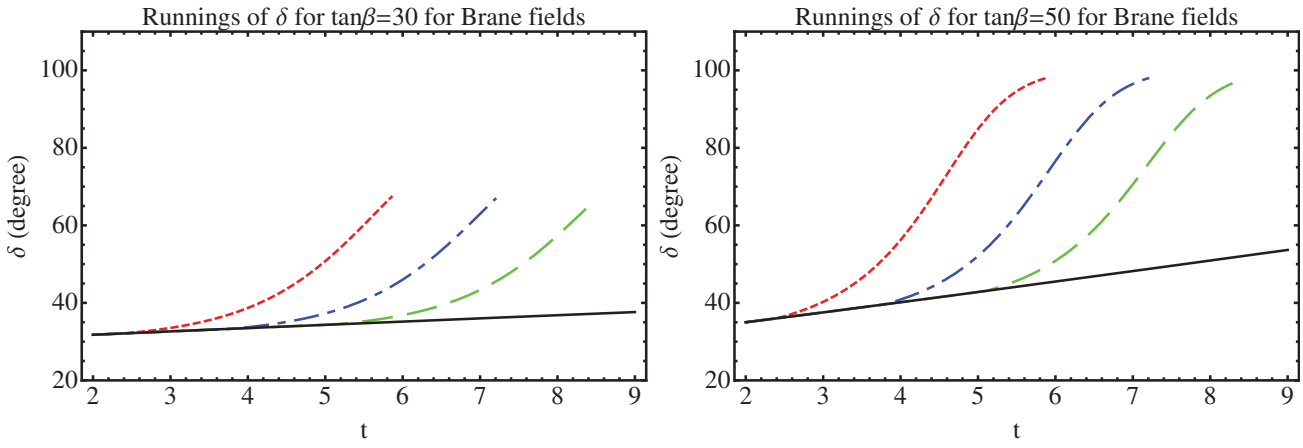

Figure 3.12: Evolution of the phase δ as a function of the parameter $t = \ln(\mu/M_Z)$ with matter fields constrained to the brane for $\tan\beta = 30$ (left panel) and $\tan\beta = 50$ (right panel) in the 5D MSSM respectively. The black line is the MSSM evolution, the red one (small dashes) is for $R^{-1} \sim 1$ TeV, the blue (dash-dotted) $R^{-1} \sim 4$ TeV, and the green (large dashes) $R^{-1} \sim 15$ TeV.

be found in Ref. [137].

The running of the mixing angles are entangled with the CP-violating phases [103,104]. The phases ϕ_1 and ϕ_2 do not affect directly the running of the masses, while the phase δ has a direct effect on the size of dm/dt, although its importance is somewhat reduced by the magnitude of θ_{13}. For further discussions of the correlation between these phases and mixing angles, refer to Refs [124,138] for details.

Finally, whilst the above results and analysis were for the normal hierarchy of neutrino masses, we did also consider an inverted hierarchy, where from an analysis of the equations presented in the appendix D we obtain the same features and results for neutrino mass runnings (though with different initial values at the M_Z scale). As such, the figures for Δm^2_{sol} and Δm^2_{atm} remain unchanged. Possible changes in the angles and phases arise from the different signs for the $(m_j - m_i)/(m_j + m_i)$ terms present in each evolution equation, where the θ_{12} results remain approximately the same (given the relative ordering of masses in these two hierarchies), and the small runnings of θ_{13} and θ_{23} would be up rather than down (though as already discussed, these runnings are quite small).

3.3 Summary and Outlook

The present work of the renormalisation group evolution of the masses, mixing angles and phases of the UED models in the quark and lepton sectors brings together the results we and other groups have obtained in the recent years in this subject using a common notation. The important physical points are discussed and the equations are written in compact way to show the unified approach to the different sectors of these models. For more technical details we refer to the existing literature.

Concerning the UED standard model the evolution of the gauge couplings has a rapid variation in the presence of the KK modes and this leads to a much lower unification scale than in the SM. Due to the power law running of the Yukawa couplings, the rapid decrease of the Yukawa couplings with energy is in contrast to the logarithmic running predicted by the SM. The UED model has substantial effects on the hierarchy between the quark and lepton sectors and provides a very desirable scenario for grand unification. As for the energy scaling of the Jarlskog parameter J, the contribution of KK modes is substantial. Its numerical analysis shows that its variation can be raised to more than 30%. The scale deviation of renormalisation curves from the usual SM one depends closely on the value of the compactified radius R. The smaller the radius is, the higher the energy scale we need to differentiate the UED curve from the SM one. A comparison between theoretical predictions and experimental measurements will be available once the LHC will be running at its full centre of mass energy. This will set limits on the parameters of the UED model, and a precise determination of J, $|V_{ub}|$ or $|V_{cb}|$ at high energy may lead to a discrimination between the SM and extra dimensional models.

In the case of the 5D MSSM, we have reviewed the behaviour of the evolution equations for the quark and neutrino sector in a minimal supersymmetric model with one extra-dimension. For quarks, the 5D MSSM scenarios with matter fields in the bulk or on the brane, give both results with small or no quark flavour mixings at high energies, especially for the mixings with

the heavy generation. The evolution equations are particularly important in view of testing the evolution of the Yukawa couplings. The evolution of these CKM parameters have a rapid variation prior to reaching a cut-off scale where the top Yukawa coupling develops a singularity point and the model breaks down. For the brane localised matter fields model, we can only observe similar behaviour for small values of $\tan\beta$, while for large $\tan\beta$, the initial top Yukawa coupling becomes smaller, the gauge couplings then play a dominant role during the evolution of the Yukawa couplings, and therefore the Yukawa couplings decrease instead of increasing. As such the variations of these CKM parameters have a relatively milder behaviour, and the theory is valid up the gauge coupling unification scale. Concerning the neutrino sector, the evolution equations for the mixing angles, phases, Δm^2_{sol} and Δm^2_{atm}, within the two distinct scenarios, is also considered. A larger $\tan\beta$ typically leads to larger renormalisation group corrections. Neutrino masses evolve differently in the two models due to the sign of the (different) dominant contributions in the bulk and in the brane cases. For the brane case we find the approximate degenerate neutrino mass spectrum becomes more favourable at the ultraviolet cut-off. In the bulk case, the neutrino splitting becomes even more severe as the unitarity bounds of the effective theory are reached faster. Contrary to the large renormalisation effect of θ_{12}, the runnings of θ_{13} and θ_{23} are relatively mild. We found a non-zero value for θ_{13} during the evolution, which has no appreciable RGE running effects, even when power law evolution effects are considered. Therefore it is necessary to introduce new physics effects in order to achieve the tri-bimaximal pattern. The maximum CP violation case, $\delta = \frac{\pi}{2}$, could be achieved starting from a relatively small initial value. In general we can see that radiative effects may have a significant impact on neutrino physics. A non-zero Jarlskog invariant, which measures the magnitude of leptonic CP violation (expected to be measured in future long baseline neutrino oscillation experiments), could open the door for measurable CP violation in the leptonic sector.

We would like to note some of the remaining incomplete areas of investigation in the study of quark and lepton sector runnings in UED models. Whilst we have reviewed the simplest SM and MSSM UED models, other alternative extra-dimensional geometries exist. Note that our two scenarios of all matter fields freely propagating in the bulk or brane localised represent the only possibilities for calculating unitary CKM or PMNS matrices, where extensions to the runnings of Yukawas with different numbers of matter fields in the bulk or brane are trivial extensions of the equations already reviewed here. Alternative extra-dimensional geometries are still to be investigated, such as 2UED models (preliminary work [139] contains errors and is an incomplete study of these sectors) or situations with warped Randall-Sundrum style extra-dimensions; though warp factors provide an additional problem of vertex factors now depending on the KK numbers, and so the equations would become of a completely different form to the ones provided here (excepting extreme limiting cases).

Part II

AMSB, HCAMSB and MMAMSB

Introduction

The search for supersymmetry and its breaking, in addition to the direct searches at LEP, B-factories, Tevatron and the Large Hadron Collider (LHC), is actively pursued using the WMAP limits on the relic density constraints. However, because the lightest supersymmetric particle relic density is sensitive to the cosmological expansion rate before Big-Bang Nucleosynthesis (BBN), the relic density can be modified considerably by variations of the expansion rate, even if these variations are modest and have no for the cosmological observations. Such variations could therefore change the constraints on the supersymmetric parameter space [59, 61].

In standard cosmology the dominant component before BBN is radiation, however energy density and entropy content can be modified. The precision of the WMAP data should therefore not make us forget the hypotheses which are implied by the use of standard cosmology. We discuss the implications of precision B-physics, direct searches and cold dark matter relic abundance for anomaly mediated models in three cases: firstly, the case of minimal anomaly mediated supersymmetry breaking [140, 141], secondly, mixed moduli-anomaly mediation [142] and thirdly, hypercharge anomaly mediation [143]. We do this for both standard cosmology as well as for scenarios of alternative cosmologies. We also discuss similar supersymmetry breaking scenarios in the case of the next-to-minimal supersymmetric standard model [144].

In section 4.1 we discuss the different anomaly mediated supersymmetry breakings in the MSSM in terms of the parameter spaces for these models. In section 4.2 we show the constraints from flavour observables due to the present data from particle physics experiments and the relic dark matter density assuming the standard model of cosmology. In section 4.3 we describe and comment the plots in different models. In section 4.4 similar scenarios are considered in the Next-to-Minimal Supersymmetric Standard Model (NMSSM) and the corresponding particle and cosmological bounds are discussed. In section 4.5 we discuss how alternative cosmological models can affect dramatically the bounds on the parameter space of the models we have considered while letting unchanged the observable cosmology. Four different alternatives to the standard cosmology are discussed which share this behaviour. Section 4.6 and section 4.7 discuss respectively the constraints implied by these different cosmological scenarios and the perspectives at the LHC for a list of benchmark points which are representative of the available parameter space for these AMSB models. The conclusions of chapter 4 are given in section 4.8.

We update our results in chapter 5 and we add new constraints from the Higgs sector. In section 5.2 the implications of the flavour physics and relic density constraints are presented, as well as the Higgs mass constraints and the possibilities to obtain branching ratios for the light CP-even Higgs in agreement with the present results at the LHC for the parameter spaces of the different AMSB models. Results and discussion are presented in section 5.3. Conclusions of chapter 5 are given in section 5.4.

Chapter 4

Dark matter in Anomaly Mediated SUSY breaking scenarios in standard and alternative cosmology

4.1 Anomaly mediated symmetry breaking in the MSSM

The superconformal Anomaly Mediated Supersymmetry Breaking (AMSB) mechanism [140, 141] is one of the most well-known and attractive set-ups for supersymmetry breaking. Supersymmetry breaking effects in the observable sector have in this framework a gravitational origin. Superconformal symmetry is classically preserved in theories without dimensional parameters and it is in general broken by the quantum effects. As anomalies only depend on the low-energy effective theory, the same will be true for the soft terms. Usually the AMSB scenario cannot be applied to the MSSM, as it leads to tachyonic sleptons. However the presence of an intermediate threshold can displace the soft terms and avoid this problem. In superconformal gravity one introduces a chiral superfield playing the role of the compensating multiplet for super-Weyl transformations, called the Weyl or conformal compensator. The F-term vacuum expectation value of the conformal compensator is turned on by the supersymmetry breaking in the hidden sector and the soft breaking of supersymmetry in the visible sector appears through the chiral anomaly supermultiplet. As the soft SUSY breaking terms arise from the anomaly, the supersymmetry breaking terms do not dominate at tree-level. Several soft SUSY breaking scenarios can be realised starting from this setup. We discuss in the following some of these realisations.

4.1.1 Minimal AMSB

The minimal AMSB (mAMSB) scenario [140] has very attractive properties, since the soft SUSY breaking terms are calculated in terms of one single parameter, namely the gravitino mass $m_{3/2}$, and the soft terms are renormalisation group invariants which can be calculated for any scale choice. However, the AMSB scenarios suffer from the problem that slepton squared masses are found to be negative, leading to tachyonic states. A solution to this problem is to

consider that the scalar particles acquire a universal mass m_0 at the GUT scale, which when added to the AMSB soft SUSY breaking terms, makes them positive. Therefore, the mAMSB model relies on only four parameters:

$$m_0, m_{3/2}, \tan\beta, \mathrm{sgn}(\mu)\ . \tag{4.1}$$

The Planck mass scale is set by the VEV of a scalar field ϕ that is part of a non-dynamical chiral supermultiplet (called the conformal compensator). As the field acquires a VEV of $\langle\phi\rangle$=1, the local superconformal invariance is spontaneously broken. In the presence of spontaneous SUSY breaking $\langle F\rangle \neq 0$ in the hidden brane, the auxiliary field component obtains a non-zero VEV as well:

$$\langle F_\phi\rangle \sim \frac{\langle F\rangle}{M_P} \sim m_{3/2} \tag{4.2}$$

The conformal compensator ϕ is dimensionless so that F_ϕ has dimensions of mass. The soft terms are [141]:

$$\begin{aligned} M_a &= \langle F_\phi\rangle \frac{\beta_{g_a}}{g_a}, \\ (m^2)^i_j &= \frac{1}{2}|\langle F_\phi\rangle|^2 \frac{d}{dt}\gamma^i_j = \frac{1}{2}|\langle F_\phi\rangle|^2 \left[\beta_{g_a}\frac{\partial}{\partial g_a} + \beta_{y^{kmn}}\frac{\partial}{\partial y^{kmn}} + \beta_{y^*_{kmn}}\frac{\partial}{\partial y^*_{kmn}}\right]\gamma^i_j, \\ a^{ijk} &= -\langle F_\phi\rangle \beta_{y^{ijk}}, \end{aligned} \tag{4.3}$$

where γ^i_j are the anomalous dimensions.

This scenario has been thoroughly studied in the literature, but is known to have cosmological consequences incompatible with the WMAP observations of the dark matter density [145].

4.1.2 HCAMSB

Another possibility to solve the negative slepton squared masses of the original AMSB scenario has been proposed: the hypercharge anomaly mediated supersymmetry breaking (HCAMSB) scenario [143], in which the MSSM resides on a D-brane and the hypercharge gaugino mass is generated in a geometrically separated hidden sector [146]. In this way, additional contribution to the gaugino mass M_1 is generated, and the large value of M_1 then increases the weak scale slepton masses beyond tachyonic values, solving the generic AMSB problem [143].

The HCAMSB scenario has four parameters:

$$\alpha = \frac{\tilde{M}_1}{m_{3/2}}, m_{3/2}, \tan\beta, \mathrm{sgn}(\mu)\ . \tag{4.4}$$

where $\tilde{M}_1$ is the HCAMSB contribution to M_1.

Not only does the anomaly mediation and hypercharge mediation have common theoretical setup , but also they are able to heal phenomenological shortcomings of each other. The minimal AMSB model predicts a negative mass squared for the sleptons (and features relatively

heavy squarks). Nevertheless, the pure hypercharge mediation suffers from negative squared masses for stops and sbottoms (and features relatively heavy sleptons). Eventually ,combining the hypercharge and anomaly mediation will result in a phenomenologically viable spectra for a sizable range of the parameter space of the model. The electroweak symmetry is broken radiatively by the large top-quark Yukawa coupling and the symmetry breaking gives the following masses and parameters values [146]:

$$\begin{aligned} M_1 &= \tilde{M}_1 + \frac{b_1 g_1^2}{16\pi^2} m_{3/2}, \\ M_a &= \frac{b_a g_a^2}{16\pi^2} m_{3/2}, \quad a = 2, 3 \\ m_i^2 &= -\frac{1}{4}\left\{ \frac{d\gamma}{dg}\beta_g + \frac{d\gamma}{df}\beta_f \right\} m_{3/2}^2 \\ A_f &= \frac{\beta_f}{f} m_{3/2}, \end{aligned} \tag{4.5}$$

where (b_1, b_2, b_3)=(33/5,1,-3), β_f is the beta function for the corresponding superpotential coupling, and $\gamma = \frac{\partial ln Z}{\partial ln \mu}$ with Z the wave function renormalisation constant. The wino and gluino masses (M_2 and M_3) receive a contribution from the bino mass at the two loop level [146].

4.1.3 MMAMSB

Contrary to the two previous AMSB scenarios, the Mixed Modulus Anomaly mediated SUSY breaking (MMAMSB) scenario [142] provides viable dark matter candidates, in addition to solving the negative slepton mass problem naturally. This scenario is based on type-IIB superstrings with stabilised moduli [147]. The study of supersymmetric scale gives predictions on what the string theory gives at an energy of order 1 TeV (SUSY phenomenology). Since the physical couplings are determined by the fundamental states of this moduli, the presence of some flat directions in the space of scalar Fields (the moduli) aids in determining the physical couplings. The spatial extra dimensions are compactified (reduction of space dimension) with flux that conduce to a minimum in the potential of moduli and represent a starting point to find fundamental state that lead to MSSM at low energy and is compatible with the constraints of cosmologie [147]. In this scenario, an interesting result is that the soft SUSY breaking terms receive comparable contributions from both anomaly and modulus, resulting in positive slepton masses. We examine here the minimal MMAMSB scenario [1], which relies on four parameters:

$$\alpha, m_{3/2}, \tan\beta, \mathrm{sgn}(\mu) \ . \tag{4.6}$$

α here parametrises the relative contributions of modulus mediation and anomaly mediation to the soft breaking terms: the largest α is, the more mediation comes from modulus; indeed

1. We note that in the general MMAMSB, there are two more parameters, n_i and l_α, which represent respectively the modular weights of visible sector of the matter fields and the gauge kinetic function, and which can modify the mass spectra.

in the limit where $\alpha \to 0$, we obtain the SSB terms which are purely AMSB with a negative squared mass for the sleptons. For an intermediate values of α which are more interesting for our studies, the problem of tachyonic sleptons is absent [142].

The mass scale of supersymmetry breaking parameters is given by the gravitino mass $m_{3/2}$. The gaugino mass parameters, trilinear parameters and sfermion mass parameters, all renormalized just below the unification scale (which we take to be Q = M_{GUT}), are respectively given by [147]

$$\begin{aligned} M_a &= M_s(l_a\alpha + b_a g_a^2), \\ A_{ijk} &= M_s(-a_{ijk}\alpha + \gamma_i + \gamma_j + \gamma_k), \\ m_i^2 &= M_s^2(c_i^2 + 4\alpha\xi_i - \dot{\gamma}_i). \end{aligned} \tag{4.7}$$

where $M_s = m_{3/2}/(16\pi^2)$, b_a are the gauge β function coefficients for gauge group a and g_a are the corresponding gauge couplings, and

$$c_i = 1 - n_i,\ a_{ijk} = 3 - n_i - n_j - n_k,\ \xi_i = \textstyle\sum_{j,k} a_{ijk}\frac{y_{ijk}^2}{4} - \sum_a l_a g_a^2 C_2^a(f_i).$$

where n_i are the modular weights of visible sector of the matter fields, l_a are the gauge kinetic function, y_{ijk} are the superpotential Yukawa couplings, C_2^a is the quadratic Casimir for the a^{th} gauge group corresponding to the representation to which the sfermion $\tilde{f}_i$ belongs, γ_i is the anomalous dimension and $\dot{\gamma}_i = 8\pi^2\frac{\partial\gamma_i}{\partial log\mu}$.

4.2 Flavour constraints and Tools

The first flavour observable that we consider here is the branching ratio of $B \to X_s\gamma$, which has been thoroughly studied in the literature and is still under scrutiny. This observable is very interesting, as its SM contributions only appear at loop level, and its theoretical uncertainties as well as the experimental errors are now under control. It provides strong constraints on the supersymmetric parameter space, especially for large $\tan\beta$, where it receives large enhancements from its supersymmetric contributions. We use the following interval at 95% C.L. [148, 149]:

$$2.16 \times 10^{-4} < \mathrm{BR}(B \to X_s\gamma) < 4.93 \times 10^{-4}\ . \tag{4.8}$$

Another interesting observable is the branching fraction of $B_s \to \mu^+\mu^-$, which is also a loop level observable, and which can receive extremely large contributions from SUSY at large $\tan\beta$, and can receive an enhancement of several orders of magnitude compared to the SM branching ratio. This decay mode has not yet been observed, and we have at 95% C.L. [148, 150] :

$$\mathrm{BR}(B_s \to \mu^+\mu^-) < 4.7 \times 10^{-8}\ . \tag{4.9}$$

We also consider a set of tree-level observables which are very sensitive to the charged Higgs mass as well as $\tan\beta$, and we use the following 95% level intervals, which include the theoretical

and experimental errors [148, 151, 152]:

$$0.56 < \frac{\mathrm{BR}(B \to \tau\nu)}{\mathrm{BR}_{SM}(B \to \tau\nu)} < 2.70 \,, \tag{4.10}$$

$$4.7 \times 10^{-2} < \mathrm{BR}(D_s \to \tau\nu) < 6.1 \times 10^{-2} \,, \tag{4.11}$$

$$0.151 < \frac{\mathrm{BR}(B \to D^0\tau\nu)}{\mathrm{BR}(B \to D^0 e\nu)} < 0.681 \,, \tag{4.12}$$

$$0.982 < \mathrm{R}_{\ell 23}(K \to \mu\nu) < 1.018 \,. \tag{4.13}$$

The observable $\mathrm{R}_{\ell 23}(K \to \mu\nu)$ is related to the decay of $K \to \mu\nu$ and is detailed in [152].
For the relic density constraint, we use the WMAP constraints [44] increased by 10% of theoretical error to account for the uncertainties in the calculation of the relic density:

$$0.088 < \Omega_{DM} h^2 < 0.123 \,. \tag{4.14}$$

We perform here an updated analysis of the mAMSB parameter space constraints from flavour physics and cosmological relic density. For this study, we generate mass spectra and couplings using Isajet 7.80 [153]. The calculation of flavour observables and the computation of the relic density are performed with SuperIso Relic v3.0 [148, 154]. In the following, we disregard the case of negative $\mathrm{sgn}(\mu)$ since it is disfavoured by the muon anomalous magnetic moment constraint, and we scan over the intervals $m_0 \in [0, 2000]$ GeV, $m_{3/2} \in [0, 100]$ TeV and $\tan\beta \in [0, 60]$.

4.3 Description of results

Figure 4.1 presents projection plots of the parameter space into the possible different planes. The green region in the plots corresponds to the parameter zone which is not excluded by flavour constraints or mass limits. The red stars corresponds to points leading to a favoured relic density but excluded by other constraints, whereas black stars are favoured by all the presented constraints, including the relic density constraint. As can be seen, no black star is visible in these plots, and the whole parameter space presented here is disfavoured either by flavour or direct constraints, or by the relic density constraint which tends to favour the low $m_{3/2}$ region. Disregarding the relic density constraint, a large zone at low $m_{3/2}$ is excluded.

In fig. 4.2, we show the relic density values as a function of the AMSB parameters. The green zones correspond to regions favoured by the flavour and direct constraints, whereas the other points are either excluded by these constraints or by cosmological considerations (charged relic or sneutrino relic, which interact therefore strongly). Two green zones clearly appear on the m_0 and $\tan\beta$ plots, for Ωh^2 around 10^{-4} and 10^{-9}. These areas are far from the WMAP dark matter allowed interval, making the mAMSB scenario disfavoured by the standard cosmology.

In fig. 4.3, we scan over the whole parameter space, and project the results in two-dimensional planes. The results are somehow similar to those of the mAMSB scenario: the constraints exclude low $m_{3/2}$ values. A large part of the parameter space is favoured by flavour

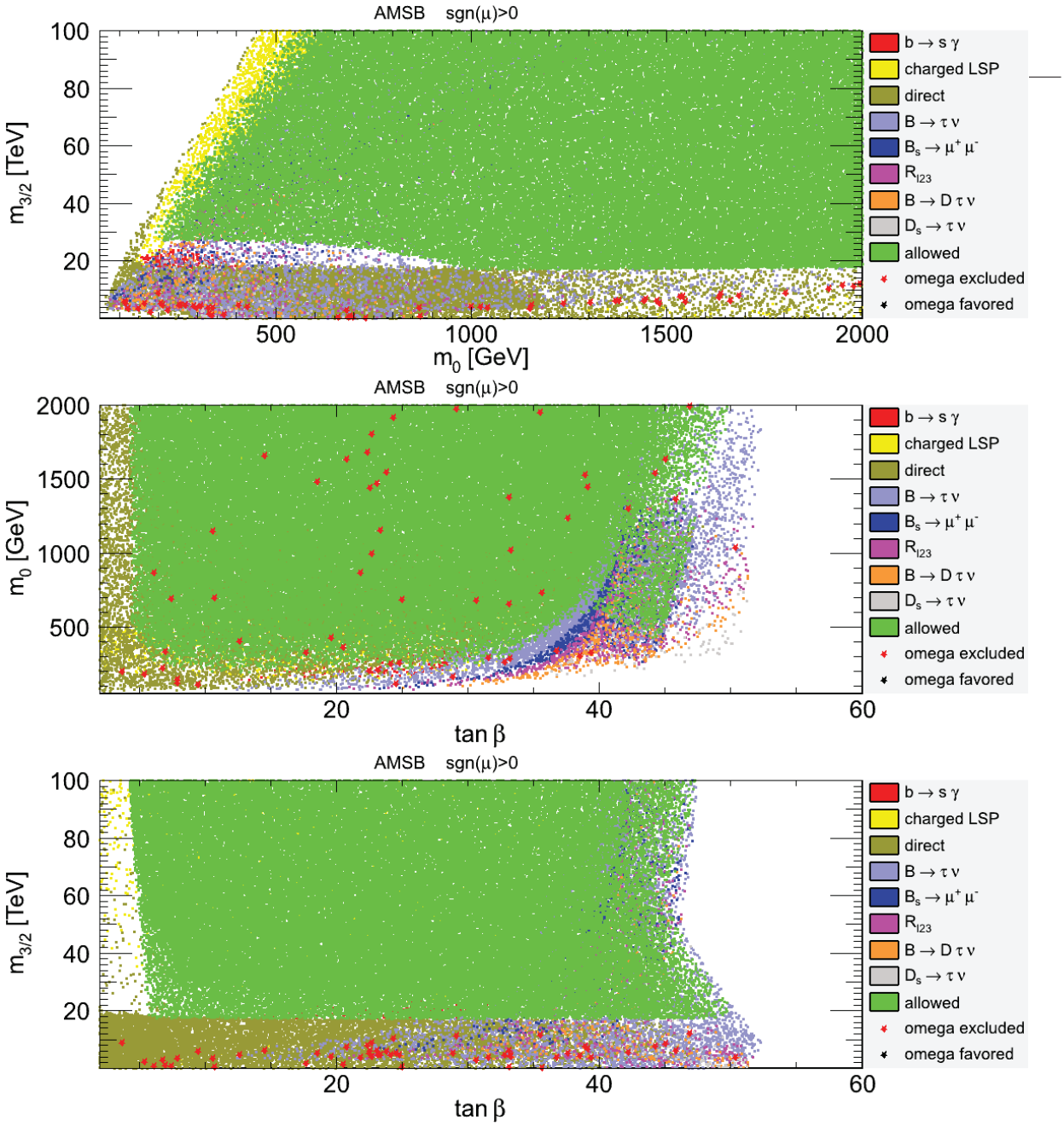

Figure 4.1: Constraints on the minimal AMSB parameter space. The exclusion regions are plotted in the order given in the legend. The red zones are excluded by the inclusive branching ratio of $B \to X_s\gamma$, the yellow ones correspond to charged LSP, the olive-green areas are excluded by direct collider constraints, the light blue zones are excluded by BR($B \to \tau\nu$), the dark blue zones by BR($B_s \to \mu^+\mu^-$), the magenta zones by $R_{\ell 23}$, the orange zones by BR($B \to D\tau\nu$) and the grey zones by BR($D_s \to \tau\nu$). The green area are in agreement with all the previously mentioned constraints. The stars are points favoured by the relic density observable, in red if disfavoured by any other constraints and in black if in agreement with all the constraints simultaneously.

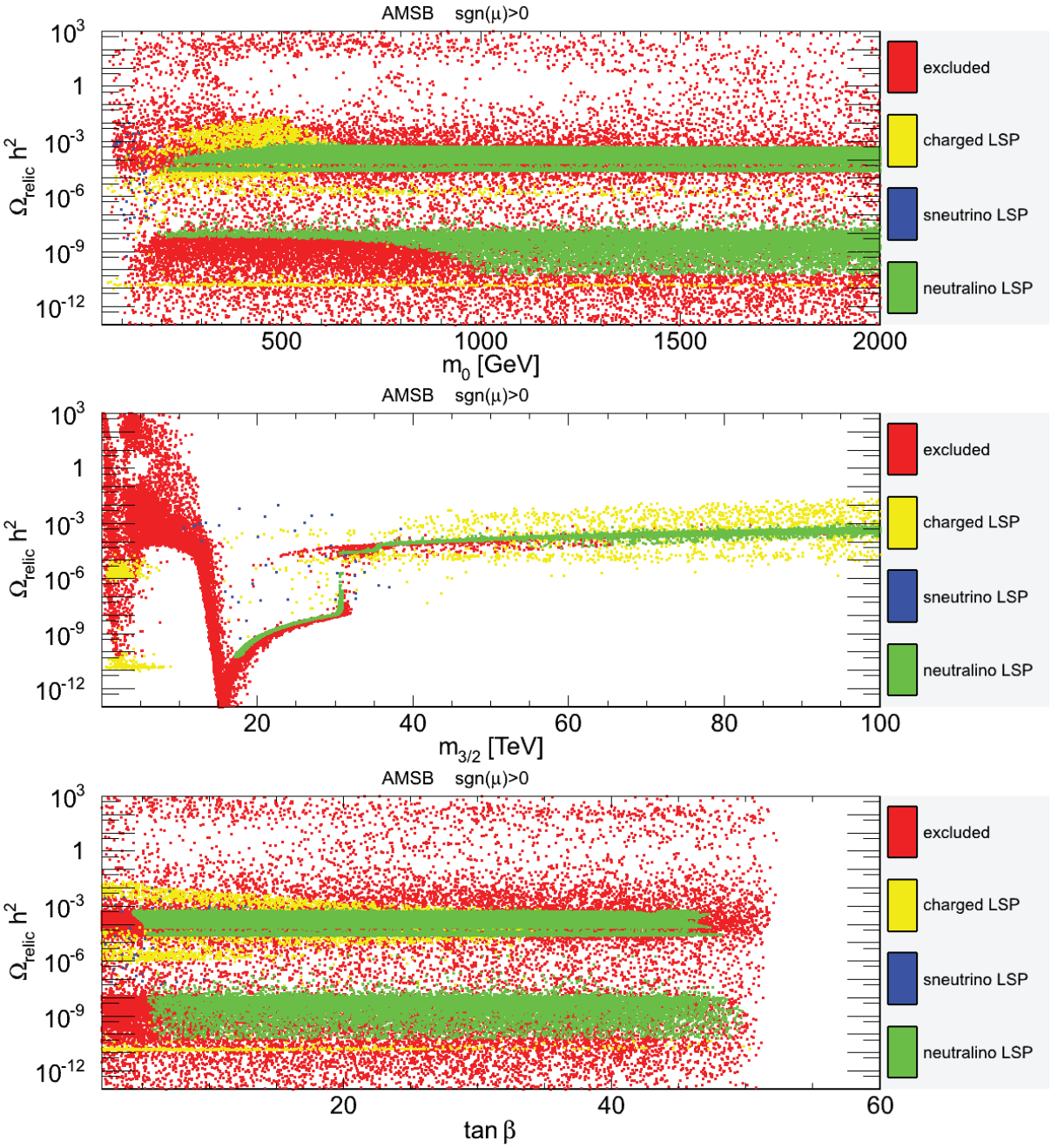

Figure 4.2: Relic density in function of the AMSB parameters. The green points are favoured by all the constraints, the yellow points corresponds to a charged LSP, the blue points correspond to left sneutrino LSP, and the red points are excluded by the other constraints (flavour and direct limits).

and direct constraints, but unfortunately no part of the parameter space respects at the same time the relic density and the other constraints, so that HCAMSB is also disfavoured by the standard cosmology.

In fig. 4.4, we show the relic density values as a function of the HCAMSB parameters. Again, the results are similar to those of the mAMSB scenario, with two distinct zones which are not excluded by flavour and direct constraints, corresponding to a relic density Ωh^2 around 10^{-4} and 10^{-8}.

In fig. 4.5, the parameter space is scanned over, and it is projected in two-dimensional planes. The resulting plots are different from those of mAMSB and HCAMSB. Indeed, a large part of parameter space escapes the flavour and direct constraints, and zones around $\alpha \sim 0$ or at low $m_{3/2}$ also fulfil the relic density constraint.

In fig. 4.6, we present the relic density values in function of the MMAMSB parameters. The relic density of points favoured by flavour and direct constraints takes values between 10^{-9} and 10^3. We can notice however that most of the points are in the interval $[1, 10^3]$, and some points fit in the WMAP interval. For this reason, MMAMSB is a scenario which can appear as attractive, as it fulfils simultaneously the standard cosmology and particle physics constraints.

4.4 Anomaly mediated symmetry breaking in the NMSSM

An interesting extension of the MSSM is the NMSSM, which brings a solution to the μ-problem [155]. It has an extended Higgs sector involving additional Higgs bosons, modifying the relic density and flavour physics constraints. Moreover, the couplings being modified, the NMSSM can escape direct constraints, and new parameter zones can be allowed by the constraints used in the previous section.

We consider here the simplest version of the NMSSM, where the term $\mu \hat{H}_u \cdot \hat{H}_d$ of the MSSM superpotential is replaced by

$$\lambda \hat{H}_u \cdot \hat{H}_d \hat{S} + \frac{\kappa}{3} \hat{S}^3 \,, \tag{4.15}$$

in order for the superpotential to be scale invariant. The soft breaking terms

$$m_{H_u}^2 |H_u|^2 + m_{H_d}^2 |H_d|^2 + m_S^2 |S|^2 + \left(\lambda A_\lambda S H_u \cdot H_d + \frac{1}{3} \kappa A_\kappa S^3 + \text{h.c.} \right) , \tag{4.16}$$

are *a priori* independent. Using the minimisation conditions for the potential, the scalar mass parameters $m_{H_{u,d}}$ can be replaced by the vacuum expectation values of the doublet v_u and v_d, with

$$v_u^2 + v_d^2 = v^2 \approx (174 \text{ GeV})^2 \quad , \qquad \tan\beta = \frac{v_u}{v_d} \,. \tag{4.17}$$

The singlet field mass parameter can also be replaced by the singlet expectation value v_s. Expanding the singlet field S around v_s gives rise to an effective parameter $\mu_{eff} = \lambda v_s$.

One can also define an effective doublet mass such as

$$m_A^2 \equiv \frac{\lambda v_s}{\sin\beta \cos\beta} (A_\lambda + \kappa v_s) \,. \tag{4.18}$$

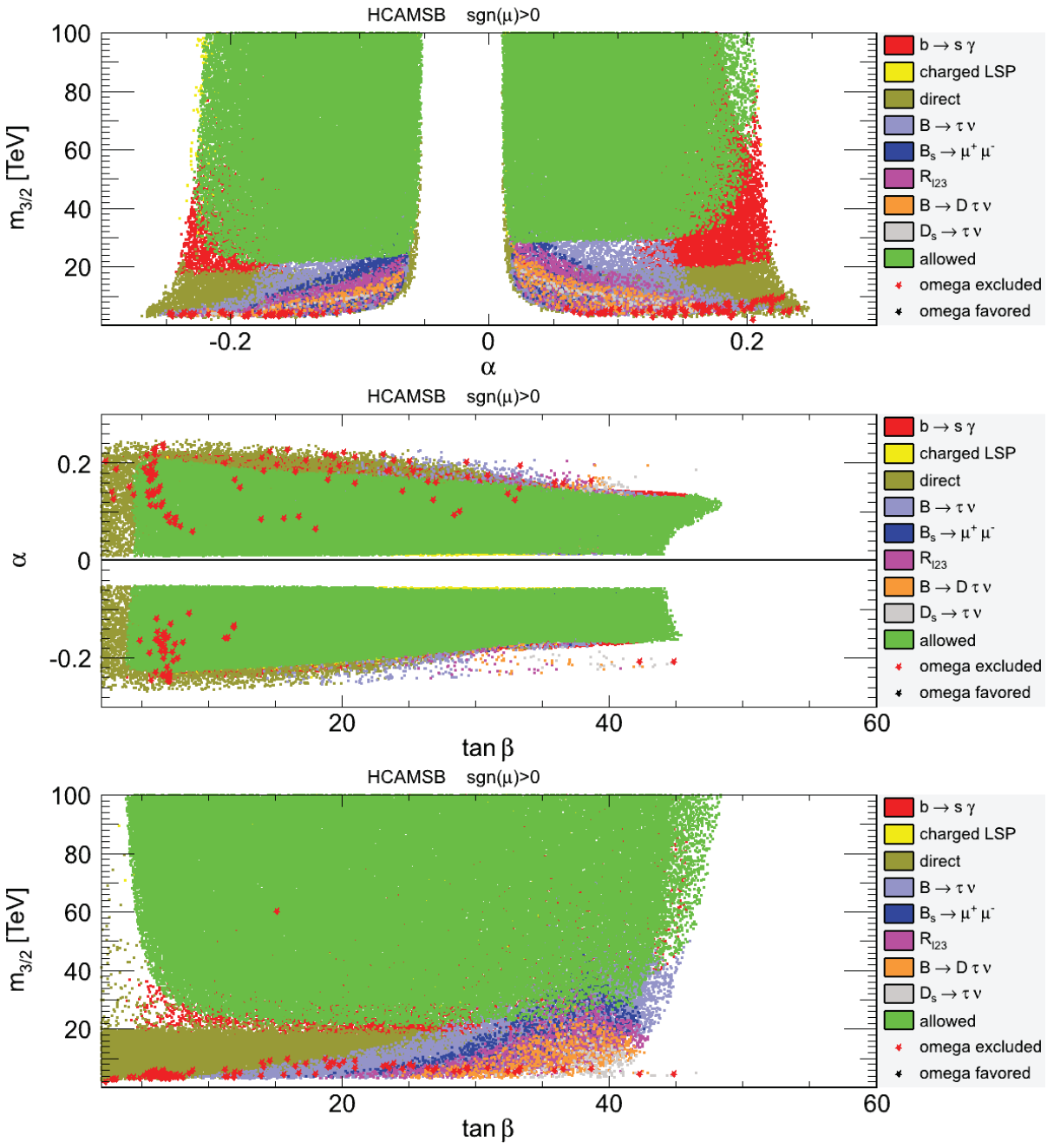

Figure 4.3: Constraints on the HCAMSB parameter space. The colour codes are the same as in fig. 4.1.

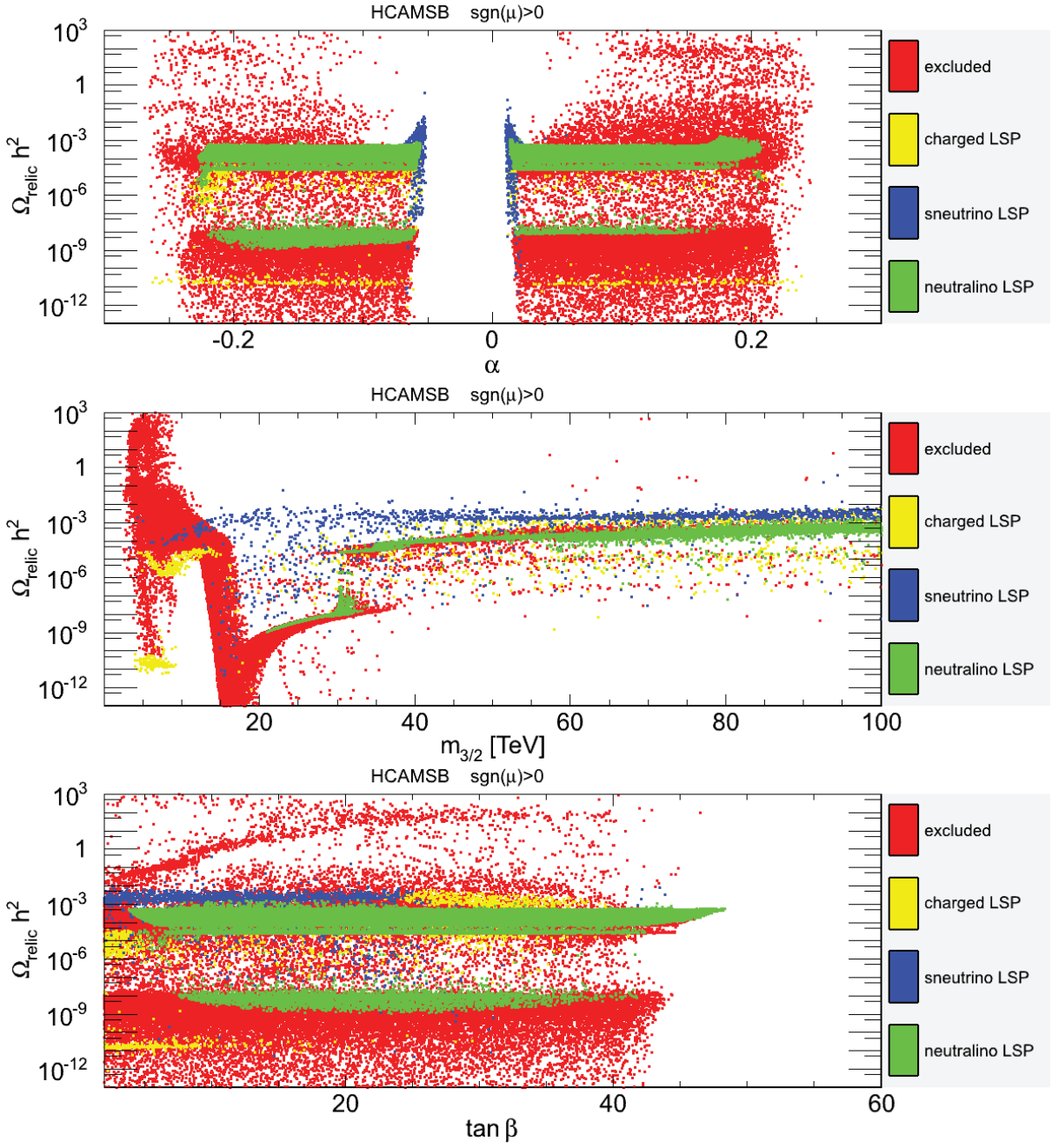

Figure 4.4: Relic density in function of the HCAMSB parameters. The colour codes are the same as in fig. 4.2.

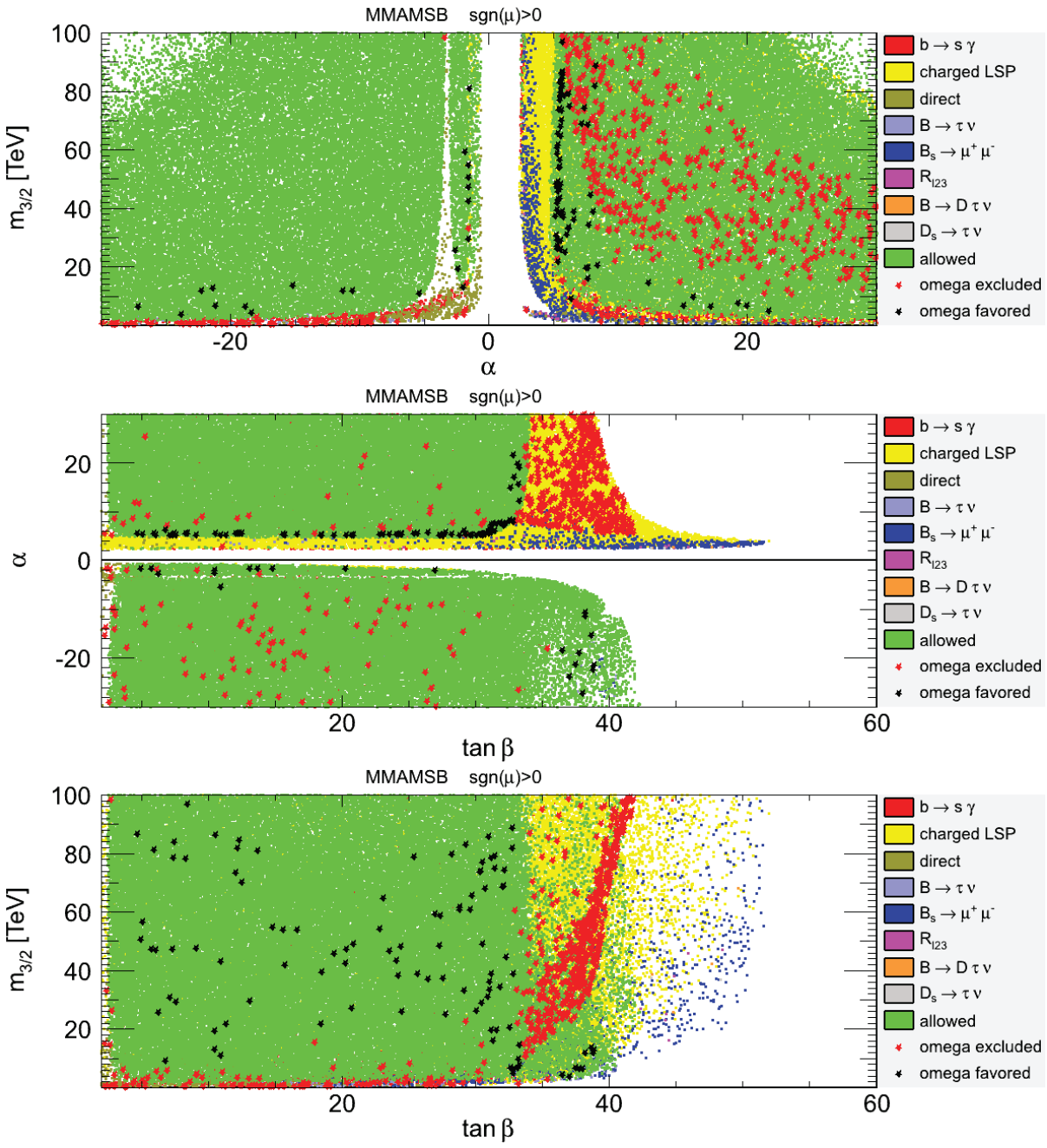

Figure 4.5: Constraints on the MMAMSB parameter space. The colour codes are the same as in fig. 4.1.

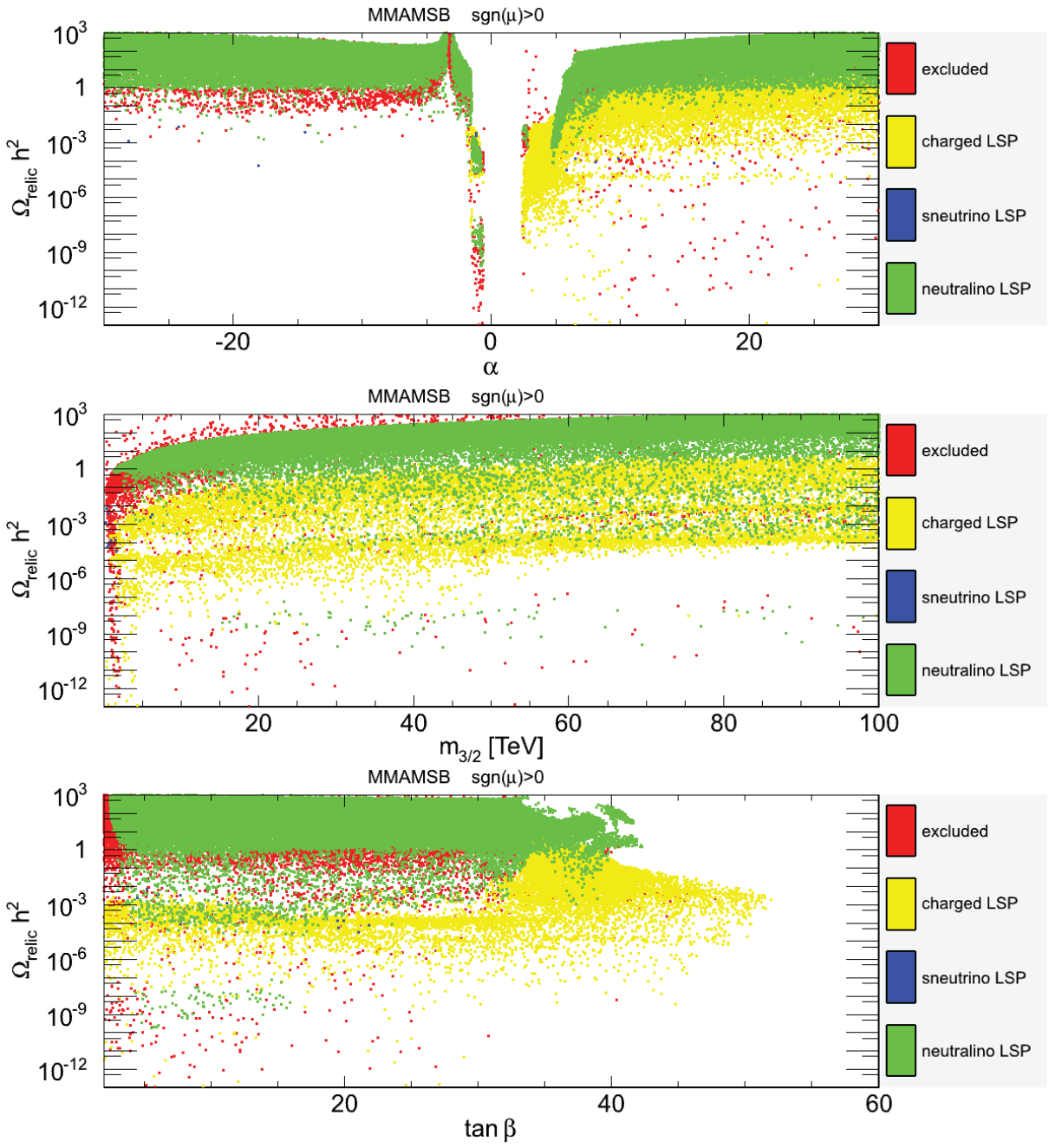

Figure 4.6: Relic density in function of the MMAMSB parameters. The colour codes are the same as in fig. 4.2.

Once the MSSM-like parameters (and in particular μ_{eff}) have been fixed by the specification of the AMSB scenario, we are left with four additional independent NMSSM-specific parameters:

$$\lambda, \kappa, A_\kappa, M_A \ . \tag{4.19}$$

We scan over the intervals $\lambda \in [-0.7, 0.7]$ GeV, $\kappa \in [-0.7, 0.7]$, $A_\kappa \in [-2000, 2000]$ GeV and $M_A \in [5, 1000]$. We review in the following the differences between the different AMSB scenarios when applied to the NMSSM.

4.4.1 mNAMSB

Minimal NMSSM-AMSB (mNAMSB) parameter points are generated here using NMSSMTools 2.3.4 [156], and flavour constraints and relic density are computed with SuperIso Relic v3.0 [148, 154].

In fig. 4.7, the parameter space of mNAMSB is presented. As in fig. 4.1, no point satisfy simultaneous flavour, direct and relic density constraints. The direct limits are less constraining than in the MSSM, but the flavour constraints are stronger and exclude a larger part of the NAMSB parameter space in comparison with AMSB.

Fig. 4.8 reveals more differences between the mAMSB and mNAMSB models. First, the zone not excluded by flavour and direct constraints having a relic density around 10^{-9} does not exist in the NAMSB, a new green zone appears for $m_{3/2} > 60$, and its relic density around 10^{-2} is much closer to the WMAP constraint. However, as in the mAMSB scenario, the mNAMSB model is globally disfavoured by the standard cosmology.

4.4.2 NHCAMSB

We generate the NMSSM-HCAMSB (NHCAMSB) parameter points using NMSSMTools 2.3.4 [156]. The obtained constraints are shown in fig. 4.9. Again, we see that no parameter point satisfies at the same time the relic density constraint and the direct and flavour constraints. Similarly to the mNAMSB scenario, NHCAMSB is less constrained by the direct mass limits, but is more excluded by the flavour constraints.

Fig. 4.10 shows the relic density in function of the different parameters. The green region that exists in the HCAMSB scenario for a relic density around 10^{-8} disappears in the NHCAMSB, and a new region opens up around 10^{-2}. However, as the mNAMSB scenario, the NHCAMSB scenario remains also disfavoured by the standard cosmology.

4.4.3 NMMAMSB

The NMSSM-MMAMSB (NMMAMSB) scenario leads to similar results as the MMAMSB scenario. As can be seen in fig. 4.11, there exists many points satisfying all the constraints, including relic density, especially for values of α near to 0.

Fig. 4.12 reveals a difference, as the calculated relic density takes values between 10^{-4} and 10^3, which is more restrictive in comparison to the MSSM case.

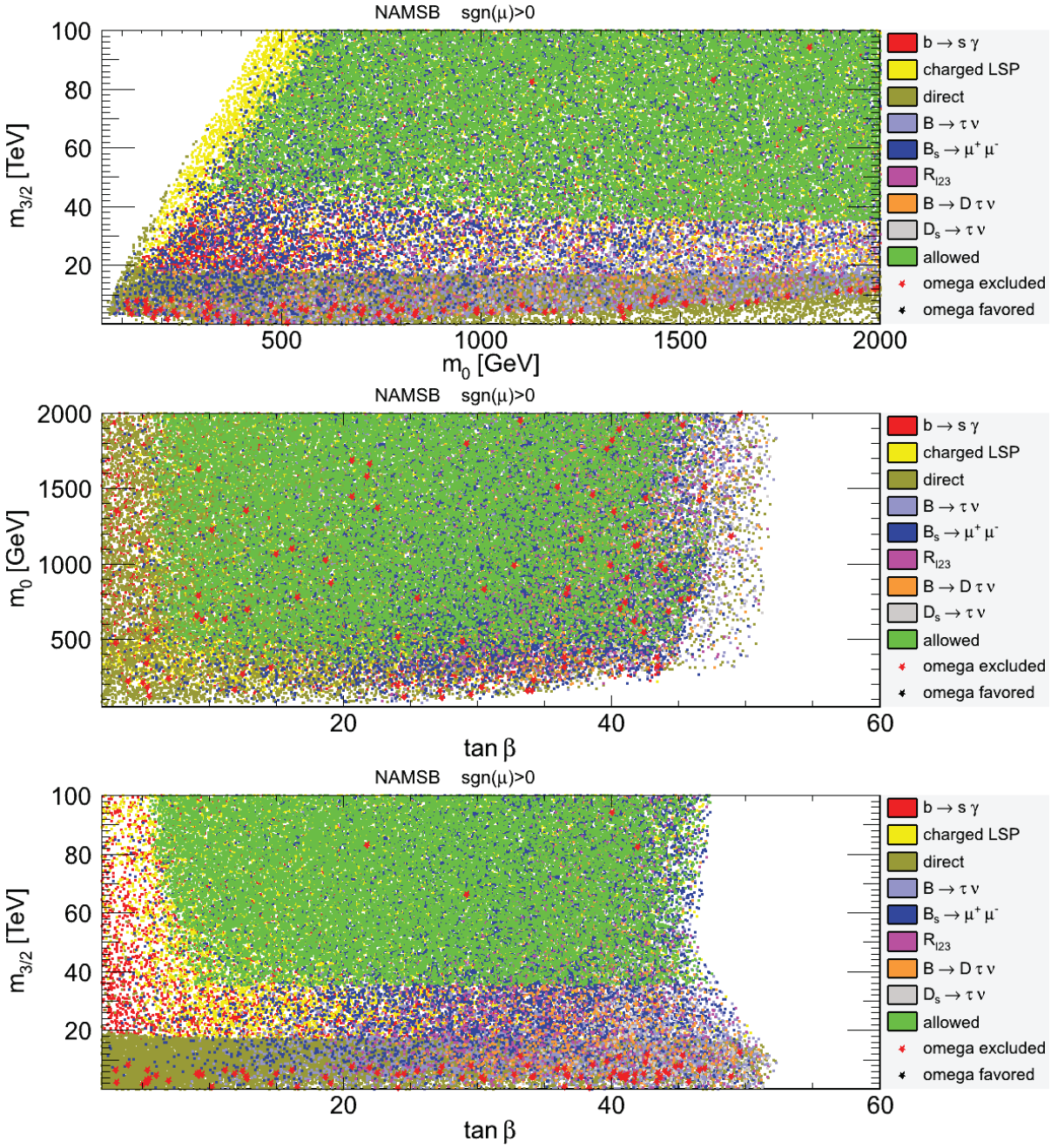

Figure 4.7: Constraints on the mNAMSB parameter space. The colour codes are the same as in fig. 4.1.

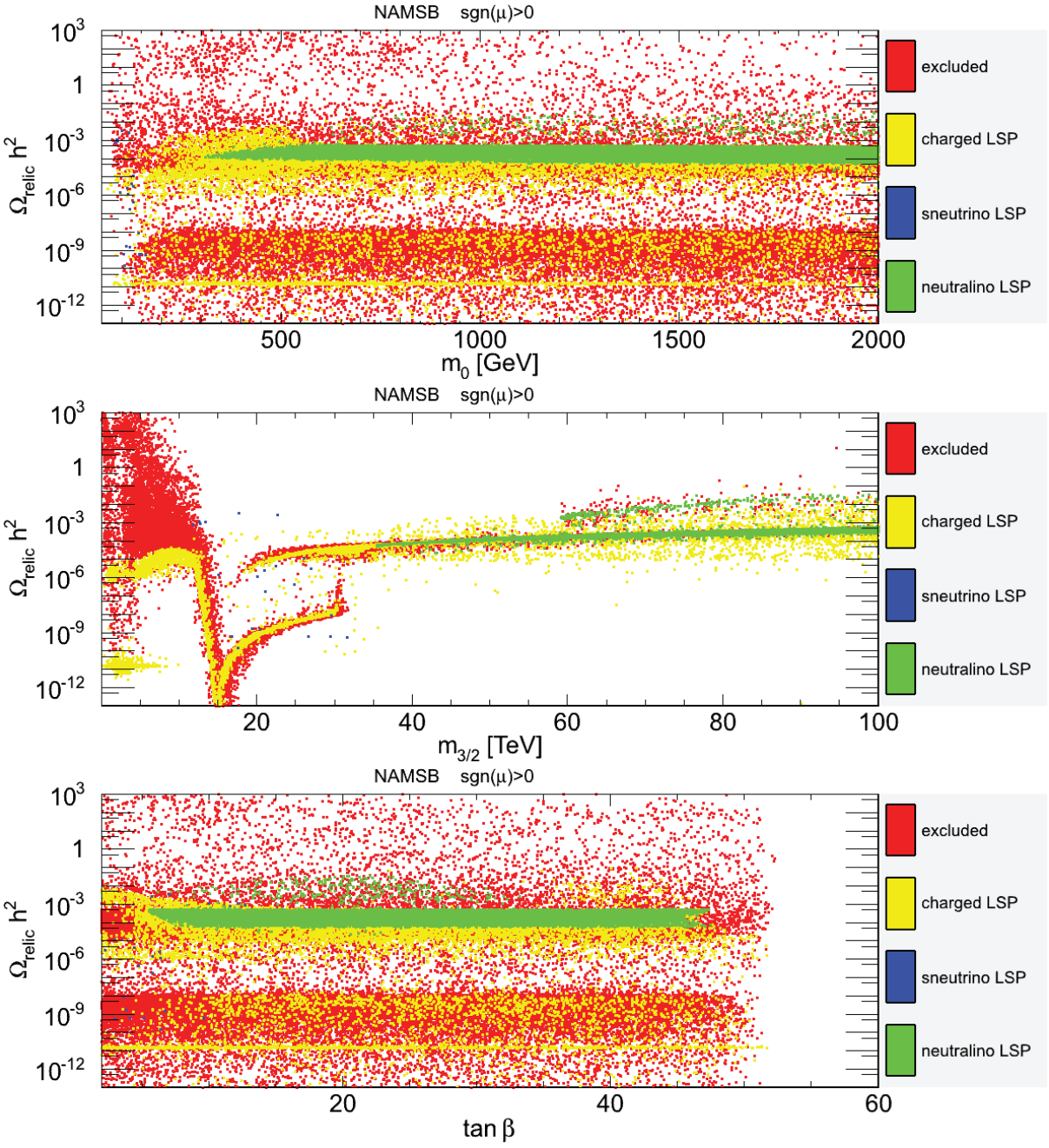

Figure 4.8: Relic density in function of the mNAMSB parameters. The colour codes are the same as in fig. 4.2.

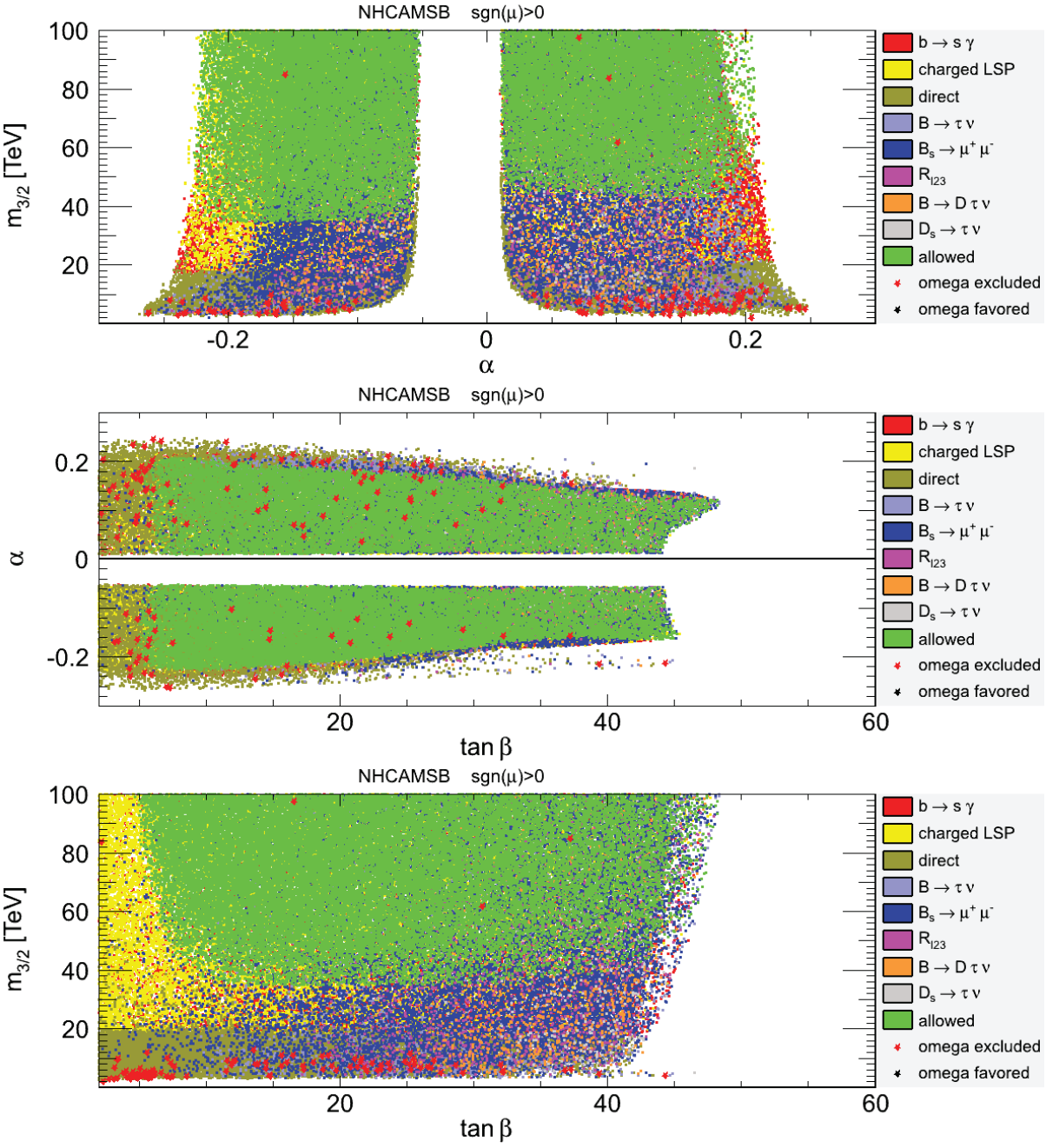

Figure 4.9: Constraints on the NHCAMSB parameter space. The colour codes are the same as in fig. 4.1.

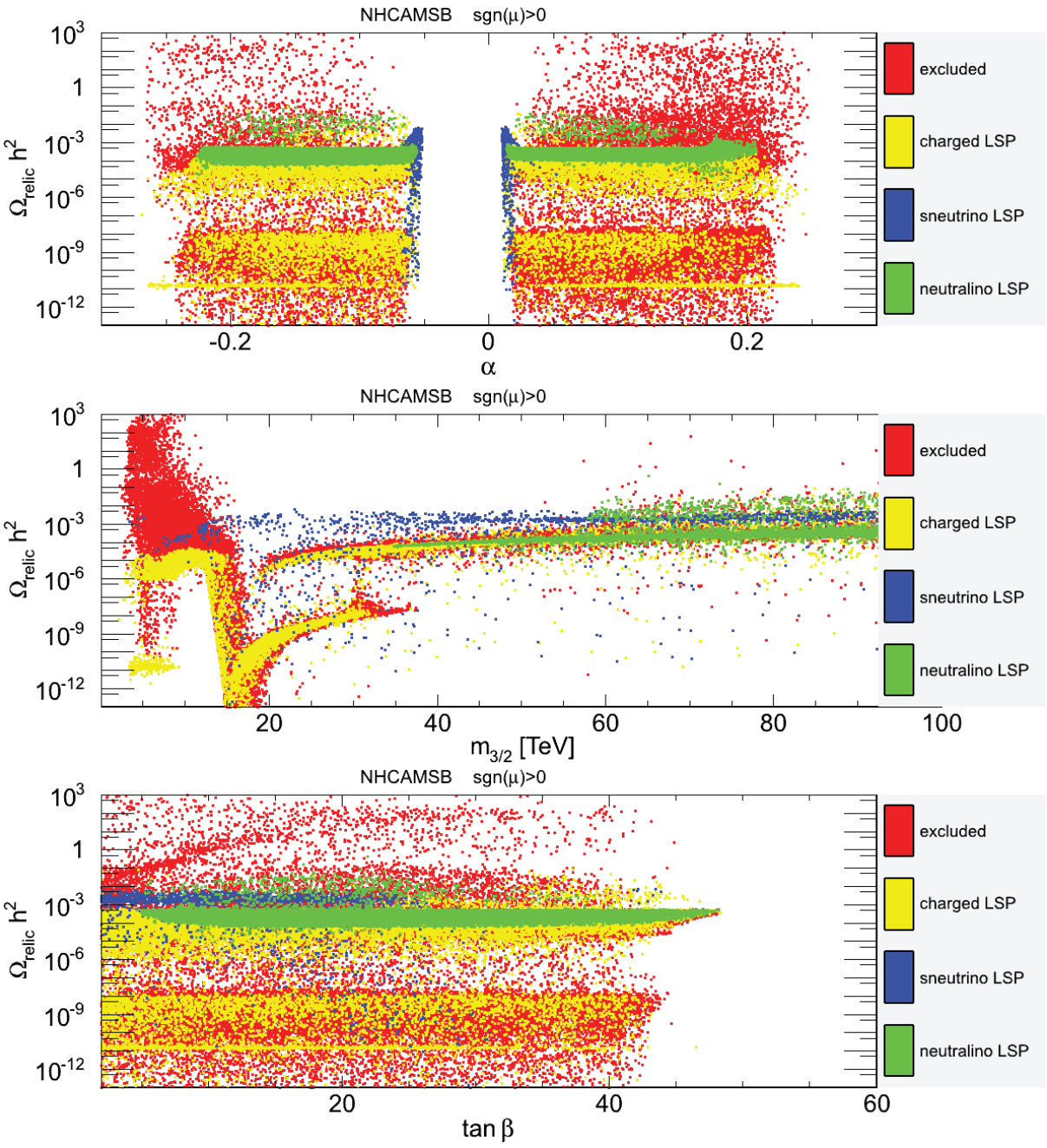

Figure 4.10: Relic density in function of the NHCAMSB parameters. The colour codes are the same as in fig. 4.2.

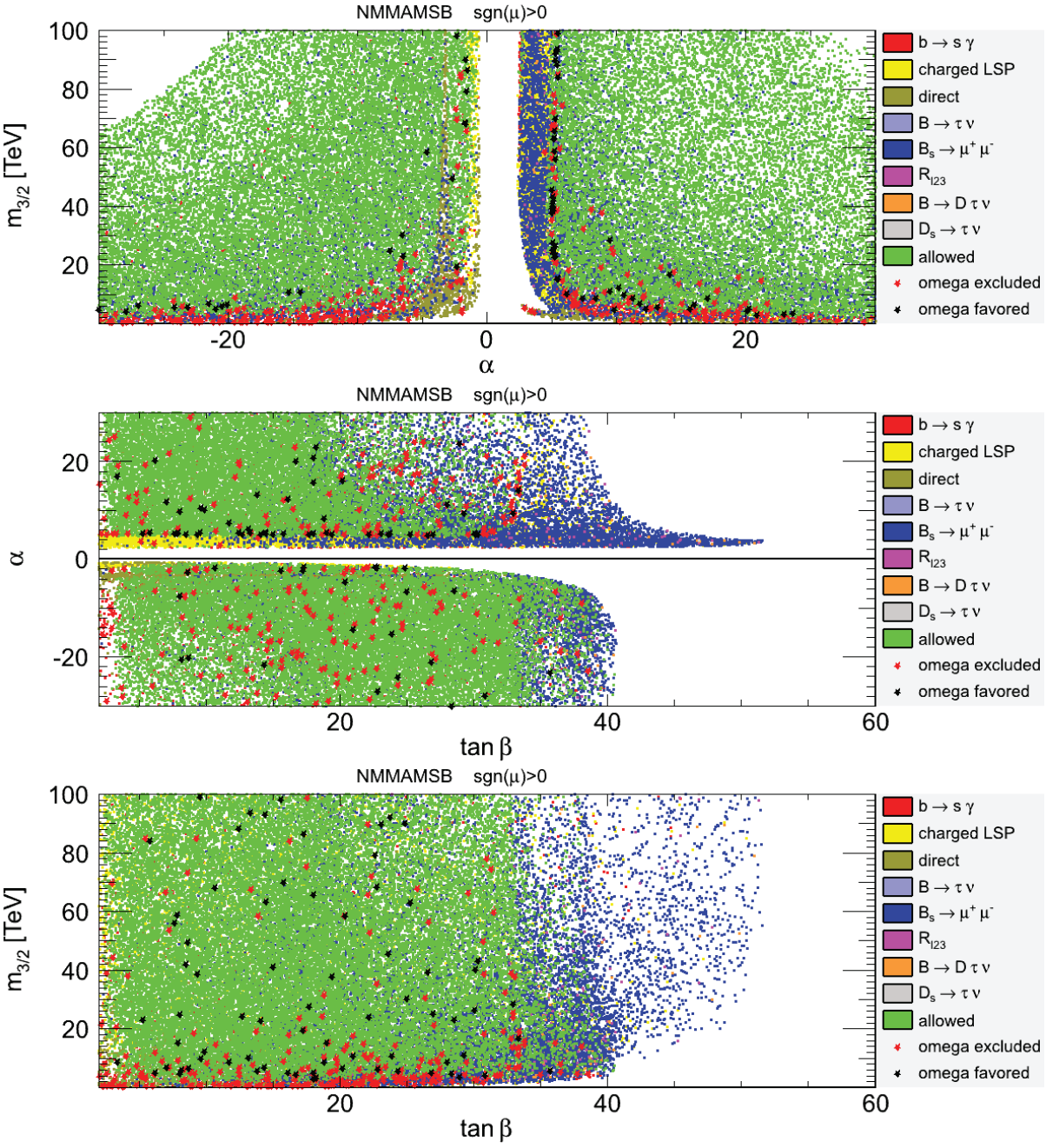

Figure 4.11: Constraints on the NMMAMSB parameter space. The colour codes are the same as in fig. 4.1.

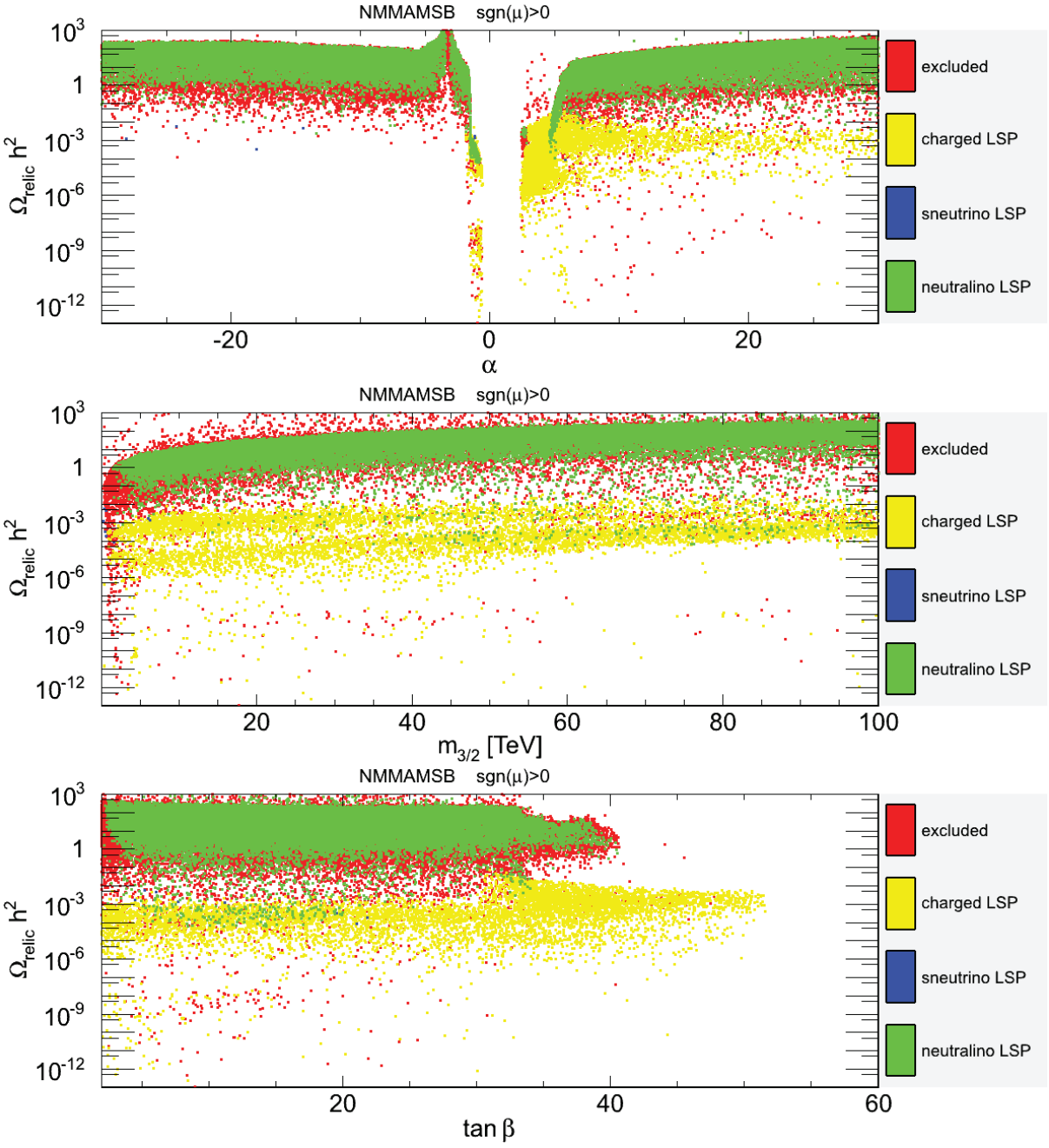

Figure 4.12: Relic density as a function of the NMMAMSB parameters. The colour codes are the same as in fig. 4.2.

4.5 AMSB and relic density in alternative cosmology

We have seen in the previous section that the relic density imposes severe constraints to the parameter spaces, excluding a major part of the AMSB scenarios. However, the relic density calculation is generally based on the simplistic standard model of cosmology. In this section, we reinterpret the previous results by considering four different alternatives to the cosmological standard scenario described in section 1.4. For this study, we focus our interest on six different benchmark points, which are described in Table 4.1 and are representative of the allowed parameter space in the different models. The mass spectra associated to these points are shown in fig. 4.13.

4.5.1 BBN constraints and modified relic density

The different scenarios discussed in section 1.4 do not have impact on the cosmological observations, but they can modify the abundance of the elements. We compute with AlterBBN [62] the abundance of the elements in the different scenarios for each benchmark points, varying the single parameter for a given scenario, and we apply the following conservative constraints [157]:

$$0.240 < Y_p < 0.258\ , \qquad 1.2\times10^{-5} < {}^2H/H < 5.3\times10^{-5}\ , \tag{4.20}$$
$$0.57 < {}^3H/{}^2H < 1.52\ , \qquad {}^7Li/H > 0.85\times10^{-10}\ , \qquad {}^6Li/{}^7Li < 0.66\ ,$$

for the helium abundance Y_p and the primordial ${}^2H/H$, ${}^3H/{}^2H$, ${}^7Li/H$ and ${}^6Li/{}^7Li$ ratios.

In fig. 4.14, we consider the relic density calculated for each of the benchmark points (A-F, from top to bottom) and for different cosmological scenarios (from left to right).

These plots reveal that the quintessence and inflaton scenarios globally increase the relic density, while the entropy and reheating scenarios decrease it. The comparison with the BBN constraints is also represented, and the red part of the curves is excluded at 95% C.L., while the blue part gives a correct abundance of the elements. As general features, the quintessence and inflaton scenarios can increase the relic density by three orders of magnitudes without interfering with the BBN constraints, and the entropy and reheating scenarios can decreased to a factor of 10^6. Therefore, apart from point B which has an extremely low relic density value in the standard cosmological scenario, all the other benchmark points can have a relic density value compatible with the cosmological observations if a non minimal cosmological scenario is considered.

4.6 Generalised relic density constraints

We have shown with different well-known cosmological scenarios, that the relic density constraints can be very strongly relaxed. Therefore, we propose to compare the relic density calculated in the standard model of cosmology to the following interval

$$10^{-4} < \Omega_{DM}h^2 < 10^5 \tag{4.21}$$

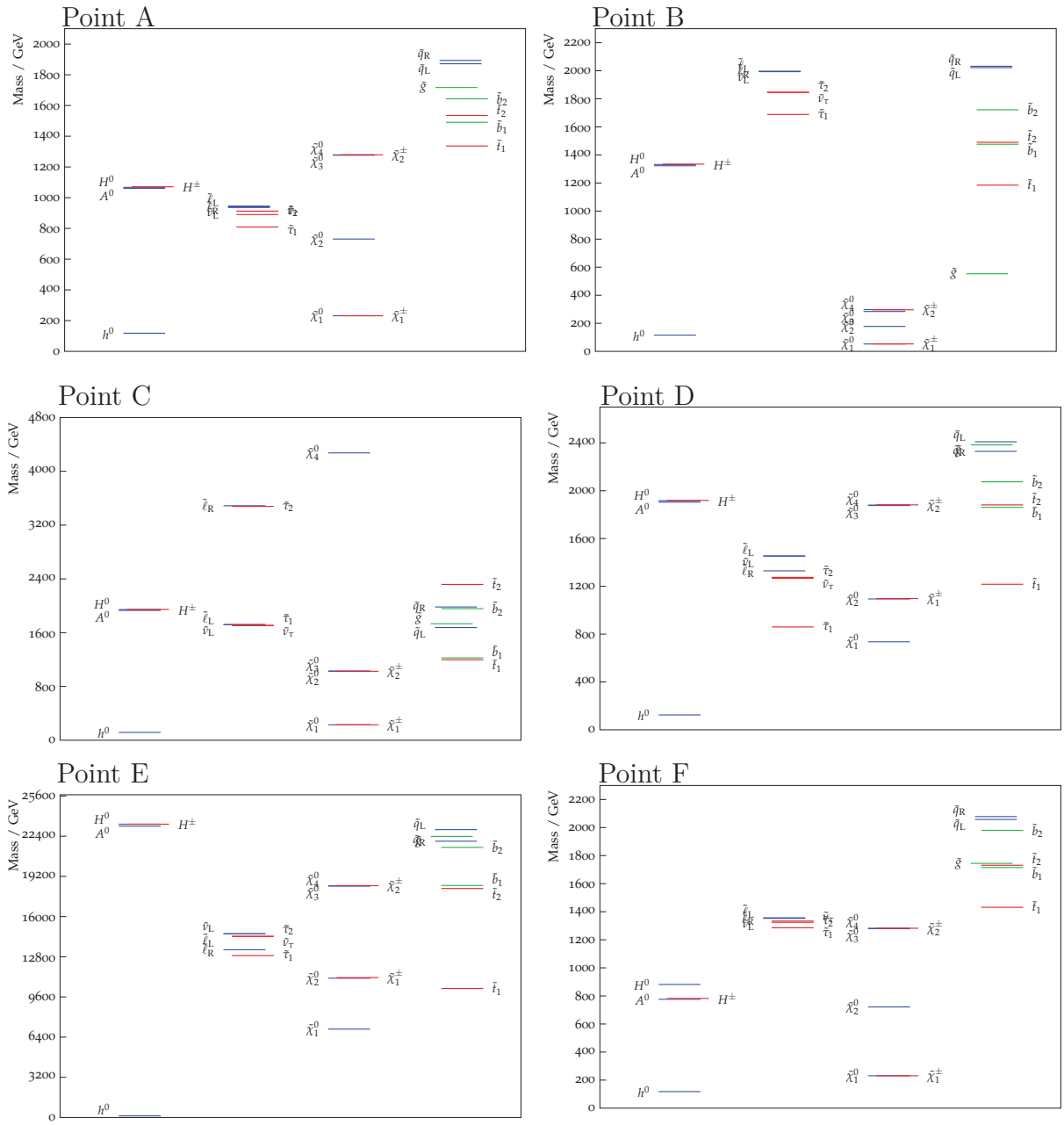

Figure 4.13: Mass spectra of the six benchmark points. Note that the scales are not identical for all spectra.

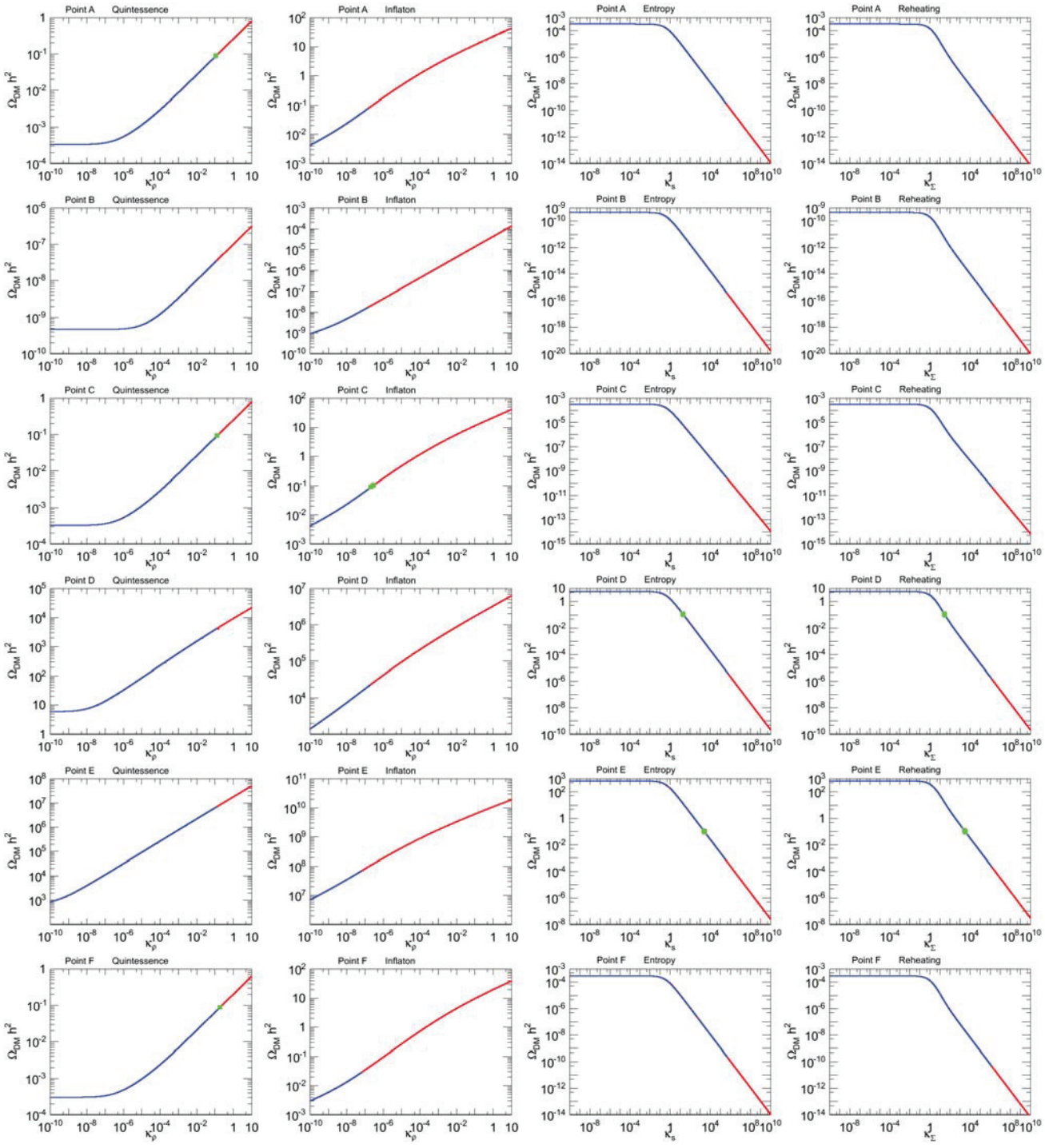

Figure 4.14: Relic density in function of the cosmological model parameters. The red lines correspond to points excluded by the BBN constraints in Eq.(4.20), whereas the blue lines correspond to a region with a correct abundance of the elements. The green squares correspond to points allowed by the BBN constraints and giving a relic density in agreement with the WMAP dark matter interval.

Point	Model	$\Omega_{DM}h^2$	m_0 (GeV)	α	$m_{3/2}$ (TeV)	$\tan\beta$	M_A(GeV)	m_{h_0} (GeV)
A	mAMSB	3.33×10^{-4}	1000	n/a	80	30	1060.5	118.15
B	mAMSB	4.63×10^{-10}	2000	n/a	20	40	1322.8	115.7
C	HCAMSB	3.24×10^{-4}	n/a	0.1	80	10	1931.3	116.32
D	MMAMSB	5.98	n/a	10	20	30	1904.4	124.31
E	MMAMSB	6.95×10^{2}	n/a	20	100	10	2320.5	128.24
F	mNAMSB	1.21×10^{-2}	1300	n/a	70	20	770	118

Table 4.1: Benchmark points for testing alternative cosmology scenarios. All these points have $\mu > 0$ and are in agreement with all the flavour and direct search constraints but would be excluded by WMAP constraints based on the standard cosmology. For the point F extra parameters are needed to specify a point in the parameter space, which are chosen to be: $\lambda = -0.1$, $\kappa = 0.5$ and $A_\kappa = 1500$ GeV.

to take into consideration the fact that it is possible to increase any relic density calculated in the standard cosmology by three orders of magnitude, and to decrease it by six orders, with non-standard cosmological scenarios in agreement with the current cosmological data. We can re-apply the relic density constraints, and the results are shown in figs. 4.15-4.20. As in the figures of section 4.1, the green zones correspond to regions in agreement with all flavour and direct constraints, but not necessarily with the relic density constraint. We added in the figures black points, which correspond to regions also in agreement with the new dark matter interval. It is clear that the allowed regions are therefore much larger than with the initial relic density interval, but a surprising result is that even with the very large interval we use here for the relic density, the relic density constraint still excludes large part of the parameter spaces. In particular, in the mAMSB and HCAMSB scenarios and their NMSSM counterparts, the relic density constraints clearly exclude the region $m_{3/2} \lesssim 40$ TeV. The MMAMSB scenario however is not constrained anymore when using the new dark matter interval.

4.7 LHC phenomenology

The benchmark points selected for testing alternative cosmology scenarios are in agreement with precision flavour and direct search constraints. It turns out that the phenomenology expected at the LHC is quite peculiar. The mass spectra for the benchmark points we considered show that the lightest neutralino is the LSP and the lightest chargino is in most cases very close in mass to the neutralino (points A, B, C, F). This will give rise to peculiar signatures due to the very limited number of open channels for the decay modes. We analyse in more detail in the following each of the six benchmark points previously selected. Production of charginos and neutralinos takes place at the LHC via cascade decays of squark and gluinos and via the direct production channels

$$pp \to \tilde{\chi}_i \tilde{\chi}_j + X \tag{4.22}$$

where the s-channel exchange of an off-shell W or Z or photon, and the contribution of SUSY-QCD diagrams are important. Indeed these cross-sections receive important SUSY-QCD cor-

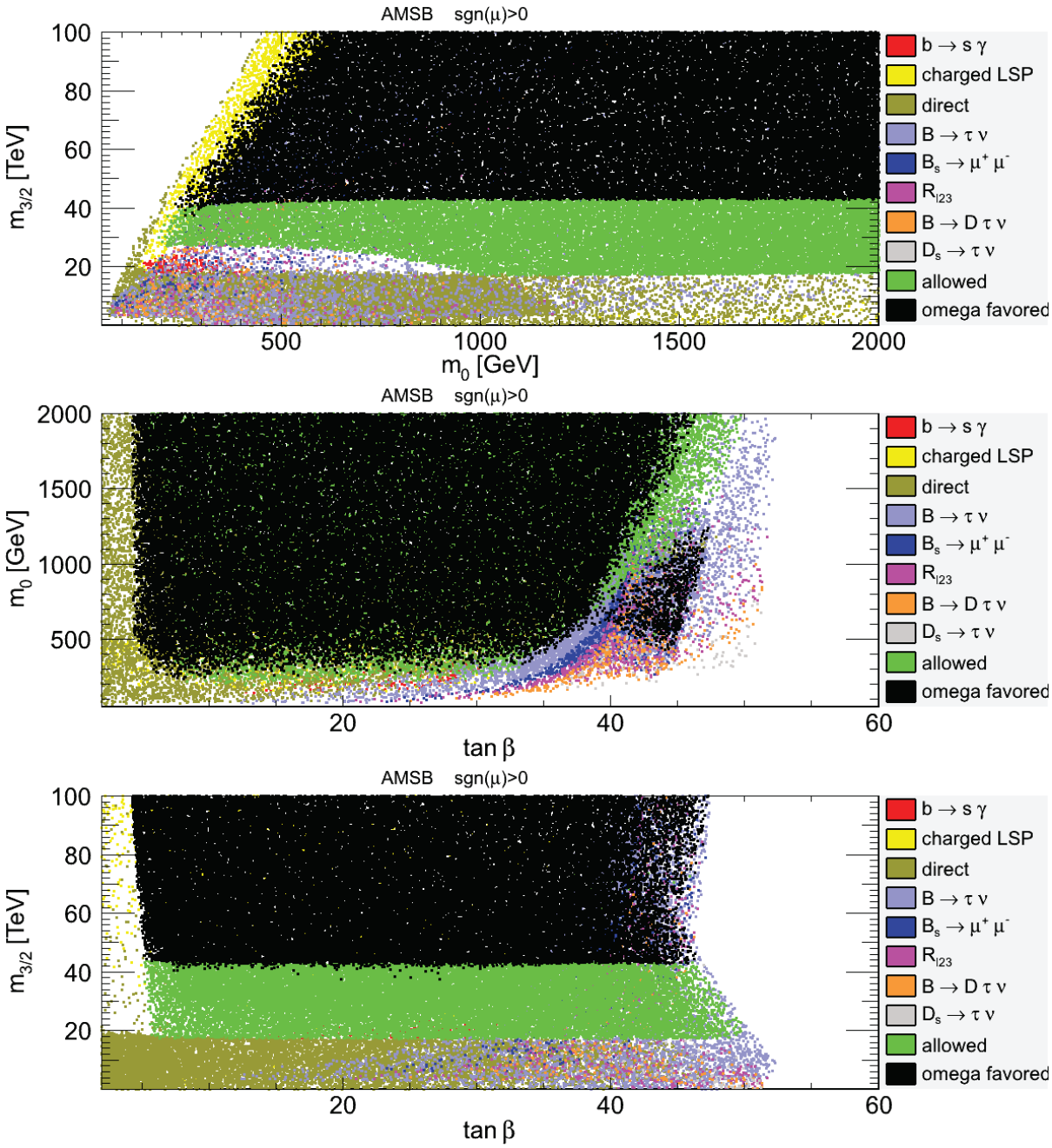

Figure 4.15: Constraints on the minimal AMSB parameter space. The exclusion regions are plotted in the order given in the legend. The red zones are excluded by the inclusive branching ratio of $B \to X_s\gamma$, the yellow ones correspond to charged LSP, the olive green area is excluded by direct collider constraints, the light blue zones are excluded by BR($B \to \tau\nu$), the dark blue zones by BR($B_s \to \mu^+\mu^-$), the magenta zones by $R_{\ell 23}$, the orange zones by BR($B \to D\tau\nu$) and the grey zones by BR($D_s \to \tau\nu$). The green areas are in agreement with all the previously mentioned constraints. The black area corresponds to parameters in agreement with all constraints, including the revised relic density interval given in Eq.(4.21).

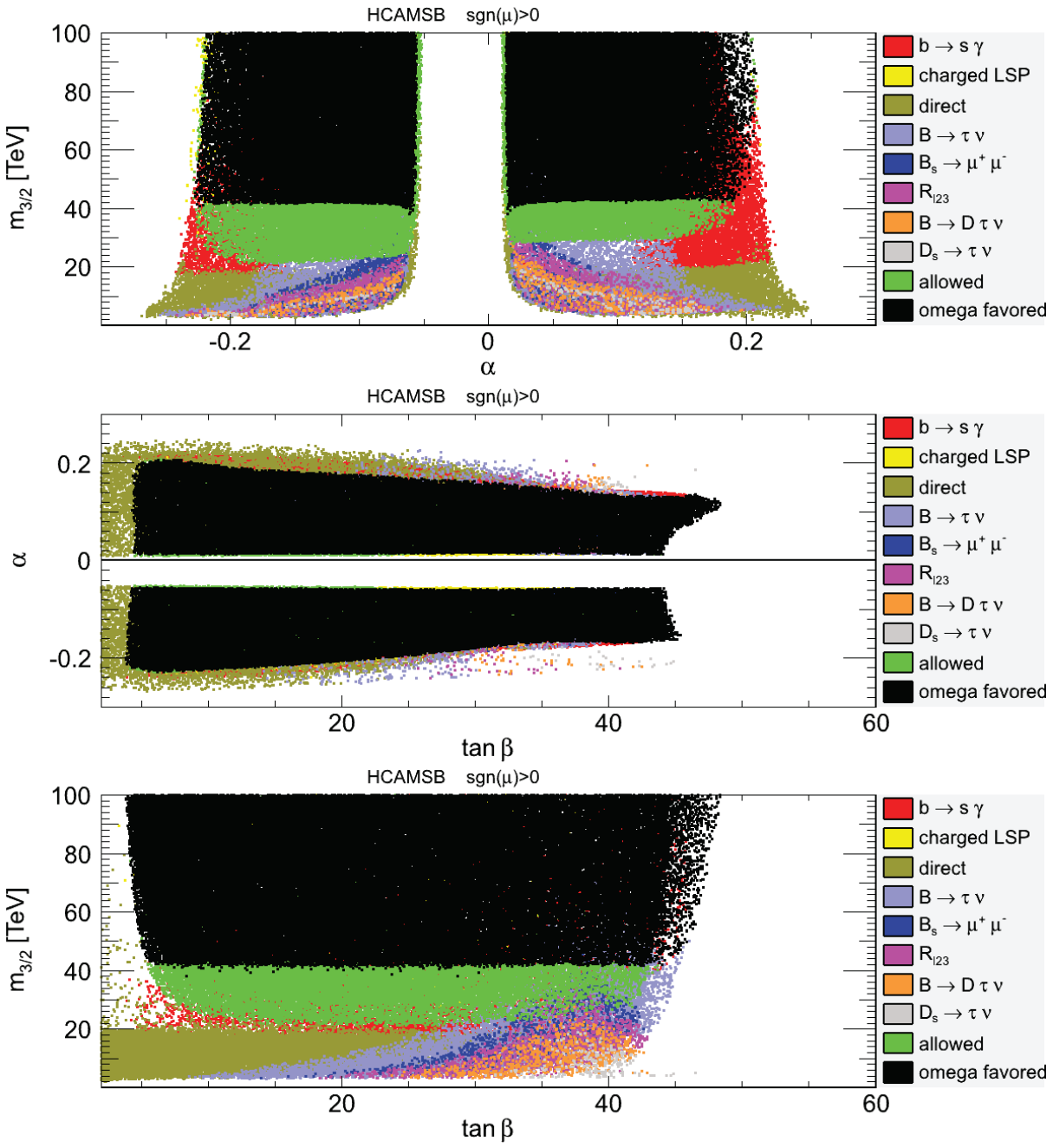

Figure 4.16: Constraints on the HCAMSB parameter space with the revised relic density interval given in Eq.(4.21). The colour codes are the same as in fig. 4.15.

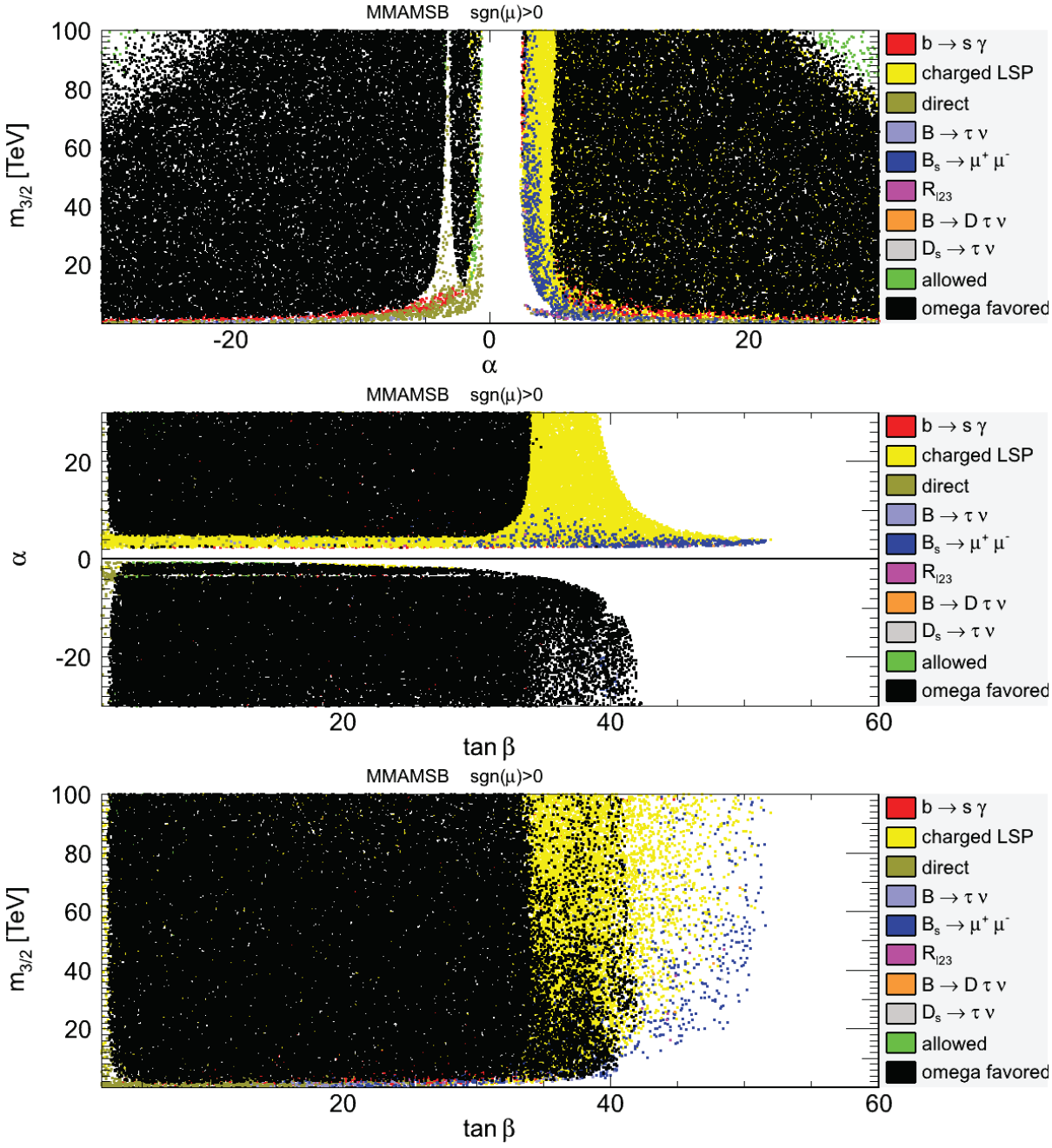

Figure 4.17: Constraints on the MMAMSB parameter space with the revised relic density interval given in Eq.(4.21). The colour codes are the same as in fig. 4.15.

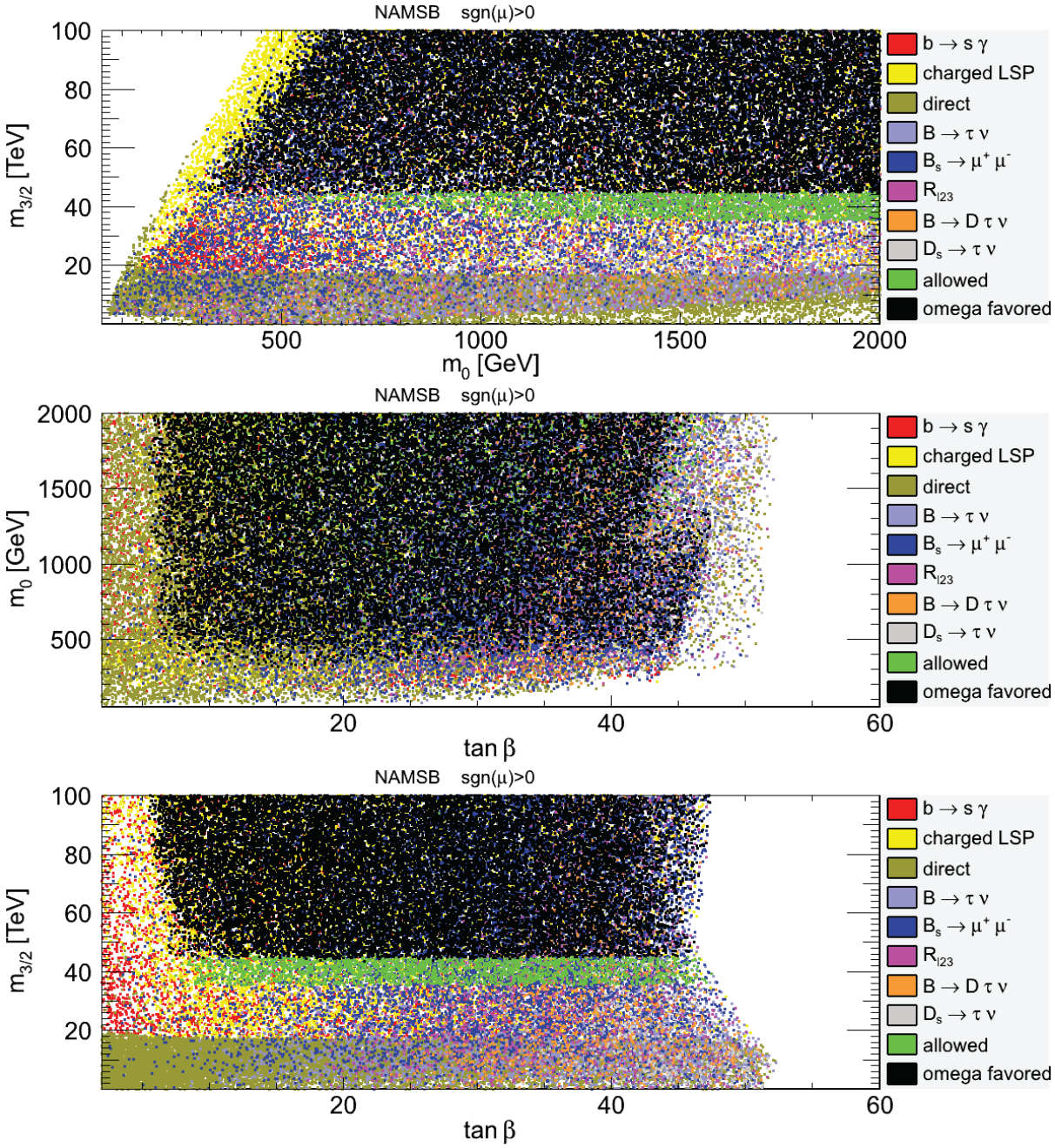

Figure 4.18: Constraints on the mNAMSB parameter space with the revised relic density interval given in Eq.(4.21). The colour codes are the same as in fig. 4.15.

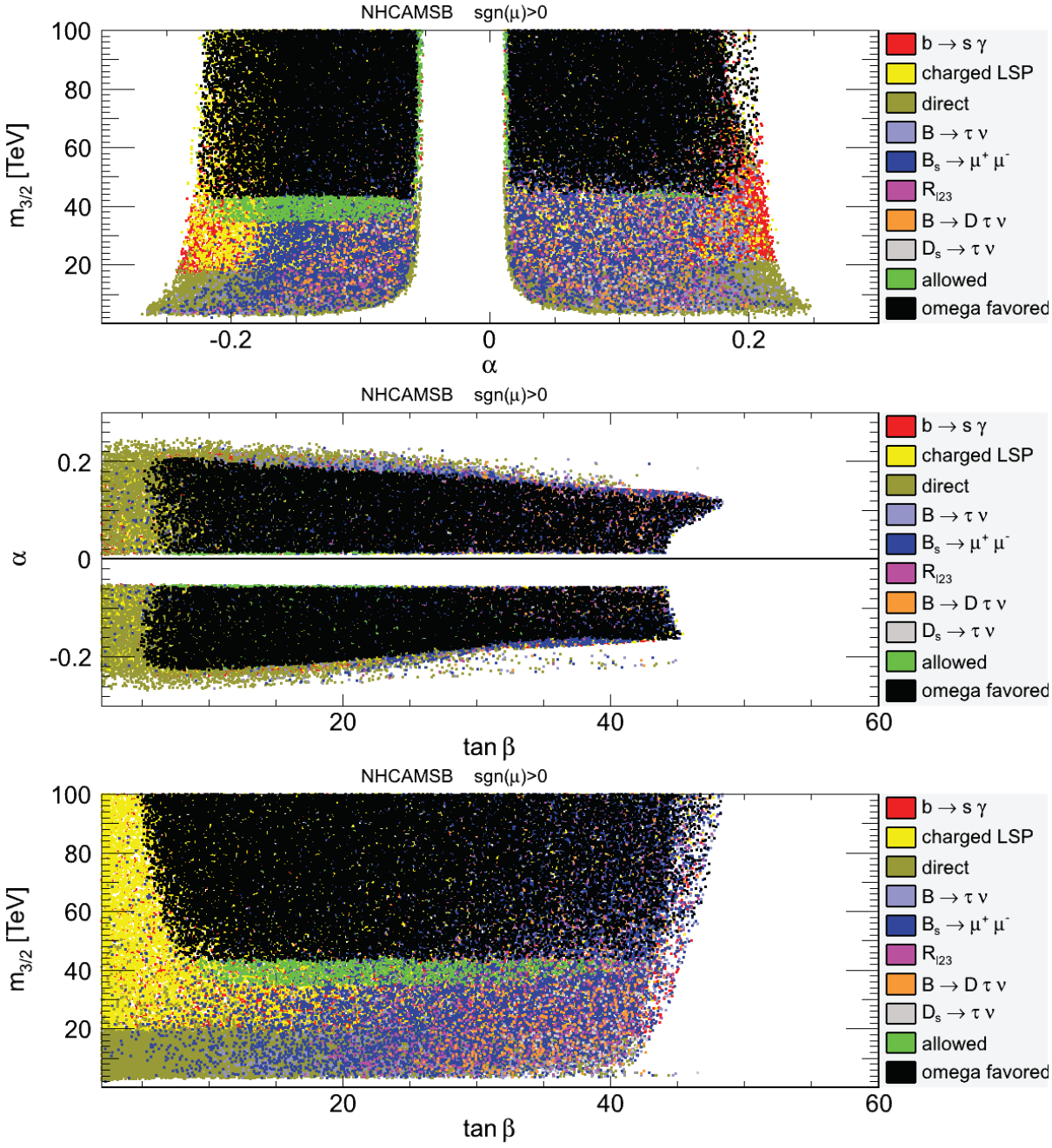

Figure 4.19: Constraints on the NHCAMSB parameter space with the revised relic density interval given in Eq.(4.21). The colour codes are the same as in fig. 4.15.

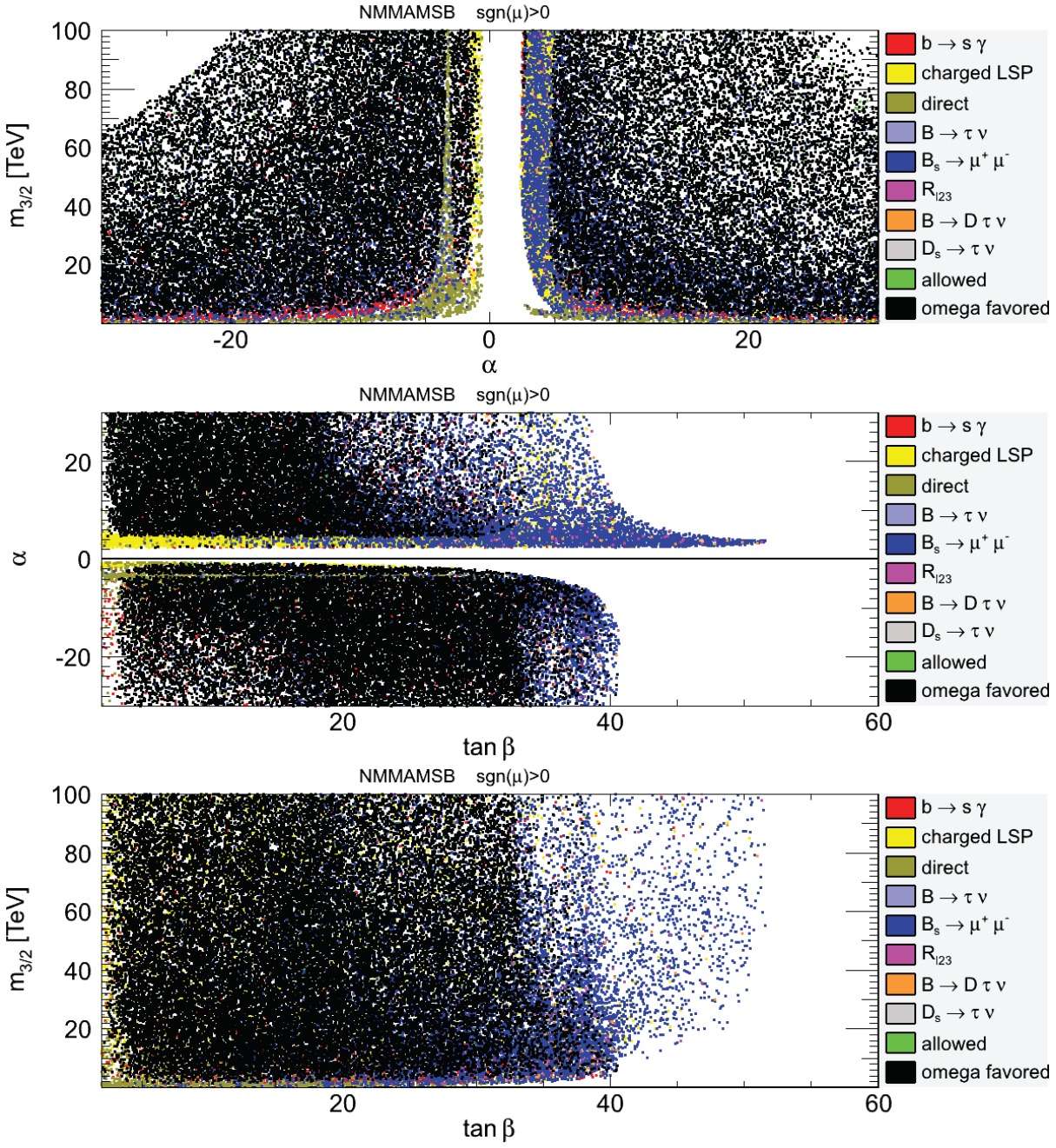

Figure 4.20: Constraints on the NMMAMSB parameter space including the revised relic density interval. The colour codes are the same as in fig. 4.15.

rections, typical values are given in [158] or can be obtained using a Monte Carlo program including the relevant K-factors or the detailed next-to-leading matrix elements.

4.7.1 mAMSB point A

The minimal AMSB scenario is disfavoured by the standard cosmology as very far from the WMAP dark matter allowed interval. The region allowed in our more general analysis typically favours points in which the lightest chargino and neutralino are very close in mass and not so heavy. For point A, $m_{\tilde{\chi}_1^0} = 231.76$ GeV and $m_{\tilde{\chi}_1^+} = 231.93$ GeV so that the mass splitting is only 170 MeV. Due to this small mass splitting, the open decay modes for the $\tilde{\chi}_1^+$ are (neglecting very small modes below the 10^{-3} level) $\tilde{\chi}_1^+ \to \tilde{\chi}_1^0 l\nu$, where

$$\mathrm{BR}(\tilde{\chi}_1^+ \to \tilde{\chi}_1^0 \mu^+ \nu_\mu) \simeq 1.87 \times 10^{-2} \tag{4.23}$$

$$\mathrm{BR}(\tilde{\chi}_1^+ \to \tilde{\chi}_1^0 e^+ \nu_e) \simeq 1.87 \times 10^{-2} \tag{4.24}$$

$$\mathrm{BR}(\tilde{\chi}_1^+ \to \tilde{\chi}_1^0 \pi^+ \to \tilde{\chi}_1^0 e^+ \nu_e) \simeq 0.96\,, \tag{4.25}$$

so that $l = e$ and $l = \mu$ have the same branching through the three body decays while most of the signal with $\tilde{\chi}_1^0 e^+ \nu_e$ is through the two body production of a charged pion. The next lightest particle is the $\tilde{\chi}_2^0$, decaying mainly to $\tilde{\chi}_1^+$ and W or $\tilde{\chi}_1^0$ and SM-like Higgs as for the light Higgs for this point (118.15 GeV) the decay is kinematically allowed :

$$\mathrm{BR}(\tilde{\chi}_2^0 \to \tilde{\chi}_1^\pm W^\mp) \simeq 0.75 \tag{4.26}$$

$$\mathrm{BR}(\tilde{\chi}_2^0 \to \tilde{\chi}_1^0 h^0) \simeq 0.19 \tag{4.27}$$

$$\mathrm{BR}(\tilde{\chi}_2^0 \to \tilde{\chi}_1^0 l^+ l^-) \simeq 5.5 \times 10^{-3}\,, \tag{4.28}$$

where $l = e, \mu$. Since the branching of the mode $\tilde{\chi}_1^\pm \to \tilde{\chi}_1^0 l^\pm \nu$ is 100% and the mode $\tilde{\chi}_2^0 \to \tilde{\chi}_1^0 l^+ l^-$ is non-negligible one can study the clean trilepton signal usually suggested at hadron colliders [159, 160].

4.7.2 mAMSB point B

The benchmark point B is in the minimal AMSB scenario too. The situation is similar to the previous point with in this case the lightest chargino and neutralino lighter than the SM-like Higgs boson. For point B, $m_{\tilde{\chi}_1^0} = 52.70$ GeV and $m_{\tilde{\chi}_1^+} = 53.07$ GeV so that the mass splitting is only 63 MeV. The decay modes for the lightest chargino are similar to the previous case

$$\mathrm{BR}(\tilde{\chi}_1^+ \to \tilde{\chi}_1^0 \mu^+ \nu_\mu) \simeq 5.26 \times 10^{-2} \tag{4.29}$$

$$\mathrm{BR}(\tilde{\chi}_1^+ \to \tilde{\chi}_1^0 e^+ \nu_e) \simeq 5.26 \times 10^{-2} \tag{4.30}$$

$$\mathrm{BR}(\tilde{\chi}_1^+ \to \tilde{\chi}_1^0 \pi^+ \to \tilde{\chi}_1^0 e^+ \nu_e) \simeq 0.89\,, \tag{4.31}$$

and for the second neutralino

$$\begin{aligned} \mathrm{BR}(\tilde{\chi}_2^0 \to \tilde{\chi}_1^\pm W^\mp) &\simeq 0.8 && (4.32)\\ \mathrm{BR}(\tilde{\chi}_2^0 \to \tilde{\chi}_1^0 h^0) &\simeq 0.1 && (4.33)\\ \mathrm{BR}(\tilde{\chi}_2^0 \to \tilde{\chi}_1^0 Z^0) &\simeq 9.6 \times 10^{-2}\ . && (4.34) \end{aligned}$$

The SM-Higgs boson (with a mass of 115.7 GeV) decays with a sizeable branching to pairs of lightest charginos and pairs of lightest neutralinos (branching 1.1×10^{-1} and 7.9×10^{-2} respectively) while the largest mode is $h^0 \to b\bar{b}$ with a branching of 6.5×10^{-1}.

4.7.3 HCAMSB point C

The HCAMSB scenario is disfavoured by standard cosmology and excluded by the WMAP dark matter allowed interval as for the minimal AMSB scenario discussed above. Also in this case the lightest chargino and neutralino are very close in mass. The masses are $m_{\tilde{\chi}_1^0} = 229.41$ GeV and $m_{\tilde{\chi}_1^+} = 229.58$ GeV with a splitting of only 17 MeV. In this situation the lightest chargino decays are very close to the numbers for point A. The decay modes for the lightest chargino are :

$$\begin{aligned} \mathrm{BR}(\tilde{\chi}_1^+ \to \tilde{\chi}_1^0 \mu^+ \nu_\mu) &\simeq 1.72 \times 10^{-2} && (4.35)\\ \mathrm{BR}(\tilde{\chi}_1^+ \to \tilde{\chi}_1^0 e^+ \nu_e) &\simeq 1.72 \times 10^{-2} && (4.36)\\ \mathrm{BR}(\tilde{\chi}_1^+ \to \tilde{\chi}_1^0 \pi^+ \to \tilde{\chi}_1^0 e^+ \nu_e) &\simeq 0.96\ , && (4.37) \end{aligned}$$

and for the second neutralino

$$\begin{aligned} \mathrm{BR}(\tilde{\chi}_2^0 \to \tilde{\chi}_1^\pm W^\mp) &\simeq 0.67 && (4.38)\\ \mathrm{BR}(\tilde{\chi}_2^0 \to \tilde{\chi}_1^0 h^0) &\simeq 7.3 \times 10^{-2} && (4.39)\\ \mathrm{BR}(\tilde{\chi}_2^0 \to \tilde{\chi}_1^0 Z^0) &\simeq 0.26 && (4.40) \end{aligned}$$

In this case the trilepton mode $pp \to \tilde{\chi}_1^\pm \tilde{\chi}_2^0 \to 3l + \not{E}_T$ is especially interesting as the branching fraction $\tilde{\chi}_1^+ \to \tilde{\chi}_1^0 l\nu$ is 100% and the one for $\tilde{\chi}_2^0 \to \tilde{\chi}_1^0 Z^0$ is 26%.

4.7.4 MMAMSB point D

The Mixed Modulus AMSB supersymmetry breaking scenario allows for viable dark matter candidates. Benchmark point D has the neutralino LSP with a mass $m_{\tilde{\chi}_1^0} = 736$ GeV. The next-to-lightest supersymmetric particle is the stau with a mass $m_{\tilde{\tau}} = 860$ GeV while the lightest chargino and the second lightest neutralino are heavier and almost degenerate with a mass of 1095 and 1098 GeV respectively. The stau decays to tau and the lightest neutralino

$$\mathrm{BR}(\tilde{\tau} \to \tilde{\chi}_1^0 \tau) = 1\ , \qquad (4.41)$$

while the lightest chargino decays mainly to

$$\mathrm{BR}(\tilde{\chi}_1^+ \to \tilde{\tau}\nu_\tau) \simeq 0.84 \tag{4.42}$$

$$\mathrm{BR}(\tilde{\chi}_1^+ \to \tilde{\chi}_1^0 W) \simeq 0.16\,. \tag{4.43}$$

The second lightest neutralino decays to stau and tau while as the SM-like Higgs is light enough to be produced (124.3 GeV), the decay $\tilde{\chi}_2^0 \to \tilde{\chi}_1^0 h^0$ is also kinematically open

$$\mathrm{BR}(\tilde{\chi}_2^0 \to \tilde{\tau}\tau) \simeq 0.83 \tag{4.44}$$

$$\mathrm{BR}(\tilde{\chi}_2^0 \to \tilde{\chi}_1^0 h^0) \simeq 0.16\,. \tag{4.45}$$

4.7.5 MMAMSB point E

For the same model as in the previous paragraph we have also an example of a higher mass spectrum in which all supersymmetric partners are quite heavy with the neutralino LSP above 7 TeV and all other particles above 10 TeV.

4.7.6 mNAMSB point F

NMSSM with minimal AMSB scenario is one of the models considered in the previous sections. It is disfavoured by the relic density constraints if standard cosmology is assumed. Point F is in the allowed zone for flavour, low energy and direct search constraints and is allowed if standard cosmology constraints are relaxed as discussed in the previous sections. From the point of view of LHC searches, this point is similar to point A. For point F, $m_{\tilde{\chi}_1^0} = 230.03$ GeV and $m_{\tilde{\chi}_1^+} = 231.02$ GeV so that the mass splitting is 99 MeV. Apart from these two particles, the next supersymmetric particle (in terms of mass) is the second neutralino (see fig. 4.13) with a mass of 721 GeV.

4.8 Conclusions and perspectives

We have considered in details the constraints on different possible realisations of superconformal anomaly mediation breaking mechanisms in supersymmetry. These constraints include the usual LEP, B-factories, Tevatron and LHC searches, but also precision constraints of cosmological origin, namely the WMAP limits on the relic density of cold dark matter. We have discussed the standard cosmological approach and also alternative cosmological scenarios which do not change the cosmological observations but which can affect strongly the constraints on the parameter space of these supersymmetric models based on the relic abundance of dark matter. We therefore show how the dark matter constraints can be weakened in order to avoid strong model dependent assumptions in the choice of the cosmological model. Based on different benchmark points for AMSB models, we performed a detailed analysis of the constraints imposed by particle data and cosmology (both standard and alternative) and finally we gave the typical mass spectra and decay modes relevant for the LHC searches. The main lesson that

can be learnt in such an exercice is that usual bounds on the parameter space of these models are too restrictive and bear a strong hidden cosmological model dependence in the assumption of the standard cosmological scenario. Concerning the LHC searches, points which are excluded in the standard analysis but permitted in this more general approach, may be quite relevant for testing not only the particle theory models themselves but also alternative cosmological scenarios at the LHC, as in many cases relatively low mass supersymmetric particles are allowed with a peculiar spectrum where the lightest neutralino and chargino are very close in mass.

Chapter 5

Impact of Higgs data on AMSB, HCAMSB and MMAMSB

5.1 Introduction

The ATLAS and CMS experiments at the Large Hadron Collider (LHC) have reported the discovery of a new boson compatible with the Standard Model (SM) Higgs in July 2012 [161, 162], and updated results of the measurements of the Higgs couplings with more precision have been recently released [163–168] and [177, 178, 178–183]. All the results are compatible with the predictions for a SM Higgs boson with a mass of about 126 GeV. This discovery is especially important in the context of new physics models, and in particular supersymmetry (SUSY), where the Higgs mass and decay rates can be related to the SUSY parameters.

The mass of the lightest CP-even Higgs particle is bounded from above and it depends on SUSY parameters that enter radiative corrections

$$M_h^{\max} \approx M_Z |\cos(2\beta)| + \text{radiative corrections} \leq 110 - 135\text{GeV} \tag{5.1}$$

The requirement that h boson mass coincides with the value of the Higgs particle observed at LHC would place strong constraints on the MSSM parameters through their contributions to radiative corrections to Higgs sector. At the one-loop level, M_h receives corrections that grow as the fourth power of the top quark mass m_t, and logarithmically with the SUSY breaking scale. Also the trilinear coupling in the stop sector A_t plays an important role.

$$\epsilon = \frac{3\, m_t^4}{2\pi^2 v^2 \sin^2\beta}\left(\log\frac{M_S^2}{m_t^2} + \frac{X_t^2}{2M_S^2}\left(1 - \frac{X_t^2}{6M_S^2}\right)\right) \tag{5.2}$$

where $M_S = \sqrt{m_{\tilde{t}_1} m_{\tilde{t}_2}}$ and $X_t = A_t - \frac{\mu}{\tan\beta}$.

We obtain a large value for M_h in the so-called *maximal mixing* scenario where $X_t = \sqrt{6} M_S$ [1]. One can also obtain a larger value for M_h if we have heavy stops (we choose M_S ∼3 TeV as

1. We note that there is also the *no mixing* scenario in which the radiative corrections are smaller for $X_t \sim 0$. Another scenario is the *typical mixing* one in which X_t is of the same order of M_S, i.e. $X_t \sim M_S$.

maximal value to have acceptable fine-tuning) and if we are in the *decoupling regime* where the pseudo-scalar Higgs boson is heavy $M_A \sim$ TeV [169].

5.2 Tools and Constraints

In order to study the different AMSB scenarios, we used `ISAJET 7.82` [153] to generate the SUSY spectra, compute the flavour observables and relic density with `SuperIso Relic v3.2` [148, 154], and we generate the Higgs branching fractions and decay widths with `HDECAY 5.11` [170]. In the following, we disregard the case of negative sign(μ) since it is disfavored by the muon anomalous magnetic moment constraint. Also, we impose the condition on the SUSY breaking scale $M_S = \sqrt{m_{\tilde{t}_1} m_{\tilde{t}_2}} < 3$ TeV as a typical scale to limit fine-tuning.

5.2.1 flavour bounds

It is well known that flavour physics observables provide important constraints on the MSSM. Similar considerations apply also in the case of the models under study. The first flavour observable that we consider here is the inclusive branching ratio of $B \to X_s\gamma$, which has been thoroughly studied in the literature and is still under scrutiny. This observable is very interesting, as its SM contributions only appear at loop level, and its theoretical uncertainties as well as the experimental errors are now very well under control. It provides strong constraints on the supersymmetric parameter space, especially for large $\tan\beta$, where it receives large enhancements from its supersymmetric contributions. We use the following interval at 95% C.L. [148, 149]:

$$2.63 \times 10^{-4} < \mathrm{BR}(B \to X_s\gamma) < 4.23 \times 10^{-4} \, . \tag{5.3}$$

Another interesting observable is the branching fraction of $B_s \to \mu^+\mu^-$, which is also a loop level observable, and which can receive extremely large contributions from SUSY at large $\tan\beta$, and can be enhanced by several orders of magnitude as compared to the SM branching ratio. The first evidence for this decay has been reported by the LHCb collaboration very recently [171]. We use the following 95% C.L. interval which includes 10% theoretical error :

$$0.99 \times 10^{-9} < \mathrm{BR}(B_s \to \mu^+\mu^-)_{\mathtt{untag}} < 6.47 \times 10^{-9} \, , \tag{5.4}$$

where `untag` denotes the untagged branching fraction, which can be derived from the CP-averaged branching fraction and directly compared to the experimental measurement [172–174].

The purely leptonic decay of $B_u \to \tau\nu$ on the other hand is sensitive to supersymmetry through the exchange of a charged Higgs boson already at tree level, which does not suffer from the helicity suppression of the SM contribution with the exchange of a W boson. This decay can therefore provide stringent constraints, and we use:

$$0.56 \times 10^{-4} < \mathrm{BR}(B_u \to \tau\nu) < 2.7 \times 10^{-4} \, . \tag{5.5}$$

Other flavour observables could be added to this list, however we have just included the most stringent ones for this analysis. A more complete analysis including all flavour information

requires in principle a global fit to all observables, similar to the ones performed to test the Standard Model. This however goes beyond the scope of this preliminary screening of the extensions of AMSB models discussed here.

5.2.2 Relic density

The WMAP data [44] provide precise observations of the cold dark matter density in the Universe. We use them to impose constraints on the AMSB parameter spaces by computing the relic density with `SuperIso Relic`. We consider the WMAP interval at 95% C.L. increased by 10% of theoretical error to account for the uncertainties in the calculation of the relic density:

$$0.068 < \Omega_\chi h^2 < 0.155 \, . \tag{5.6}$$

However the relic density constraint can be falsified in alternative cosmological model [61] or if dark matter is composed by more than one species, and we therefore also consider a loose interval:

$$10^{-4} < \Omega_\chi h^2 < 0.155 \, , \tag{5.7}$$

in which we relaxed the lower bound.

In addition to these bounds, we impose the neutralino to be the lightest supersymmetric particle (LSP) to avoid problems with charged or not-so-weakly-interacting relics. This constraints could be avoided if R-parity is violated or if a lighter neutral SUSY particle like a gravitino is present.

5.2.3 Higgs searches

The discovery of a Higgs-like particle at the LHC provides important information on the MSSM [169, 175, 176]. In the following, we associate the newly discovered boson to the lightest CP-even Higgs h. The Higgs mass value close to 126 GeV brings constraints on the parameter

	Value	Experiment
M_h	125.7±2.1 GeV	ATLAS [177], CMS [178]
$\mu_{\gamma\gamma}$	1.20±0.30	ATLAS [179], CMS [180]
μ_{ZZ}	1.10±0.22	ATLAS [181], CMS [178]
μ_{WW}	0.77±0.21	ATLAS [182], CMS [183]
$\mu_{b\bar{b}}$	1.12 ± 0.45	ATLAS [184], CMS [185], CDF,D0 [186]
$\mu_{\tau\tau}$	1.01 ± 0.36	ATLAS [184], CMS [187]

Table 5.1: Experimental average for the Higgs mass and rates.

space of supersymmetric models due to the well known fact that the Higgs boson mass is linked to the electroweak scale and can not be much larger than the Z-boson mass in low scale supersymmetry. The extra information provided by the measurements of Higgs branching ratios, provides extra useful constraints. The latest LHC measurements of the Higgs mass and

decay rates are summarized in Table 5.1. We use in the following the by now standard notation of signal strengths normalized to the SM expectation, and defined as:

$$\mu_{\gamma\gamma,VV} = \frac{\sigma(\text{gluon fusion})}{\sigma_{\text{SM}}(\text{gluon fusion})} \frac{\text{BR}(h \to \gamma\gamma, VV)}{\text{BR}_{\text{SM}}(H \to \gamma\gamma, VV)} , \tag{5.8}$$

$$\mu_{\tau\tau} = \frac{\sigma(\text{VBF})}{\sigma_{\text{SM}}(\text{VBF})} \frac{\text{BR}(h \to \tau\tau)}{\text{BR}_{\text{SM}}(H \to \tau\tau)} , \tag{5.9}$$

$$\mu_{b\bar{b}} = \frac{\sigma(\text{HV})}{\sigma_{\text{SM}}(\text{HV})} \frac{\text{BR}(h \to b\bar{b})}{\text{BR}_{\text{SM}}(H \to b\bar{b})} , \tag{5.10}$$

where VV refers to vector boson ZZ or WW production, and VBF and HV stand for vector boson fusion and associated Higgs vector boson production.

To evaluate the Higgs production cross sections normalized to the SM values, we use:

$$\frac{\sigma(\text{gluon fusion})}{\sigma_{\text{SM}}(\text{gluon fusion})} \approx \frac{\Gamma^h}{\Gamma^H_{\text{SM}}} \frac{\text{BR}(h \to gg)}{\text{BR}_{\text{SM}}(H \to gg)} , \tag{5.11}$$

$$\frac{\sigma(\text{VBF})}{\sigma_{\text{SM}}(\text{VBF})} \approx \frac{\sigma(\text{HV})}{\sigma_{\text{SM}}(\text{HV})} \approx \frac{\Gamma^h}{\Gamma^H_{\text{SM}}} \frac{\text{BR}(h \to VV)}{\text{BR}_{\text{SM}}(H \to VV)} , \tag{5.12}$$

where Γ^h and Γ^H_{SM} are respectively the MSSM h and SM H total decay widths.

In the following, we do not impose strict intervals on the calculated signal strengths, but we comment on the compatibility of the results with the experimental data.

5.3 Results

We consider the constraints from flavour physics, dark matter and LHC Higgs searches in the context of minimal AMSB, hypercharge AMSB and mixed-moduli AMSB. We show in the following how the available parameter space is reduced in these different models when applying the available constraints.

5.3.1 mAMSB

To study the mAMSB scenario, we perform flat scans by varying the parameters in the following ranges:

$$m_0 \in [50, 10000] \text{ GeV}; m_{3/2} \in [0, 500] \text{ TeV}; \tan\beta \in [1, 55] , \tag{5.13}$$

and use a sample of more than 3 million points.

We first consider the constraints obtained from the Higgs mass measurement. In fig. 5.1, we present the light CP-even Higgs mass as a function of $\tan\beta$ and X_t/M_S, and show the points compatible with the flavour and relic density constraints. First, we see that M_h is limited

to values below 122 GeV, as already pointed out in [175]. The reason is related to the fact that the points of the mAMSB scenario, X_t/M_S is small, corresponding to a no mixing regime which leads to a lower Higgs mass. Second, no mAMSB point is compatible with the tight relic density interval of Eq. (5.6), but there exist points compatible with the loose relic density interval of Eq. (5.7). One of the limiting factors for the light CP-even Higgs mass comes from the restriction $M_S < 3$ TeV that we impose to limit fine-tuning [188].

We consider now the Higgs signal strengths in fig. 5.2 as a function of $\tan\beta$. We include the 2-σ constraint from the Higgs mass on the plots. We first notice that most of the valid points are close to the SM values of the Higgs strengths. Also, all the Higgs strengths can be strongly decreased, which corresponds to a strong suppression in the production cross-sections. Concerning the Higgs to diphoton decay, the predicted strength mainly stands below the 2σ experimental lower bound. We see however that points not compatible with the cosmology constraints can have an increased signal in $\gamma\gamma$ for $\tan\beta \sim 20$. However, all these points correspond to a scenario in which the lightest supersymmetric particle (LSP) is a stau, and the increase is induced by light stau loops as described in [189]. Nevertheless, scenarios with charged LSP are strongly disfavored by the cosmology requirements for a neutral dark matter stable particle.

As a consequence, the mAMSB scenario is compatible with the Higgs mass measurements only marginally at the two-sigma level since the maximum attainable Higgs mass is below 122 GeV, and also the relic abundance constraint can only be met with the loose bounds described above.

5.3.2 HC-AMSB

The HC-AMSB scenario provides a modification of the M_1 bino mass, as discussed in Sec. **??**. We have generated a sample of more than 2 million points through flat scans over the parameters in the following intervals:

$$\alpha \in [-0.3, 0.3]; m_{3/2} \in [0, 500] \text{ TeV}; \tan\beta \in [1, 55] \, . \tag{5.14}$$

In fig. 5.3, we plot the light Higgs mass as functions of $\tan\beta$ and X_t/M_S. Contrary to the mAMSB scenario, the Higgs mass can reach 126 GeV and therefore be fully consistent with the mass constraint. The sfermions are lighter in this scenario as compared to in the mAMSB scenario and X_t/M_S can reach larger values. On the other hand, no point in this scenario is at the same time consistent with the tight relic density constraint of Eq.(5.6), but many points fulfil both the Higgs and loose relic density bounds. More specifically, the allowed points have $\tan\beta \gtrsim 5$ and $X_t \gtrsim M_S$, and therefore correspond to the typical or maximal mixing regimes.

In fig. 5.4, we consider the μ_{WW}, $\mu_{\gamma\gamma}$, $\mu_{b\bar{b}}$ and $\mu_{\tau\tau}$ signal strengths of the Higgs as a function of $\tan\beta$. First, the bulk of points compatible with the flavour constraints are consistent with the SM signal strengths. When imposing the Higgs mass constraint, $\tan\beta$ is restricted to large values, as already noticed in fig. 5.3, and most of the points with low signal strengths are removed. We notice that in the region of $\tan\beta \sim 25 - 30$, the Higgs to two photon channel can be enhanced as in the mAMSB due to the presence of light staus. Finally, we impose the neutralino LSP and loose relic density constraints, and note that this requirement

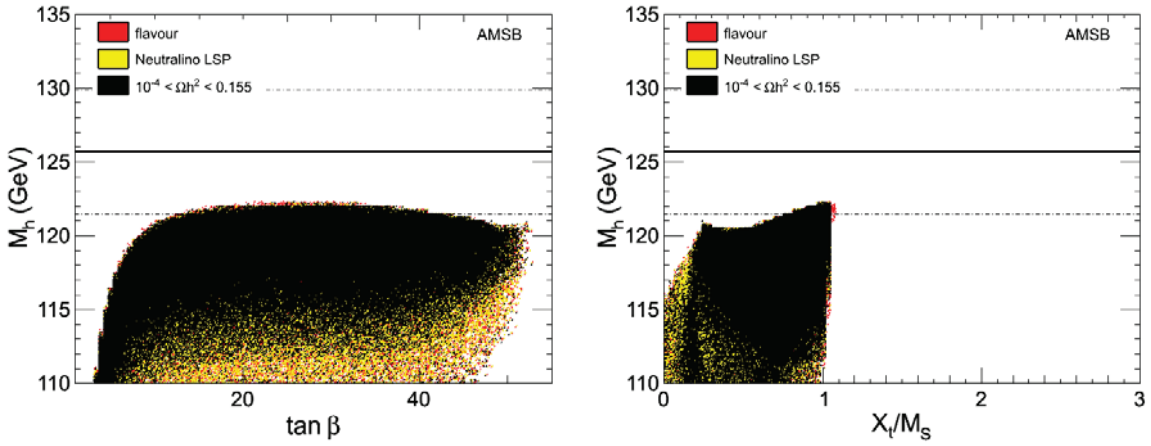

Figure 5.1: Light Higgs mass as functions of $\tan\beta$ (left panel) and X_t/M_S (right panel) in mAMSB. The red points are all points compatible the constraints from flavour physics described in Sec. 5.2.1. The yellow points have also a neutralino LSP. The black points are in addition consistent with the upper bound of the relic density constraint. The horizontal solid line corresponds to the central value of the Higgs mass and the dashed lines to the 2σ deviations.

removes points with enhanced $\gamma\gamma$ signal strength. While this scenario is well compatible with the latest Higgs search results, it may be disfavoured in the future if the $\gamma\gamma$ signal strength value is confirmed to be larger than the SM value. Thus, the HC-AMSB model can explain simultaneously flavour physics, loose relic density bounds and the current Higgs search results, but can be challenged by future more precise data.

5.3.3 MM-AMSB

As we already showed in [144], the MM-AMSB has the advantage of providing solutions consistent with the tight relic density constraint. We confront here this model to the latest Higgs constraints. To study this scenario, we vary the parameters in the following ranges:

$$\alpha \in [-30, 30]; m_{3/2} \in [0, 500] \text{ TeV}; \tan\beta \in [1, 55] \ , \tag{5.15}$$

using flat scans generating more than 2 million points.

In fig. 5.5, we plot the light Higgs mass as functions of $\tan\beta$ and X_t/M_S. As for the HC-AMSB scenario, the Higgs mass can reach 126 GeV, in a region corresponding to typical and maximal mixing regimes in the stop sector. In this scenario, both the sfermion masses and trilinear couplings are modified by the modulus mediation. We note that imposing the lower bound of the relic density constraint makes apparent two distinct regions of compatibility: a large one with $\tan\beta \lesssim 30$ and $X_t/M_S \gtrsim 1-2$ corresponding to a typical mixing, and a narrow strip around $\tan\beta \sim 37$ and $X_t \gtrsim 2M_S$ corresponding to a maximal mixing.

In fig. 5.6 we consider the effects of the constraints in the $(\alpha, \tan\beta)$ and $(m_{3/2}, \tan\beta)$ parameter planes. We see clearly the difference between the two regions highlighted in fig. 5.5:

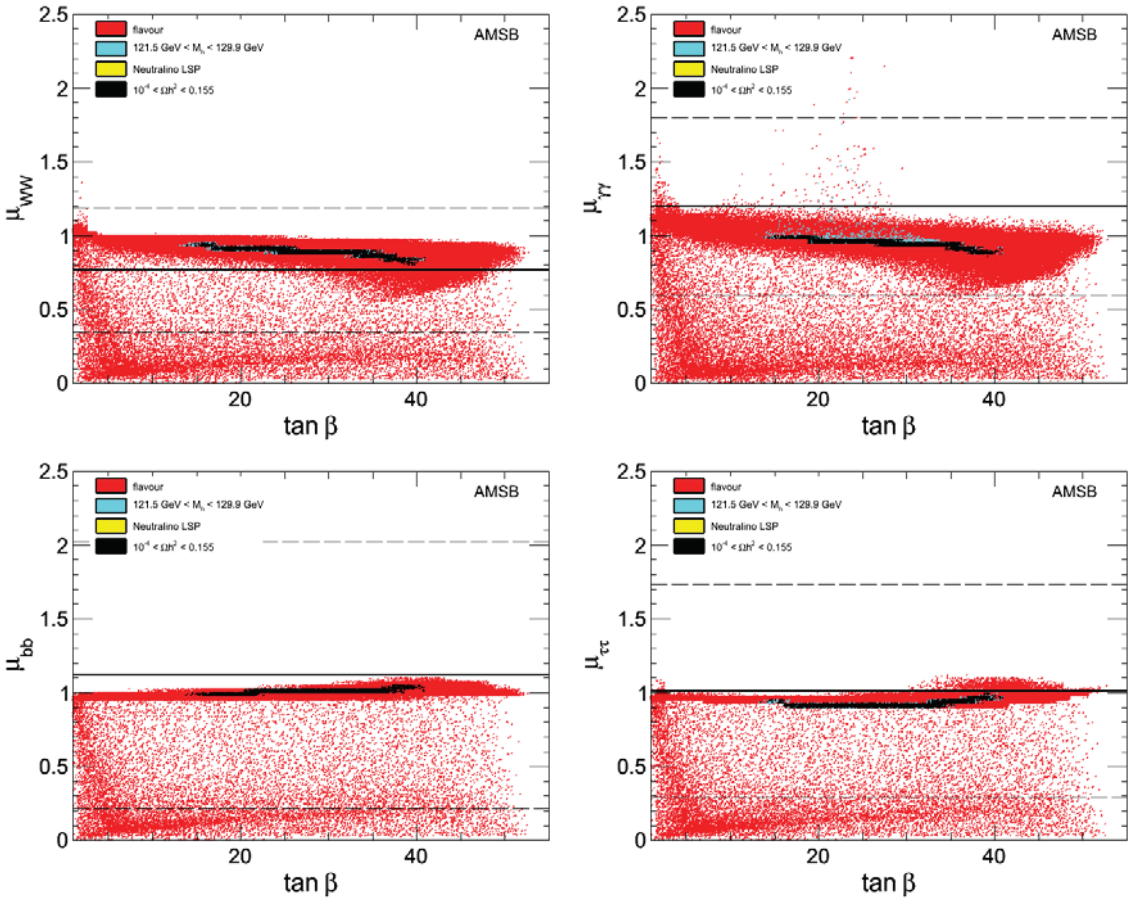

Figure 5.2: μ_{WW} (top left), $\mu_{\gamma\gamma}$ (top right), $\mu_{b\bar{b}}$ (bottom left) and $\mu_{\tau\tau}$ (bottom right) as functions of $\tan\beta$ in the mAMSB model. The red points are favored by the flavour physics constraints, the cyan points are compatible with the Higgs mass constraint, the yellow points have a neutralino LSP and the black points in addition are compatible with the upper bound of the relic density constraint. The horizontal solid line corresponds to the experimental central value given in Table 5.1 and the dashed lines to the 2σ values.

the low $\tan\beta$ region has positive values of α typically around 6, while the $\tan\beta \sim 37$ strip corresponds to negative α and small $m_{3/2}$. In terms of physical spectra, in both scenarios the neutralino is relatively heavy ($\gtrsim 500$ GeV). The negative α region corresponds to Higgs resonances, with a bino-like neutralino 1 mass approximately half the H and A Higgs masses, while the positive α region has stau and stop masses close to the neutralino mass, resulting in important co-annihilations, and the neutralino 1 is a mixed bino-wino state.

In fig. 5.7, we consider the μ_{WW}, $\mu_{\gamma\gamma}$, $\mu_{b\bar{b}}$ and $\mu_{\tau\tau}$ signal strengths of the Higgs as a function of $\tan\beta$. In comparison with the other AMSB scenarios, we find for the MM-AMSB model a situation similar to the one of the HC-AMSB model, where the Higgs mass constraint is satisfied, the signal strength for the decay of the Higgs boson to two photons is consistent with

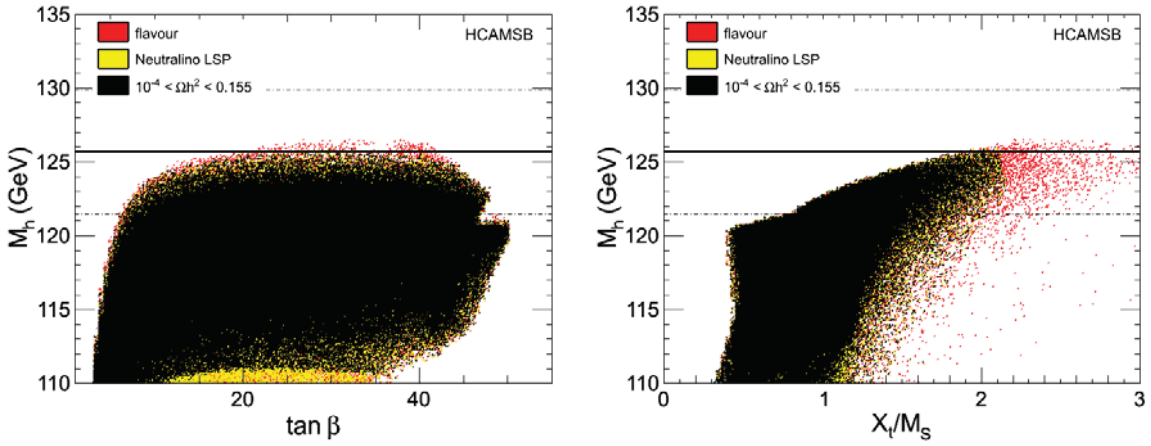

Figure 5.3: Light Higgs mass as functions of $\tan\beta$ (left panel) and X_t/M_S (right panel) in HC-AMSB. The red points are all points compatible the constraints from flavour physics described in Sec. 5.2.1, the yellow points have a neutralino LSP and the black points are in addition consistent with the upper bound of the relic density constraint. The horizontal solid line corresponds to the central value of the Higgs mass and the dashed lines to the 2σ deviations.

the preferred dark matter region of the parameter space within two sigmas.

We can also note that before imposing the the cosmology constraints, there is a possible enhancement for $\mu_{\gamma\gamma}$ at small $\tan\beta \sim 17$, but similarly to mAMSB and HC-AMSB, the LSP in this case is the stau, and is therefore disfavored by cosmology.

5.4 Conclusions

Anomaly mediation and its extensions including hypercharge and moduli for supersymmetry breaking are attractive models from the theoretical point of view. The well-known shortcomings of these models have been largely discussed and corrected in the literature. However detailed phenomenological implications of the recent dark matter, Higgs, flavour and collider data were not yet considered. In this paper we have discussed these limits, taking into account the most important recent flavour and Higgs search results, together with the dark matter constraints in order to establish, which among these models are still compatible with data.

The minimal AMSB model is consistent with the loose relic density dark matter constraints, but consistency is only marginal at the two-sigma level, especially due to the Higgs mass constraint. We consider therefore this minimal scenario much less attractive, once the phenomenological constraints are imposed.

Concerning the HC-AMSB model, it is consistent with the loose relic density dark matter constraints and with the Higgs mass value. Relaxing the neutralino LSP requirement and the relic density constraints allows for points with increased $\mu_{\gamma\gamma}$ in the region of light stau masses. This scenario with light staus has been thoroughly studied in the literature, however in the HC-AMSB scenario it corresponds to a region in which the stau is the LSP, making it inconsistent

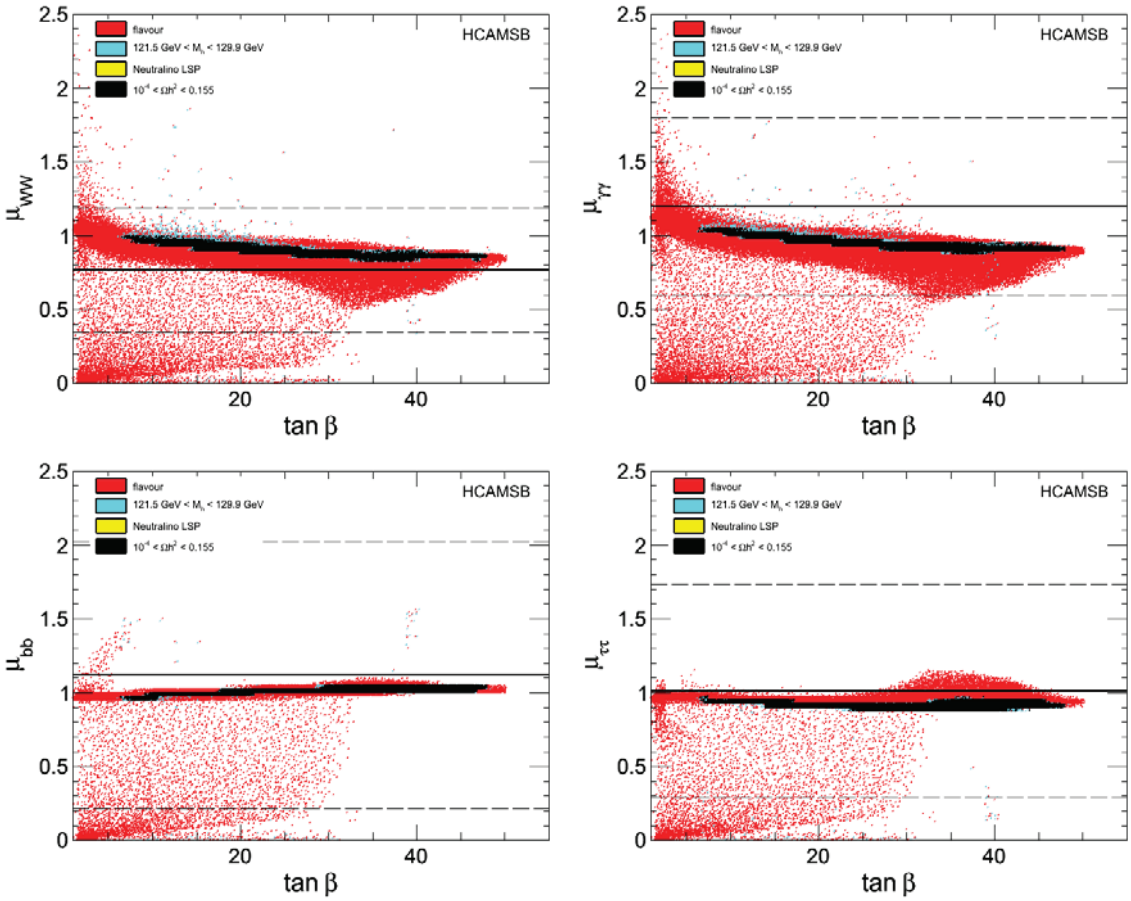

Figure 5.4: μ_{WW} (top left), $\mu_{\gamma\gamma}$ (top right), $\mu_{b\bar{b}}$ (bottom left) and $\mu_{\tau\tau}$ (bottom right) as functions of $\tan\beta$ in the HC-AMSB model. The red points are favored by the flavour physics constraints, the cyan points are compatible with the Higgs mass constraint, the yellow points have a neutralino LSP and the black points in addition are compatible with the upper bound of the relic density constraint. The horizontal solid line corresponds to the experimental central value given in Table 5.1 and the dashed lines to the 2σ values.

with cosmology. However, models with gravitino LSP could revive such possibility.

Contrary to the mAMSB and the HC-AMSB, the MM-AMSB model provides solutions compatible with flavour, collider data and the full relic density constraint. It also features the same $\mu_{\gamma\gamma}$ enhancement possibility by light staus. Therefore, the MM- and, to a lesser extent, the HC-AMSB model, are attractive solutions of supersymmetry breaking which are also consistent with present data. Future improvements in the precision of the Higgs mass measurements may easily rule out the minimal AMSB model if the present central value is confirmed. The MM- and HC-AMSB models will be still consistent in that case, but further constraints can be obtained from more precise determinations of the signal strength in the measured decay channels. This shows the importance of present and future LHC data, in combination with flavour and dark

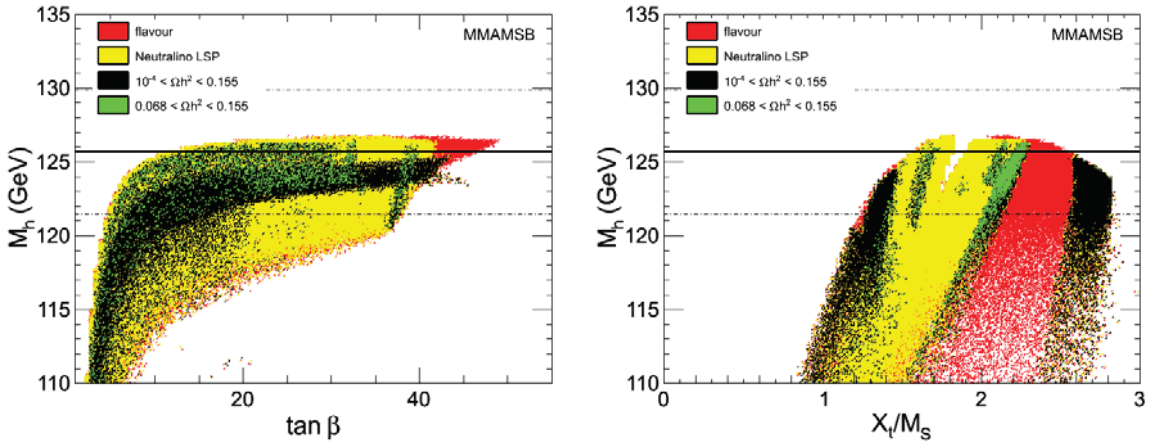

Figure 5.5: Light Higgs mass as functions of $\tan\beta$ (left panel) and X_t/M_S (right panel) in MM-AMSB. The red points are all points compatible with the constraints from flavour physics described in Sec. 5.2.1. The yellow points have also a neutralino LSP. The black points are consistent with the loose relic density constraint of Eq.(5.7). The green points are in addition consistent with the tight relic density constraint given in Eq.(5.6). The horizontal solid line corresponds to the central value of the Higgs mass and the dashed lines to the 2σ deviations.

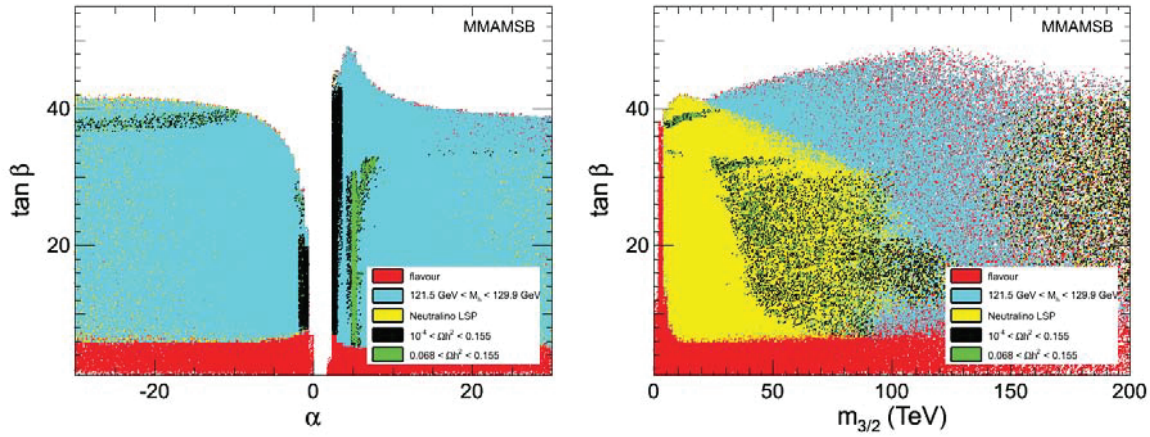

Figure 5.6: Constraints from flavour physics, Higgs mass and relic density in the $(\alpha, \tan\beta)$ (left panel) and $(m_{3/2}, \tan\beta)$ parameter planes (right panel) in the MM-AMSB model. The red points are favored by the flavour physics constraints, the cyan points are compatible with the Higgs mass constraint, the yellow points have a neutralino LSP, and the green points are in addition compatible with the tight relic density constraint.

matter constraints to suggest the path to be followed in the investigation of physics beyond the standard model.

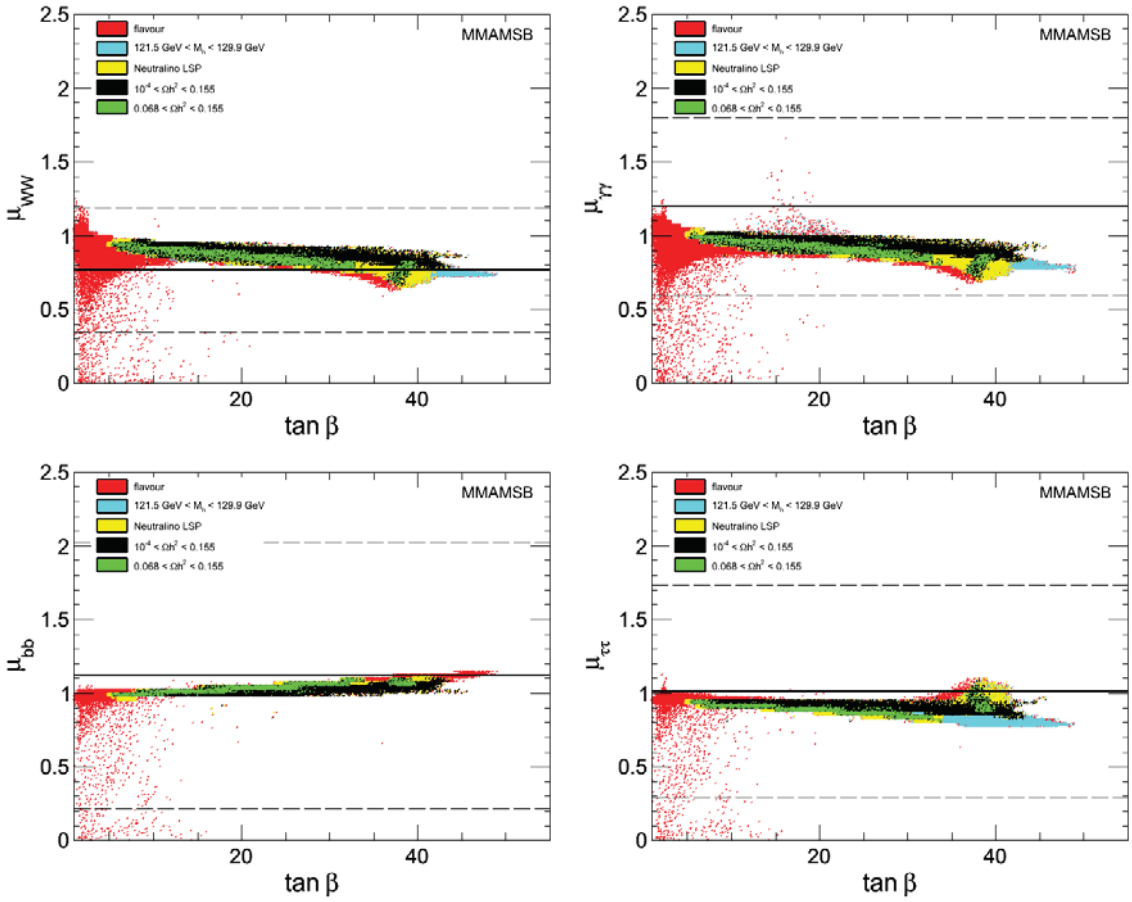

Figure 5.7: μ_{WW} (top left), $\mu_{\gamma\gamma}$ (top right), $\mu_{b\bar{b}}$ (bottom left) and $\mu_{\tau\tau}$ (bottom right) as functions of $\tan\beta$ in the MM-AMSB model. The red points are favoured by the flavour physics constraints, the cyan points are compatible with the Higgs mass constraint, the yellow points have a neutralino LSP, and the green points in addition are compatible with the tight relic density constraint. The horizontal solid line corresponds to the experimental central value given in Table 5.1 and the dashed lines to the 2σ values.

Conclusion & perspectives

In this thesis I discussed the one-loop expressions of the quark Yukawa couplings in two supersymmetric five-dimensional models, with bulk matter fields and with brane-localized matter fields. I derived the cutoff dependence of the CKM mixing matrix and found that the brane-localized matter with large $\tan\beta$ has rather different dependence from the others.

For the two 5D MSSM scenarios with matter fields in the bulk or on the brane, I performed the numerical analysis of the evolution of the various parameters of the CKM matrix, and both cases give us a scenario with small quark flavor mixings at high energies, especially for the mixings with the heavy generation. The evolution equations which relate various observables at different energies, and also allow the study of their asymptotic behaviours, are particularly important in view of testing the evolution of the Yukawa couplings. In the universal 5D MSSM model, the evolution of these CKM parameters have a rapid variation prior to reaching a cut-off scale where the top Yukawa coupling develops a singularity point and the model breaks down. For the brane localised matter fields model, I can only observe similar behaviours for small values of $\tan\beta$, while for large $\tan\beta$, the initial top Yukawa coupling becomes smaller, the gauge couplings then play a dominant role during the evolution of the Yukawa couplings, which cause the Yukawa couplings to decrease instead of increasing. As such the variations of these CKM parameters have a relatively milder behaviour, and the theory is valid up the gauge coupling unification scale.

I studied also, in the same framework, the neutrino sector using the updated value of θ_{13} and other mixing parameters. We have presented the evolution equations for the physical mixing angles, phases, Δm^2_{sol} and Δm^2_{atm}, within two distinct scenarios, where a larger $\tan\beta$ typically leads to more significant renormalization group corrections. Neutrino masses evolve differently in the two models due to the sign of the (different) dominant contributions in the bulk and in the brane cases. For the brane case we find the approximate degenerate neutrino mass spectrum becomes more favourable at the ultraviolet cut-off, whilst in the bulk case, the neutrino splitting becomes even more severe as the unitarity bounds of the effective theory are rapidly reached. As the evaluation of RGEs may play a crucial role in searching for realistic mixing patterns we also studied the evolution of mixing angles and phases. Contrary to the large renormalization effect of θ_{12}, the runnings of θ_{13} and θ_{23} were relatively mild. We found a non-zero value for θ_{13} during the evolution, which has no appreciable RGE running effects, even when power law evolution effects are considered. Therefore it is necessary to introduce new physics effects in order to achieve the tri-bimaximal pattern. Here, we also find the maximum CP violation case, $\delta = \frac{\pi}{2}$, could be achieved starting from a relatively small initial value. In this regard, radiative effects have a very significant impact on neutrino physics. A non-zero

Jarlskog invariant, which measures the magnitude of leptonic CP violation and is expected to be measured in future long baseline neutrino oscillation experiments, could open the door for CP violation in the lepton sector.

We provide also in this thesis a detailed phenomenological analysis, focusing particularly on the dark matter aspect of several SUSY breaking scenarios involving the anomaly mediation as one of the major components. Anomaly mediation models are well motivated supersymmetry breaking scenarios which appear as alternatives to the mSUGRA paradigm. These models are quite compelling from the theoretical point of view and it is therefore important to test if they are also viable models for phenomenology. We perform a study of these models in the light of all standard flavor, collider and dark matter constraints, including also the recent Higgs boson measurements for the mass and signal strengths in the different decay channels. The minimal AMSB scenario can satisfy in part of its parameter space both the dark matter requirement and is marginally consistent with the current Higgs boson mass value within a two sigma deviation. The HyperCharge-AMSB and Mixed Moduli-AMSB scenarios can better describe present data from dark matter, flavor, low energy physics and are consistent with the measured mass of the Higgs boson. The inclusion of the preferred signal strengths for the Higgs boson decay channels shows that in the range $5 < \tan\beta < 50$ the HC-AMSB and MM-AMSB models are consistent with the present Higgs boson channels. In contrast the minimal AMSB has a narrower allowed range in $\tan\beta$. These different AMSB scenarios, while consistent with present Higgs boson measurements, can be further tested by future more precise data in the Higgs boson sector. We study also alternative cosmology: the possibility to loosen the dark matter constraint on AMSB model and its extensions by modifying the cosmological scenario and this is a new result which includes also a very detailed analysis of some interesting parameter points.

Appendix A

Example for Loop calculation in 5D

We present in this appendix an example of loop calculation in the 5D MSSM which is the first diagram (a) in fig. 2.2. We draw this diagram more clearly as shown in fig. A.1, and we present in fig. A.2 the vertex needed to do the calculation.

We start by presenting the Feynman rules for supergraphs [28, 29] ;

- Integrate over $\int d^4\theta$ at each vertex.
- For a chiral vertex with n external lines, $(n-1)$ factors $[-\frac{1}{4}\bar{D}^2]$ act on the propagators.
- For an anti-chiral vertex with n external lines, $(n-1)$ factors $[-\frac{1}{4}D^2]$ act on the propagators.
- Multiply by a symmetry factor.
- For every loop with momentum k running in it, integrate over $\int \frac{d^4k}{(2\pi)^4}$.
- For every external line, write a chiral superfield Φ or $\bar{\Phi}$.

The chiral and vector propagators are

$$= \frac{-i}{p^2 + \frac{n^2}{R^2} - i\epsilon}\delta_{ij}\delta_{mn}\delta^4(\theta_1 - \theta_2)$$

$$= \frac{i}{p^2 + \frac{n^2}{R^2} - i\epsilon}\delta_{ab}\delta_{mn}\delta^4(\theta_1 - \theta_2)$$

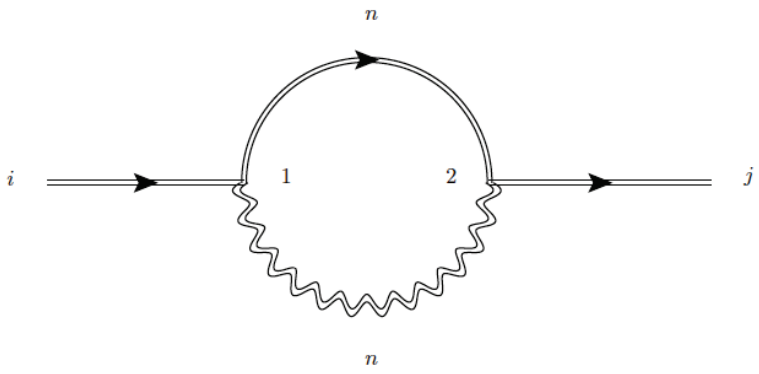

Figure A.1: The one-loop diagram correction for chiral superfields with two KK states running in the loop for Φ and V.

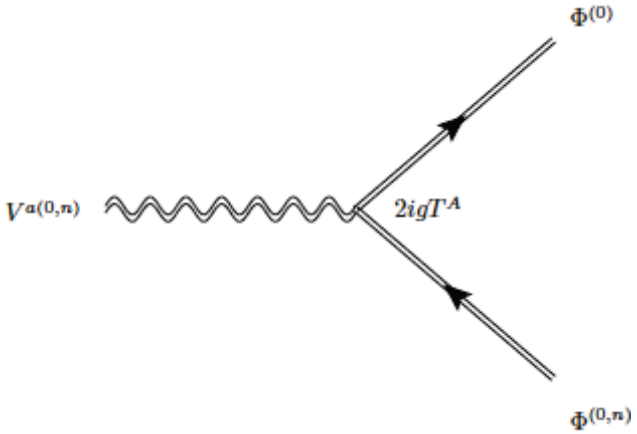

Figure A.2: The $V\Phi\Phi$ vertex relevant for our one loop calculation in fig. A.1.

$$
\begin{aligned}
\delta Z_{ij}^{(a)} &= \sum_{n\geq 0}\int \frac{d^4k}{(2\pi)^4} d^4\theta_1 (2igT^A)\frac{i\delta^{(4)}(\theta_1-\theta_2)}{2(k^2+\frac{n^2}{R^2})}\times(-\frac{1}{4}\bar{D}_1^2) \\
&\times(-\frac{1}{4}D_2^2)d^4\theta_2(2igT^A)\frac{(-i)\delta^{(4)}(\theta_1-\theta_2)\delta_{ij}}{(p+k)^2+\frac{n^2}{R^2}} \\
&\times \Phi_i^{(0)}(\theta_1)\bar{\Phi}_j^{(0)}(\theta_2) \\
&= (-4g^2T^AT^A)\delta_{ij}\sum_{n\geq 0}\int \frac{d^4k}{(2\pi)^4} d^4\theta_1 d^4\theta_2 \frac{i\delta^{(4)}(\theta_1-\theta_2)}{2(k^2+\frac{n^2}{R^2})} \\
&\times(\frac{1}{16}\bar{D}_1^2D_2^2)\frac{(-i)\delta^{(4)}(\theta_1-\theta_2)}{(p+k)^2+\frac{n^2}{R^2}}\times\Phi_i^{(0)}(\theta_1)\bar{\Phi}_j^{(0)}(\theta_2)
\end{aligned}
\tag{A.1}
$$

From Eq.(2.17), we have $T^A T^A = C_2(R)$ and if we integrate over $d^4\theta_2$, we obtain

$$\delta Z_{ij}^{(a)} = [-2g^2 C_2(R)]\delta_{ij} \sum_{n\geq 0} \int \frac{d^4k}{(2\pi)^4} d^4\theta_1 \times (\frac{1}{16}\bar{D}_1^2 D_2^2)\delta^{(4)}(\theta_1 - \theta_2)$$
$$\times \frac{1}{\left(k^2 + \frac{n^2}{R^2}\right)\left((p+k)^2 + \frac{n^2}{R^2}\right)} \times \Phi_i^{(0)}(\theta_1)\bar{\Phi}_j^{(0)}(\theta_1) \tag{A.2}$$

However, $\delta^{(4)}(\theta_1 - \theta_2) = \delta^{(2)}(\theta_1 - \theta_2)\delta^{(2)}(\bar{\theta}_1 - \bar{\theta}_2)$ and

$$\int d^4\theta_1 \bar{D}_1^2 D_2^2 \delta^{(2)}(\theta_1 - \theta_2)\delta^{(2)}(\bar{\theta}_1 - \bar{\theta}_2) = 16 \int d^4\theta_1 \tag{A.3}$$

So we will have

$$\delta Z_{ij}^{(a)} = -2g^2 C_2(R)\delta_{ij} \sum_{n\geq 0} \int \frac{d^4k}{(2\pi)^4} \frac{1}{\left(k^2 + \frac{n^2}{R^2}\right)\left((p+k)^2 + \frac{n^2}{R^2}\right)}$$
$$\times \int d^4\theta_1 \Phi_i^{(0)}(\theta_1)\bar{\Phi}_j^{(0)}(\theta_1) \tag{A.4}$$

One can divide the sum into two parts $n = 0$ and $n \geq 1$

$$\delta Z_{ij}^{(a)} = -2g^2 C_2(R)\delta_{ij}\Big(\int \frac{d^4k}{(2\pi)^4} \frac{1}{k^2(p+k)^2} + \sum_{n\geq 1} \int \frac{d^4k}{(2\pi)^4} \frac{1}{\left(k^2 + \frac{n^2}{R^2}\right)\left((p+k)^2 + \frac{n^2}{R^2}\right)}\Big)$$
$$\times \int d^4\theta_1 \Phi_i^{(0)}(\theta_1)\bar{\Phi}_j^{(0)}(\theta_1) \tag{A.5}$$

The first integral of the first line in this equation contains logarithmic divergence and the second one contains both logarithmic and linear divergences as we can see easily by a simple power counting. These two integrals are calculated in the paper [98] ,

$$\delta Z_{ij}^{(a)} = \frac{-2g^2 C_2(R)\delta_{ij}}{16\pi^2}\Big(2\log(\Lambda R) + 2\Lambda R - \log(\Lambda R)\Big) \times \int d^4\theta_1 \Phi_i^{(0)}(\theta_1)\bar{\Phi}_j^{(0)}(\theta_1)$$
$$= \frac{-2g^2 C_2(R)\delta_{ij}}{16\pi^2}\Big(2\Lambda R + \log(\Lambda R)\Big) \times \int d^4\theta_1 \Phi_i^{(0)}(\theta_1)\bar{\Phi}_j^{(0)}(\theta_1) \tag{A.6}$$

In the same way we can obtain the wave function renormalization constants for the other one-loop diagrams in fig. 2.2. We find respectively for diagrams b), c), d) and e)

$$\begin{aligned}
\delta Z_{ij}^{(b)} &= \frac{-2g^2 C_2(R)\delta_{ij}}{16\pi^2}\Big(2\Lambda R - \log(\Lambda R)\Big) \\
\delta Z_{ij}^{(c)} &= \frac{\lambda_{ikl}\lambda^*_{jkl}}{16\pi^2}\log(\Lambda R) \\
\delta Z_{ij}^{(d)} &= \frac{\lambda_{ikl}\lambda^*_{jkl}}{16\pi^2}\Big(4\Lambda R - \log(\Lambda R)\Big) \\
\delta Z_{ij}^{(e)} &= \frac{\lambda_{ikl}\lambda^*_{jkl}}{16\pi^2}\Big(2\pi(\Lambda R)^2 - 8\Lambda R + \log(\Lambda R)\Big)
\end{aligned} \tag{A.7}$$

We only displayed the integral over the θ coordinate for the first contribution, omitting it in the others. Summing the different contributions, we obtain the result in Eq.(2.20).

For the brane case, the calculation is quite similar and we will not have contributions from the last diagram, this is why the quadratic divergence term $(\Lambda R)^2$ is absent.

Appendix B

Gauge Coupling Coefficient Calculation in 5D MSSM

The evolution of the gauge couplings

$$16\pi^2 \frac{dg_i}{dt} = b_i {g_i}^3 \tag{B.1}$$

In the Standard Model

$$(b_1, b_2, b_3) = (\tfrac{41}{6}, -\tfrac{19}{6}, -7) \tag{B.2}$$

$$\text{or } (b_1, b_2, b_3) = (\tfrac{41}{6} \times \tfrac{3}{5}, -\tfrac{19}{6}, -7) = (\tfrac{41}{10}, -\tfrac{19}{6}, -7) \tag{B.3}$$

in the SU(5) normalization. (refer to Ref. [111])

In the 4D MSSM

$$(b_1, b_2, b_3) = (11, 1, -3) \tag{B.4}$$

$$\text{or } (b_1, b_2, b_3) = (11 \times \tfrac{3}{5}, 1, -3) = (\tfrac{33}{5}, 1, -3) \tag{B.5}$$

in the SU(5) normalization. (refer to Ref. [111])

In the 5D MSSM

$$16\pi^2 \frac{dg_i}{dt} = [{b_i}^{\text{MSSM}} + (S(t) - 1)\tilde{b}_i] {g_i}^3 \tag{B.6}$$

where ${b_i}^{MSSM} = (\frac{33}{5}, 1, -3)$,

$$\tilde{b}_i = (\frac{66}{5}, 10, 6) \tag{B.7}$$

(refer to Eq.(11) of Ref. [87])

Possible hints to check the beta function of the gauge couplings:

a. Consider the normal 4D MSSM gauge beta functions, especially for the Feynman diagrams of the gauge A_μ field (Not the vector superfield)

b. At each KK level, the only new one-loop contributions to the A_μ Feynman diagrams are from the wave function renormalization of A_μ, contributed by:
the coupling of A_μ with the complex scalar field and its super-partner in the superfield χ (the superfield described after Eq.(2.9)
the coupling of A_μ with the new fermion field and its super-partner in the superfield Φ^c (the superfield Φ^c described after Eq.(2.11), includes Φ^c corresponding to the two doublet of the Higgs fields, and the matter fields in the bulk)

The RGE of the gauge couplings have the following form in the standard model [18]:

$$16\pi^2\frac{dg}{dt} = [-\frac{11}{3}C_2(G) + \frac{2}{3}\sum T_i(R) + \frac{1}{3}\sum T_a(R)]g^3 \tag{B.8}$$

And in the 4D MSSM [18]:

$$16\pi^2\frac{dg}{dt} = [-3C_2(G) + \sum T_i(R) + \sum T_a(R)]g^3 \tag{B.9}$$

Where the first term is related to the gauge (and gaugino) field contributions, the second term is related to the fermion (and s-fermion) field contributions, the third one related to the scalar (and s-scalar) field contributions, and $C_2(G) = N$ for SU(N) group, $T(R) = \frac{1}{2}$ for fundamental representation.

In 5D MSSM, all the matter field in the bulk, for g_3, at each KK level,

$$\begin{aligned} b_3^{\text{5D MSSM}} &= b_3^{\text{4D MSSM}}(\text{Feynman diagram mirror 4D MSSM}) \\ &+ C_2(G)(\text{Superfield } \chi \text{ scalar and fermion contribution}) \\ &+ \sum T_i(R)(\text{Superfield } \Phi^C \text{ scalar and fermion contribution}) \\ &= -3 + 3 + \frac{1}{2} \times 12(\text{total 12 flavor } u_L, u_R, d_L \text{ etc}) \\ &= 6 \end{aligned} \tag{B.10}$$

for g_2, at each KK level,

$$\begin{aligned} b_2^{\text{5D MSSM}} &= b_2^{\text{4D MSSM}}(\text{Feynman diagram mirror 4D MSSM}) \\ &+ C_2(G)(\text{Superfield } \chi \text{ scalar and fermion contribution}) \\ &+ \sum T_i(R)(\text{Superfield } \Phi^C \text{ scalar and fermion contribution for matter field}) \\ &+ \sum T_R(R)(\text{Superfield } \Phi^C \text{ scalar and fermion contribution for 2 Higgs doublet}) \\ &= 1 + 2 + \frac{1}{2} \times (3 \text{ (color)for quark doublet} + 1 \text{ (lepton doublet)}) \times 3 \text{ (generation)} \\ &+ \frac{1}{2} \times 2(\text{Higgs doublet}) \\ &= 1 + 2 + \frac{1}{2} \times 12 + \frac{1}{2} \times 2 \\ &= 10 \end{aligned} \tag{B.11}$$

for g_1, at each KK level, no χ coupling to the gauge field (abelian group)

$$\begin{aligned}
b_1^{\text{5D MSSM}} &= b_1^{\text{4D MSSM}}(\text{Feynman diagram mirror 4D MSSM}) \\
&+ \sum T_i(R)(\text{Superfield } \Phi^C \text{ scalar and fermion contribution for matter field}) \\
&+ \sum T_R(R)(\text{Superfield } \Phi^C \text{ scalar and fermion contribution for 2 Higgs doublet}) \\
&= \frac{33}{5} + 2(T(R) \text{ is 2 for doublet}) \times \frac{1}{6}(\text{quark doublet hypercharge}) \\
&\times \frac{1}{6} \times 3 \text{ (generation)} \times 3 \text{ (color)} \\
&+ 2(T(R) \text{ is 2 for doublet}) \times \frac{1}{2}(\text{lepton doublet hypercharge}) \times \frac{1}{2} \times 3 \text{ (generation)} \\
&+ 1(T(R) \text{ is 1for singlet}) \times \frac{1}{3}(\text{quark singlet hypercharge}) \\
&\times \frac{1}{3} \times 3 \text{ (generation)} \times 3 \text{ (color)} \\
&+ 1(T(R) \text{ is 1for singlet}) \times \frac{2}{3}(\text{quark singlet hypercharge}) \\
&\times \frac{2}{3} \times 3 \text{ (generation)} \times 3 \text{ (color)} \\
&+ 1(T(R) \text{ is 1for singlet}) \times 1 \text{ (lepton singlet hypercharge)} \times 1 \times 3(\text{generation}) \\
&+ 2(T(R) \text{ is 2 for doublet}) \times \frac{1}{2}(\text{Higgs doublet hypercharge}) \times \frac{1}{2} \times 2 \text{ (two Higgs doublet)} \\
&= \frac{33}{5} + 11 \times (\frac{3}{5} \text{ rescale}) \\
&= \frac{66}{5}
\end{aligned} \tag{B.12}$$

In 5D MSSM, if there are η generation matter fields in the bulk, for g_3, at each KK level,

$$\begin{aligned}
b_3^{\text{5D MSSM}} &= C_2(G)(\text{superfield } \chi \text{ scalar and fermion contribution}) \\
&+ b_3^{\text{4D MSSM}}(\text{Feynman diagram 4D MSSM related to gauge gaugino contribution}) \\
&+ b_3^{\text{4D MSSM}}(\text{Feynman diagram 4D MSSM related to } \eta \text{ generation matter contribution}) \\
&+ T(R)(\eta \text{ generation superfield } \Phi^C \text{ contribution}) \\
&= 3 - 9 + \frac{1}{2} \times 4 \times \eta + \frac{1}{2} \times 4 \times \eta \\
&= -6 + 4\eta
\end{aligned} \tag{B.13}$$

for g_2, at each KK level,

$$\begin{aligned} b_2^{\text{5D MSSM}} &= C_2(G)(\text{Superfield } \chi \text{ scalar and fermion contribution}) \\ &+ b_2^{\text{4D MSSM}}(\text{Feynman diagram 4D MSSM related to gauge gaugino contribution}) \\ &+ b_2^{\text{4D MSSM}}(\text{Feynman diagram 4DMSSM related to } \eta \text{ generation matter contribution}) \\ &+ T(R)(\eta \text{ generation superfield } \Phi^C \text{ contribution}) \\ &+ T(R)(\text{two Higgs superfield mirror 4D MSSM contribution}) \\ &+ T(R)(\text{two Higgs superfield for } \Phi^C) \\ &= 2 - 6 + \frac{1}{2} \times 4 \times \eta + \frac{1}{2} \times 4 \times \eta + 1 + 1 \\ &= -2 + 4\eta \end{aligned} \tag{B.14}$$

for g_1, at each KK level,

$$\begin{aligned} b_1^{\text{5D MSSM}} &= b_1^{\text{4DMSSM}}(\text{Feynman diagram 4DMSSM related to } \eta \text{ generation matter contribution}) \\ &+ T(R)(\text{two Higgs superfield mirror 4D MSSM contribution}) \\ &+ T(R)(\eta \text{ generation superfield } \Phi^C \text{ contribution}) \\ &+ T(R)(\text{two Higgs superfield for } \Phi^C) \\ &= (\frac{10}{3} \times \eta + 1 + \frac{10}{3} \times \eta + 1)\frac{3}{5} \\ &= (\frac{20}{3} \times \eta + 2)\frac{3}{5} \\ &= \frac{6}{5} + 4 \times \eta \end{aligned} \tag{B.15}$$

So

$$(b_1, b_2, b_3)^{\text{5D MSSM}} = (\frac{6}{5}, -2, -6) + 4\eta \tag{B.16}$$

Appendix C

Higgs Self Coupling Evolution in 5D UED SM

In the SM, the Higgs boson mass is given by $m_H = \sqrt{\lambda}\, v$, where λ is the Higgs self-coupling parameter and v is the vacuum expectation value of the Higgs field (where $v = (\sqrt{2}G_F)^{-1/2} = 246$ GeV is fixed by the Fermi coupling G_F). From the requirement that the scalar potential energy of the vacuum be bounded from below, the quartic coupling λ should be positive at any energy scale. If m_H is too small, λ becomes negative at certain energy scales and then induces a false and deep minimum at large field values, destabilizing the EW vacuum. Therefore, above that scale, the validity of the SM is expected to fail and must be embedded in some more general theories that give rise to a wealth of new physics phenomena.

In the five dimensional UED model compactified on a circle of radius R with a Z_2 orbifolding, motivated by the new bounds on the mass of the SM Higgs boson around 125 GeV of ATLAS and CMS collaborations [190] , we quantitatively analyse the Higgs self coupling evolution from the EW scale up to the unification scale and exploit its evolution behaviors for different compactification radii.

The kinetic term of the scalar doublet has the following forms in the 5D UED model:

$$\mathcal{L}_{Higgs} = \int_0^{\pi R} dy (D_M \Phi(x,y))^\dagger D^M \Phi(x,y) \,, \tag{C.1}$$

where the covariant derivative is

$$D_M \Phi(x,y) = \left\{ \partial_M + i g_2^5 T^a W_M + \frac{i}{2} g_1^5 B_M \right\} \Phi(x,y) \,, \tag{C.2}$$

where the gauge fields $G_M(x,y)$ $\left(G_M^A \frac{\lambda^A}{2}\right)$, $W_M(x,y)$ $\left(W_M^a \frac{\tau^a}{2}\right)$ and $B_M(x,y)$ refer to the $SU(3)$, $SU(2)$ and $U(1)$ gauge groups respectively. Note also the five dimensional gauge coupling constants g_3^5, g_2^5 and g_1^5 are related to the four dimensional SM coupling constants (up to a normalization factor) by $g_i = \frac{g_i^5}{\sqrt{\pi R}}$, and similarly for the quartic coupling $\lambda = \frac{\lambda^5}{\sqrt{\pi R}}$.

The evolution of the Higgs quartic coupling is given by the beta function as follows

$$16\pi^2\frac{d\lambda}{dt} = \beta_\lambda^{SM} + \beta_\lambda^{UED}\,, \tag{C.3}$$

where [191]

$$\begin{aligned}\beta_\lambda^{SM} &= 12\lambda^2 - \left(\frac{9}{5}g_1^2 + 9g_2^2\right)\lambda + \frac{9}{4}\left(\frac{3}{25}g_1^4 + \frac{2}{5}g_1^2g_2^2 + g_2^4\right) + 4\lambda Tr[3Y_U^\dagger Y_U + 3Y_D^\dagger Y_D + Y_E^\dagger Y_E] \\ &\quad -4Tr[3(Y_U^\dagger Y_U)^2 + 3(Y_D^\dagger Y_D)^2 + (Y_E^\dagger Y_E)^2]\end{aligned} \tag{C.4}$$

and

$$\begin{aligned}\beta_\lambda^{UED} &= (S(t)-1)\left\{12\lambda^2 - 3\left(\frac{3}{5}g_1^2 + 3g_2^2\right)\lambda + \left(\frac{9}{25}g_1^4 + \frac{6}{5}g_1^2g_2^2 + 3g_2^4\right)\right\} + 2(S(t)-1) \\ &\quad \left\{4\lambda Tr[3Y_U^\dagger Y_U + 3Y_D^\dagger Y_D + Y_E^\dagger Y_E] - 4Tr[3(Y_U^\dagger Y_U)^2 + 3(Y_D^\dagger Y_D)^2 + (Y_E^\dagger Y_E)^2]\right\}\end{aligned} \tag{C.5}$$

for the UED bulk model, [87, 192] where both the fermion fields and the boson fields can propagate in the bulk, and

$$\beta_\lambda^{UED} = (S(t)-1)\left\{12\lambda^2 - 3\left(\frac{3}{5}g_1^2 + 3g_2^2\right)\lambda + \left(\frac{9}{25}g_1^4 + \frac{6}{5}g_1^2g_2^2 + 3g_2^4\right)\right\} \tag{C.6}$$

for the UED brane model [112] , where the SM matter fields are localized to the brane, whilst the gauge and Higgs fields are propagating in the bulk. Note that the pure gauge terms in Eq.(C.6) are different from these in Ref. [122, 193] . Explicitly, these terms cannot exactly resemble what is in the SM, since there are extra contributions from the couplings of the Higgs field with the A_5 component in the bulk space as well.

In Fig.C.1, starting from the initial value of $m_H = 125$ GeV, we focus on the evolution of the Higgs self-coupling and explore its behavior and constraints on the compactification radii for which the validity of the theory is satisfied. For interesting values of a Higgs mass around 125 GeV, we can observe that, in the whole range from the EW scale up to the gauge unification scale, in the UED brane model the Higgs self coupling $\lambda(t)$ remains positive and its trajectory goes upward but remains finite when approaching the unification scale, whilst for the SM and the UED bulk model $\lambda(t)$ evolves towards a zero value before reaching the unification scale, which then incurs the vacuum instability and introduces an ultraviolet cutoff for the theory.

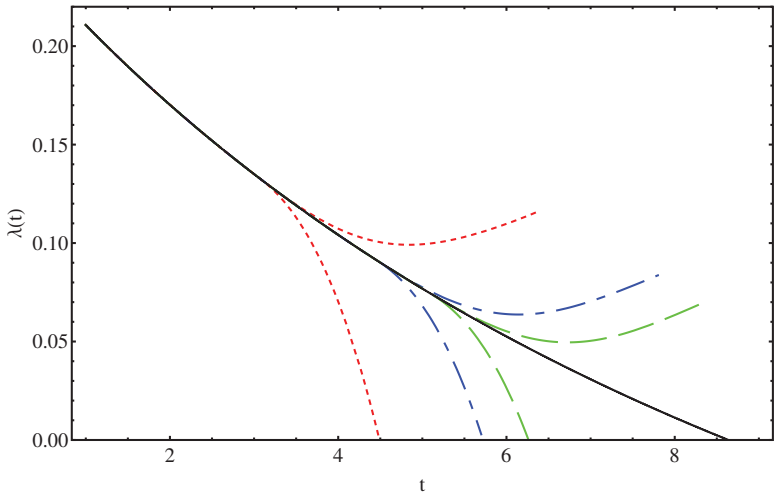

Figure C.1: The evolution of the Higgs self coupling for $m_H = 125$ GeV, where the solid (black) line is the SM, the upward [downward] dotted (red) line is the $R^{-1} = 2$ TeV UED brane model [UED bulk model], the upward [downward] dotted-dashed (blue) line is the $R^{-1} = 8$ TeV UED brane model [UED bulk model], and the upward [downward] dashed (green) line is the $R^{-1} = 15$ TeV UED brane model [UED bulk model]. The ultraviolet cutoff incurred from the vacuum instability are observed around $t = 4.5, 5.7, 6.3$ for $R^{-1} = 2, 8, 15$ TeV respectively in the UED bulk model.

Appendix D

Mass and mixing angles evolution

As such, for the four dimensional MSSM, where $C = 1$ and $\alpha = 6Tr(Y_u^\dagger Y_u) - \frac{6}{5}g_1^2 - 6g_2^2 = 6(y_t^2 + y_c^2 + y_u^2) - \frac{6}{5}g_1^2 - 6g_2^2$, we have:

$$\begin{aligned}
16\pi^2\frac{dm_1}{dt} &= m_1\Big\{\alpha + Cy_\tau^2\Big(2\sin^2(\theta_{12})\sin^2(\theta_{23}) - \sin(\theta_{13})\sin(2\theta_{12})\sin(2\theta_{23})\cos(\delta) \\
&\qquad +2\sin^2(\theta_{13})\cos^2(\theta_{12})\cos^2(\theta_{23})\Big)\Big\}\ , \\
16\pi^2\frac{dm_2}{dt} &= m_2\Big\{\alpha + Cy_\tau^2\Big(2\cos^2(\theta_{12})\sin^2(\theta_{23}) + \sin(\theta_{13})\sin(2\theta_{12})\sin(2\theta_{23})\cos(\delta) \\
&\qquad +2\sin^2(\theta_{13})\sin^2(\theta_{12})\cos^2(\theta_{23})\Big)\Big\}\ , \\
16\pi^2\frac{dm_3}{dt} &= m_3\Big\{\alpha + Cy_\tau^2\Big(2\cos^2(\theta_{13})\cos^2(\theta_{23})\Big)\Big\}\ ,
\end{aligned} \tag{D.1}$$

and for the mixing angles:

$$\begin{aligned}
16\pi^2\frac{d\theta_{13}}{dt} &= \frac{1}{2}Cy_\tau^2\Bigg(\frac{m_1+m_3}{m_1-m_3}\cos(\delta-\frac{\phi_1}{2})\cos(\theta_{12})\cos(\theta_{13})\Big(-\cos(\frac{\phi_1}{2})\sin(\theta_{12})\sin(2\theta_{23}) \\
&\quad + 2\cos(\delta-\frac{\phi_1}{2})\cos(\theta_{12})\sin(\theta_{13})\cos^2(\theta_{23})\Big) \\
&\quad + \frac{m_2+m_3}{m_2-m_3}\cos(\delta-\frac{\phi_2}{2})\sin(\theta_{12})\Big(\cos(\frac{\phi_2}{2})\cos(\theta_{12})\cos(\theta_{13})\sin(2\theta_{23}) \\
&\quad + \cos(\delta-\frac{\phi_2}{2})\sin(\theta_{12})\sin(2\theta_{13})\cos^2(\theta_{23})\Big)\Bigg)\ ,
\end{aligned} \tag{D.2}$$

$$
\begin{aligned}
16\pi^2\frac{d\theta_{12}}{dt} &= \frac{1}{2}Cy_\tau^2\Bigg(\frac{m_1+m_2}{m_1-m_2}\cos(\frac{\phi_1-\phi_2}{2})\Big(\frac{1}{2}\cos(\frac{\phi_1-\phi_2}{2})\cos^2(\theta_{13})\sin(2\theta_{12}) \\
&+ \{\frac{1}{4}\cos(\frac{\phi_1-\phi_2}{2})(-3+\cos(2\theta_{13}))\cos(2\theta_{23})\sin(2\theta_{12}) - [\cos\delta\cos(\frac{\phi_1-\phi_2}{2})\cos(2\theta_{12}) \\
&+ \sin\delta\sin(\frac{\phi_1-\phi_2}{2})]\sin(\theta_{13})\sin(2\theta_{23})\}\Big) \\
&+ \frac{m_1+m_3}{m_1-m_3}\cos(\delta-\frac{\phi_1}{2})\sin(\theta_{12})\sin(\theta_{13})\Big(-\cos(\frac{\phi_1}{2})\sin(\theta_{12})\sin(2\theta_{23}) \\
&+ 2\cos(\delta-\frac{\phi_1}{2})\cos(\theta_{12})\sin(\theta_{13})\cos^2(\theta_{23})\Big) \\
&+ \frac{m_2+m_3}{m_2-m_3}\cos(\delta-\frac{\phi_2}{2})\cos(\theta_{12})\tan(\theta_{13})\Big(\cos(\frac{\phi_2}{2})\cos(\theta_{12})\cos(\theta_{13})\sin(2\theta_{23}) \\
&+ \cos(\delta-\frac{\phi_2}{2})\sin(\theta_{12})\sin(2\theta_{13})\cos^2(\theta_{23})\Big)\Bigg)\ , \qquad \text{(D.3)} \\
16\pi^2\frac{d\theta_{23}}{dt} &= \frac{1}{2}Cy_\tau^2\Bigg(\frac{m_1+m_3}{m_1-m_3}\cos(\frac{\phi_1}{2})\sin(\theta_{12})\Big(\cos(\frac{\phi_1}{2})\sin(\theta_{12})\sin(2\theta_{23}) \\
&-2\cos(\delta-\frac{\phi_1}{2})\cos(\theta_{12})\sin(\theta_{13})\cos^2(\theta_{23})\Big) \\
&+ \frac{m_2+m_3}{m_2-m_3}\cos(\frac{\phi_2}{2})\cos(\theta_{12})\sec(\theta_{13})\Big(\cos(\frac{\phi_2}{2})\cos(\theta_{12})\cos(\theta_{13})\sin(2\theta_{23}) \\
&+ \cos(\delta-\frac{\phi_2}{2})\sin(\theta_{12})\sin(2\theta_{13})\cos^2(\theta_{23})\Big)\Bigg)\ , \qquad \text{(D.4)}
\end{aligned}
$$

As we have already mentioned, the transition to the bulk case will be done by making the replacement of $C = C(\mu) = \pi\mu^2R^2 = \pi S(t)^2$ and $\alpha = 6\pi S(t)^2 Tr(Y_u^\dagger Y_u) - (\frac{6}{5}g_1^2 + 6g_2^2)S(t)$. Similarly, we will also have the same equations in the brane case, and with $C = C(\mu) = 2\mu R = 2S(t)$ and $\alpha = 6Tr(Y_u^\dagger Y_u) - (\frac{9}{5}g_1^2 + 9g_2^2)S(t)$.

Appendix E

Dirac and Majorana phases evolution

As already discussed, in the MSSM $C = 1$, in the 5D brane case $C = 2\mu R = 2S(t)$, and in the bulk case $C = C(\mu) = \pi\mu^2 R^2 = \pi S(t)^2$. In which case, the equations for the evolution of the phases can be expressed as:

$$
\begin{aligned}
16\pi^2 \frac{d\phi_1}{dt} &= \frac{1}{2} C y_\tau^2 \left(\frac{1}{2} \frac{m_1 + m_2}{m_1 - m_2} \sin(\frac{\phi_1 - \phi_2}{2}) \cot(\theta_{12}) \Big(-2 \cos(\frac{\phi_1 - \phi_2}{2}) \cos^2(\theta_{13}) \sin(2\theta_{12}) \right. \\
&- \Big\{ \cos(\frac{\phi_1 - \phi_2}{2})(-3 + \cos(2\theta_{13})) \cos(2\theta_{23}) \sin(2\theta_{12}) \\
&- 4 \Big[\cos\delta \cos(\frac{\phi_1 - \phi_2}{2}) \cos(2\theta_{12}) + \sin\delta \sin(\frac{\phi_1 - \phi_2}{2}) \Big] \sin(\theta_{13}) \sin(2\theta_{23}) \Big\} \Big) \\
&+ \frac{m_1 + m_3}{m_1 - m_3} 2 \cos(\theta_{13}) \Big(-\cot(\theta_{23}) \sin(\frac{\phi_1}{2}) \sin(\theta_{12}) \sec(\theta_{13}) + 2 \cos(\theta_{12}) \sin(\delta - \frac{\phi_1}{2}) \tan(\theta_{13}) \\
&+ \sec(\theta_{13}) \tan(\theta_{23}) \sin(\frac{\phi_1}{2}) \sin(\theta_{12}) \Big) \Big(-2 \cos(\delta - \frac{\phi_1}{2}) \cos(\theta_{12}) \sin(\theta_{13}) \cos^2(\theta_{23}) \\
&+ \cos(\frac{\phi_1}{2}) \sin(\theta_{12}) \sin(2\theta_{23}) \Big) \\
&+ \frac{m_2 + m_3}{m_2 - m_3} \Big(\sin(\delta - \frac{\phi_2}{2}) \sin(\theta_{12}) \tan(\theta_{13}) + \cos(\theta_{12}) \Big\{ \cot(\theta_{23}) \sec(\theta_{13}) \sin(\frac{\phi_2}{2}) \\
&- \cos(\frac{\phi_2}{2}) \cot(\theta_{12}) \sin\delta \tan(\theta_{13}) + \sin(\frac{\phi_2}{2}) \cos(\theta_{12}) \cos\delta \tan(\theta_{13}) - \sec(\theta_{13}) \tan(\theta_{23}) \sin(\frac{\phi_2}{2}) \Big\} \Big) \\
&\times \Big(-2 \cos(\frac{\phi_2}{2}) \cos(\theta_{12}) \cos(\theta_{13}) \sin(2\theta_{23}) \\
&- 2 \cos(\delta - \frac{\phi_2}{2}) \sin(\theta_{12}) \sin(2\theta_{13}) \cos^2(\theta_{23}) \Big) \Big) \ , \qquad \text{(E.1)}
\end{aligned}
$$

$$
\begin{aligned}
16\pi^2\frac{d\phi_2}{dt} &= \frac{1}{2}Cy_\tau^2\left(\frac{1}{2}\frac{m_1+m_2}{m_1-m_2}\sin(\frac{\phi_1-\phi_2}{2})\tan(\theta_{12})\Big(-2\cos(\frac{\phi_1-\phi_2}{2})\cos^2(\theta_{13})\sin(2\theta_{12})\right.\\
&- \{\cos(\frac{\phi_1-\phi_2}{2})(-3+\cos(2\theta_{13}))\cos(2\theta_{23})\sin(2\theta_{12})-4[\cos\delta\cos(\frac{\phi_1-\phi_2}{2})\cos(2\theta_{12})\\
&+ \left.\sin\delta\sin(\frac{\phi_1-\phi_2}{2})]\sin(\theta_{13})\sin(2\theta_{23})\}\right)\\
&- \frac{m_1+m_3}{m_1-m_3}2\cos(\theta_{13})\Big(\cot(\theta_{23})\sin(\frac{\phi_1}{2})\sin(\theta_{12})\sec(\theta_{13})-\cos(\theta_{12})\sin(\delta-\frac{\phi_1}{2})\tan(\theta_{13})\\
&+ \sin(\theta_{12})\{\sin\delta\cos(\frac{\phi_1}{2})\tan(\theta_{12})\tan(\theta_{13})-\sin(\frac{\phi_1}{2})\cos\delta\tan(\theta_{12})\tan(\theta_{13})\\
&- \sin(\frac{\phi_1}{2})\sec(\theta_{13})\tan(\theta_{23})\}\Big)\\
&\times \Big(-2\cos(\delta-\frac{\phi_1}{2})\cos(\theta_{12})\sin(\theta_{13})\cos^2(\theta_{23})+\cos(\frac{\phi_1}{2})\sin(\theta_{12})\sin(2\theta_{23})\Big)\\
&+ \frac{m_2+m_3}{m_2-m_3}\Big(\sin(\frac{\phi_2}{2})\cos(\theta_{12})\cos(2\theta_{23})\csc(\theta_{23})\sec(\theta_{13})\sec(\theta_{23})\\
&+ 2\sin(\delta-\frac{\phi_2}{2})\sin(\theta_{12})\tan(\theta_{13})\Big)\\
&\times \Big(-2\cos(\frac{\phi_2}{2})\cos(\theta_{12})\cos(\theta_{13})\sin(2\theta_{23})\\
&- 2\cos(\delta-\frac{\phi_2}{2})\sin(\theta_{12})\sin(2\theta_{13})\cos^2(\theta_{23})\Big)\Big)\ , \qquad \text{(E.2)}
\end{aligned}
$$

$$
\begin{aligned}
16\pi^2\frac{d\delta}{dt} &= \frac{1}{4}Cy_\tau^2\left(\frac{m_1+m_2}{m_1-m_2}\sin(\frac{\phi_1-\phi_2}{2})\csc(2\theta_{12})\Big(-2\cos(\frac{\phi_1-\phi_2}{2})\cos^2(\theta_{13})\sin(2\theta_{12})\right.\\
&- \Big\{\cos(\frac{\phi_1-\phi_2}{2})(-3+\cos(2\theta_{13}))\cos(2\theta_{23})\sin(2\theta_{12}) - 4[\cos\delta\cos(\frac{\phi_1-\phi_2}{2})\cos(2\theta_{12})\\
&+ \left.\sin\delta\sin(\frac{\phi_1-\phi_2}{2})]\sin(\theta_{13})\sin(2\theta_{23})\Big\}\right)\\
&- \frac{m_1+m_3}{8(m_1-m_3)}\Big(\cos(\frac{\phi_1}{2})\Big\{2-6\cos(2\theta_{12})+\cos(2\theta_{12}-2\theta_{13})-6\cos(2\theta_{13})\\
&+ \cos(2\theta_{12}+2\theta_{13})\Big\}\csc(\theta_{13})\sec(\theta_{12})\sin\delta + 4\cos(\theta_{12})(-3+\cos(2\theta_{13}))\csc(\theta_{13})\sin(\delta-\frac{\phi_1}{2})\\
&+ \sin(\frac{\phi_1}{2})\Big\{-\cos(\delta)[2-6\cos(2\theta_{12})+\cos(2\theta_{12}-2\theta_{13})-6\cos(2\theta_{13})\\
&+ \cos(2\theta_{12}+2\theta_{13})]\csc(\theta_{13})\sec(\theta_{12}) + 16\sin(\theta_{12})\cot(\theta_{23}) - 16\sin(\theta_{12})\tan(\theta_{23})\Big\}\Big)\\
&\times \Big(-2\cos(\delta-\frac{\phi_1}{2})\cos(\theta_{12})\sin(\theta_{13})\cos^2(\theta_{23}) + \cos(\frac{\phi_1}{2})\sin(\theta_{12})\sin(2\theta_{23})\Big)\\
&- \frac{m_2+m_3}{4(m_2-m_3)}\Big([\frac{-5}{2}+\frac{3}{2}\cos(2\theta_{12})-\frac{1}{4}\cos(2\theta_{12}-2\theta_{13})-\frac{1}{2}\cos(2\theta_{13})-\frac{1}{4}\cos(2\theta_{12}+2\theta_{13})]\\
&\times \csc(\theta_{12})\csc(\theta_{13})\sec(\theta_{13})\sin(\delta-\frac{\phi_2}{2}) + \cos(\theta_{12})\sec(\theta_{13})\\
&\times [-\cos(\frac{\phi_2}{2})(-3+\cos(2\theta_{13}))\cot(\theta_{12})\csc(\theta_{13})\sin\delta\\
&- 4\sin(\frac{\phi_2}{2})\cot(\theta_{23}) + \sin(\frac{\phi_2}{2})\cos\delta(-3+\cos(2\theta_{13}))\cot(\theta_{12})\csc(\theta_{13}) + 4\sin(\frac{\phi_2}{2})\tan(\theta_{23})]\Big)\\
&\times \Big(-2\cos(\frac{\phi_2}{2})\cos(\theta_{12})\cos(\theta_{13})\sin(2\theta_{23})\\
&- 2\cos(\delta-\frac{\phi_2}{2})\sin(\theta_{12})\sin(2\theta_{13})\cos^2(\theta_{23})\Big)\Big)\ . \qquad \text{(E.3)}
\end{aligned}
$$

References

[1] J. Iliopoulos, "Progress in gauge theories", Rapporteur's talk given at the 17th International Conf. on High Energy Physics, London 1974. 5

[2] L.D. Landau, Zh. Eksp. Teor. Fiz. **7** 19 (1937), L. Landau, Phys. Z. Sowjetunion **11** 26 (1937). 5

[3] L. D. Landau, Zh. Eksp. Teor. Fiz. **7** 627 (1937), L. Landau, Phys. Z. Sowjetunion **11** 545 (1937) 5

[4] P. W. Higgs, "Broken symmetries, massless particles and gauge fields," Phys. Lett. **12** (1964) 132. 5

[5] F. Englert and R. Brout, "Broken Symmetry and the Mass of Gauge Vector Mesons," Phys. Rev. Lett. **13** (1964) 321. 5

[6] P. W. Higgs, "Broken Symmetries and the Masses of Gauge Bosons," Phys. Rev. Lett. **13** (1964) 508. 5

[7] G. S. Guralnik, C. R. Hagen and T. W. B. Kibble, "Global Conservation Laws and Massless Particles," Phys. Rev. Lett. **13** (1964) 585. 5

[8] P. W. Higgs, "Spontaneous Symmetry Breakdown without Massless Bosons," Phys. Rev. **145** (1966) 1156. 5

[9] S.L. Glashow, "Partial Symmetries of Weak Interactions", Nucl. Phys. **22** (1961) 279. 5, 6

[10] A. Salam, "Renormalizability of gauge theories," Phys. Rev. **127** (1962) 331. 5, 6

[11] S. Weinberg, "A Model of Leptons," Phys. Rev. Lett. **19** (1967) 1264. 5, 6

[12] M. Gell-Mann, "A Schematic Model of Baryons and Mesons," Phys. Lett. **8** (1964) 214. 6

[13] G. Zweig, "An $SU(3)$ Model for Strong Interaction Symmetry and its Breaking", CERN Report No.8182/TH.401. 6

[14] M. Y. Han and Y. Nambu, "Three Triplet Model with Double SU(3) Symmetry," Phys. Rev. **139** (1965) B1006. 6

[15] R. F. Schwitters, Proc. 1975 Int. Symposium on Lepton-Photon Interactions at High Energies, Stanford, 1975, p. 5.

[16] R. Brandelik *et al.* [TASSO Collaboration], Phys. Lett. B **86** (1979) 243. 6

[17] M. E. Peskin and D. V. Schroeder, "An Introduction to quantum field theory," Reading, USA: Addison-Wesley (1995) 842. 6

[18] H. Baer and X. Tata, "Weak scale supersymmetry: From superfields to scattering events," Cambridge, UK: Univ. Pr., 2006. 6
11, 16, 17, 58, 61, 154
[19] T. Aaltonen *et al.* [CDF and D0 Collaborations], arXiv:1103.3233 [hep-ex]. 11
[20] J. Beringer *et al.* [Particle Data Group Collaboration], Phys. Rev. D **86** (2012) 010001. 11, 13, 14
[21] http://lepewwg.web.cern.ch/LEPEWWG/ 12
[22] Observation of a new boson with a mass near 125 GeV, Technical Report CMS-PAS-HIG-12-020, CERN, Geneva, November 2012 12
[23] R. Barate *et al.* [LEP Working Group for Higgs boson searches and ALEPH and DELPHI and L3 and OPAL Collaborations], Phys. Lett. B **565** (2003) 61 [hep-ex/0306033]. 11
[24] M. E. Peskin and T. Takeuchi, Phys. Rev. D **46** (1992) 381-409. 12
[25] F. Quevedo, S. Krippendorf and O. Schlotterer, arXiv:1011.1491 [hep-th]. 16, 26
[26] S. P. Martin, In *Kane, G.L. (ed.): Perspectives on supersymmetry II* 1-153 [hep-ph/9709356]. 16, 17, 18, 19, 24, 25
[27] R. Nevzorov, arXiv:1201.0115 [hep-ph]. 16, 24
[28] P. C. West, "Introduction to Supersymmetry and Supergravity," Singapore, Singapore: World Scientific, 1986. 16, 19, 56, 58, 149
[29] J. Wess and J. Bagger, "Supersymmetry and supergravity," Princeton, USA: Univ. Pr., 1992. 16, 19, 56, 149
[30] M. Drees, R.M. Godbole and P. Roy, "Theory and Phenomenology of Sparticles," Singapore: World Scientific Publishing, 2004. 16, 19, 56
[31] T. Flacke, DESY-THESIS-2003-047. 24, 55
[32] T. S. Ray, arXiv:1103.5939 [hep-ph]. 26
[33] J. Lesgourgues, astro-ph/0409426. 28, 29
[34] "Official wmap webpage," http://map.gsfc.nasa.gov/. 31, 32, 35
[35] G. Bertone, D. Hooper, J. Silk and , Phys. Rept. **405** (2005) 279 [hep-ph/0404175]. 30, 36
[36] E. S. Sheldon *et al.* [SDSS Collaboration], Astrophys. J. **703** (2009) 2232 [arXiv:0709.1162 [astro-ph]]. 32
[37] D. Clowe, M. Bradac, A. H. Gonzalez, M. Markevitch, S. W. Randall, C. Jones and D. Zaritsky, Astrophys. J. **648** (2006) L109 [astro-ph/0608407]. 32, 33
[38] K. G. Begeman, A. H. Broeils, and R. H. Sanders, *Mon. Not. Roy. Astron. Soc.* **249** (1991) 523. 32, 33
[39] M. Milgrom, Acta Phys. Polon. B **32** (2001) 3613 [astro-ph/0112069]. 33
[40] A. A. Penzias and R. W. Wilson, *Astrophys. J.* **142** (1965) 419-421. 34
[41] C. L. Bennett, A. Kogut, G. Hinshaw, A. J. Banday, E. L. Wright, K. Gorski, D. T. Wilkinson and R. Weiss *et al.*, Astrophys. J. **436** (1994) 423 [astro-ph/9401012]. 34
[42] J. Dunkley *et al.* [WMAP Collaboration], Astrophys. J. Suppl. **180** (2009) 306 [arXiv:0803.0586 [astro-ph]]. 34

[43] M. Kowalski *et al.* [Supernova Cosmology Project Collaboration], Astrophys. J. **686** (2008) 749 [arXiv:0804.4142 [astro-ph]]. 34, 36, 37

[44] E. Komatsu *et al.* [WMAP Collaboration], "Seven-Year Wilkinson Microwave Anisotropy Probe (WMAP) Observations: Cosmological Interpretation," Astrophys. J. Suppl. **192** (2011) 18 [arXiv:1001.4538]. 34, 103, 135

[45] K. Agashe, R. Contino and A. Pomarol, Nucl. Phys. B **719** (2005) 165 [hep-ph/0412089]. 34

[46] W. J. Percival *et al.* [SDSS Collaboration], Mon. Not. Roy. Astron. Soc. **401** (2010) 2148 [arXiv:0907.1660 [astro-ph.CO]]. 35

[47] N. Jarosik, C. L. Bennett, J. Dunkley, B. Gold, M. R. Greason, M. Halpern, R. S. Hill and G. Hinshaw *et al.*, Astrophys. J. Suppl. **192** (2011) 14 [arXiv:1001.4744 [astro-ph.CO]]. 36

[48] T. Falk, K. A. Olive, M. Srednicki and , Phys. Lett. B **339** (1994) 248 [hep-ph/9409270]. 38

[49] J. L. Feng, A. Rajaraman, F. Takayama and , Phys. Rev. Lett. **91** (2003) 011302 [hep-ph/0302215]. 38

[50] M. Pospelov, Phys. Rev. Lett. **98** (2007) 231301 [hep-ph/0605215]. 38

[51] W. Buchmuller, L. Covi, K. Hamaguchi, A. Ibarra, T. Yanagida and , JHEP **0703** (2007) 037 [hep-ph/0702184 [HEP-PH]]. 38

[52] L. J. Rosenberg, K. A. van Bibber and , Phys. Rept. **325** (2000) 1. 38

[53] S. A. Bonometto, F. Gabbiani, A. Masiero and , Phys. Rev. D **49** (1994) 3918 [hep-ph/9305237]. 38

[54] L. Covi, H. -B. Kim, J. E. Kim, L. Roszkowski and , JHEP **0105** (2001) 033 [hep-ph/0101009]. 38

[55] G. Servant and T. M. P. Tait, Nucl. Phys. B **650** (2003) 391 [hep-ph/0206071]. 39

[56] K. Griest and D. Seckel, Phys. Rev. **D43** (1991) 3191-3203. 39, 41

[57] P. Gondolo and G. Gelmini, Nucl. Phys. B **360** (1991) 145; J. Edsjo and P. Gondolo, Phys. Rev. D **56** (1997) 1879 [hep-ph/9704361]. 39

[58] E. W. Kolb and M. S. Turner, *Front. Phys.* **69** (1990) 1-547.klei 41

[59] A. Arbey and F. Mahmoudi, JHEP **1005** (2010) 051 [arXiv:0906.0368]; A. Arbey and F. Mahmoudi, Nuovo Cim. C **33** (2010) 151 [arXiv:1002.4096]. 42, 43, 44, 97

[60] P. Salati, Phys. Lett. B **571** (2003) 121 [astro-ph/0207396]. 42

[61] A. Arbey and F. Mahmoudi, Phys. Lett. B **669** (2008) 46 [arXiv:0803.0741]. 42, 43, 97, 135

[62] A. Arbey, Comput. Phys. Commun. **183** (2012) 1822 [arXiv:1106.1363 [astro-ph.CO]]. 42, 118

[63] G.B. Gelmini and P. Gondolo, Phys. Rev. D **74** (2006) 023510 [hep-ph/0602230]. 43

[64] G. Gelmini, P. Gondolo, A. Soldatenko and C.E. Yaguna, Phys. Rev. D **74** (2006) 083514 [hep-ph/0605016]. 43, 44

[65] N. Okada and O. Seto, Phys. Rev. D **70** (2004) 083531 [hep-ph/0407092]. 43

[66] J. C. Pati and A. Salam, Phys. Rev. D **10**, 275 (1974) [Erratum-ibid. D **11**, 703 (1975)]; H. Georgi and S. L. Glashow, Phys. Rev. Lett. **32**, 438 (1974); H. Fritzsch and P. Minkowski, Annals Phys. **93**, 193 (1975); F. Gursey, P. Ramond and P. Sikivie, Phys. Lett. B **60**, 177 (1976). 47

[67] H. Georgi, H. R. Quinn and S. Weinberg, Phys. Rev. Lett. **33**, 451 (1974). 47

[68] K. R. Dienes, E. Dudas and T. Gherghetta, Nucl. Phys. B **537** (1999) 47 [arXiv:hep-ph/9806292]. K. R. Dienes, E. Dudas and T. Gherghetta, Phys. Lett. B **436** (1998) 55 [arXiv:hep-ph/9803466]. 47, 55

[69] O. Klein, Z. Phys. **37** (1926) 895 [Surveys High Energ. Phys. **5** (1986) 241]. 47

[70] I. Antoniadis, Phys. Lett. B **246** (1990) 377. 48

[71] N. Arkani-Hamed, S. Dimopoulos and G. R. Dvali, Phys. Lett. B **429** (1998) 263 [hep-ph/9803315]. 48

[72] I. Antoniadis, N. Arkani-Hamed, S. Dimopoulos and G. R. Dvali, Phys. Lett. B **436** (1998) 257 [hep-ph/9804398]. 48

[73] N. Arkani-Hamed, S. Dimopoulos and G. R. Dvali, Phys. Rev. D **59** (1999) 086004 [hep-ph/9807344]. 48

[74] N. Arkani-Hamed, L. J. Hall, D. Tucker-Smith and N. Weiner, Phys. Rev. D **62** (2000) 105002 [hep-ph/9912453]. 48

[75] L. Randall and R. Sundrum, Phys. Rev. Lett. **83** (1999) 3370 [hep-ph/9905221]. 48

[76] N. Arkani-Hamed, S. Dimopoulos, G. R. Dvali and J. March-Russell, Phys. Rev. D **65** (2002) 024032 [hep-ph/9811448]. N. Arkani-Hamed and M. Schmaltz, Phys. Rev. D **61** (2000) 033005 [hep-ph/9903417]. B. Lillie, JHEP **0312** (2003) 030 [hep-ph/0308091]. 48

[77] K. R. Dienes, E. Dudas and T. Gherghetta, Phys. Lett. B **436** (1998) 55 [hep-ph/9803466]. K. R. Dienes, E. Dudas and T. Gherghetta, Nucl. Phys. B **537** (1999) 47 [hep-ph/9806292]. M. S. Carena, A. Delgado, E. Ponton, T. M. P. Tait and C. E. M. Wagner, Phys. Rev. D **68** (2003) 035010 [hep-ph/0305188]. L. Randall and M. D. Schwartz, JHEP **0111** (2001) 003 [hep-th/0108114]. 48

[78] G. Cacciapaglia, C. Csaki, C. Grojean and J. Terning, Phys. Rev. D **71** (2005) 035015 [hep-ph/0409126]. C. Csaki, C. Grojean, J. Hubisz, Y. Shirman and J. Terning, Phys. Rev. D **70** (2004) 015012 [hep-ph/0310355]. C. Csaki, C. Grojean, L. Pilo and J. Terning, Phys. Rev. Lett. **92** (2004) 101802 [hep-ph/0308038]. C. Csaki, C. Grojean, H. Murayama, L. Pilo and J. Terning, Phys. Rev. D **69** (2004) 055006 [hep-ph/0305237]. Y. Nomura, JHEP **0311** (2003) 050 [hep-ph/0309189]. H. Davoudiasl, J. L. Hewett, B. Lillie and T. G. Rizzo, JHEP **0405** (2004) 015 [hep-ph/0403300]. H. Davoudiasl, J. L. Hewett, B. Lillie and T. G. Rizzo, Phys. Rev. D **70** (2004) 015006 [hep-ph/0312193]. R. Barbieri, A. Pomarol and R. Rattazzi, Phys. Lett. B **591** (2004) 141 [hep-ph/0310285]. 48

[79] G. Servant and T. M. P. Tait, Nucl. Phys. B **650** (2003) 391 [hep-ph/0206071]. H. -C. Cheng, K. T. Matchev and M. Schmaltz, Phys. Rev. D **66** (2002) 036005 [hep-ph/0204342]. T. Appelquist, H. -C. Cheng and B. A. Dobrescu, Phys. Rev. D **64** (2001) 035002 [hep-ph/0012100]. 48

[80] S. Dimopoulos and G. L. Landsberg, Phys. Rev. Lett. **87** (2001) 161602 [hep-ph/0106295]. S. B. Giddings and S. D. Thomas, Phys. Rev. D **65** (2002) 056010 [hep-ph/0106219]. 48

[81] I. Antoniadis, K. Benakli and M. Quiros, Phys. Lett. B **331** (1994) 313 [hep-ph/9403290], I. Antoniadis, C. Munoz and M. Quiros, Nucl. Phys. B **397** (1993) 515 [hep-ph/9211309]. 48

[82] E. Accomando, I. Antoniadis and K. Benakli, Nucl. Phys. B **579** (2000) 3 [hep-ph/9912287]. 48

[83] A. Delgado, A. Pomarol and M. Quiros, Phys. Rev. D **60** (1999) 095008 [hep-ph/9812489]. 48

[84] T. Appelquist, H. C. Cheng and B. A. Dobrescu, Phys. Rev. D **64**, 035002 (2001) [arXiv:hep-ph/0012100]. 48

[85] N. Arkani-Hamed, H. C. Cheng, B. A. Dobrescu and L. J. Hall,, Phys. Rev. D **62**, 096006 (2000) [arXiv:hep-ph/0006238]. 48

[86] T. Appelquist, B. A. Dobrescu, E. Ponton and H. U. Yee, Phys. Rev. Lett. **87**, 181802 (2001). 48

[87] G. Bhattacharyya, A. Datta, S. K. Majee and A. Raychaudhuri, arXiv:hep-ph/0608208. 48, 52, 53, 153, 158

[88] A. J. Buras, A. Poschenrieder, M. Spranger and A. Weiler, Nucl. Phys. B **678**, 455 (2004) [arXiv:hep-ph/0306158]; A. J. Buras, M. Spranger and A. Weiler, Nucl. Phys. B **660**, 225 (2003) [arXiv:hep-ph/0212143]. 48

[89] D. Hooper and S. Profumo, Phys. Rept. **453**, 29 (2007) [arXiv:hep-ph/0701197]; 48

[90] P. Colangelo, F. De Fazio, R. Ferrandes and T. N. Pham, Phys. Rev. D **77**, 055019 (2008) [arXiv:0709.2817 [hep-ph]] and references therein. 48

[91] A. Datta, K. Kong and K. T. Matchev, New J. Phys. **12**, 075017 (2010) [arXiv:1002.4624 [hep-ph]]. 48

[92] M. Kobayashi and T. Maskawa, Prog. Theor. Phys. **49**, 652 (1973): N. Cabibbo, Phys. Rev. Lett. **10**, 531 (1963). 48

[93] A. Pomarol and M. Quiros, Phys. Lett. B **438** (1998) 255 [hep-ph/9806263]. 51

[94] A. Delgado, A. Pomarol and M. Quiros, JHEP **0001** (2000) 030 [hep-ph/9911252]. 51

[95] A. S. Cornell and L. -X. Liu, Phys. Rev. D **83** (2011) 033005 [arXiv:1010.5522 [hep-ph]]. 53, 61, 66, 70

[96] L. -X. Liu and A. S. Cornell, PoS KRUGER **2010**, 045 (2010) [arXiv:1103.1527 [hep-ph]]. 53

[97] T. P. Cheng, E. Eichten and L. F. Li, Phys. Rev. D **9**, 2259 (1974). 53, 63

[98] A. Deandrea, J. Welzel, P. Hosteins and M. Oertel, Phys. Rev. D **75** (2007) 113005 [hep-ph/0611172]. 55, 56, 57, 67, 151

[99] C. Bouchart, A. Knochel and G. Moreau, Phys. Rev. D **84**, 015016 (2011) [arXiv:1101.0634 [hep-ph]]. 55

[100] A. Hebecker, Nucl. Phys. B **632** (2002) 101 [hep-ph/0112230]. 55

[101] N. Arkani-Hamed, T. Gregoire and J. G. Wacker, JHEP **0203**, 055 (2002) [arXiv:hep-th/0101233]. N. Marcus, A. Sagnotti and W. Siegel, Nucl. Phys. B **224**, 159 (1983). E. A. Mirabelli and M. E. Peskin, Phys. Rev. D **58**, 065002 (1998) [arXiv:hep-th/9712214]. I. L. Buchbinder, S. J. J. Gates, H. S. J. Goh, W. D. I. Linch, M. A. Luty, S. P. Ng and J. Phillips, Phys. Rev. D **70**, 025008 (2004) [arXiv:hep-th/0305169]. 55

[102] A. S. Cornell, A. Deandrea, L. -X. Liu and A. Tarhini, Phys. Rev. D **85** (2012) 056001 [arXiv:1110.1942 [hep-ph]]. 55, 56, 62, 64, 70

[103] A. S. Cornell, A. Deandrea, L. -X. Liu and A. Tarhini, Eur. Phys. J. Plus **128** (2013) 6 [arXiv:1206.5988 [hep-ph]]. 55, 83, 92

[104] A. S. Cornell, A. Deandrea, L. -X. Liu and A. Tarhini, Mod. Phys. Let. A **28** (2013) 1330007 [arXiv:1209.6239 [hep-ph]]. 55, 92

[105] I. Antoniadis, Phys. Lett. B **246** (1990) 377; C. Csaki, arXiv:hep-ph/0404096. Y. A. Kubyshin, arXiv:hep-ph/0111027. V. A. Rubakov, Phys. Usp. **44**, 871 (2001) [Usp. Fiz. Nauk **171**, 913 (2001)] [arXiv:hep-ph/0104152]. A. Perez-Lorenzana, J. Phys. Conf. Ser. **18**, 224 (2005) [arXiv:hep-ph/0503177]. M. Quiros, arXiv:hep-ph/0302189; 55

[106] N. Arkani-Hamed, T. Gregoire and J. G. Wacker, JHEP **0203** (2002) 055 [hep-th/0101233]. 55

[107] J. Iliopoulos and B. Zumino, Nucl. Phys. B **76** (1974) 310; J. Wess and B. Zumino, Phys. Lett. B **49** (1974) 52. 56

[108] P. H. Chankowski and Z. Pluciennik, Phys. Lett. B **316** (1993) 312 [hep-ph/9306333]. 57, 65

[109] S. Antusch, M. Drees, J. Kersten, M. Lindner and M. Ratz, Phys. Lett. B **519** (2001) 238 [hep-ph/0108005]. 57, 59, 65

[110] S. Antusch, M. Ratz and , JHEP **0207** (2002) 059 [hep-ph/0203027]. 59

[111] K. S. Babu, Z. Phys. C **35**, 69 (1987). 61, 63, 77, 153

[112] L. -X. Liu and A. S. Cornell, arXiv:1204.0532 [hep-ph]. 61, 67, 70, 71, 158

[113] M. Bando, T. Kobayashi, T. Noguchi and K. Yoshioka, Phys. Rev. D **63**, 113017 (2001) [arXiv:hep-ph/0008120]. M. Bando, T. Kobayashi, T. Noguchi and K. Yoshioka, Phys. Lett. B **480**, 187 (2000) [arXiv:hep-ph/0002102]. 62

[114] K. Sasaki, Z. Phys. C **32**, 149 (1986). 63

[115] M. E. Machacek and M. T. Vaughn, Nucl. Phys. B **236**, 221 (1984). 63

[116] L. X. Liu, Int. J. Mod. Phys. A **25**, 4975 (2010), arXiv:0910.1326 [hep-ph]. 63

[117] C. Balzereit, T. Mannel and B. Plumper, Eur. Phys. J. C **9**, 197 (1999) [arXiv:hep-ph/9810350]. 63

[118] T. K. Kuo and L. X. Liu, arXiv:hep-ph/0511037. 63

[119] Z. -z. Xing, H. Zhang and S. Zhou, Phys. Rev. D **77**, 113016 (2008) [arXiv:0712.1419 [hep-ph]]. 64

[120] K. Nakamura *et al.* [Particle Data Group Collaboration], J. Phys. G G **37** (2010) 075021 and 2011 partial update for the 2012 edition. 64, 83

[121] S. Weinberg, Phys. Rev. Lett. **43** (1979) 1566. 65

[122] M. Blennow, H. Melbeus, T. Ohlsson and H. Zhang, JHEP **1104** (2011) 052 [arXiv:1101.2585 [hep-ph]]. 65, 66, 67, 158

[123] P. H. Chankowski and Z. Pluciennik, Phys. Lett. B **316** (1993) 312 [hep-ph/9306333]. K. S. Babu, C. N. Leung and J. T. Pantaleone, Phys. Lett. B **319** (1993) 191 [hep-ph/9309223]. 65, 66

[124] S. Antusch, J. Kersten, M. Lindner and M. Ratz, Nucl. Phys. B **674** (2003) 401 [hep-ph/0305273]. 65, 67, 82, 92

[125] B. Aubert *et al.* [BABAR Collaboration], Nucl. Instrum. Meth. A **479** (2002) 1 [hep-ex/0105044]. 70

[126] A. Abashian *et al.*, Nucl. Instrum. Meth. A479 (2002) 117-232. 70

[127] M. Blennow, H. Melbeus, T. Ohlsson and H. Zhang, Phys. Lett. B **712**, 419 (2012) [arXiv:1112.5339 [hep-ph]]. 71

[128] R. N. Mohapatra, S. Antusch, K. S. Babu, G. Barenboim, M. -C. Chen, A. de Gouvea, P. de Holanda and B. Dutta *et al.*, Rept. Prog. Phys. **70** (2007) 1757 [hep-ph/0510213]. 81

[129] M. Raidal, A. van der Schaaf, I. Bigi, M. L. Mangano, Y. K. Semertzidis, S. Abel, S. Albino and S. Antusch *et al.*, Eur. Phys. J. C **57** (2008) 13 [arXiv:0801.1826 [hep-ph]]. 81, 90

[130] F. P. An *et al.* [DAYA-BAY Collaboration], Phys. Rev. Lett. **108** (2012) 171803 [arXiv:1203.1669 [hep-ex]]. 81, 83

[131] Y. Abe *et al.* [DOUBLE-CHOOZ Collaboration], Phys. Rev. Lett. **108** (2012) 131801 [arXiv:1112.6353 [hep-ex]]. 81

[132] J. K. Ahn *et al.* [RENO Collaboration], Phys. Rev. Lett. **108**, 191802 (2012) [arXiv:1204.0626 [hep-ex]]. 81

[133] P. Minkowski, Phys. Lett. B **67** (1977) 421. R. N. Mohapatra and G. Senjanovic, Phys. Rev. Lett. **44** (1980) 912. 82

[134] Z. Maki, M. Nakagawa and S. Sakata, Prog. Theor. Phys. **28** (1962) 870. 82

[135] P. F. Harrison, D. H. Perkins and W. G. Scott, Phys. Lett. B **530**, 167 (2002) [hep-ph/0202074]. 88

[136] W. Buchmuller, P. Di Bari and M. Plumacher, Nucl. Phys. B **665** (2003) 445 [hep-ph/0302092]. 90

[137] P. -H. Gu, Phys. Rev. D **81** (2010) 073002 [arXiv:1001.1340 [hep-ph]]. 92

[138] S. Luo and Z. -z. Xing, arXiv:1203.3118 [hep-ph]. 92

[139] T. Ohlsson and S. Riad, Phys. Lett. B **718**, 1002 (2013) [arXiv:1208.6297 [hep-ph]]. 93

[140] G.F. Giudice, M.A. Luty, H. Murayama and R. Rattazzi, JHEP **9812** (1998) 027 [hep-ph/9810442]; A. Pomarol and R. Rattazzi, JHEP **9905** (1999) 013 [hep-ph/9903448]; D.W. Jung and J.Y. Lee, JHEP **0903** (2009) 123 [arXiv:0902.0464]. 97, 99

[141] L. Randall and R. Sundrum, Nucl. Phys. B **557** (1999) 79 [hep-th/9810155]. 97, 99, 100

[142] K. Choi, K.S. Jeong and K.I. Okumura, JHEP **0509** (2005) 039 [hep-ph/0504037]. 97, 101, 102

[143] R. Dermisek, H. Verlinde and L.T. Wang, Phys. Rev. Lett. **100** (2008) 131804 [arXiv:0711.3211]. 97, 100

[144] A. Arbey, A. Deandrea and A. Tarhini, JHEP **1105** (2011) 078 [arXiv:1103.3244]. 97, 138

[145] H. Baer, R. Dermisek, S. Rajagopalan and H. Summy, JCAP **1007** (2010) 014 [arXiv:1004.3297]. 100

[146] H. Baer, R. Dermisek, S. Rajagopalan and H. Summy, JHEP **0910** (2009) 078 [arXiv:0908.4259]. 100, 101

[147] H. Baer, E.K. Park, X. Tata and T.T. Wang, JHEP **0608** (2006) 041 [hep-ph/0604253]. 101, 102

[148] F. Mahmoudi, Comput. Phys. Commun. **178** (2008) 745 [arXiv:0710.2067]; F. Mahmoudi, Comput. Phys. Commun. **180** (2009) 1579 [arXiv:0808.3144]; `http://superiso.in2p3.fr` F. Mahmoudi, Comput. Phys. Commun. **180** (2009) 1718, `http://superiso.in2p3.fr` 102, 103, 111, 134

[149] F. Mahmoudi, JHEP **0712** (2007) 026 [arXiv:0710.3791]. 102, 134

[150] CDF collaboration, "Search for $B_s^0 \to \mu^+\mu^-$ and $B_d^0 \to \mu^+\mu^-$ Decays in 3.7 fb^{-1} of $p\bar{p}$ Collisions with CDF II," CDF public note **9892** (2009). 102

[151] A. G. Akeroyd and F. Mahmoudi, JHEP **0904** (2009) 121 [arXiv:0902.2393]. 103

[152] M. Antonelli *et al.* [FlaviaNet Working Group on Kaon Decays], arXiv:0801.1817 [hep-ph]. 103

[153] F. E. Paige, S. D. Protopopescu, H. Baer and X. Tata, hep-ph/0312045. 103, 134

[154] A. Arbey and F. Mahmoudi, Comput. Phys. Commun. **181** (2010) 1277 [arXiv:0906.0369], `http://superiso.in2p3.fr/relic` 103, 111, 134

[155] For recent reviews, see: M. Maniatis, Int. J. Mod. Phys. A **25** (2010) 3505 [arXiv:0906.0777]; U. Ellwanger, C. Hugonie and A.M. Teixeira, Phys. Rept. **496** (2010) 1 [arXiv:0910.1785]. 106

[156] U. Ellwanger and C. Hugonie, Comput. Phys. Commun. **177** (2007) 399 [hep-ph/0612134]. 111

[157] K. Jedamzik, Phys. Rev. D **74** (2006) 103509 [hep-ph/0604251]. 118

[158] W. Beenakker, M. Klasen, M. Kramer, T. Plehn, M. Spira and P.M. Zerwas, Phys. Rev. Lett. **83** (1999) 3780 [Erratum-ibid. **100** (2008) 029901] [hep-ph/9906298]. 128

[159] H. Baer and X. Tata, Phys. Rev. D **47** (1993) 2739. 128

[160] H. Baer, C.H. Chen, F. Paige and X. Tata, Phys. Rev. D **50** (1994) 4508 [hep-ph/9404212]. 128

[161] G. Aad *et al.* [ATLAS collaboration], Phys. Lett. B716 (2012) 1 [arXiv:1207.7214]. 133

[162] S. Chatrchyan *et al.* [CMS collaboration], Phys. Lett. B716 (2012) 30 [arXiv:1207.7235]. 133

[163] [ATLAS Collaboration], Note ATLAS-CONF-2012-160. 133

[164] [ATLAS Collaboration], Note ATLAS-CONF-2012-161. 133

[165] [CMS Collaboration], Note CMS PAS HIG-2012-043. 133

[166] [CMS Collaboration], Note CMS PAS HIG-2012-044. 133

[167] [ATLAS Collaboration], Note ATLAS-CONF-2012-168. 133
[168] [ATLAS Collaboration], Note ATLAS-CONF-2012-169. 133
[169] A. Arbey, M. Battaglia, A. Djouadi and F. Mahmoudi, JHEP **1209** (2012) 107 [arXiv:1207.1348 [hep-ph]]. 134, 135
[170] A. Djouadi, J. Kalinowski and M. Spira, Comput. Phys. Commun. 108 (1998) 56. 134
[171] R. Aaij *et al.* [LHCb Collaboration], arXiv:1211.2674 [hep-ex]. 134
[172] K. De Bruyn, R. Fleischer, R. Knegjens, P. Koppenburg, M. Merk, A. Pellegrino and N. Tuning, Phys. Rev. Lett. **109** (2012) 041801 [arXiv:1204.1737 [hep-ph]]. 134
[173] K. De Bruyn, R. Fleischer, R. Knegjens, P. Koppenburg, M. Merk and N. Tuning, Phys. Rev. D **86** (2012) 014027 [arXiv:1204.1735 [hep-ph]]. 134
[174] A. Arbey, M. Battaglia, F. Mahmoudi and D. Martinez Santos, arXiv:1212.4887 [hep-ph]. 134
[175] A. Arbey, M. Battaglia, A. Djouadi, F. Mahmoudi and J. Quevillon, Phys. Lett. B **708** (2012) 162 [arXiv:1112.3028 [hep-ph]]. 135, 137
[176] A. Arbey, M. Battaglia, A. Djouadi and F. Mahmoudi, arXiv:1211.4004 [hep-ph].
[177] [ATLAS Collaboration], Note ATLAS-CONF-2013-014. 135
[178] [CMS Collaboration], Note CMS PAS HIG-2013-002. 133, 135
[179] [ATLAS Collaboration], Note ATLAS-CONF-2013-012. 133, 135
[180] [CMS Collaboration], Note CMS PAS HIG-2013-001. 133, 135
[181] [ATLAS Collaboration], Note ATLAS-CONF-2013-013. 133, 135
[182] [ATLAS Collaboration], Note ATLAS-CONF-2013-030. 133, 135
[183] [CMS Collaboration], Note CMS PAS HIG-2013-003. 133, 135
[184] [ATLAS Collaboration], Note ATLAS-CONF-2012-161. 133, 135
[185] [CMS Collaboration], Note CMS PAS HIG-2012-044. 135
[186] T. Aaltonen *et al.* [CDF and D0 Collaborations], Phys. Rev. Lett. **109** (2012) 071804 [arXiv:1207.6436 [hep-ex]]. 135
[187] [CMS Collaboration], Note CMS PAS HIG-2012-004. 135
[188] A. Arbey, A. Deandrea, F. Mahmoudi and A. Tarhini, Phys. Rev. D 87 (115020) 2013 [arXiv:1304.0381 [hep-ph]]. 135
[189] See e.g., M. Carena et al., JHEP **1207** (2012) 175; M. Carena, I. Low and C. E. M. Wagner, JHEP **1208** (2012) 060; G. F. Giudice, P. Paradisi, and A. Strumia, JHEP **1210** (2012) 186; U. Haisch and F. Mahmoudi, arXiv:1210.7806 [hep-ph]. 137
137
[190] G. Aad *et al.* [ATLAS Collaboration], Phys. Lett. B **710**, 49 (2012) [arXiv:1202.1408 [hep-ex]]. S. Chatrchyan *et al.* [CMS Collaboration], Phys. Lett. B **710**, 26 (2012) [arXiv:1202.1488 [hep-ex]]. 157
[191] P. Kielanowski and S. R. Juarez Wysozka, Phys. Rev. D **72**, 096003 (2005). 158
[192] A. S. Cornell and L. -X. Liu, Phys. Rev. D **84**, 036002 (2011) [arXiv:1105.1132 [hep-ph]]. 158
[193] G. Bhattacharyya, S. Goswami and A. Raychaudhuri, Phys. Rev. D **66**, 033008 (2002) [hep-ph/0202147]. 158